Faculty of Engineering and Science

An Analytical and Experimental Study on Wire Rope Isolators for Vibration Isolation of Equipment and Structures

Balaji Palani Selvaraj

THIS THESIS IS PRESENTED FOR THE DEGREE OF
Doctor of Philosophy
of
Curtin University

November 2016

Statement of Originality

To the best of my knowledge and belief, this thesis contains no material previously published by any other person except where due acknowledgement has been made.

This thesis contains no material, which has been accepted for the award of any other degree or diploma in any university.

Signature :

Date : 23/11/2016

Acknowledgement

I take this opportunity to express my deep sense of gratitude to my thesis supervisors, Dr. Leblouba Moussa, A/Prof.Muhammad Ekhlasur Rahman and Prof. Ir. Lau Hieng Ho for their constant guidance and insightful comments during the course of work. I also would like to express my gratitude for their expert guidance and for inspiring me to do this research work. I shall always cherish my association with them for their constant encouragement and freedom to thought and action that rendered to me throughout the thesis work.

I also like to extend my gratitude to Professor Marcus Lee for his valuable comments in the preparation of my research proposal.

I am thankful to Ministry of Higher Education (MOHE), Malaysia under the ERGS grant scheme and Curtin University for providing the financial support for my research work.

Finally, I wish to express my special thanks to my wife Mrs. Amudhasri Balaji and my daughter Ms. Sivasakthi, for their great encouragement and maintaining patience throughout my project, as well as to my parents for their continual support and encouragement.

List of Publications

JOURNAL PUBLICATIONS

1. P.S.Balaji, Leblouba Moussa, M.E.Rahman, Lau Hieng Ho, 2016 “Static lateral stiffness of wire rope isolators”, *Mechanics Based Design of Structures and Machines, An International Journal, Taylor and Francis* 2016. DOI: http://dx.doi.org/10.1080/15397734.2015.1116996.(Impact Factor : 0.84)

2. P.S.Balaji, Leblouba Moussa, M.E.Rahman, Lau Hieng Ho, 2016 “An analytical study on the static vertical stiffness of wire rope Isolators”, *Journal of Mechanical Science and Technology, Springer,* 30 (1) 287-295. (Impact Factor : 0.838)

3. P.S. Balaji, L. Moussa, M.E. Rahman, L. Vuia, 2015 “Experimental investigation on the hysteresis behaviour of the wire rope isolators”, *Journal of Mechanical Science and Technology*, Springer, 29 (4) 1527-1536. (Impact Factor : 0.838)

4. P.S. Balaji, M. Rahman, L. Moussa, H. Lau, 2015 “Wire rope isolators for vibration isolation of equipment and structures–A review”, IOP Conference Series: Materials Science and Engineering. (IOP Publishing, 2015), 012001.

INTERNATIONAL CONFERENCES

(1) P.S.Balaji, M.E.Rahman, Leblouba Moussa, Lau Hieng Ho, 2015, "Vibration isolation of structures and equipment using Wire rope isolators", *Proceeding of 4th International Conference on Recent Trends in Engineering & Technology*, 2nd-4th July 2015, SNJB College of Engineering, Nasik, India.

(2) P.S.Balaji, L.Moussa, M.E.Rahaman, P.L.Y.Tiong, Lau Hieng Ho, A. Adnan, "Performance study of wire rope isolators for vibration isolation equipment and structures", *2nd International Conference on Design, Analysis, Manufacturing & Simulation (ICDAMS 2016)*, 7–8 April 2016, Saveetha University, Chennai, India.

Abstract

Vibrations due to earthquake ground motions or the operation of heavy machinery can affect the functionality of equipment and cause damage to the hosting structures. Hence adding a discrete system to isolate vibrations from these type of sources has become a necessity. The Wire Rope Isolator (WRI) is known to be effective in isolating shocks and vibrations and can be used for both lightweight structures and equipment. The primary advantage of the WRI is it can provide isolation in all three planes and in any orientation. The isolation of equipment is generally provided by decoupling the equipment from the base through a system of isolators. The isolation ability of WRI can be characterized by evaluating its stiffness and damping characteristics.

The primary aim of this research work is to evaluate the stiffness and damping characteristics of WRIs in both the vertical and lateral directions through analytical and experimental studies. The analytical models for the vertical and lateral stiffness of WRIs were developed based on Castigliano's second theorem and the study has identified that the wire rope diameter significantly influences the stiffness of the WRI more than the other geometric characteristics. The damping characteristic of WRI was studied through a series of cyclic loading tests. In addition, mathematical models were also developed for the hysteresis behaviour in both vertical and lateral directions using the Bouc-Wen model of hysteresis. The cyclic loading tests on the WRIs in the vertical direction are asymmetric in the hysteresis behaviour, whereas in the lateral direction the hysteresis behaviour is symmetric. Therefore, the original Bouc-Wen model of hysteresis was used for the lateral direction and a modified version of the same model was developed for the asymmetric hysteresis behaviour in the vertical direction. This study identified the damping characteristics of the WRI is effectively influenced by varying the height-to-width ratio for a given wire rope diameter.

Recent studies in vibration isolation have suggested the raised floor technique can provide better isolation than the direct isolation approach. Hence, in this research

work, a case study on the isolation of equipment using WRI by the raised floor technique has also been investigated. The performance of WRIs in the isolation of equipment using the raised floor technique was studied using numerical simulations. The performance of WRIs was evaluated using 34 earthquake excitations having different characteristics. The WRI reduced the acceleration of the equipment by 68% on average for the cases considered in this study. This reduction in the acceleration was achieved at the expense of increased lateral displacements.

This study enhanced the understanding of the stiffness and damping characteristics of WRIs and improved the knowledge on the behaviour of WRI as a vibration isolation device. The mathematical and numerical models developed in this work, for the behaviour and performance respectively, can be used to simulate the static and dynamic behaviour of wire rope isolators and to determine their effectiveness in isolating lightweight structures and equipment from external vibrations.

Table of Contents

List of Figures

List of Tables

Nomenclature

A_{Loop}	Area of hysteresis curve
A	Bouc-Wen parameter
C	Damping coefficient of the system
E	Young's Modulus
EDR	Equivalent Damping ratio
F	Restoring Force
F_{1s}	Non-Hysteretic term
F_{2s}	Nonlinear hysteretic term
F_{max}	Maximum force
F_{min}	Minimum force
F_Y	Yield force
H	Height of the isolator
I	Moment of Inertia
K	Stiffness of the system
k_v	Vertical stiffness of the WRI
k_h	Lateral stiffness of the WRI
K_{eff}	Effective stiffness
$K_{rope,}$ K_{cs}, K_{gs}	Bending stiffness of the rope, central core and general strand respectively.
L	Half-Width of the metal retainer
R	Radius of the arc
M	Mass of the system
M_1,M_2	Bending moment in the region 1 and 2 respectively
M_o	Statically indeterminate bending moment
n	Bouc-Wen parameter
Q	Characteristic strength
U	Displacement
X_{max}	Maximum Displacement
X_{min}	Minimum Displacement
Y	Yield displacement
Z	hysteresis dimensionless quantity

Greek Symbols

α	Ratio of post to pre-yield stiffness
β,γ	Bouc-Wen parameters
ω	frequency
δ_v, δ_h	Vertical and lateral displacement respectively.
ϕ	Helix angle

Chapter 1. INTRODUCTION

1.1. NEED FOR VIBRATION ISOLATION

Vibrations are present in every engineering application and when they become excessive, can cause structural damage and affect equipment functionality. However, in many cases, these vibrations will be within tolerable limits. In other cases where the vibration becomes intolerable, adding an isolation system to counter the vibrations becomes necessary (Klembczyk, 2014). For example, the El Centro earthquake in 1940 has caused significant damages to the property and loss of life, and such destructive effects from harmful vibrational disturbance can be reduced by using vibration isolation systems. The application of a vibration isolation system requires understanding the components of vibration control, namely, the source, path and receiver of the vibration (Simmons, 2007).

The source of the vibration can be either natural, such as an earthquake, wind, ocean waves, etc. or human-induced, such as due to the operation of heavy machinery, construction works etc. The path is the medium through which the vibration is transmitted, such as building components, accessories etc. The receiver refers to the building or equipment that receives the vibrations emitted from the source. The vibration control is employed based on the level of vibrations that a receiver can withstand without, either, undergoing structural damage or affecting its functionality. In cases where the level of vibrations are unacceptable, an isolation system is applied to cut off the path of the vibration to enhance the safety of the receiver (Klembczyk, 2014;Mallik, 1990).

1.2. BASIC CONCEPT OF VIBRATION ISOLATION

The term ‘vibration isolation’ refers to the mitigation of the vibratory response of the receiver to external excitations(Rivin, 2003).In general, the isolation system can be used in two different cases. Case 1: To reduce the vibratory disturbance from the equipment to its surrounding, as in the case of heavy machinery or Case 2: To isolate the

sensitive equipment whose precision can be affected by its disturbing surrounding. However, the basic principle of vibration isolation remains the same for both cases (Mallik, 1990). The basic concept of vibration isolation can be best explained using a single degree of freedom system (SDOF)(Den Hartog, 1985). Consider the case of a SDOF system as shown in Figure 1.1, in which the isolator having stiffness (K) and Damping (C) support the mass of equipment (M). The natural frequency (ω_n) of the undamped SDOF system is given by Eq(1.1). Assuming a harmonic force (F_B) with a forcing frequency ω in the base excites the system. Now, the ratio of the force (F) experienced by the isolated mass to the external harmonic force is called transmissibility (T).

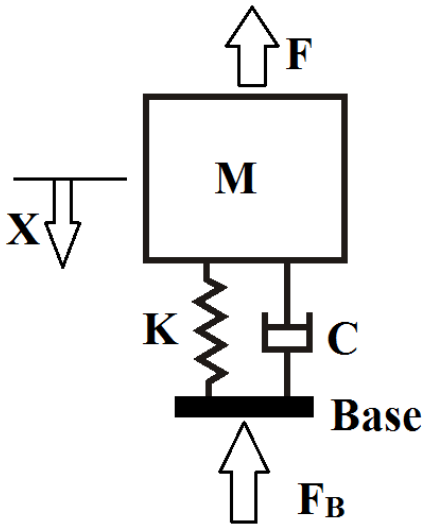

Figure 1.1 Schematic of a SDOF system (Abolfathi, 2012)

$$\omega_n = \sqrt{K/M} \quad in \quad rad/\sec \tag{1.1}$$

Transmissibility of a SDOF system for various damping ratios are shown in Figure 1.2. It can be seen that there is a peak in the transmissibility curve at the frequency ratio of 1, which is the resonance condition. When the transmissibility of a system is less than unity, it means the force experienced by the isolated mass is less than the external force and this is the intended condition by using an isolator. From Figure 1.2, it can be seen that all the curves cross below the line of unit transmissibility at the point where the frequency ratio is $\sqrt{2}$. This frequency is referred as the isolation

frequency(Abolfathi, 2012). Hence, it is clear that to achieve the isolation effect, it is required to reduce the natural frequency of the system lower than the forcing frequency and at a higher frequency ratio, lower transmissibility can be achieved. The amount of transmissibility required for an application differs in each case and depends mainly on the criticalness of the application. In general, transmissibility of about 3% (0.03) for critical applications and 5% (0.05) for sensitive applications and 10% (0.1) for non-sensitive are the accepted standards applied (Simmons, 2007) and the values indicated here, are only for reference.

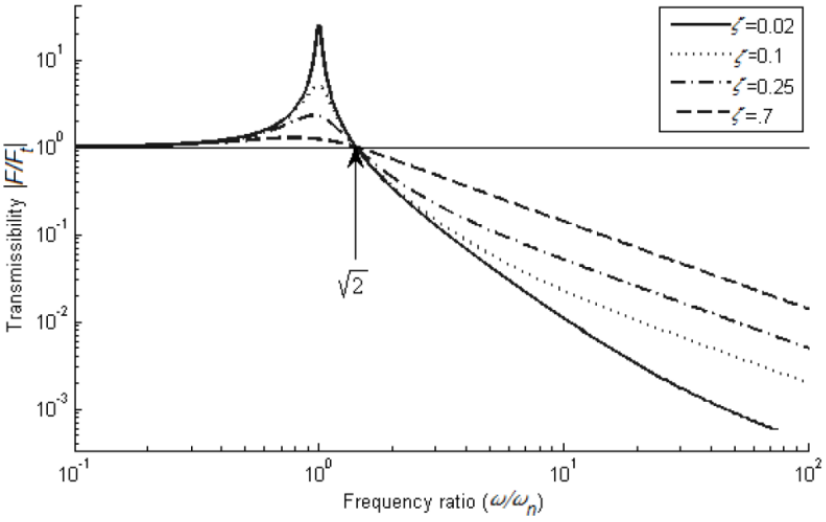

Figure 1.2 Transmissibility of SDOF system (Abolfathi, 2012)

1.2.1. ISOLATION METHODS

In general, the mitigation of vibrational response on equipment and structures can be performed through three approaches (Hamidi and El Naggar, 2007;Ismail *et al.*, 2009b) (see Figure 1.3.): (1) Isolation of the entire housing structure, (2) Isolation of individual equipment, (3) Isolation of a raised floor system. The first approach is suitable for new construction where isolators are installed between the structure and foundation to reduce the damage to both primary structure and equipment (Naeim and Kelly, 1999). The second approach concentrates only on the equipment; the isolation system is inserted at the base of the equipment to reduce the transmission of vibration. However, both approaches are confronted with the difficulty of achieving the desired long time period within an affordable displacement (Demetriades *et al.*, 1993).

In the third approach, the raised floor approach, several equipment are fixed to a secondary floor which decouples from the structural floor by an isolation system. This approach provides potential benefit to both new and existing constructions. The raised floor approach also possesses advantages such as low cost when compared with the first approach and it can also provide long period while maintaining an affordable displacement (Ismail *et al.*, 2012a;Ismail *et al.*, 2012b). The raised floor approach is a newly introduced concept and it needs to be explored further. However, the concept of an isolation system design remains similar for all the approaches.

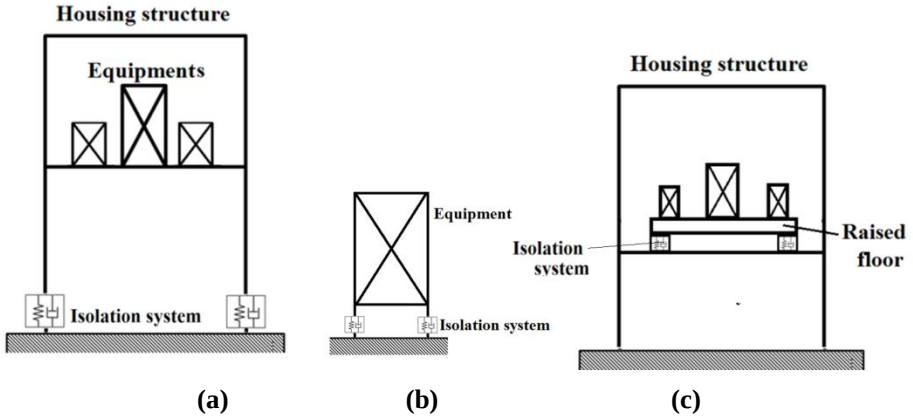

Figure 1.3 Types of isolation methods (a) Entire structure (b) individual equipment (c) raised floor method (De Silva, 2006)

1.3. IDENTIFICATION OF THE PROBLEM

It is clear from the preceding section that vibration isolation can be achieved by lowering the natural frequency than the forcing frequency. It may not be desirable to increase the mass of the system; instead reducing the stiffness of the isolator is usually the preferable practical approach. The earlier developed isolators for vibration isolation applications are passive in type and possessing linear relation in Force-Displacement (F-D) characteristics. The linear type isolators possess constant stiffness and the selection of isolator stiffness for applications depends on the value of the forcing frequency and the amount of transmissibility required. Hence, the linear isolation system requires a careful estimation of forcing frequency to achieve the vibration isolation. However, during severe environmental disturbances such as impact loading, shocks or random ground motions, their spectrum can contain dangerous low-frequency components, which can cause excessive displacement and may even damage the entire system

(Ibrahim, 2008).The limitation of linear isolators can be overcome by introducing nonlinear isolators (Ibrahim, 2008).

Figure 1.4 shows the typical F-D characteristics of a nonlinear isolator with softening behaviour. The slope of the F-D curve at any point is referred to as dynamic stiffness or tangent stiffness (Abolfathi, 2012). It can be seen that the tangent stiffness decreases for higher displacement that in turn reduces the natural frequency of the system. This benefit of the nonlinear isolator provides better isolation than the linear type. The nonlinearity possess challenges in the design of these types of isolators. Though the linear isolators have some drawbacks, they have been widely used in many applications because of their well-documented theories in the literature (Snowdon, 1968;Rivin, 2003). Due to the lack of studies on the nonlinear isolators, the applications areas of nonlinear isolators are very limited. Hence, the nonlinear isolators need to be studied and further the mathematical models to predict its stiffness and damping characteristics are highly desired to widen the application area.

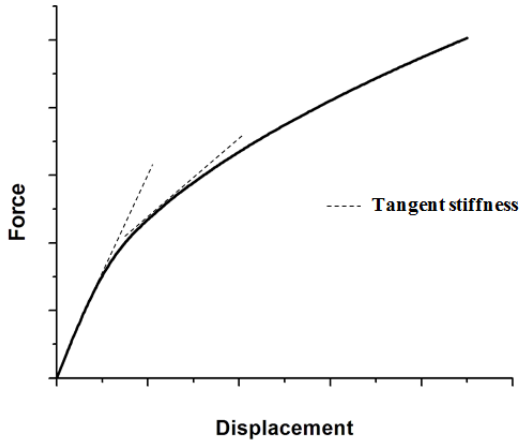

Figure 1.4 Typical F-D characteristics of a nonlinear isolator with softening behaviour (De Silva, 2006)

This research work focuses on a wire rope based nonlinear isolator called the Wire Rope Isolator (WRI) in order to explore its dynamic characteristics and to enhance the understanding of wire rope based isolators. In addition, in this study, due to the advantages of the raised floor approach a case study on the performance of WRI in the vibration isolation of equipment will also be performed. Accordingly, the aim and

objectives are framed and they are stated in the next section. The background and review of the literature on the nonlinear isolators are discussed in Chapter 2.

1.4. AIMS AND OBJECTIVES

The aims of this research work are:

I. To evaluate the static stiffness and damping characteristics in both vertical and lateral directions of the wire rope isolators through an analytical and experimental study.
II. To investigate a case study on the performance of wire rope isolators in the vibration isolation of equipment by the raised floor method.

The objectives of the proposed work are listed below:

1. To develop analytical models of the static stiffness of wire rope isolators in both vertical and lateral directions and to validate the models with the monotonic loading tests.
2. To study the damping characteristics of the wire rope isolators in both vertical and lateral directions using mathematical modelling and cyclic loading tests.
3. To numerically study the performance of wire rope isolators, in the vibration isolation of equipment by raised floor method, using the static stiffness and damping characteristics obtained from objectives 1 and 2.

1.5. SCOPE OF THE WORK

In this research work the stiffness and damping characteristics of the WRI is studied. The objective 1 is to develop the analytical model of the static stiffness in the vertical and lateral directions. The Castigliano's second theorem is applicable for a linear elastic structure and hence the models were developed in the linear region, which is the case at the small displacement of WRI. The vertical and lateral stiffness analytical models of WRI are developed as a function of geometric characteristics (such as wire rope diameter, width, Height and number of turns) and wire rope properties (such as flexural rigidity).

Further, in the objective 2, the cyclic loading test was done at different displacement amplitudes and in this study was conducted at 3 mm, 6 mm and 9 mm displacement amplitudes and the Bouc-Wen model parameters were also identified and validated at all the test displacement amplitudes. The modeling asymmetric hysteresis curve is developed using the bilinear approximation as a function in the Bouc-Wen model and this bilinear approximation shows to be in good agreement with test results.

The scope of the work on the performance study is limited to Raised floor method. The equipment of Demetriades *et al.*(1993) is also considered in this work to numerically study the performance of WRI. The methodology is obtained from Ismail *et al.*(2009b). The isolator results obtained is relevant to the considered excitations in this study, however similar methodology can be used to study performance of WRI at other excitations data.

1.6. THESIS OUTLINE

This thesis is composed of six chapters, following the Chapter 1 on introduction,

Chapter 2 presents a review of the literatures on the development of nonlinear isolators and reviews the literature on the stiffness, damping characteristics, and performance of wire rope isolators.

Chapter 3 presents the first objective of this work, which is the development of analytical models of vertical and lateral stiffness of WRI.

Chapter 4 discusses the second objective of this study, the experimental and mathematical study on the damping characteristics of WRI

Chapter 5 presents a case study on the performance of WRI in the vibration isolation of equipment using the raised floor approach.

Finally, Chapter 6 provides the conclusions and Recommendation for future work.

Chapter 2. BACKGROUND AND LITERATURE REVIEW

2.1. INTRODUCTION

This chapter provides the background information on the development of nonlinear isolators and discusses the existing literature on the characteristics and performance of these isolators. The review of the literature on nonlinear isolators is presented initially followed by the literatures on the stiffness and damping characteristics of wire rope isolators. Finally, previous research on the performance study is reviewed, to provide the overall development in this field. A summary is also provided at the end of this chapter to highlight the research gap relevant to wire rope isolators.

2.2. RESEARCH WORK ON NONLINEAR VIBRATION ISOLATORS

The need for nonlinearity in the force-displacement characteristics of isolators has led to studies on the implementation of nonlinearity found in other fields of engineering for isolator applications. A considerable number of studies have been published on nonlinear isolators so only those relevant to wire rope isolators will be discussed in this chapter. Accordingly in this review, the isolators are discussed under two categories 1) Beam as nonlinear springs and 2) Materials with nonlinear behaviour. These categories were made based on the distinguishing features of the isolators. In the first category, the focus is on influencing the stiffness of the isolators and in the second category; both stiffness and damping are influenced for the vibration isolation application.

2.2.1. BEAMS AS NONLINEAR SPRINGS

The beams, which undergoes large deflection, exhibit nonlinearity in the force-deflection relationship and thus can be used as a nonlinear spring for isolators (Abolfathi, 2012). This type of isolators majorly focuses on reducing the natural frequency of the system by incorporating beams that exhibits softening behaviour in tangent stiffness under large deflections. The nonlinearity of the beam is used in the application by designing a suitable mechanism causing it to undergo large deflections.

The beams are either axially loaded, transversely loaded or both using suitable arrangements. In this section, the Euler springs and beam-column isolators are discussed.

2.2.1.1. Euler springs

When columns are loaded axially, they will exhibit nonlinear force-deflection characteristics and this makes them suitable as a nonlinear spring element in the isolators. Winterflood *et al.*(2002a; 2002b) have utilized the Euler buckling mode of the column springs as a stiffness element in vibration isolators (Figure 2.1). They also developed a mathematical model for the stiffness of Euler spring using the Euler theory for column buckling (Winterflood *et al.*, 2002a). They developed the stiffness model in relation to the geometric characteristics of the column to enable the design of such springs. Virign and Davis (2003) also have proposed a vibration isolator using buckled struts and have used second order approximation for force-defection relation for stiffness characterisation.

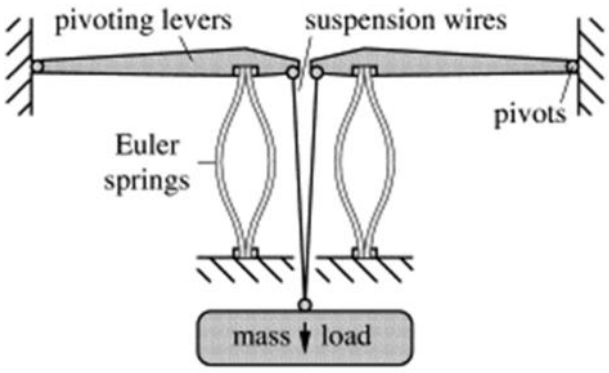

Figure 2.1 Euler spring for vibration isolation (Winterflood *et al.*, 2002a)

2.2.1.2. Beam-Column

The beams also exhibit nonlinearity in the force-deflection when loaded transversely and hence the nonlinearity in both axial and transverse directions lead to the development of Beam-Column isolators. Figure 2.2 shows a simple representation of beam-column isolators in applications and how they are used with suitable fixtures. Platus (1992) has discussed the various applications of beam-column effect for vibration isolation and why these kinds of isolators are preferred used in micro and nano-

mechanical applications. Haberman (2007) has conducted mathematical and experimental research on the force-displacement characteristics of these kinds of isolators. Abolfathi (2012) has developed a mathematical model of the static stiffness as a function of initial curvature angle of curved beams, and the eccentricity of the loading.

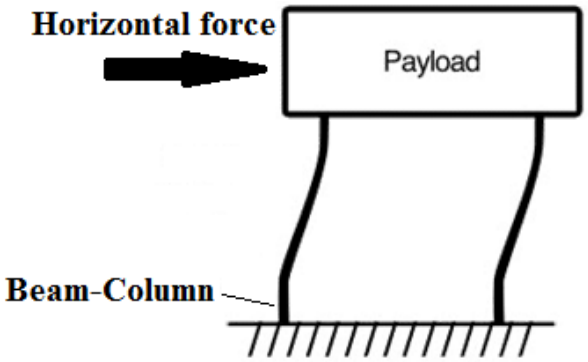

Figure 2.2 Schematic representation of the isolator using beam-column (Platus, 1992)

2.2.2. MATERIALS WITH NONLINEAR BEHAVIOUR

In these kinds of isolators, materials with nonlinear behaviour, such as rubber, composite materials, wire rope, etc., are used as a spring element and additionally, these materials possess energy dissipation capabilities due to inherent damping. A rubber material is used in vibration isolation applications, due to its inherent visco-elastic damping, and has been studied by various researchers. One of the early work was performed by McCallion and Davies (1955), who studied the effects of frequency and amplitude of oscillation as well as the effect of temperature on the mechanical properties of rubber isolators. They also attempted to develop a mathematical expression for the dynamic behaviour of the rubber isolators. The rubber –type isolators were also found to possess transmissibility less than the linear isolators (Shaska *et al.*, 2006). Attempts were also made to incorporate these rubber materials into the spring isolators in order to introduce the damping ability. Leblouba *et al.*(2015) have developed the elliptical leaf spring incorporating lead-rubber (Figure 2.3) and their study has shown that the damping was improved significantly due to the addition of rubber.

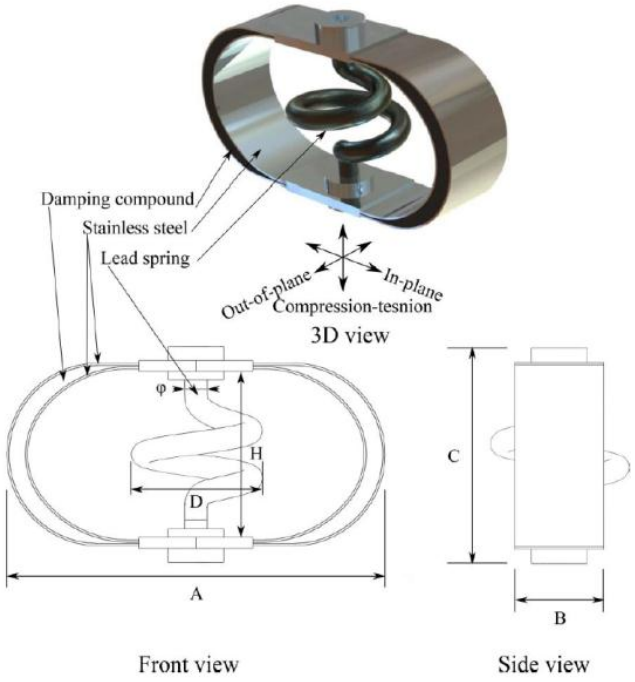

Figure 2.3 Elliptical leaf spring compound with Lead-Rubber (Leblouba *et al.*, 2015)

One of the early work on composite materials for vibration isolation applications was performed by Mallick (1987) who has developed composite elliptical springs to replace the steel elliptical spring in aerospace applications to provide better strength to weight ratio and achieve weight savings. The application of composite materials in aerospace applications has increased significantly since the theoretical research on their impressive characteristics was established. Latter, Tse *et al.*(2002) have studied the force–displacement in both vertical and lateral directions of elliptical composite springs. They also developed a mathematical model of both the vertical and lateral stiffness using Castigliano's second theorem to relate force and displacement in terms of geometric and composite material properties.

Several attempts have also been made to utilize the nonlinear properties of smart materials such as electro-rheological fluids, magneto-hydro-rheological fluids and piezo-electrics. The stiffness and damping properties of these materials can be adjusted using an electric field for electro-rheological fluids, a magnetic field for magneto-hydro-rheological fluids, or mechanical inputs for piezo-electrics (Ibrahim, 2008). One of the first studies of electro-rheological fluids was performed by Tandon *et al.*(1999) using

two colloidal suspensions, one based on silica powder and the other on starch powder. They found that the stiffness and damping properties of this type of fluid could be controlled using electric fields. Guyomar *et al.*(2008) experimented wtih peizo-electric materials in vibration applications and suggested the piezo-electric materials converted excitation energy (mechanical) in to electrical energy and then, dissipates the electrical energy as a heat through electric shunt circuits. The smart materials, although having the beneficial ability to modify its dynamic characteristics, also need a large external power to function as well as suffering from design complexity. Hence, nonlinearity is preferred to achieve using the techniques that are more passive.

2.2.3. SUMMARY

The nonlinearity found in other fields of engineering was subsequently utilized in the vibration isolators. The beams as nonlinear springs discussed in this section have the ability to provide nonlinearity in terms of force-deflection characteristics; however the major drawback to this system is they need a large static deflection for vibration isolation against the low frequency (Abolfathi, 2012). These isolators mainly achieve their isolation by functioning as a nonlinear-spring element and they lack any damping element to restrict displacement magnitude during a resonance condition which may occur due to unforeseen circumstances. Furthermore, these kinds of beams are presently limited to micro and nano mechanical applications.

Likewise, materials with nonlinear properties such as electro-rheological fluids, magneto-hydro-rheological fluids and piezo-electrics have their own limitations in terms of large power requirements and a complex support system. Rubber materials have limitations in terms of being temperature dependent and incurring high manufacturing costs. Hence, further research was needed for developing materials with nonlinear behaviour, yet simple in design and of a passive type; this is what led to the development of wire rope based isolators. The wire rope based isolator is the focus of this research and the developmental work and related literatures are discussed in Section 2.3.

2.3. WIRE ROPE FOR VIBRATION ISOLATION

2.3.1. WIRE ROPE

Wire ropes have been used widely in many engineering and industrial applications, such as in elevator lifting, mine hoists, suspension bridges etc., due to its ability to support large tensile loads. The wire rope consists of individual thin metallic wires, which are helically twisted to form strands, and in turn, multiple strands are laid around a core to form the wire rope as shown in Figure 2.4. The core of the wire rope can be either a wire rope, natural fibers or polypropylene (Costello, 1997). However, the majority of the load is carried by the strands and the core provides the support under normal bending and loading conditions for the strands (Miller, 2004). One of the major contributors on examining wire rope characteristics in various configurations is Velinsky (1988; 1989; 2004). His studies have reported nonlinearity in the force-displacement relation. This nonlinearity is due to the complex interaction between the individual wires with each other and with the core. This poses challenges to developing accurate analytical models and closed form solutions for force-displacement relation.

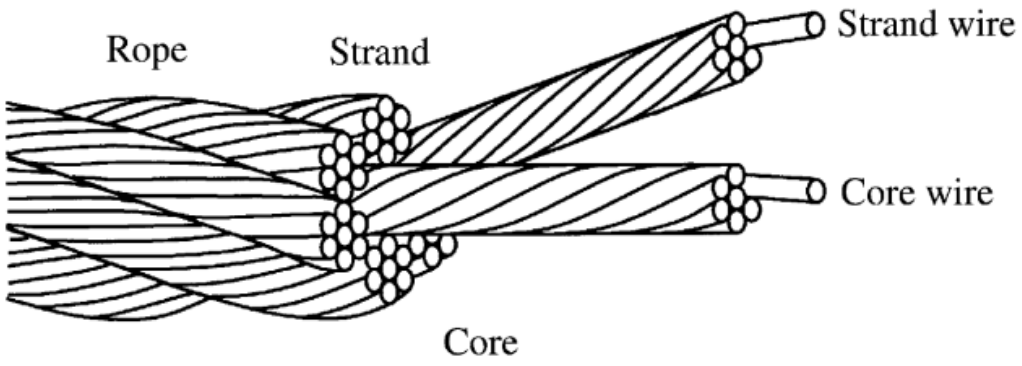

Figure 2.4 Wire rope components (Miller, 2004)

2.3.2. WIRE ROPE FOR VIBRATIONISOLATION

The wire rope has wire strands that are in frictional contact, and hence, have inherent frictional damping. The advantages of exhibiting nonlinear force-displacement and an inherent damping mechanism make it a suitable candidate for vibration isolation applications. One of the early applications of wire rope for vibration control can be

found it cable bridges and in Stockbridge dampers (Figure 2.5). In these applications, wire rope is used as a damping element in bridge cables to dampen wind induced vibrations or in electric transmission lines (Barry *et al.*, 2013).

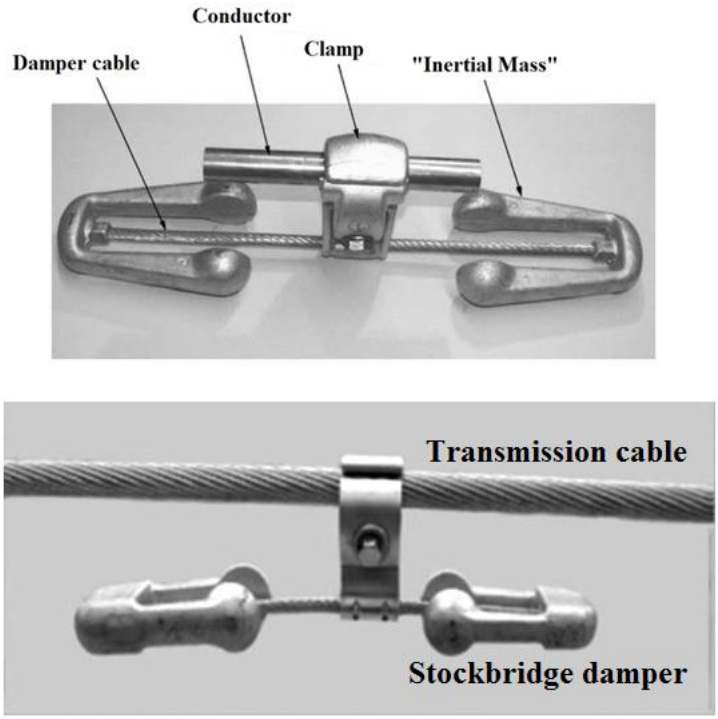

Figure 2.5Application of Stockbridge damper (Barry *et al.*, 2015)

One of the early designs of a wire rope as an isolator called Wire Rope Isolator (WRI), for vibration isolation application was proposed by Constantinous *et al.*(1991). WRI consists of wire rope held between two metal retainer bars in the form of a helix shape as shown in Figure 2.6 (a) or of a polycal shape as shown in Figure 2.6. As the name implies, wire rope isolators use a metal wire rope made up of individual wire strands that are in frictional contact with each other. It acquires its elastic characteristics from the spring design of stranded wire rope and provides energy dissipation through the inherent frictional damping between the wire rope strands (Ni *et al.*, 1999b). The wire rope has the ability to attenuate the vibration and to absorb the energy impact efficiently (Chungui *et al.*, 2009;Weimin *et al.*, 1997). Both the helical and polycal WRI are similar in characteristics and function. However, this research work focuses on helical-type WRI due its ability to be used in large scale applications. Figure 2.7 shows the geometric characteristics of WRI. The most commonly used orientations of WRI are

shown in Figure 2.8 and such orientations induce tension/compression, shear and roll load on the WRI (Demetriades *et al.*, 1993).

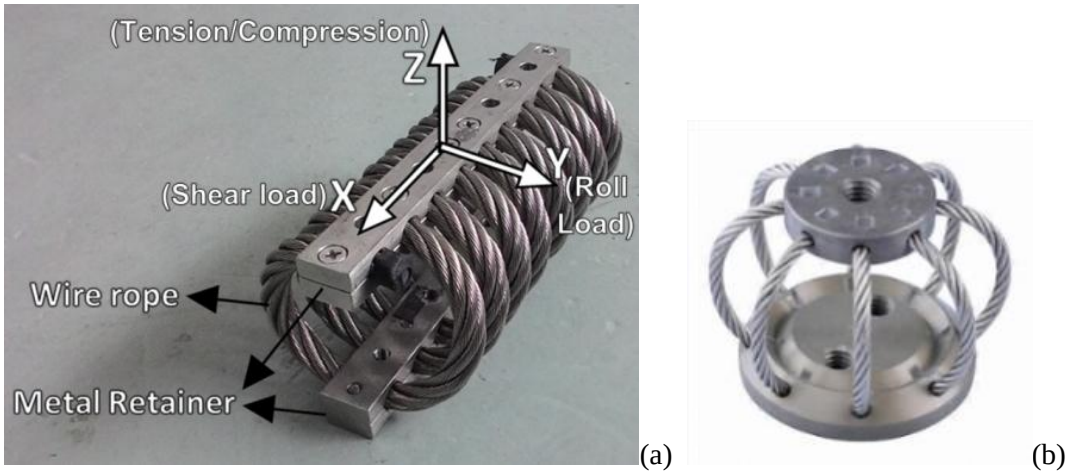

Figure 2.6 (a)Wire rope isolator and loading modes (b) Polycal Wire rope isolator

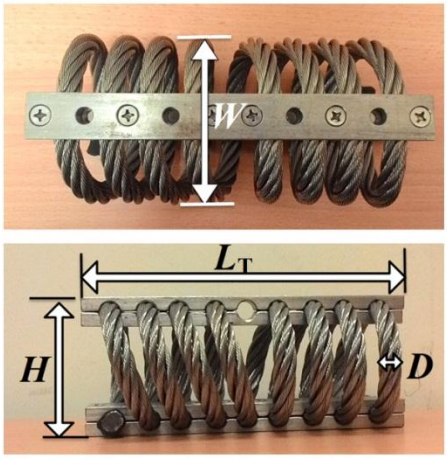

W = Width; L_T = Length; H = Height
D = Wire rope diameter

Figure 2.7 Geometric characteristics of WRI

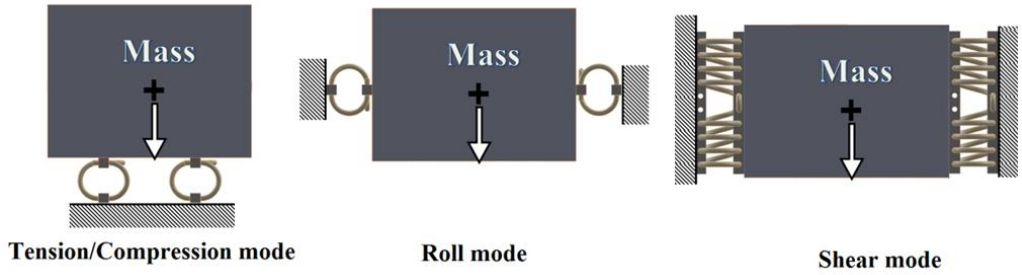

Figure 2.8 Orientation of WRI used in the applications

WRI is a typical non-linear hysteretic damping device (Ni *et al.*, 1999b). It is also effective for controlling both shock and vibrations (Tinker and Cutchins, 1992). Hence, WRI can be an effective isolator for shock and vibration isolation. The WRI is an economical passive isolation device and has many applications. The application of WRI includes vibration isolation for industrial and defense equipment (Demetriades *et al.*, 1993), light steel structures(Pagano and Strano, 2013), aerospace systems and rocket engines (Tinker and Cutchins, 1992), sensitive electronic systems (Veprik and Babitsky, 2000), cargo shipments (Chaudhuri and Kushwaha, 2008) isolation of pipes in nuclear power plants (Loziuk, 1988) and in the petroleum industry. The potential of the WRI to be applied for vibration isolation in wide areas makes it essential to understand fully its characteristics (Tinker and Cutchins, 1992).

WRI has two main components namely, stiffness and energy dissipation. The stiffness component provides the restoring force and is achieved by the wire spring design of the WRI. It has different stiffness values in different directions and exhibits nonlinear relation between force-displacement. The helical spring design enables the WRI to contribute as both stiffness and damping element in the vibration isolation applications. The stiffness is obtained from the spring design of the WRI and the damping is achieved from the inherent frictional damping. In the literature, the study of WRI has focused on both the stiffness and damping characteristics. In this section, the major contributors to the research of these characteristic are discussed in detail in the next section.

2.4. RESEARCH ON THE STIFFNESS CHARACTERISTICS OF WRI

The static stiffness can be obtained through the monotonic loading test in each direction (Ni *et al.*, 1999b). The static stiffness of WRI provides the understanding of the hardening and softening nature of the wire rope for increasing displacements. Among the existing literature on WRI, most have focused their research on the cyclic loading behaviour of WRI and only a very few researchers have studied on the static stiffness. Ni *et al.*(1999b) have experimentally studied the static stiffness in each direction through shear, roll and tension-compression loadings (Figure 2.9). The static

stiffness can provide an initial estimation of the loading carrying capacity of the WRI and an understanding of the tangent stiffness of wire rope springs.

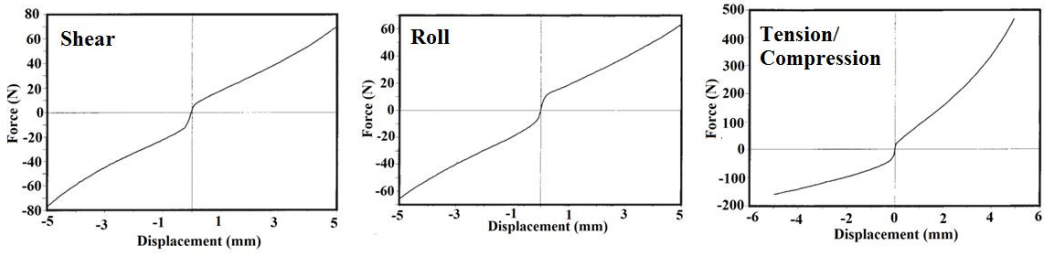

Figure 2.9 Static stiffness curve of the WRI (Ni *et al.*, 1999b)

The study conducted by Demetriades *et al.*(1993) found that the stiffness characteristics of WRI are a function of the geometric characteristics and wire rope properties. These studies have shown the stiffness required for any application can be achieved by the WRI through proper design of its geometric characteristics and wire rope properties. An analytical model with these parameters is highly desired. However, the existing literatures lacks the detailed analytical and experimental research on the stiffness characteristics of WRI and one of the possible reasons could be due to the complexity of the analytical model for the wire strand interactions. The design and function of WRI is similar to the Elliptical leaf spring (ELS) in terms of supporting the load through the bending of a curved beam. Tse *et al.*(2002) have developed the stiffness model of the ELS using Castigliano's second theorem. This similarity in design enables applying similar methodology for development of the stiffness characteristics of WRI.

Further, Castigliano's second theorem relates the force with displacement through the geometric characteristics of the spring design and flexural rigidity (EI) of wire rope. The flexural rigidity of wire rope takes account of the wire rope contribution to the bending or displacement of WRI. Velinsky (2004, 1988) proposed a simplified analytical model for the flexural rigidity (EI) of a wire rope using assumptions to simplify the complex wire interaction. He assumed the flexural rigidity of a wire rope is a sum of the flexural rigidity of individual wires and wire strands. Costello (1997) also considered similar assumption to study the strength and stress distribution of wire rope and his research yielded satisfactory results. In another study, Zhu and Meguid(2007)

have obtained the flexural rigidity of the wire rope using the transverse bending test in a similar procedure as per the test for beams. Overall, it can be summarized that the stiffness characteristics of WRI can be estimated using Castigliano's theorem, due to the similarity in design of WRI with the ELS and further, EI needed for the estimation, which accounts the wire rope properties, can be estimated using the transverse bending test.

2.5. RESEARCH ON DAMPING BEAVHIOUR OF WRI

The behaviour of the WRI under cyclic loading provides an understanding of the energy dissipation capability of the WRI. The study on this behaviour also enables greater understanding of the WRI as a vibration isolation device. Demetriades *et al.*(1993) performed one of the first research studies on the cyclic loading behaviour. This study has verified and confirmed the WRI exhibits a hysteresis curve under cyclic loading. This hysteretic nature indicates that the restoring force is a function of instantaneous displacement and on the history of displacement (Ismail *et al.*, 2009a).This dependency can be described as a memory effect, which means the history of displacements also influences the response of the WRI for a given load (Demetriades *et al.*, 1993;Wang *et al.*, 2015). This hysteresis is a natural way, for mechanical and structural systems to provide restoring forces against movements and dissipate energy (Ismail *et al.*, 2009a).

Tinker and Cutchins (1992) have identified the mode of energy dissipation of WRI as through the friction between its wire strands. They identified the mode by comparing the hysteresis curve obtained by the WRI with the hysteresis curve due to a Coulomb friction hysteresis curve. The hysteresis behaviour, in general, was majorly studied by the researchers through experimental work due to the limitation in the development of the analytical model in terms of wire rope properties. Any detailed modeling of the force-displacement relation with the geometric and wire rope properties is a challenging task. Hence, earlier studies have developed the model based on the understanding of the hysteretic system. Here, experimental work are initially discussed then followed by the mathematical approaches attempted in the earlier researchers.

2.5.1. EXPERIMENTAL WORK AND ITS OBSERVATIONS ON CYCLIC BEHAVIOUR

Ni *et al.* (1999b) has been one of the major contributors research on cyclic loading behaviour of WRI. The hysteresis behaviour obtained by Ni *et al.*(1999b) under cyclic loading in three directions is shown in the Figure 2.10. This study has identified a critical observation in the hysteresis behaviour. The hysteresis behaviour for shear and roll is symmetric; however, for tension/compression it is asymmetric. However, the hysteresis curve is symmetric for small displacement amplitude and becomes asymmetric for a higher displacement. Demetriades *et al.*(1993) have studied the behaviour of WRI under different loadings and have suggested the hardening and softening can be due to the interaction between the wire strands under tension and compression loading. Under tension load, the wire strands come close to each other and hence the contact surface increases which results in the increased frictional force. This increase in the frictional force resists further displacement and therefore, is attributed as hardening under tension load. On the other hand, under a compressive load, wire strands move far from each other and this result in the reduced contact surface and hence reduced resistance to displacement and defined as softening.

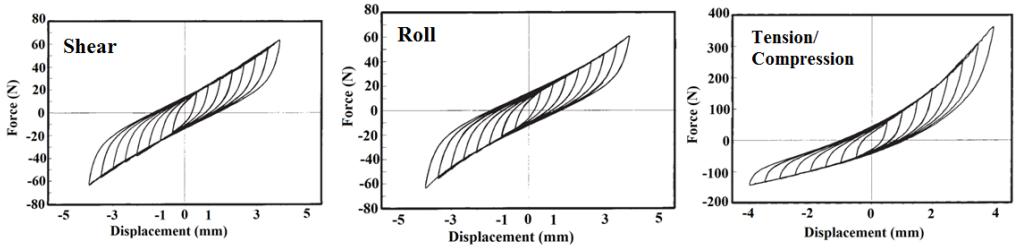

Figure 2.10 Hysteresis behaviour of WRI under cyclic loading (Ni *et al.*, 1999b)

Foss (2006) proposed two parameters that can be derived from the hysteresis curve, to study the hysteresis curve. Those two parameters are effective stiffness and the hysteresis area. The effective stiffness provides the details of amplitude-dependent stiffness behaviour of the WRI under cyclic loading and the energy dissipation can be obtained from the hysteresis area. Later, Wang *et al.*(2015)have used these parameters to experimentally study the influence of displacement amplitude on the effective stiffness and found a reduction in the effective stiffness for higher displacement as shown in Figure 2.11. This reduction can be understood from the wire strand interaction

during the higher displacements. In such a case, the wire strands move away from each other resulting in less contact surface for frictional resistance and hence attributed as reduced effective stiffness.

On the other hand, the hysteresis area increases with increased displacements as shown in Figure 2.11. This can be observed in Figure 2.10, for higher displacement the hysteresis curve increases in area. However, the main criterion to be considered in the effectiveness of the WRI for damping characteristics is Energy Loss Ratio (ELR) (Foss, 2006). ELR plays a significant role in defining the damping property of the WRI. ELR is the amount of energy being dissipated due to frictional resistance between the wire strands during a cyclic loading test with respect to viscous damping. The ELR can be obtained from Eq.(2.1).

$$ELR = \frac{Area\ of\ Hysteresisloop}{\pi\left(\frac{F_{max} - F_{min}}{2}\right)\left(\frac{X_{max} - X_{min}}{2}\right)} \tag{2.1}$$

where F_{max} and F_{min} are the maximum and minimum force respectively, and X_{max} and X_{min} are the maximum and minimum displacement respectively. These forces and displacements are obtained from the hysteresis curve for particular displacement amplitude. ELR provides the information on the damping of the WRI and a higher value of ELR indicates an increased damping capability of WRI.

Another interesting observation made in the studies of Demetriades *et al.*(1993) and Paolacci and Giannini (2008) is hysteresis behaviour under shear is similar to the hysteresis behaviour under roll. This can also be observed in Figure 2.11, that both the area of hysteresis loop and effective stiffness curves of WRI under roll and shear lies close to each other. The rate independency of WRI's hysteresis behaviour was tested by Demetriades *et al.*(1993) and Wang *et al.*(2015), by exciting the WRI under cyclic loading of various frequencies and the results showed that the hysteresis curves were similar to each other as shown in Figure 2.12.

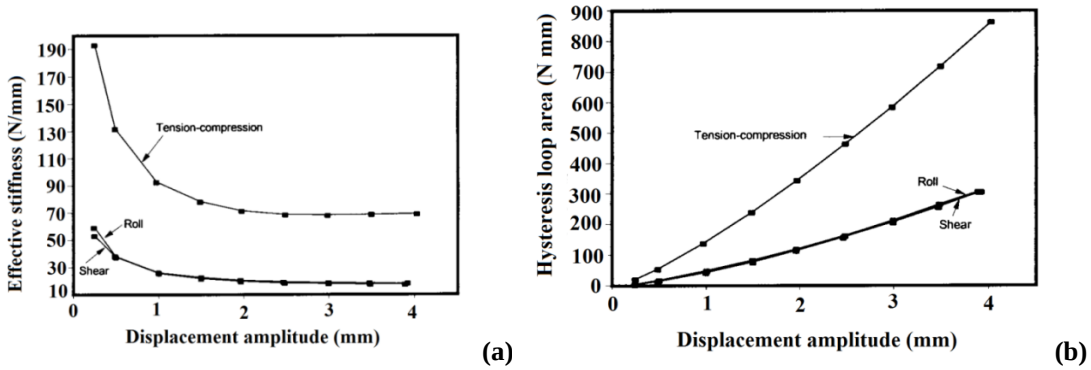

Figure 2.11 (a)Effective stiffness versus displacement amplitude (Ni *et al.*, 1999b) (b) Hysteresis loop area versus displacement amplitude (Ni *et al.*, 1999b)

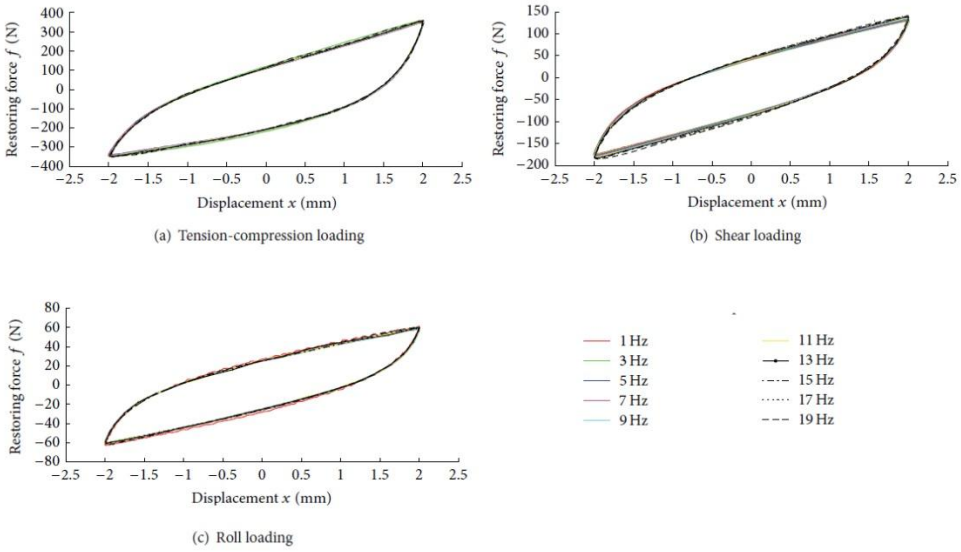

Figure 2.12 Effect of frequency on the hysteresis behaviour of WRI (Wang *et al.*, 2015)

2.5.2. MATHEMATICAL MODELLING OF HYSTERESIS BEHAVIOUR

The development of an analytical model with a closed form solution for hysteresis behaviour by relating mechanical properties and boundary conditions with output parameters is an arduous task. This is due to the lack of analytical understanding of wire strands interaction. Further, the models obtained were often very complex to use in practical applications involving system characterizations, identification and control (Ismail *et al.*, 2009a). Hence researchers prefer to model this behaviour through the physical understanding of the hysteretic system and for this reason, some researchers also have referred to their models as "semi-physical" (Ismail *et al.*, 2009a). A hysteretic semi-physical model was proposed initially by Bouc in 1971 and later, generalized by

Wen in 1976 (Ismail *et al.*, 2009a). Hence, this model is referred to as the Bouc-Wen model in the literature. This model has been used extensively in the modelling of hysteresis in mechanical and civil engineering. The Bouc-Wen model is a first-order non-linear differential equation that hysterically relates input displacement with the output restoring force (Demetriades *et al.*, 1993;Wen, 1976;Song and Kiureghian, 2006).

Earlier attempts were also made by researchers to model the hysteresis through a different formulation. Cutchines *et al.*(1987) proposed a model involving n-th power velocity damping and nonlinear stiffness to represent the research findings of their work (Tinker and Cutchins, 1992). However, this model needs different model parameters for the hysteresis loop obtained under different amplitudes (Ni *et al.*, 1999b). Another study (Haiyan and Yuefeng, 1989) presented a nonlinear model to explain the behaviour of the cable type isolator. However, this model primarily explains the bilinear hysteresis behaviour.

Researchers also attempted to research on the mathematical modelling of stranded wire rope response (Wang *et al.*, 2013;Zhou *et al.*, 2011). The application of Bouc-Wen differential model for the wire rope hysteresis was initially performed by Lo *et al.*(1988). Later, the Bouc-Wen model and its refinement was applied by Demetriades *et al.*(1992, 1993) for an analytical description of the hysteresis behaviour of wire rope isolators (Ni *et al.*, 1999b). Ismail *et al.*(2009a) have presented a detailed survey on the hysteresis behaviour and its application. Generally, the Bouc-Wen model can be used to model symmetric hysteresis loop, as in the case of shear and roll load behaviour. However for tension/compression, the hysteresis loop is asymmetric hence some modifications needs to be incorporated. This section presents the application of the Bouc-Wen model with some modifications suggested by previous studies to predict symmetric and asymmetric hysteresis behaviour.

2.5.2.1. Bouc-Wen model for symmetric hysteresis behaviour.

The Bouc-Wen model used by the earlier studies (Demetriades *et al.*, 1992;Massa *et al.*, 2013), which relates restoring force with the displacement

hysterically, is illustrated in Equations (2.2-2.3). This Bouc-wen model is suitable for explaining the symmetric hysteresis behaviour as discussed in roll and shear cyclic loading behaviour (Figure 2.10). The generalized Bouc-Wen model of the hysteresis curve (Figure 2.13) is:

$$F = \alpha \frac{F_Y}{Y} U + (1-\alpha) F_Y Z \tag{2.2}$$

where F is the restoring force, U = displacement, F_Y = yield force, Y = Yield displacement, α= ratio of post to pre-yield stiffness and Z is a hysteresis dimensionless quantity defined by the following differential equations:

$$Y\dot{Z} + \gamma \left|\dot{U}\right| Z \left|Z\right|^{n-1} + \beta \dot{U} \left|Z\right|^{n} - A\dot{U} = 0 \tag{2.3}$$

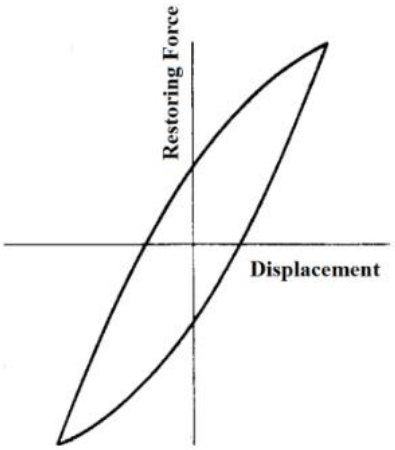

Figure 2.13 Typical Hysteresis curve

In Eq. (2.3) the model parameters A, γ, β *and* n govern the amplitude, the shape of the hysteresis loop, and the smoothness of transition from the elastic to the inelastic region. Different model parameters control the shape of the hysteresis curve. From the previous studies (Ni *et al.*, 1999b;Ismail *et al.*, 2009a) it was observed that hardening and softening is related to the sign of the expression β+γ. The study also showed that parameter *A* controls hysteresis loop's slope at *Z* =0 and an increase in parameters *A* and *n* makes the hysteresis loop narrower. When employing the Bouc-Wen model to a practical application, these parameters must be identified with respect to initial experimental data to enable the BW model to predict the response. This identification of the model parameters can be performed using different system identification techniques. Many researchers have used techniques like the least square method (Loh and Chung,

1993), the Kalman filter method (Jeen-Shang and Yigong, 1994) and the genetic algorithm based identification (Ortiz *et al.*, 2013) to identify the system parameters, so the output of the model matches as accurately as possible with the experimental data (Xie *et al.*, 2013).

In general, various hysteresis based isolation system exhibits softening behaviour due to dynamic loading but divergently exhibit hardening stiffness beyond certain large deformations. Such phenomenon is referred to as soft-hardening hysteresis or post-hardening of the hysteresis curve (Ni *et al.*, 1999b). While, the Bouc-Wen model can exhibit a wide variety of softening, hardening or a quasi-linear hysteretic system, it lacks the ability to display such a soft–hardening hysteresis system. In view of that, Ni *et al.*(1999b) proposed a soft-hardening hysteresis model as shown by Eqs.(2.4-7) which were derived from a Duhem operator.

$$F(t) = F_{1s}(t)F_{2s}(t) \tag{2.4}$$

$$F_{1s}(t) = 1 + k_2 x^2(t) + k_3 \,\mathrm{sgn}(x) x^3(t) \tag{2.5}$$

$$F_{2s}(t) = bx(t) + z(t) \tag{2.6}$$

$$\dot{z}(t) = \alpha\dot{x}(t) - \beta|\dot{x}(t)|\; z(t)\,|z(t)|^{n-1} - \gamma\,\dot{x}(t)\,|z(t)|^{n} \tag{2.7}$$

where $F_{1s}(t)$ is a non-hysteretic term, x is displacement. $F_{2s}(t)$ is a nonlinear hysteretic term and is a combination of linear restoring force and hysteretic variable z(t) which satisfies the Bouc-Wen differential equation (Eq.(2.7)) and k_2, $k3$ are hysteresis model parameters.

2.5.2.2. Bouc-Wen model for Asymmetric hysteresis behaviour

The asymmetric nature of the hysteresis is due to the hardening and softening of the WRI under tension and compression, respectively. As such, the hysteresis curve can be represented by two sets of model parameters, each for loading and unloading respectively. The Bouc-Wen model under such cases can be demonstrated by (Ni *et al.*, 1999b;a)

$$F(t) = bx(t) + z(t) \tag{2.8}$$

$$\dot{z}(t) = \begin{cases} \dot{x}(t)\left\{\alpha_1 - \left[\gamma_1 + \beta_1 \operatorname{sgn}(z)\right]\left[z(t)\right]^{n_1}\right\}, & \dot{x} \geq 0 \\ \dot{x}(t)\left\{\alpha_2 - \left[\gamma_2 + \beta_2 \operatorname{sgn}(z)\right]\left[z(t)\right]^{n_2}\right\}, & \dot{x} < 0 \end{cases} \tag{2.9}$$

The slope of the hysteresis loops is governed by the following equations:

$$\frac{dF}{dx} = \begin{cases} b + \alpha_1 + (\beta_1 - \gamma_1)|z|^{n_1}, & \dot{x} \geq 0, \quad z < 0 \\ b + \alpha_1 - (\beta_1 + \gamma_1)|z|^{n_1}, & \dot{x} \geq 0, \quad z \geq 0 \\ b + \alpha_2 + (\beta_2 - \gamma_2)|z|^{n_2}, & \dot{x} < 0, \quad z \geq 0 \\ b + \alpha_2 - (\beta_2 + \gamma_2)|z|^{n_2}, & \dot{x} < 0, \quad z < 0 \end{cases} \tag{2.10}$$

A different variety of hysterics loops can be obtained from the different combinations of α_1,β_1,α_2 and β_2. Figure. 2.14 shows the asymmetric hysteresis loops generated from the Eqs.(2.8-10). Although, these equations provide the asymmetric curves as desired and have good agreement with experimental results, these curves lack in exhibiting the hardening overlap of the asymmetric hysteresis curve. Therefore, this major drawback needs to be addressed.

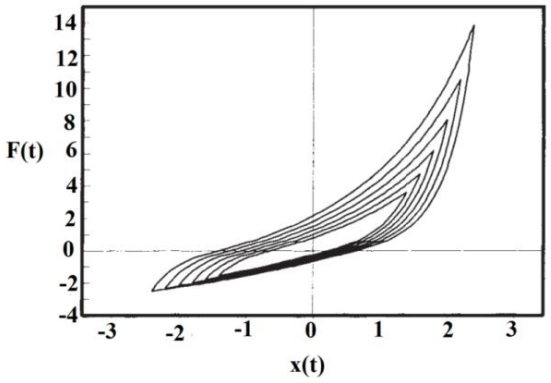

Figure 2.14 Asymmetric hysteresis loops generated by the modified Bouc–Wen model (Eqs. (2.8-10)) (Ni *et al.*, 1999b;a)

This section presented various models used by researchers to demonstrate the symmetric and asymmetric hysteresis behaviour. These models were based on the understanding of the hysteresis curve. Nevertheless, improvements in these models are needed for enhancing the post-hardening behaviour expression. The hysteresis behaviour model, which relates wire rope spring dimensions and wire rope properties

with the response of the WRI, is also required to predict the hysteresis behaviour without the need of a complex algorithm to determine model parameters.

The models used in the earlier studies also suffer from weaknesses in terms of increased model parameters. For instance; Demetriades *et al.*(1992, 1993) proposed a model which has 9 to 11 parameters and a model by Ni *et al.*(1999b;a) has 9 other parameters which need to be calibrated with the initial experimental data (Gerges, 2008). These models express only the behaviour of WRI; however, greater understanding of how the WRI performs in vibration isolation also needs to be developed. There is also a need to develop the mathematical model of the static stiffness curve in terms of WRI dimensions and wire rope properties, which could have benefits in the design of the WRI. The literature on the performance of WRI is presented in the next section.

2.6. PERFORMANCE OF WRI IN VIBRATION ISOLATION

This section presents the background and literatures on the performance of nonlinear isolators. The investigation of the performance of nonlinear isolators is generally carried out using the equivalent linearized model. Many studies have adopted this approach to examine the performance of nonlinear isolators. In the performance study, nonlinear isolators can be evaluated based on frequency-domain response and time-domain response. In the frequency-domain response approach, the isolated system is evaluated for various frequency ranges and is studied to identify the resonance condition and transmissibility. In the time-domain response approach, a comparison is made between the non-isolated and isolated system and hence, relative performance of an isolated system with respect to a non-isolated system is obtained. The selection of an isolator for the vibration application is based on the peak acceleration response of the system. The response obtained from the time domain can be converted to s frequency domain and vice versa, using the Fourier and inverse Fourier transform respectively (De Silva, 2006) .

The responses types of nonlinear isolators that are evaluated for the performance study are acceleration response and displacement response. The isolation effect is

achieved at the expense of the isolator displacement and in this process, the external excitation energy is dissipated. This mechanism results in the reduced acceleration and increased displacement response of the isolated system(Tustin and Jariwala, 2005). The isolation of a system can be performed using three approaches, 1. Isolation of entire the housing structure, 2. Isolation of the individual equipment and 3. Isolation using the raised floor approach. The first approach is used to isolate the entire structure by installing the isolator at its base. Similarly, in the second approach, only the required sensitive equipment is isolated (Ismail *et al.*, 2009b). These two approaches are the most common approaches and many studies have been conducted on these approaches for nonlinear isolators.

The third approach is the isolation of a common platform or floor, called the raised floor approach, by a group of isolators. This third method is a recently introduced method and can have certain advantages over the other two such as the ability to achieve the isolation within the reasonable isolator displacements. In first two approaches, the displacement of the isolator may be significant which can damage the isolators. Another advantage in the third approach is the heavy weight of the floor and equipment contribute to the reduction in the natural frequency (see Eq.1.1) of the isolated-raised floor and hence better isolation effect is achieved (Ismail *et al.*, 2009b). However, most of the literature has only studied the isolators of the first two approaches with limited published research on the raised-floor approach. The literature, which contributed significantly to this field are discussed in this section.

The mathematical methods for analyzing nonlinear isolators are well established in the literature (Nayfeh and Mook, 2008;Hayashi, 1964). Ravindra and Mallick (1994) studied the performance of rubber-based nonlinear isolators and considered the nonlinearities in both stiffness and damping using the second approach mentioned above. This study showed the isolator with softening behaviour provided better isolation than the isolators with hardening behaviour. Dutta and Chakraborty (2014) have studied the performance of nonlinear isolators using magneto-rheological fluids and in this study; the hysteresis behaviour was modelled using the Bouc-Wen equations. The literature shows only limited research on the performance of WRI. Further, due to this

limited research, the WRI application area has also been limited to industrial applications and its ability for seismic protection needs detailed study. This section compiles the findings and observations made in the previous studies.

Demetriades *et al.*(1993, 1992) performed the shaking tables test to study the effectiveness of the WRI in the vibration isolation of equipment. A computer cabinet was tested by supporting it over four WRI and then subjected to different real-time earthquake excitation including the 1952 Taft, the 1940 El-Centro and the 1971 Pacoima Dam records. They compared the fixed and isolated conditions in which they observed reduced acceleration responses of the isolated equipment relative to the fixed condition. However, the measured displacements in the isolated case were greater than that of the fixed case. They also studied the effect of another different installation system of the equipment alongside the WRI isolated system and observed that the WRI system was able to provide a better reduction in acceleration than other considered systems. They suggested that WRI provided an equivalent damping ratio of 0.1 of critical for large deformation and 0.2-0.3 of critical for small deformations. The stiff WRI was observed to reduce or maintain acceleration at the same level while reducing the displacements by a factor of about 10.

Alessandri *et al.*(2015b) have studied the retrofitting of an HV circuit breaker with WRI and found it to be effective in reducing the seismic acceleration and further, it also helped in the seismic demand on the structure. However, the available literature is focused on the initial evaluation of WRI as a vibration isolation device. Further, there is a need to understand the performance of WRI when subjected to various levels of base excitation. Ismail *et al.*(2009b; 2012b) proposed a novel Roll-N-Cage (RNC) Isolator for seismic protection of structures and evaluated the performance through a numerical study. The numerical model developed was subjected to various earthquake records including long period earthquake data and high acceleration earthquake data. The study also analyzed the performance of the RNC isolator in an isolated floor approach. This kind of study is also desired for WRI, to widen the application area.

2.7. SUMMARY FROM LITERATURE REVEIW

1. The nonlinearity found in other fields of engineering has been utilized in the application of vibration isolation. The stiffness characteristic of such nonlinear isolators was studied using experimental tests and previous research has developed an analytical model based on the mechanics which causes isolator displacement due to the applied force.
2. The static stiffness is one of the important parameters for selecting WRI for practical applications and it is dependent on the geometrical properties. However, only limited research has been carried out so far on the static stiffness behaviour of WRI. Due to the similarity between WRI and ELS, Castigliano's second theorem approach of ELS for the development of an analytical stiffness model can also be used for the WRI
3. Castigliano's second theorem relates the force with displacement through the geometric characteristics of spring design and flexural rigidity (EI) of wire rope. The flexural rigidity of wire rope takes account of wire ropes' contribution to the bending or displacement of WRI. However, the literature lacks the model for the analytical estimation and hence, the transverse bending test can be carried out to estimate the wire rope EI.
4. The effects of the geometrical properties on the stiffness need to be identified and a well-developed analytical model with all influencing parameters will assist both the selection process and design.
5. The damping behaviour of WRI is obtained from the inherent frictional contact between the wires in the wire rope. This damping causes the WRI to exhibit hysteresis behaviour under cyclic loadings. Hence, the damping characteristics of WRI can be studied from its hysteresis behaviour.
6. Previous work on the hysteresis behaviour of WRI has applied the Bouc-Wen model to symmetric hysteresis loop for the lateral cyclic loading. However, WRI exhibits an asymmetric hysteresis behaviour for the vertical cyclic loading and hence, development of a modified Bouc-Wen model is required to predict asymmetric hysteresis behaviour of WRI.

7. Very few studies on the effects of geometrical properties on the hysteresis behaviour of WRI are available.
8. The isolation of equipment is more effective using the raised floor approach and there has been studies done on the isolation of the entire housing structure and on the isolation of individual equipment, however, the literature lacks any studies on the performance of WRI using the raised floor approach. Therefore, there is a requirement in this area focusing on the capability of WRI using this approach.

From the literature survey the previous findings and research gap was identified. In this work, aim and objectives were developed to approach towards enhancing the understanding on the stiffness and damping characteristics.

Chapter 3. STATIC STIFFNESS OF WRI

3.1. INTRODUCTION

The basic concept to obtain vibration isolation is to reduce the natural frequency of a system below the excitation frequency (Ibrahim, 2008). In practice, the reduction in natural frequency is achieved by providing a flexible isolator at the base of the system and hence the stiffness of the isolator becomes a paramount factor to achieve vibration isolation (Abolfathi, 2012). This chapter presents the research on the static stiffness of wire rope isolators (WRI). The analytical models were developed for both vertical and lateral stiffnesses of WRI which were validated against the monotonic loading tests in the respective direction. The methodology used for the development of the analytical model is given in Section 3.2. This chapter also discusses the parametric study on the effects of wire rope diameter, width, height, and number of turns on the vertical stiffness and lateral stiffness of WRI. Finally, the WRI-Spring configuration was also studied to improve the load carrying ability of the WRI.

3.2. METHODOLOGY

The stiffness in the WRI comes from both its spring design and wire rope interactions. The spring design significantly influences the stiffness at small displacement and the wire rope interaction influences the stiffness at higher displacement. Hence, the Force-Deflection (F-D) characteristic, in both vertical and lateral directions, is linear for small displacements and becomes nonlinear for higher displacements (Demetriades *et al.*, 1993;Ni *et al.*, 1999b). As discussed in Chapter.2, the nonlinearity in the F-D characteristics of WRI is a results of its complex wire rope interaction. The nonlinear F-D characteristic of WRI at higher displacement possesses challenges in developing the analytical F-D model due to the complex wire and wire strands interaction. On the other hand, linear mechanics can be used to obtain the F-D model of WRI in the linear region due to its spring design.

The analytical models for the stiffness in the required direction can be developed by establishing a relationship between the displacement and the applied load in the respective direction. When the WRI is acted upon by the external excitation, it displaces

and when the excitation is removed, it returns to its initial position. Meanwhile, work done in overcoming the friction between the wire rope in achieving the displacement of WRI dissipates the excitation energy. Hence, the geometric and wire rope properties are the major factors in the design of the wire rope isolator. The relation between the strain energy and the displacement is provided by Castigliano's second theorem (Budynas *et al.*, 2008). Hence in this work, the analytical models of stiffness in both vertical and lateral directions was developed using Castigliano's theorem relating stiffness's with the geometric and wire rope characteristics. Further, Demetriades *et al.*(1993) has found that the force-displacement behaviours of WRI along shear and roll are similar and hence, the lateral stiffness is evaluated for the roll load only.

3.3. ANALYTICAL MODEL OF STIFFNESS

In this section, the analytical models developed for the vertical and lateral stiffnesses are discussed. The geometry of the WRI was simplified by considering a load carried by one coil of wire rope (Figure 3.1). The single wire rope coil is symmetric about both the vertical (X-X) and the horizontal (Y-Y) axes and it can be characterized by using the dimensions L and R, where L represents the half width of the top retainer and R, radius of the arc (Figure 3.2). These dimensions, L and R, can be defined using the geometric characteristic of the WRI such as width, height and thickness of the retainers. The deflection of a curved bar is usually calculated using Castigliano's theorem (Timoshenko, 1983). For the case of WRI, the cross section of the wire rope is small compared to the radius of curvature of its centerline. The loading in each directions and its corresponding reaction from the fixed base on a coil of WRI can be represented by two equal and opposite forces *F* as shown in Figure 3.3. The force on a single coil of the WRI was considered and is represented by *P/N* where P is the total load on the entire WRI and *N* is the number of turns (coils).

$$R = \frac{(H - T)}{2} \tag{3.1}$$

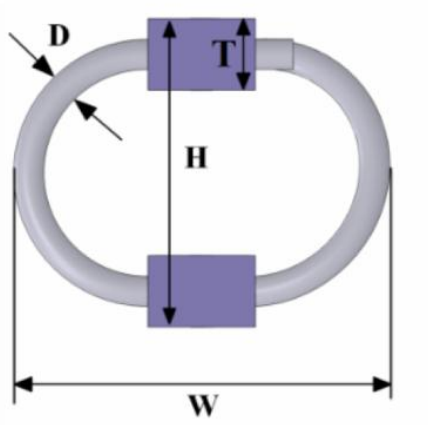

Figure 3.1 Geometry of the WRI

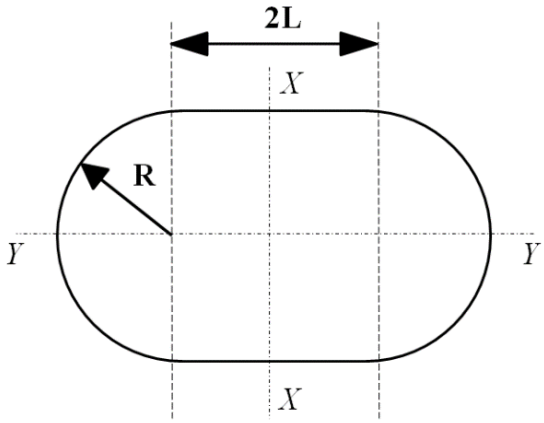

Figure 3.2 Schematic of WRI used in the analytical model

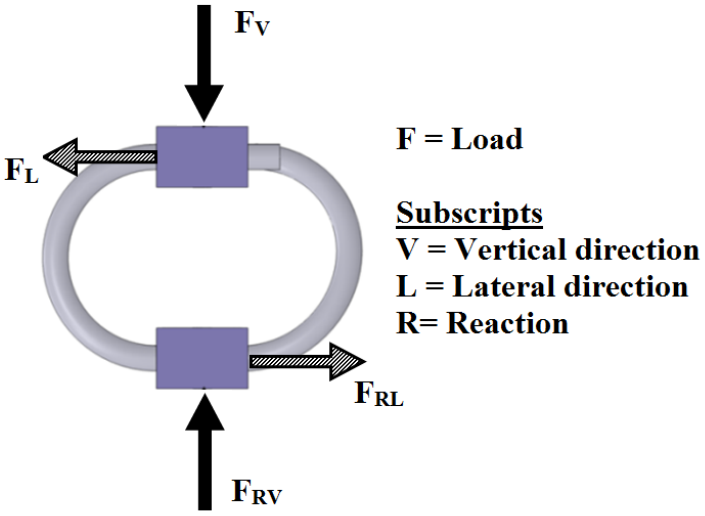

Figure 3.3 Load on the WRI

3.3.1. ASSUMPTIONS

The following assumptions are considered to simplify the development of the analytical models:

1. The wire rope is considered a solid bar with a uniform cross section;
2. The material of the wire rope is considered homogenous and isotropic;
3. The involvement of a metal retainer in resisting the load is neglected;
4. Quasi-static loading is considered;
5. The WRI is firmly mounted with no unwanted displacements.
6. Small displacement amplitudes are assumed, such that forces and displacements are linearly related.
7. The load is assumed to be equally distributed along the metal retainer

The Force-Displacement (F-D) characteristics of WRI at small displacements is significantly influenced by the spring design and hence the solid bar assumption can be considered valid for small displacements. At the small displacement conditions, the radius of curvature of the bar is not significantly altered by the loading. Furthermore, the analytical model relates the F-D through geometric characteristics and the wire rope property. The wire rope property was accounted in the model through the flexural rigidity term. This flexural rigidity was evaluated for the wire rope using the transverse bending test to calculate the stiffness using the analytical model.

3.3.2. ANALYTICAL MODEL OF VERTICAL STIFFNESS (KV)

Due to symmetry, only one quadrant of the coil was considered and this was divided into two regions - AB and BC, as shown in Figure 3.4. The shearing stress over the cross section was neglected and the compressive force on the cross section is represented by F/2. The bending moment M_0 acting on the cross section was statically indeterminate and was determined using Castigliano's theorem. Due to symmetry, the cross section did not rotate during bending of the wire rope. Hence, the displacement due to M_0 is zero, that is:

$$\frac{dU}{dM_0} = 0 \tag{3.2}$$

Where U is the strain energy of the quadrant of the wire rope.

Both regions underwent bending along their entire length. Whereas region BC is in the form of a semi-circular arc, hence it is integrated in radial coordinates. The strain energy (U) of the quarter coil model is represent by:

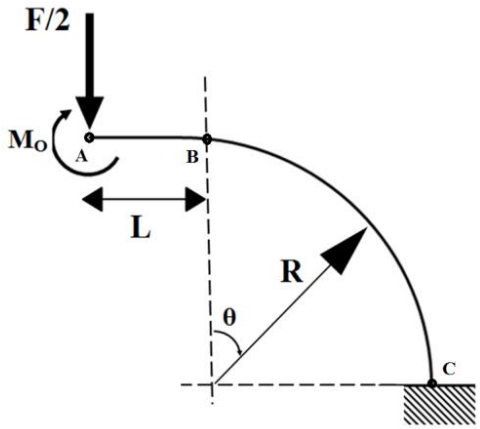

Figure 3.4 One-quarter coil of WRI under consideration

$$U = U_1 + U_2 \tag{3.3}$$

$$U_1 = \int_0^L \frac{1}{2EI} M_1^2 dx \tag{3.4}$$

$$U_2 = \int_0^\pi \frac{1}{2EI} M_2^2 R d\theta \tag{3.5}$$

The bending moment in region AB (M_1) and in region BC (M_2) are represent by:

For region AB:

$$M_1 = \frac{F}{2} x - M_0 \ , \ \ 0 \le x \le L \tag{3.6}$$

For region BC:

$$M_2 = \frac{F}{2}(L + R\sin\theta) - M_0 \ , \ \ 0 \le \theta \le \frac{\pi}{2} \tag{3.7}$$

Upon solving Eq.(3.2.) for the statically indeterminate moment M_0 the following was deduced:

$$M_0 = \frac{FL^2 + \pi FLR + 2FR^2}{(4L + 2\pi R)} \tag{3.8}$$

The bending moment at any cross section of the wire rope can be calculated using either Eq.(3.6) or Eq.(3.7) depending on the region. The deflection due to the applied load F, can be calculated using Castigliano's theorem:

$$\delta_v = \frac{dU}{dF} = \frac{F}{EI} g(L,R) \tag{3.9}$$

$$g(L,R) = \frac{2L^4 + 4L^3R\pi + 24R^2L^2 + 6R^3L\pi + 3R^4\pi^2 - 24R^4}{12(2L + R\pi)} \tag{3.10}$$

Finally, the vertical stiffness (k_v) of the complete WRI was calculated as:

$$k_v = N \times \frac{P}{\delta} = \frac{N\,EI}{g(L,R)} \tag{3.11}$$

where N is the number of coils of the WRI.

3.3.3. ANALYTICAL MODEL OF LATERAL STIFFNESS (KH)

Figure 3.5 shows the geometry of one coil of the WRI subjected to a roll load and one-half of a coil was considered in the model development. The one-half coil, having a circular cross section of diameter D, was divided into three regions, namely AB, BC and CD, as shown in Figure 3.5. The boundary limits for each region are represented as; Regions AB and CD: 0 to L and Region BC: 0 to π; where the length L is the half width of the metal retainer. The lateral load was acting in the roll configuration and the WRI was fixed to the base. The simplified model was subjected to the reduced force $F/2$ and the indeterminate shear force (Q), however, the indeterminate bending moment at A can be shown to vanish by the principle of least work (Tse *et al.*, 2002). Hence, F The strain energy (U) of the semi-circular coil model is represented by:

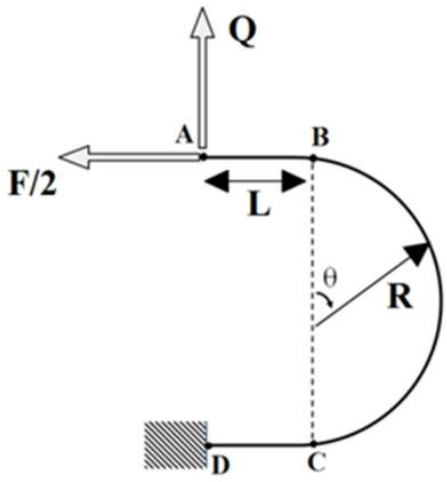

Figure 3.5 One-half coil of WRI under lateral load

$$U = U_{AB} + U_{BC} + U_{CD} \tag{3.12}$$

Where U_{AB}, U_{BC} and U_{CD} are the strain energies of the first, second and third regions, respectively:

$$U_{AB} = \int_0^L \frac{1}{2EI} M_1^2 dx \tag{3.13}$$

$$U_{BC} = \int_0^\pi \frac{1}{2EI} M_2^2 R d\theta \tag{3.14}$$

$$U_{CD} = \int_0^L \frac{1}{2EI} M_3^2 dx \tag{3.15}$$

whereM_1, M_2, and M_3 are the moment in the regions AB, BC, and CD, respectively, and are represented by:

For region AB:

$$M_1 = Qx; \qquad 0 \le x \le L \tag{3.16}$$

For region BC:

$$M_2 = Q(R\sin\theta + L) - \frac{F}{2}(R - R\cos\theta); \qquad 0 \le \theta \le \pi \tag{3.17}$$

For region CD:

$$M_3 = Qx - \frac{F}{2}(2R); \qquad 0 \le x \le L \tag{3.18}$$

The indeterminate shear force Q was determined by using Castigliano's theorem. As seen from Figure 3.5 due to symmetry, the cross-section did not rotate during bending of the wire rope. Thus, the displacement due to Q is zero, that is:

$$\frac{dU}{dQ} = 0 \tag{3.19}$$

Upon solving Eq.(3.19) for the indeterminate shear force, the following was obtained:

$$Q = \frac{3FL^2R + 3\pi FLR^2 + 6FR^3}{4L^3 + 6\pi L^2R + 24LR^2 + 3\pi R^3} \tag{3.20}$$

Hence, the total strain energy stored in the half coil wire rope was calculated to be:

$$U = \frac{F^2}{8}\frac{f(L,R)}{EI} \tag{3.21}$$

$$f(L,R) = \frac{R^2\left(20L^4 - 48R^4 + 144L^2R^2 + 9\pi^2R^4 + 6\pi^2L^2R^2 + 48\pi LR^3 + 36\pi L^3R\right)}{2\left(4L^3 + 6\pi L^2R + 24LR^2 + 3\pi R^3\right)} \tag{3.22}$$

Now, the deflection due to the lateral load, for the complete loop, was obtained from the strain energy through the Castigliano's theorem as follows:

$$\delta_v = 2 \times \frac{dU}{dF} \tag{3.23}$$

From Eq.(22), the deflection of one full coil due to the applied load F is:

$$\delta_v = \frac{F}{2}\frac{f(L,R)}{EI} \tag{3.24}$$

Eq.(3.24) represents the force-displacement relation of one full coil assuming small displacement amplitudes. Finally, the lateral stiffness, k_h, of the complete WRI was computed as:

$$k_h = N \times \frac{F}{\delta} = \frac{2NEI}{f(L,R)} \tag{3.25}$$

The term EI in both vertical and lateral stiffness, which is the product of the elastic modulus (E) and moment of inertia (I), in the analytical model (Eqs.(3.11 and 25)), represents the resistance of the wire rope to bending and is referred to as the

flexural rigidity or bending stiffness. These analytical models can be used to estimate the stiffness of the WRI and further, can also be used to design the WRI with a required stiffness value in the required directions by controlling the geometric characteristics accordingly from these models. In order to apply the equations Eq.(3.11) and Eq.(3.25), EI is required and the next section discusses the estimation of EI for wire ropes.

3.4. FLEXURAL RIGIDITY OF A WIRE ROPE

The flexural rigidity of the wire rope cable depends on its material and specification (Costello and Butson, 1982). A number of studies have been attempted to develop analytical models to determine wire rope's behavior. Velinsky (1988; 1989; 2004) has carried out detailed studies on wire ropes with various configurations. The study was primarily focused on the design and the mechanicals aspects of wire ropes under various configurations. Velinsky (1988) has developed a set of dimensionless parameters for determining the bending stiffness and the bending to axial stiffness ratio to generalize the study. The sensitivity of these dimensionless parameters were also examined with various wire rope characteristics. Costello (1997) considered the wire rope bending stiffness as the sum of the bending stiffness of the individual strands without considering the interaction among wires. Based on these assumptions, Gerges (2008) has applied the following analytical model (Eq. 3.26-3.27) for the strand's bending stiffness to a 6x19 WSC (Wire Strand Core) wire rope (see Figure 3.6):

$$K_{rope} = K_{cs} + 6K_{gs} \tag{3.26}$$

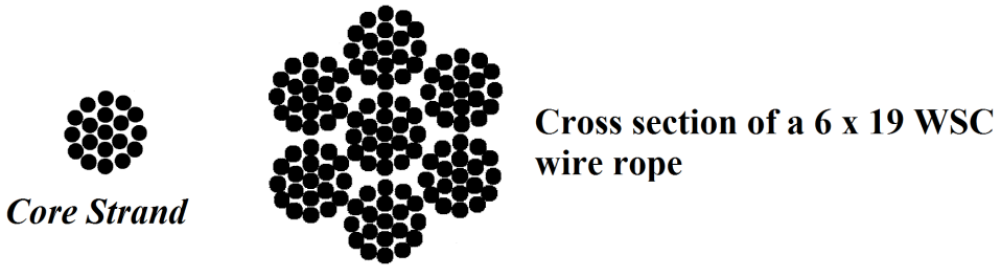

Figure 3.6 Cross-section of the 6x19 WSC wire rope (Gerges, 2008)

where K_{rope}, K_{cs}, and K_{gs} are the bending stiffness of the wire rope, core strand, and the general strand, respectively. The bending stiffness of the center strand is represented by:

$$K_{cs} = \frac{\pi E}{4}\left[R_{w1}^4 + \frac{6\sin(\phi_2)}{1+\frac{\upsilon}{2}\cos^2(\phi_2)} R_{w2}^4 + \frac{12\sin(\phi_3)}{1+\frac{\upsilon}{2}\cos^2(\phi_3)} R_{w3}^4 \right] \tag{3.27}$$

where R_{w1}, R_{w2}, and R_{w3} are the wire radii in the first, second, and third layer, respectively. ϕ_2 and $\phi_3$are the helix angles of the second and third layer. The bending stiffness of a general strand, which is in helix over helix, is represent by:

$$K_{gs} = \frac{\pi E}{4}\left[R_{w1}^4 + \frac{6\sin(\phi_2)}{1+\frac{\upsilon}{2}\cos^2(\phi_2)} R_{w2}^4 + \frac{12\sin(\phi_3)}{1+\frac{\upsilon}{2}\cos^2(\phi_3)} R_{w3}^4 \right] \times \left[\frac{\sin(\phi^*)}{1+\frac{\upsilon}{2}\cos^2(\phi^*)} \right] \tag{3.28}$$

in which ϕ^* is the helix angle of the strand around the core in the wire rope. Eq. (3.26) can be used to estimate the bending stiffness of the wire rope. However, there is always a difficulty associated with measuring the wire radii accurately and in obtaining the lay angles accurately. In general, the lay angle for strands range from 71^o to 76^o and 74^o to 105^o for wires (Gerges, 2008). Zhu and Meguid (2007) have investigated the flexural damping of the wire rope and as a part of their work; they obtained the bending stiffness of the wire rope through a transverse bending test. The analytical model of the EI is developed with many assumptions and hence, in order to gain the confidence in applying the Eq.(3.26) for EI, the transverse bending test was carried out to compare with the Eq.(3.26). In this work both analytical modeling and the transverse bending test were used to evaluate the bending stiffness of the wire rope.

3.4.1. TRANSVERSE BENDING TEST

Zhu and Meguid (2007) performed a transverse bending test for the 6×37 WSC, steel cables to evaluate the bending stiffness of the wire rope. In this work, a similar test procedure was applied to obtain the bending stiffness, EI, for the 6×19 WSC stainless

steel wire cables. ASTM A931-08 was also referred to for the geometric characterization and selection of wire rope test samples. The wire ropes, having diameters of 6.4 mm, 9.5 mm, 12.7 mm, and 15.9 mm were used for the test, in accordance with the wire rope diameter of the WRI used in this research. The bending stiffness of the cantilever beam (Figure 3.7) was determined by using the end deflection due to the point load acting at the free end. The flexural rigidity can be expressed as:

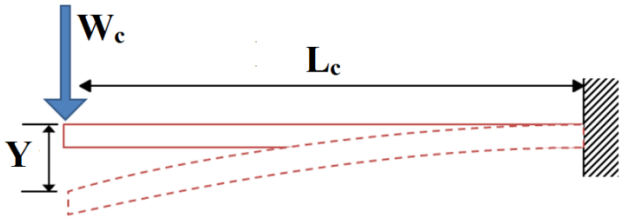

Figure 3.7 Cantilever with end load

$$EI = \frac{L_c^3}{3}\left(\frac{W_c}{Y}\right) \tag{3.29}$$

where W_c is the load acting at the free end, L_c is the beam's length, and Y is the free end deflection. The transverse force was applied at the end of the 300 mm length wire rope to measure its flexural rigidity (Figure 3.8).The deflection was measured using the ABSOLUTE Digimatic Indicator, which features an accuracy of 0.02 mm and a resolution of 0.01 mm. Three samples of wire ropes were tested and the average deflection for each load increment was calculated to plot the load-displacement curve shown in Figure 3.9. The slope (W/Y) was obtained from the best-fit linear curve (W = slope × Y). The EI of each wire rope was evaluated using the slope from the transverse bending tests (Figure 3.9) in the Eq.(3.29). Figure 3.10 shows the value of EI for various wire rope diameters. The flexural rigidity of the wire rope was observed increasing with the wire rope diameter. The third order polynomial equation was found to best fit the data points (Figure 3.10). This equation can be used to obtain EI for the 6×19 WSC stainless steel wire cables. From Figure 3.10, the EI for the wire rope was found to increase cubically with the wire rope diameter. This is attributed to the increased diameter of individual wires. The analytical model of bending stiffness as given by Eq.(16) was also used to compare the results in order to confirm the transverse bending

test, which is not a standardized procedure. Table 3-1 compares Eq.(3.26) with the transverse bending test results. The ratio of analytical to experimental bending stiffness is almost one, indicating that the test procedure was adequate and the analytical model provided a good estimation of the bending stiffness. Hence, for a preliminary design, it is recommended to use Eq.(3.26).

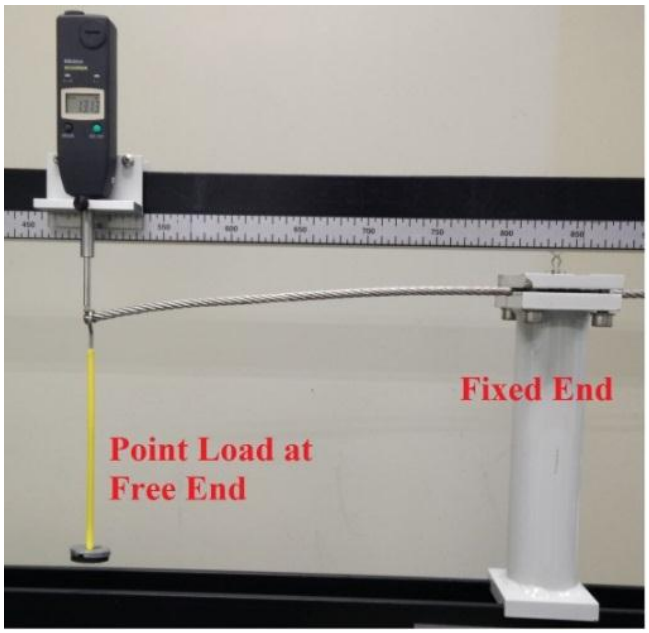

Figure 3.8 Experimental setup of the transverse bending test

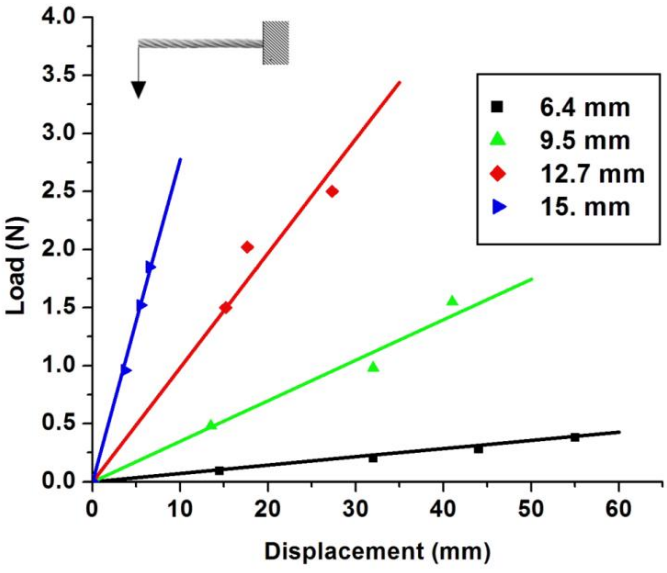

Figure 3.9 Force-Displacement plot from transverse bending tests

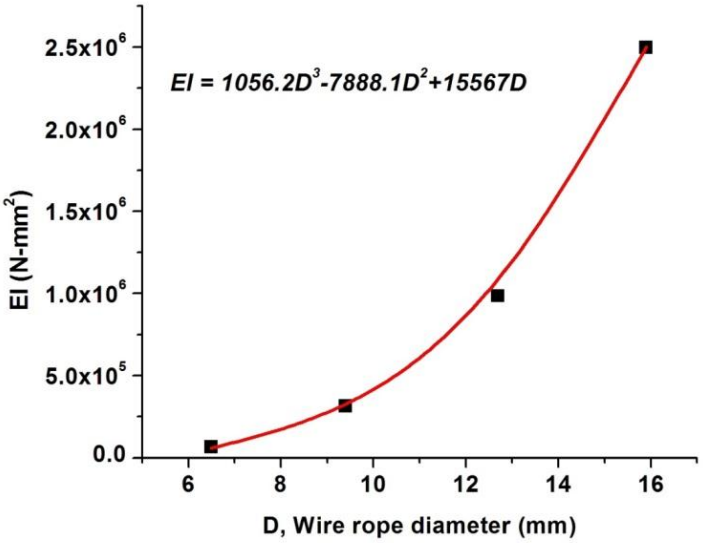

Figure 3.10 Flexural rigidity of the 6x19 IWSC wire rope cables

Table 3-1 Comparison of analytical and transverse bending test

Wire rope diameter (mm)	Bending stiffness from Eq.(16) (kN-mm^2)	Experimental Bending stiffness(kN-mm^2)	Error (%)
6.4	60.80	63.90	4.85
9.5	307.60	314.10	2.01
12.7	802.05	884.70	9.31
15.9	2373.40	2497.50	4.96

3.5. EXPERIMENTAL TEST FOR VALIDATIONS

The monotonic loading test of wire rope isolators was performed using an INSTRON 5982 machine. The test was carried out in compression and roll mode for vertical and lateral loading respectively. The set-up of the test is shown in Figure 3.11. The test was conducted in displacement-controlled mode and the corresponding force was obtained from the machine. The compressive displacement was applied on the top bar of the WRI by fixing the bottom bar. The roll displacement was applied by positioning the WRI in a suitable orientation, as shown in Figure 3.11, through the fixture designed for loading purpose.

Previous studies (Demetriades *et al.*, 1993;Paolacci and Giannini, 2008) have suggested that the WRI exhibits linear behaviour under small displacements and non-linear behaviour under higher displacement magnitudes. Hence, the loading was

performed only up to a 2 mm displacement. The validation of vertical and lateral stiffness models was performed with the isolators obtained from the supplier DPFLEX (2014a), China. This supplier was preferred due to their lower cost compared with the U.S. supplier ENDINE (2014b). However, both the DPFLEX and ENDINE suppliers follow the same standards, namely MIL-STD-810 and MIL-STD-167.The specifications of the WRIs used for the monotonic loading test is shown in Table 3-2. The isolators are intended to determine their stiffness and damping characteristics and the influence from its geometric characteristics. Hence with the available WRI sample from the supplier, one of each model was purchased with the project fund. The WRI was loaded at a rate of 2 mm/min to minimize the inertia effects and to achieve the quasi-static condition. The load was applied and the corresponding displacement was recorded after every load step. The loading was performed only up to 2 mm displacement. The load-displacement plots are shown in Figure 3.12 and Figure 3.13. The obtained data points (displacement, load) were best fitted with the first order linear polynomial curve to obtain the slope, which represents the static stiffness of the WRI

= 

(a)

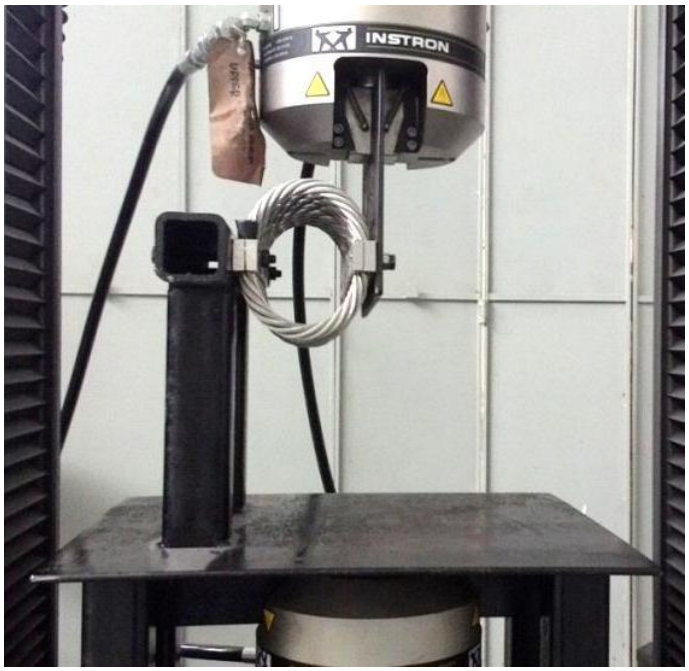

Figure 3.11 Experimental set up for (a) Tension/compression (b) Roll

Table 3-2 Geometric characteristics of WRI used in the monotonic loading test

Isolator No.	Wire rope diameter (D) (mm)	Number of coils (N)	Width (W) (mm)	Height (H) (mm)	Length (L_T) (mm)	Thickness (T) (mm)
1	6.4	8	64	54	146	14
2	6.4	8	71	59	146	14
3	6.4	8	80	64	146	14
4	6.4	8	89	65	146	14
5	9.5	8	84	71	216	18
6	9.5	8	90	75	216	18
7	9.5	8	105	76	216	18
8	12.7	8	105	86	216	20
9	12.7	8	133	105	216	20
10	15.9	8	112	99	268	27

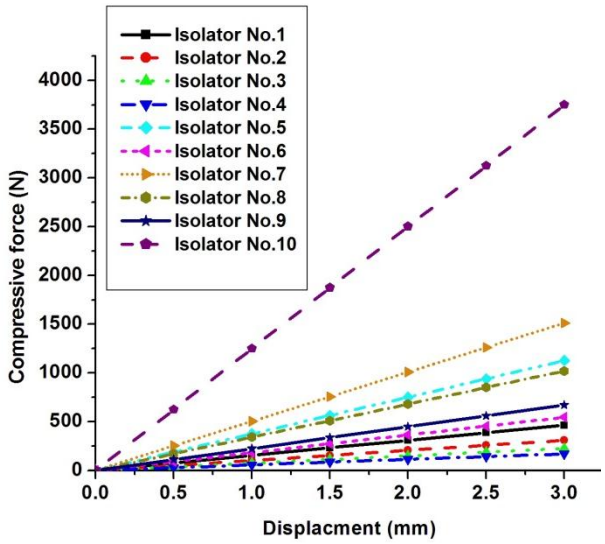

Figure 3.12 Load-Displacement plot for all the isolators under compressive load

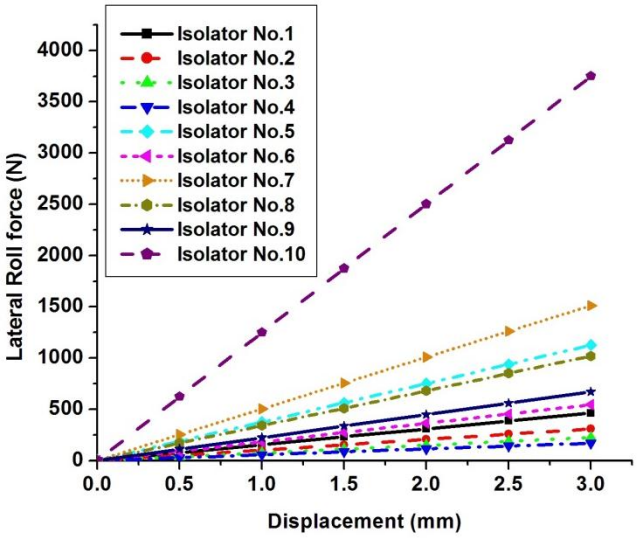

Figure 3.13 Load-Displacement plots for all the isolators under roll load

3.6. VALIDATION WITH EXPERIMENTAL RESULTS

This section presents the validation of the analytical models developed against the experimental results. The analytical model of both vertical and lateral stiffness was verified with the respective monotonic loading test. The flexural rigidity required in the analytical model was obtained from the transverse bending tests. The comparison between the analytical and the experimental test results is tabulated in Table 3-3 and

Table 3-4. The analytical model was observed have a good agreement with the experimental results of within 8% deviation for vertical stiffness and 12% error for lateral stiffness. The errors may be due to the error in the estimation of *EI*, since the analytical model of *EI* (Eq. (3.29)) and test result for *EI* is having 5% deviations. Further, the analytical models assume the wire loop of WRI is of elliptical in shape, however practically it may not be exactly elliptical.

Table 3-3 and Table 3-4 show the WRI having a different geometric shape has different stiffness values. Further, The WRI with a greater wire rope diameter can also be designed to have a lower stiffness than the smaller wire rope diameter by properly designing the width and height. The analytical model provided the stiffness in terms of the geometric properties. The analytical model related the stiffnesses to the WRI geometric and wire rope properties. The analytical study was also used to assess the effects of wire rope diameter, width, height, and number of turns (coils) on the WRI's lateral stiffness. The developed analytical model can also be used to design the WRI to obtain the desired lateral stiffness or to evaluate the modification required in the geometric properties to target a specified increase in the stiffness.

Table 3-3 Comparison of analytical and experimental vertical stiffness

Isolator No.	k_v (Experimental), N/mm	k_v (Eq.(11)), N/mm	Error (%)
1	154.60	156.58	1.26
2	102.70	110.92	7.41
3	74.80	75.40	0.80
4	56.60	54.41	4.02
5	376.10	353.91	6.27
6	182.10	173.65	4.87
7	504.50	517.07	2.43
8	340.26	326.34	4.27
9	223.80	235.36	4.91
10	1250.30	1300.50	3.86

Table 3-4 Comparison of analytical and experimental lateral stiffness results

Isolator No.	k_h (Experimental), N/mm	k_h (Eq.(25)), N/mm	Error (%)
1	39.06	40.64	3.90
2	27.53	29.23	5.40
3	19.51	21.80	10.49
4	16.54	18.53	10.72
5	84.78	93.63	9.45
6	54.30	61.50	11.72
7	111.34	115.50	3.60
8	81.78	85.50	4.35
9	53.82	60.10	10.46
10	285.24	310.00	7.99

3.7. PARAMETRIC ANALYSIS

In this section, a parametric analysis was performed to investigate the effects of different geometrical properties on the vertical compressive and lateral roll stiffnesses of WRIs. The parameters selected in this analysis were the wire rope diameter, width and height of the isolator, and the number of turns.

3.7.1. INFLUENCE OF WIRE ROPE DIAMETER

WRI is made up of wire rope cables; hence, cable diameter has a significant effect on the behaviour of WRI. The quantified effects of wire rope diameter on the stiffness of WRI have not been reported in the literature. Thus, it would be interesting to investigate the effect of wire rope diameter on the WRI's stiffness. The effect of wire rope diameter (D) on the vertical stiffness is shown in Figure 3.14. It is observed from the analytical model (Eq.(3.11)) that the vertical stiffness is highly dependent on the wire rope diameter, or in other words, one effective way to control the stiffness is to adjust the wire rope diameter. The significant increase in the vertical stiffness is due to the increase of flexural rigidity, *EI*, which in turn increases with wire rope diameter.

Increasing the diameter from 9 mm to 15 mm induces an increase of stiffness by a factor of $(15.9/9.5)^4$ ~7.85

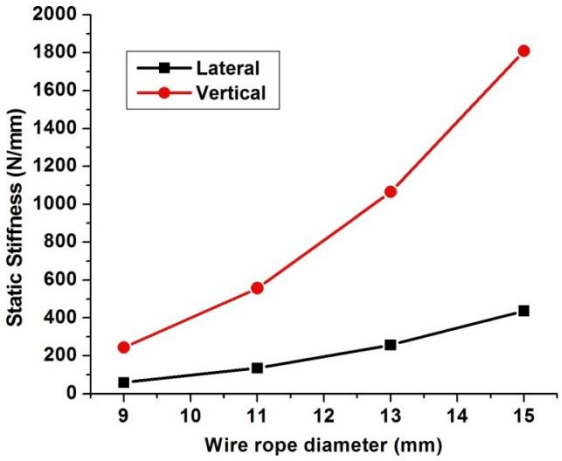

Figure 3.14 Variation of WRI's stiffness with rope diameter for *W = 90 mm, H = 75 mm* and *N = 8*).

This significant increase in the vertical and lateral stiffness is mainly due to the increase in the resistance of the wire rope to lateral deformation (i.e., flexural rigidity, *EI*), which in turn, is due to the increased diameter, and hence inertia, of individual wires. The tested WRIs are around four times stiffer in the vertical direction than in the lateral direction. The stiffness ratio determined from Eqs.(3.11) and (3.25) are dependent only on *R* and *L*:

$$\frac{k_v}{k_h} = \frac{f(R,L)}{2g(R,L)} \tag{3.30}$$

Figure 3.15 shows the variation of stiffness ratio with *R* and *L*. It is clear that the ratio is more sensitive to the variation of isolator radius *R* than the metal retain length, 2*L*; an increase in *R* increases the ratio significantly, whereas an increase in *L* decreases the stiffness ratio slowly.

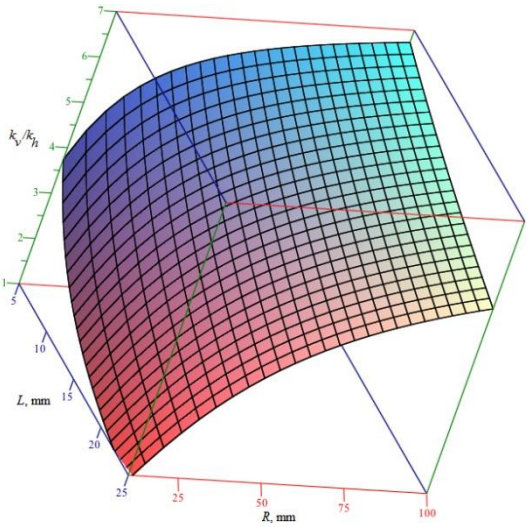

Figure 3.15 Variation of WRI's stiffness ratio with R and L.

3.7.2. INFLUENCE OF WIDTH AND HEIGHT

The width and height of the WRI control the geometry of the coil, hence, affecting the stiffness from a geometrical perspective (L and R in Eqs. (3.11 and 3.25)). An increase in width with a constant height results in a decrease of both vertical and lateral stiffness (Figure 3.16(a)). Similarly, an increase in height with a constant width results in a decrease of stiffness (Figure 3.16(b)). Figure 3.17-3.18 shows the variation of the height-to-width ratio for various wire rope diameters. It can be seen that by increasing the ratio from 0.6 to 1.2, the stiffness increases, which is significant for higher wire rope diameters. The effect of height-to-width ratio on the vertical compressive stiffness is less pronounced for small wire rope diameters.

For higher values of height-to-width ratio, the stability of the coil in the lateral direction decreases and the lateral restoring force of the WRI is reduced affecting the isolator's performance. As a consequence, the present trend in the industry is to maintain a ratio of 0.75–0.85 for a stable wire rope isolator (2014b). From the monotonic tests, it can be seen that isolator 5 and 8 have similar stiffness, however, they were made from different wire rope diameters; this can be explained by the differences in width and height. The width and height can be controlled to obtain a higher vertical stiffness from the lower diameter wire rope; however, the height-to-width ratio has to be maintained within the limits of 0.75-0.85.

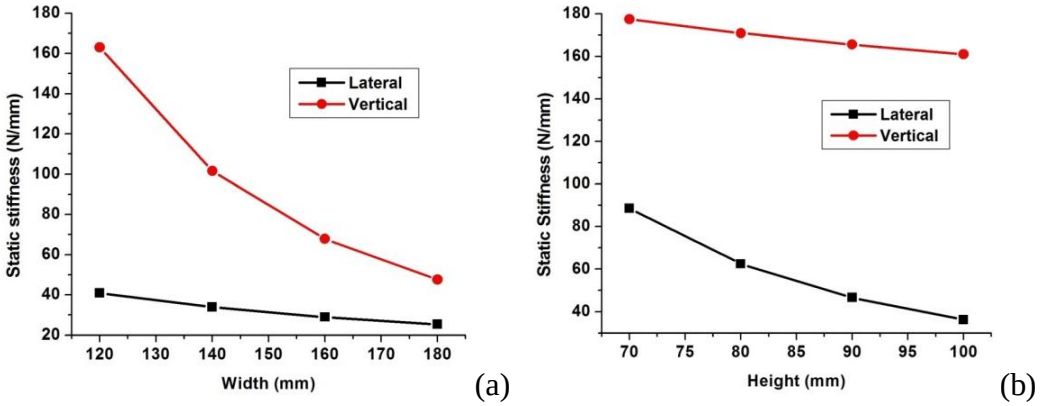

Figure 3.16 Variation of vertical stiffness with (a) Width and (b) Height*(for D = 12.7 mm and N =8*)

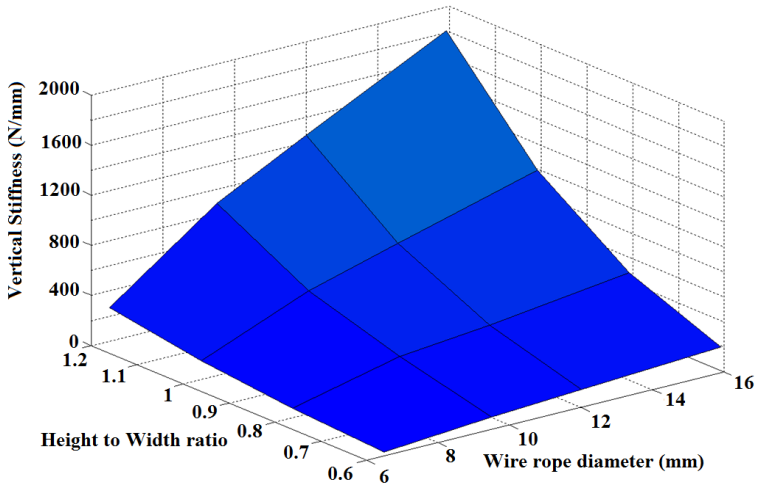

Figure 3.17 Variation of vertical stiffness with height-to-width ratio and wire rope diameter

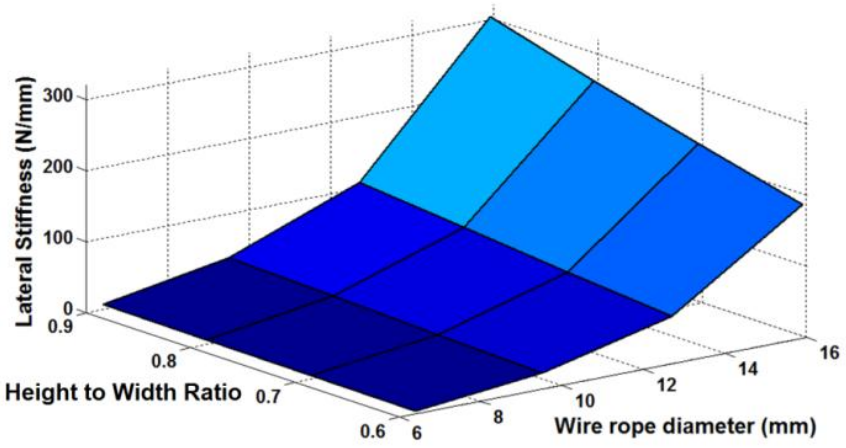

Figure 3.18 Variation of lateral stiffness with height-to-width ratio and wire rope diameter

3.7.3. INFLUENCE OF NUMBER OF TURNS

Figure 3.19 shows the influence of the number of turns on the stiffness of the WRI. The additional number of turns provides the wire loops with greater support of the equipment. From Eqs.(3.11) and (3.25), it is clear that the WRI stiffness is directly proportional to the number of turns. This is also due to the assumption that load is equally distributed in the metal retainer. In current industry practice, after establishing the stiffness of a 8 turns WRI, the stiffness of the WRI with same geometrical characteristics with different turns are estimated as a linear function of N. From the stability point of view, a stiffer WRI should be designed to have a sufficient number of turns with a small wire rope diameter rather than a small number of turns with larger wire rope diameter. Although, the WRI can be constructed with any number of turns, it is generally manufactured with an even number of turns (i.e., 2, 4, 6, or 8 turns) to provide adequate stability to the equipment.

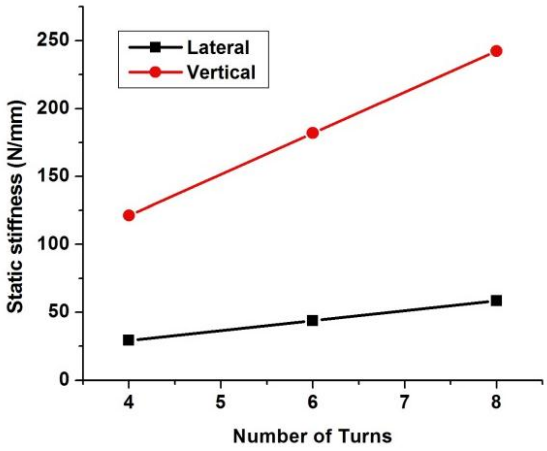

Figure 3.19 Variation of WRI's stiffness with Number of turns (For Isolator No.9)

3.8. ENHANCEMENT OF VERTICAL LOAD CARRYING ABILITY OF WRI.

As discussed in Section 1.2, the application of isolators depends to a great extent on the stiffness value required in the excitation direction to achieve the desired vibration isolation. Hence, the stiffness of the isolator at the excitation direction is of great interest to the designer in selecting an isolator. There is also a critical assessment to be made to identify the excitation direction in order to effectively isolate the system by providing the required stiffness in that direction. Traditionally available passive isolators are effective in a specific direction and hence, careful identification of excitation is required.

However, in the case of WRI, it is effective in all planes and in any directions and hence, it can provide better isolation from the excitations from any directions. This advantage also causes a disadvantage as in the case when the weight of the equipment to be supported is vertically and the excitation is acted laterally (Figure 3.20). The problem can be understood by understanding the vertical and lateral stiffness of the WRI. After estimating the lateral stiffness of the isolator for a given excitation, it is also required to select an isolator so the WRI can also support the weight of the equipment vertically as shown in Figure 3.20. Table 3-3 and Table 3-4 show the smaller WRI has less lateral stiffness however it has a lower vertical stiffness as well, hence when moving to a larger WRI and this will have an increased vertical stiffness to support the load but also an increased lateral stiffness. This bigger size with increased lateral stiffness may not provide the desired level of isolation compared to the smaller size with less lateral stiffness. Therefore, there is an interest in improving the vertical weight carrying ability of the WRI so a smaller WRI with less lateral stiffness can be used in certain applications. This problem is addressed in this section.

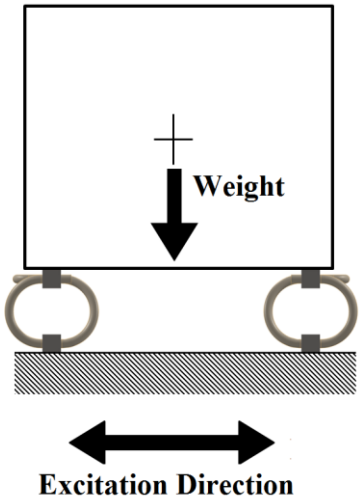

Figure 3.20 WRI carrying vertical load and subjected to lateral excitation

3.8.1. WRI-SPRING (S-WRI)

The springs are generally used to support the load along its length and further, they provide an elastic restoring force. This ability of the spring can be used with WRI to enhance the vertical load carrying ability of the WRI without affecting the lateral

stiffness of the WRI. In this study, the WRI-Spring configuration (S-WRI), shown in Figure 3.21 and Figure 3.22, was examined to determine the extent of a positive advantage gained from this configuration. In order to increase the overall knowledge of the S-WRI configuration, three S-WRI were fabricated in the lab. Table 3-5 shows the specifications of the spring and the characteristics of the spring is shown in Figure 3.23. Table 3-6 shows the WRI used for the S-WRI configuration. As shown in Table 3-6, Isolator No 4 is compounded with 3 S1 springs. The springs were selected from the catalogue of the supplier, so that they fit with the available WRI.

Figure 3.24 shows the WRI-Spring configurations and these springs were welded as shown in the Figure 3.25. The concept of making 3 sets of S-WRI was to identify and verify the ability of the spring to provide same benefits in all three cases. Hence, three WRI, each having different wire rope diameters, was used for the S-WRI. The spring was expected to improve the vertical loading carrying ability of the WRI and hence the loading in the vertical direction was performed to evaluate the stiffness of the S-WRI. The configuration was subjected to monotonic loading and the results are discussed in Section. 3.8.2.

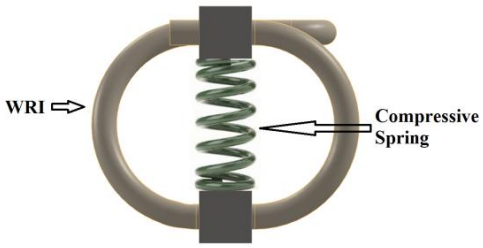

Figure 3.21 WRI with Spring

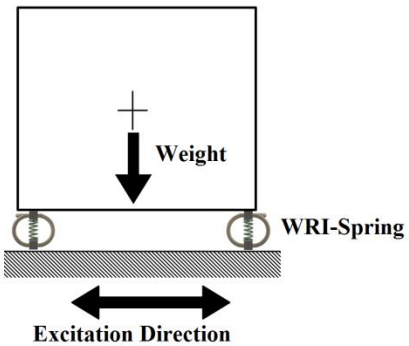

Figure 3.22 S-WRI carrying vertical load assisted by springs and subjected to lateral excitation

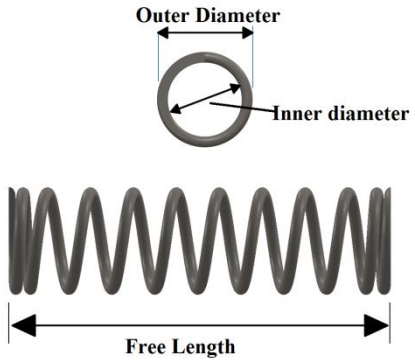

Figure 3.23 Specifications of the springs

Table 3-5 Specification for the springs

Name	Free Length (mm)	Wire diameter (mm)	No. of Coil	Outer diameter (mm)	Inside diameter (mm)	Quantity	Stiffness (N/mm)
S1	40	4	4	43	35	3	16
S2	45	6	4.5	50	38	3	49.5
S3	78	7	5	60	46	3	39.5

Table 3-6 S-WRI configurations used in this study

Name	S-WRI Configurations	
	WRI	3 Springs of type
S-WRI.1	Isolator No. 4	S1
S-WRI.2	Isolator No.6	S2
S-WRI. 3	Isolator No.9	S3

Figure 3.24 S-WRI fabricated in this work. (WRI with 3 metal springs)

Figure 3.25 View showing welding of the spring for the S-WRI configurations

3.8.2. STIFFNESS OF S-WRI CONFIGURATION

The monotonic loading test was done in both vertical and lateral directions, as discussed in Section and the test setup is shown in Figure 3.26. The test was performed to identify the spring assistance in the stiffness of the WRI. The test was performed on a small displacement range and the stiffness of the WRI is given in the Table 3-7. The vertical stiffness of the S-WRI was propotionaly enahnced by the number of springs however, the lateral stiffenss of the S-WRI was not significantly affected which is desirable for the applications. This results show that the spring can improve the vertical stiffness of the WRI and simulatenously maintin the flexibility for lateral excitation. It can also be observed from Table 3-8 that the spring produces similar effect in all 3 cases and hence it can be summarized that the spring can improve the vertical stifness of the WRI.

The vertical stiffness of the S-WRI can now be expressed analytically using the Eq. 3.31 and is given below.

$$k_v^S = k_v + n_s * s_v \tag{3.31}$$

Where k_v^S is the vertical stiffness of the S-WRI configuration, n_s is the number of springs and s_v is the stiffness of the spring. The Eq.(3.31) can be used to explain the Spring–WRI combination to obtain the requried stifness to carry the weight of the

equipment. The proper combination of Spring-WRI can be fabricated as required to obtain the desired performance.

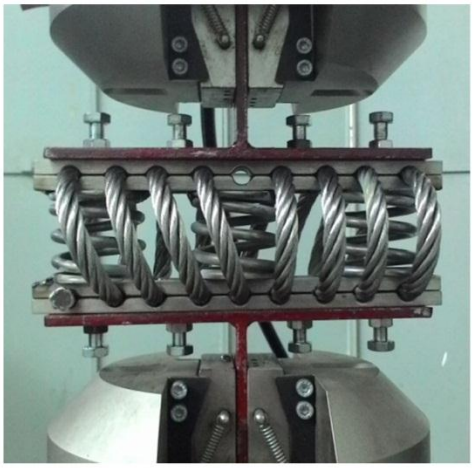

Vertical Cyclic loading

Lateral Cyclic loading

Figure 3.26 Setup for the monotonic loading test of S-WRI

Table 3-7 Stiffness of S-WRI obtained from the test

S.No	WRI-Spring	Vertical Stiffness (N/mm)	Lateral stiffness (N/mm)
1	S-WRI.1	120.50	20.50
2	S-WRI.3	369.50	75.30
3	S-WRI.3	485.50	95.30

Table 3-8 Comparison of WRI and S-WRI

Parameter	Name	WRI	S-WRI
Vertical Stiffness of S-WRI (N/mm)	S-WRI. 1	56.60	120.50
	S-WRI. 2	182.10	369.50
	S.WRI. 3	223.80	485.50

3.9. SUMMARY

This study presented two analytical models for testing the stiffness of wire rope isolators in the vertical and lateral directions. The models were validated with results obtained from a series of monotonic loading tests. The models developed can be effectively used in the analysis and design of wire rope isolators for the vibration

protection of equipment and lightweight structures. The following conclusions are drawn so far, from this study:

1. The transverse bending test was used to estimate the flexural rigidity, *EI*, of the 6x19 IWSC wire rope cables. An equation was developed to estimate *EI* for similar wire ropes with different diameters.
2. The WRI is almost four times stiffer in the vertical direction than the lateral direction.
3. The wire rope diameter significantly influences the vertical stiffness more than the width, height, and number of turns.
4. The lateral stiffness is influenced more by the wire rope diameter and height than by the width.
5. An increase in the wire rope diameter increases the WRI stiffness (vertical and lateral), however, decreasing either the width or height results in the decrease of stiffness.
6. A 10% increase in vertical stiffness can be achieved either by increasing the wire rope diameter by 2.5% or decreasing the width by 3.3 %.
7. The lateral stiffness (in the roll mode) of the WRI is more sensitive to the flexural rigidity (bending stiffness) of the wire rope cable.
8. A S-WRI configuration was developed and tested in this study. The test results show the springs can be used to enhance the vertical stiffness of the WRI.

Chapter 4. HYSTERESIS BEHAVIOUR OF WRI

4.1. INTRODUCTION

An analytical model of stiffness was discussed in Chapter 3. This stiffness model can be used to design the WRI to achieve the effective isolation. The stiffness component of the isolator provides flexibility and hence dissipates the external excitation energy through work done in the displacement (Rivin, 2003). However, the high magnitude excitation energy demands, larger displacement of the isolator and this demand can be, in some cases, more than the displacement limit of the isolators. In such cases, the displacement of the isolator can be reduced, by additionally dissipating the external excitation energy through a damping mechanism. Therefore, the damping can reduce the displacement demand of the isolator. Conversely, higher damping can affect the isolation capability since the damping induces rigidness in the isolator and this can be observed from Figure 1-2. The increased damping results in higher transmissibility. Hence the damping of the isolator needs to be studied to understand the damping ability of the isolator, in order to achieve the effective isolation.

The damping or energy dissipation capability of the WRI can be studied from its hysteresis behaviour under cyclic loading (Demetriades *et al.*, 1993). This hysteresis is a natural way, available in mechanical and structural system to provide restoring forces against movements and dissipate energy (Ismail *et al.*, 2009a). Previous studies (Demetriades *et al.*, 1993;Tinker and Cutchins, 1994, 1992;Michael Loyd, 1989) have verified and confirmed that the WRI exhibits a hysteresis curve under cyclic loading and is due to the frictional resistance between the wire strands. WRI is a typical non-linear hysteretic damping device (Ni *et al.*, 1999b). The hysteresis characteristics of WRI can be studied from its force-displacement relation. WRI has inherent frictional damping from the wire rope and hence, the loading and unloading paths are different and result in a hysteresis curve when a cyclic load is applied. The area of the hysteresis curve explains the energy dissipation capability. This chapter presents the research conducted for understanding of the hysteresis characteristics of WRI and additionally, the mathematical modelling for the hysteresis behaviour is also discussed. The methodology

used in this study is discussed in Section 4.2. In this study, a new configuration of WRI to enhance the damping ability of the WRI is also discussed at the end of this chapter.

4.2. METHODOLOGY

The hysteresis behaviour of WRI was studied using experimental tests and mathematical model is also developed for the hysteresis behaviour. Firstly, test was performed in both vertical and lateral directions to understand the hysteresis behaviour of WRI. Figure 4.1 shows the loading modes in each direction. These loading modes are defined from the orientation of WRI used in the applications. Figure 4.2 shows the loading modes used in the applications. In this study, the hysteresis behaviour in vertical loading was studied using a tension/compression load. Previous studies (Demetriades *et al.*, 1993;Paolacci and Giannini, 2008) have suggested the WRI exhibits similar hysteresis behaviour for cyclic roll and cyclic shear loading in the lateral direction. Hence the lateral cyclic behaviour was studied using a cyclic roll load. However, the similarity in hysteresis behaviour between cyclic roll and cyclic shear was initially verified from the test.

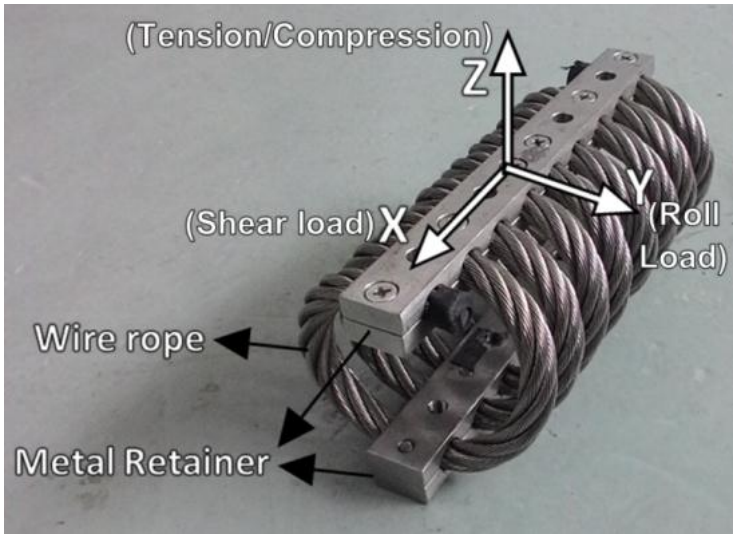

Figure 4.1 Wire rope isolator and Loading modes

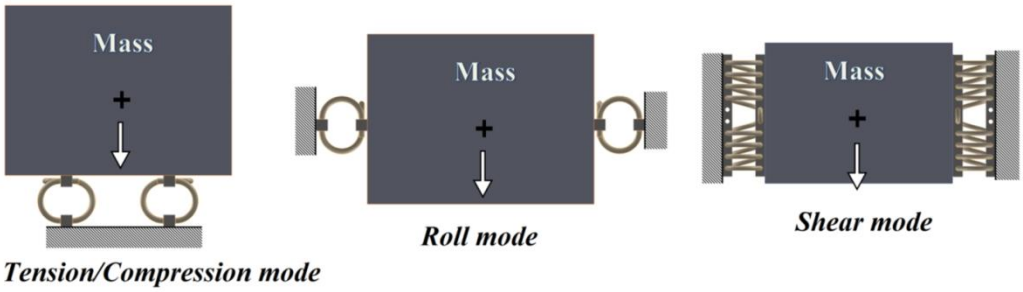

Figure 4.2 Orientation of WRI in applications

Secondly, the mathematical model of the hysteresis behaviour, for both vertical and lateral directions, was also developed using the Bouc-Wen equations. Section 2.5.2 of Chapter.2 discusses the literature on Bouc-Wen equations. The model parameters of the Bouc-Wen equations were identified using the cyclic loading test and least square method. The Bouc-Wen equations are suited for a symmetric hysteresis which was the case in lateral direction. However in the vertical direction, the WRI exhibits asymmetric behavior and hence a suitable modification was proposed in this study. The mathematical models developed, for both vertical and lateral directions, were validated with the cyclic loading test. This validation was performed at various displacement amplitudes to verify the ability of the model parameters to predict the hysteresis behaviour for ranges of displacement amplitudes. Hence, the cyclic loading test was performed at three displacement amplitudes (3 mm, 6 mm and 9 mm) to validate the mathematical model. Moreover, other published reports (Demetriades *et al.*, 1993;Tinker and Cutchins, 1992) have reported the behaviour of WRI at specific displacement amplitudes and hence this study can provide an understanding of WRI behaviour at different displacement amplitudes. This chapter also discusses the effects of the geometric characteristics of WRI on hysteresis behaviour. The influence of geometrical characteristics was evaluated based on two calculated parameters from the hysteresis curve, namely, the equivalent damping ratio and the effective stiffness.

4.3. EXPERIMENTAL STUDY ON THE HYSTERESIS BEHAVIOUR

WRI is a hysteretic damping device and hence exhibits a hysteresis curve for restoring force-displacement under cyclic loading. This hysteretic nature indicates that the restoring force is a function of both instantaneous displacement and the history of

displacement (Ismail *et al.*, 2009a).This dependency can be described as a memory effect, which means the history of displacements also influences the response of the WRI for a given load (Demetriades *et al.*, 1993;Wang *et al.*, 2015). In general, the hysteresis behaviour of the friction type damper is rate-independent (Visintin, 2013). Earlier, Demetriades *et al.*,(1993) and Wang *et al.*,(2015) also have suggested that the WRI exhibits rate independent behavior. The hysteresis in mathematics is defined as rate independent memory effect (Visintin, 2013;Ni *et al.*, 1999b).

In reality, these memory effects in damping material may not be purely rate independent due to the coupling of hysteresis with viscous-type memory (Ni *et al.*, 1999b). However, the friction type damper exhibits a dominant rate independent hysteresis effect. Ni *et al.*,(1999b;a) have shown by eliminating the effect of inertial force, the experimental hysteresis curve of WRI is almost rate independent and are identical with those obtained from a quasi-static cyclic loading test. Moreover, the quasi-static cyclic test is less contaminated with noise than the dynamic test (Ni *et al.*, 1999b). Hence, cyclic loading behavior of the WRI is studied using a quasi-static cyclic loading test. In this work, the rate independency of the WRI was also verified by subjecting the WRI to various rates of loading and comparing the resulting hysteresis behavior.

In this study, the cyclic loading was applied in both vertical and lateral directions. The tension\compression loading was applied in the vertical direction and cyclic roll was applied in the lateral direction (Figure 4.2). These directions were used in this study as in real time applications; the WRI was primarily loaded in the modes as shown in the Figure 4.2. The test was carried out in a displacement-controlled manner and hence the force was characterized as a restoring force, as this refers to the force that resists the applied displacement. The cyclic loading test was primarily performed to study the energy dissipation capability of the WRI and was evaluated using the parameter the Equivalent Damping Ratio (EDR) calculated from the hysteresis curve. The cyclic loading behavior can also be used to study the hardening and softening effect of the WRI for various displacement amplitudes. This hardening and softening refers to the stiffness characteristics of WRI. The effectiveness of the WRI under cyclic loading testing can provide information on how the stiffness of WRI varies with displacement

amplitudes. Further, the influence of the wire rope diameter and height to width ratio on hysteresis behavior was reported. In this section the experimental setup, test results and discussion on the effects of geometric characteristics of WRI on equivalent damping and effective stiffness is discussed.

4.3.1. EXPERIMENTAL SET UP

The cyclic loading test of wire rope isolators was performed using an INSTRON 5982 machine with a capacity of 100 kN. The cyclic test was carried out in both vertical and lateral directions by applying tension\compression, cyclic roll and cyclic shear loadings, respectively. The cyclic shear was performed to verify the similarity in the hysteresis curve between cyclic roll and cyclic shear. Table 4-1 shows the specifications of the isolators used in the cyclic loading test. Figure 4.3 shows the geometric characteristics of WRI. Table 4-1 is the same as Table 3-2 in chapter 3 however; Isolator No. 10 was not used in the cyclic loading test since it was dismantled, after the monotonic loading test, to identify the parts and fabrication of WRI. Furthermore, the previous studies (Demetriades *et al.*, 1993;Alessandri *et al.*, 2015b) had used only 2-3 WRI for their work. However, in this study nine WRIs were used for the hysteresis study, which were significantly more samples than previous studies done on the WRI. More samples were used so as to attain better confidence in the observations by comparing the results. Further, the study on the effects of height to width ratio and wire rope diameter was also performed in this study with the samples. Each sample was identified using the number as given in the Table 4-1.

The cyclic test was conducted in a displacement-controlled mode and the corresponding restoring force was obtained from the machine. Figure 4.4 shows the experimental setup used in this study and a suitable fixture was designed to apply the cyclic loading in the required direction. The specifications of the fixture used in the test is provided in the Appendix A. The cyclic loading behavior was studied under 3 displacement amplitudes namely 3 mm, 6 mm and 9 mm. The study also included the effect of the rate of loading on the cyclic loading behavior. The test was carried at a rate of 8 mm/min to reduce the inertia effects. The hysteresis curve from the cyclic test

results were also used for the development of the mathematical model using Bouc-Wen equations and its parametric identification and it will be discussed in Section 4.4.

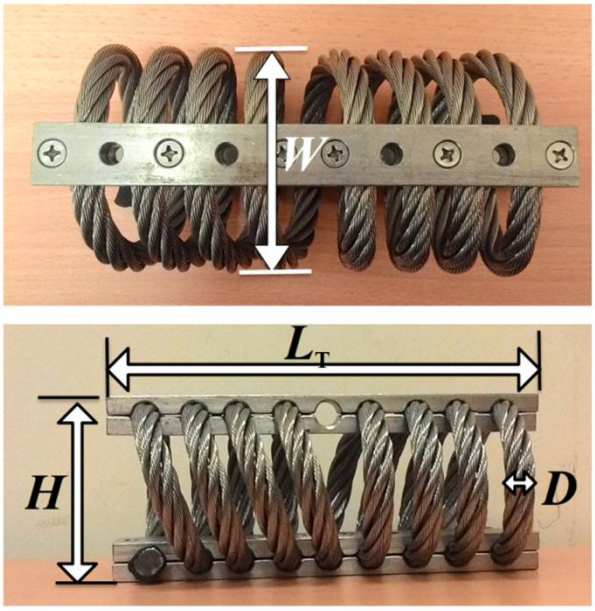

Figure 4.3 Geometric characteristics of WRI

Table 4-1 Specification of the WRI used for the cyclic loading test

Isolator No	Wire rope diameter (D) (mm)	Number of coils	Width (W) (mm)	Length (L) (mm)	Height (H) (mm)	(H/W)
No. 1	6.4	8	64	146	54	0.84
No. 2	6.4	8	71	146	59	0.83
No. 3	6.4	8	80	146	64	0.80
No. 4	6.4	8	89	146	65	0.73
No. 5	9.5	8	84	216	71	0.85
No. 6	9.5	8	105	216	76	0.72
No. 7	12.7	8	105	216	90	0.86
No. 8	12.7	8	121	216	95	0.79
No. 9	12.7	8	133	216	108	0.81

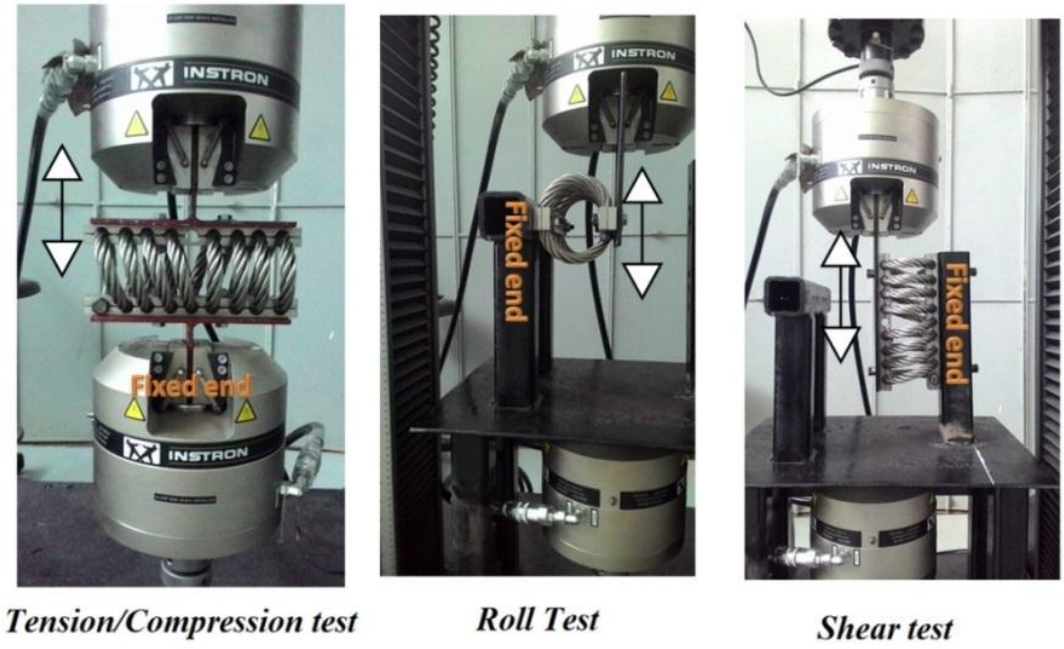

Figure 4.4 Experimental test set-up for tension/compression, cyclic roll and cyclic shear loadings

4.3.2. CYCLIC LOADING TEST RESULTS

Figure 4.5 to 4.13 show the hysteresis loops with different displacement amplitudes for each isolator under tension/compression and the selected data points are given in Appendix B. It was observed the hysteretic curve of isolators under tension/compression were asymmetrical; this indicates the variable stiffness in tension and compression modes. The amplitude of displacement has a significant impact on the hysteretic curves in the vertical direction. For small displacement amplitudes (i.e., 3 mm), the hysteresis curves were basically symmetrical in both sides with observed stiffness softening and quasi-linear behavior. Thus, the displacement increases with force in linear gradient form. The asymmetrical curves become more apparent when isolators are loaded to larger displacements; this is due to the non-linear contact between the stranded wires for higher loads

The hardening in the tension mode and softening in the compression mode was observed for higher displacement amplitudes (6 mm and 9 mm). This is because when the isolator is under tension, the wire strands contract, which increases the number of contact points, thus, the surface of friction increases. This will imply more dry friction and eventually stiffens the isolator. In contrast, when the isolator is compressed, the wire

strands tend to move further apart from each other leaving less contact points. In this case, most of the stiffness of the isolator comes from the wire strand itself.

Figure 4.14- 4.22 show the results obtained from the cyclic roll tests conducted on the isolators and the selected data points are given in Appendix C. It was observed the behavior in the roll was different from tension/compression loading. In addition, the stiffness of the WRI remained the same for both positive and negative roll. This behavior is different from vertical loading where stiffness is different in tension and compression. The hysteresis exhibits symmetric nature in cyclic roll. The symmetric nature of the hysteresis in roll is due to the circular section of the coil and an equal number of coil turns from the center of the WRI. For roll loading, the negative and positive loading results were in the similar displacement mode (Figure 4.23 (a)) in both directions, whereas in tension and compression loading both of the loads resulted in different displacement shapes as shown in the Figure 4.23 (b)

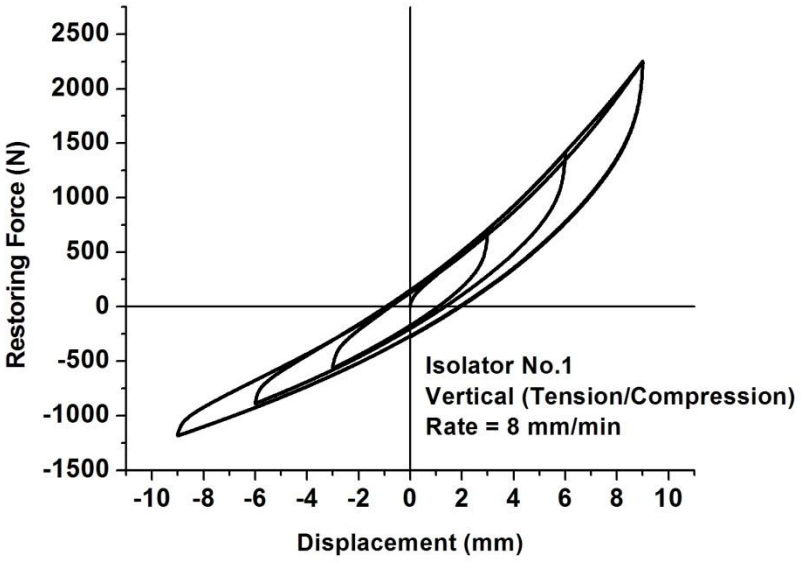

Figure 4.5 Hysteresis behavior under vertical cyclic loading (Tension/Compression) at 8 mm/min of Isolator No.1

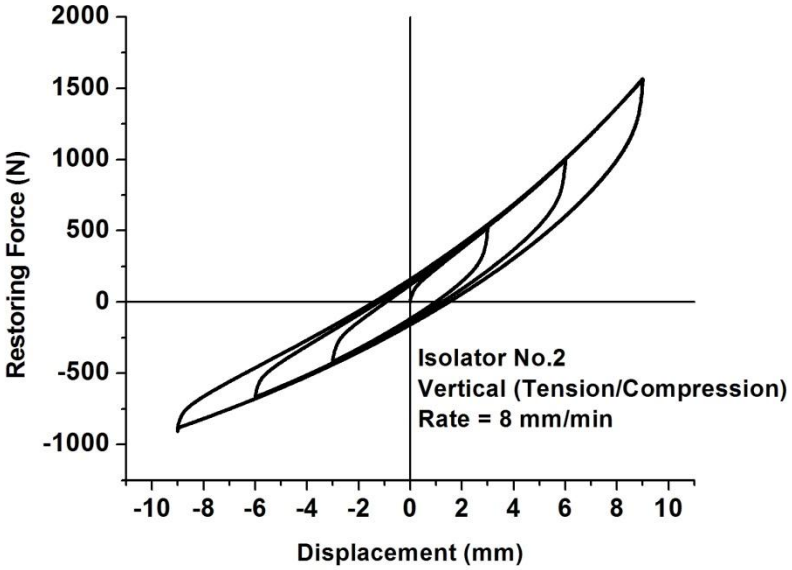

Figure 4.6 Hysteresis behavior under vertical cyclic loading (Tension/Compression) at 8 mm/min of Isolator No.2

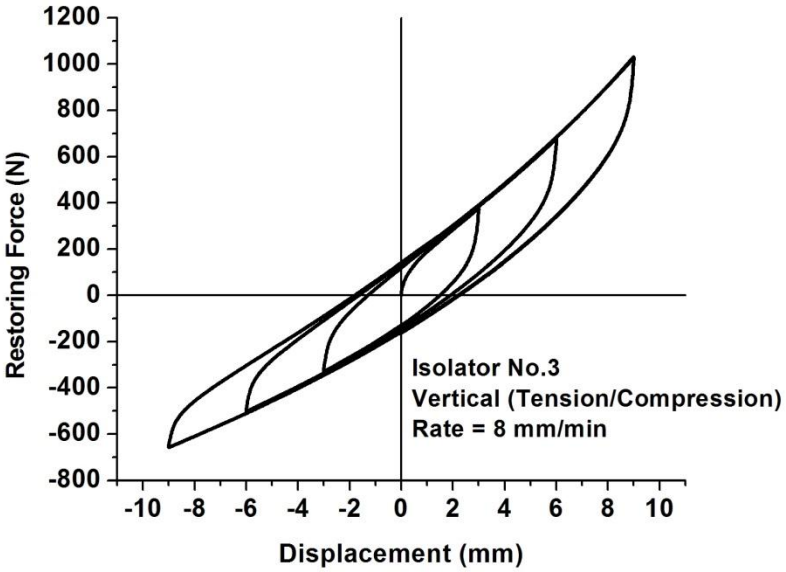

Figure 4.7 Hysteresis behavior under vertical cyclic loading (Tension/Compression) at 8 mm/min of Isolator No.3

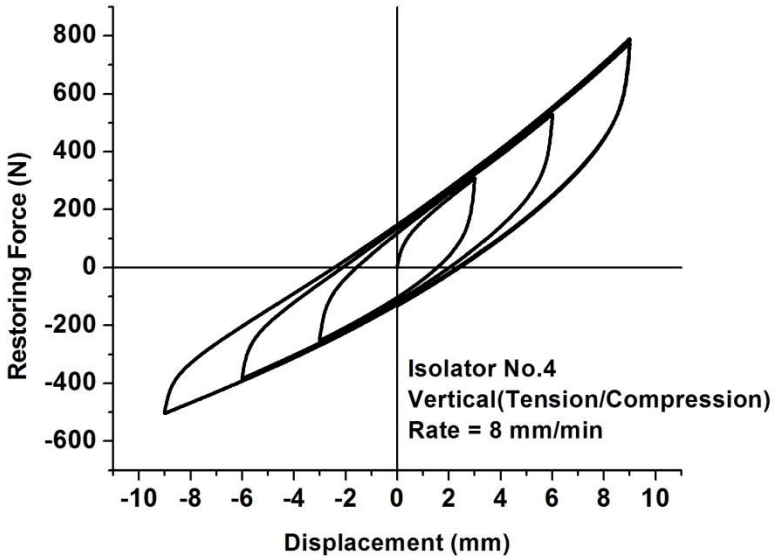

Figure 4.8 Hysteresis behavior under vertical cyclic loading (Tension/Compression) at 8 mm/min of Isolator No.4

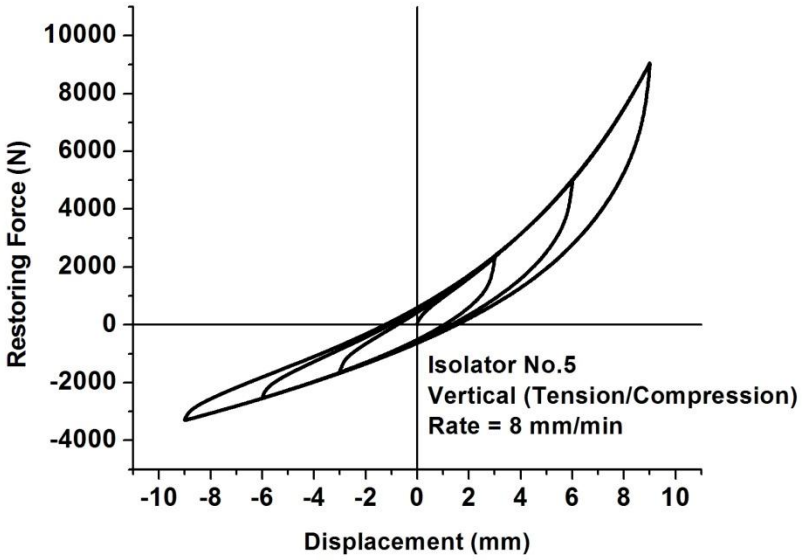

Figure 4.9 Hysteresis behavior under vertical cyclic loading (Tension/Compression) at 8 mm/min of Isolator No.5

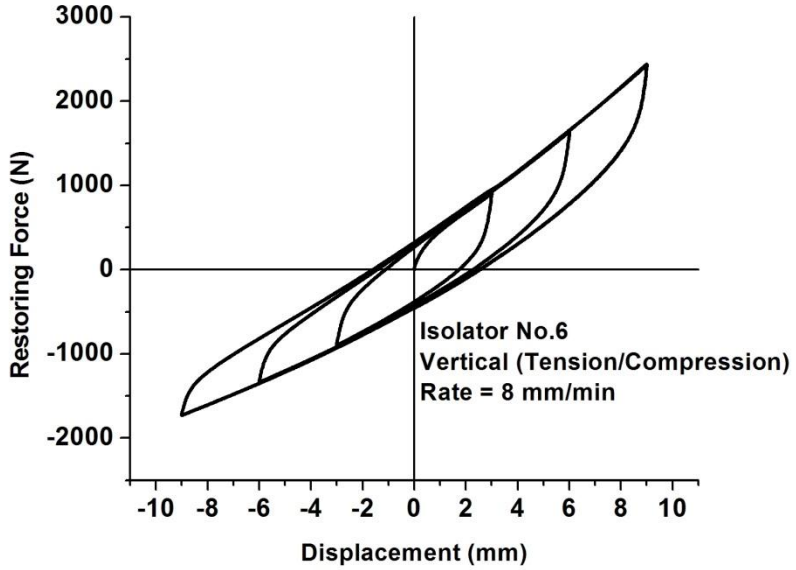

Figure 4.10 Hysteresis behavior under vertical cyclic loading (Tension/Compression) at 8 mm/min of Isolator No.6

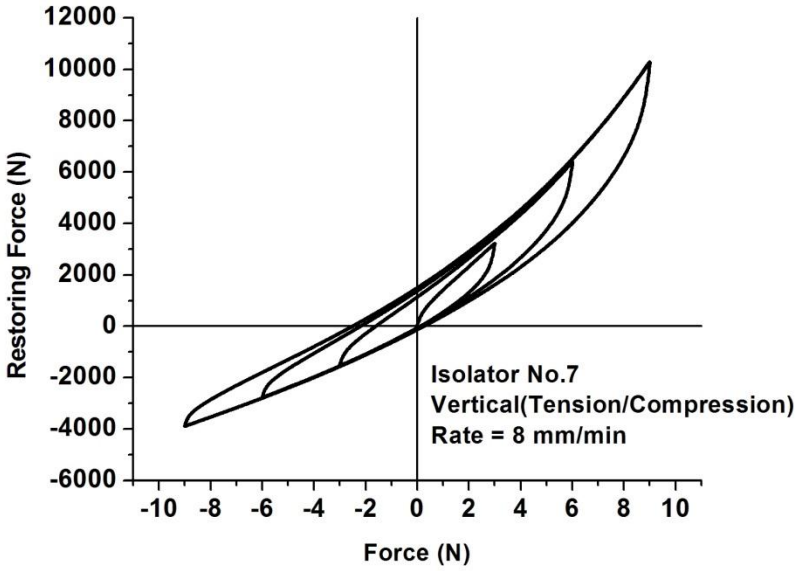

Figure 4.11 Hysteresis behavior under vertical cyclic loading (Tension/Compression) at 8 mm/min of Isolator No.7

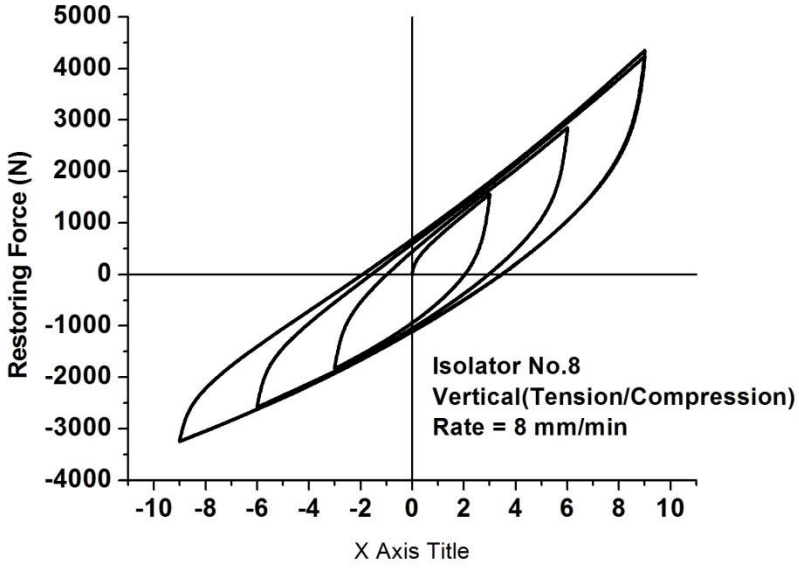

Figure 4.12 Hysteresis behavior under vertical cyclic loading (Tension/Compression) at 8 mm/min of Isolator No.8

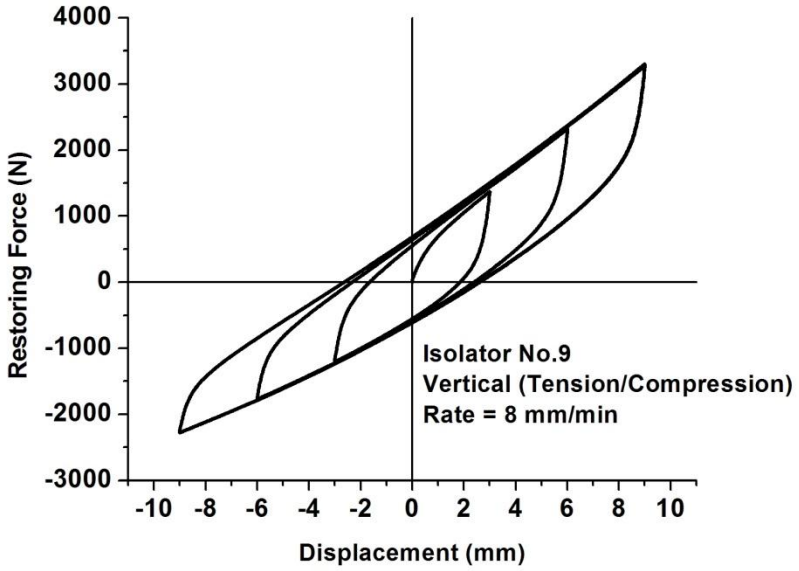

Figure 4.13 Hysteresis behavior under vertical cyclic loading (Tension/Compression) at 8 mm/min of Isolator No.9

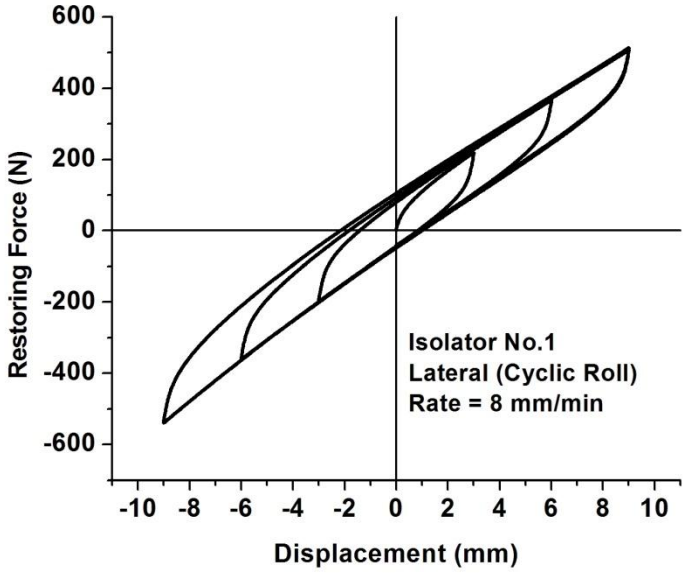

Figure 4.14 Hysteresis behavior under lateral cyclic loading (Cyclic Roll) at 8 mm/min of Isolator No.1

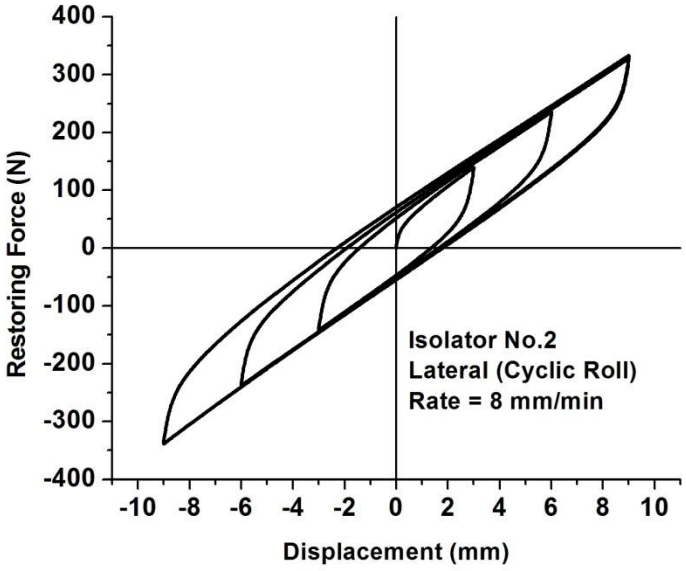

Figure 4.15 Hysteresis behavior under lateral cyclic loading (Cyclic Roll) at 8 mm/min of Isolator No.2

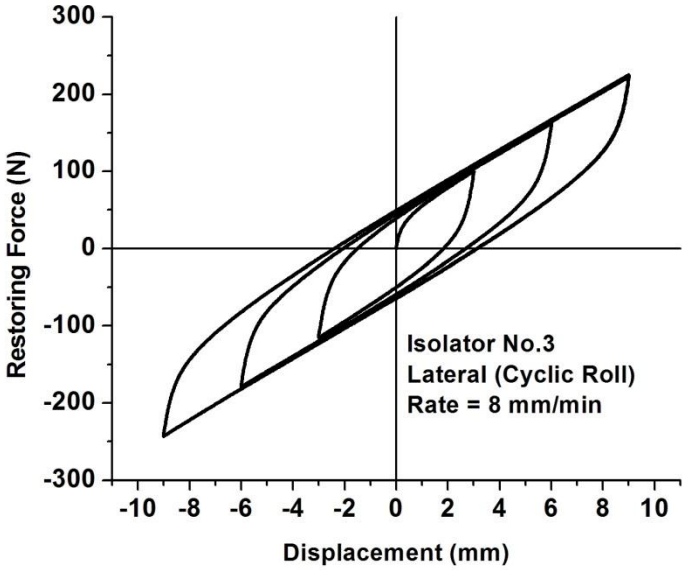

Figure 4.16 Hysteresis behavior under lateral cyclic loading (Cyclic Roll) at 8 mm/min of Isolator No.3

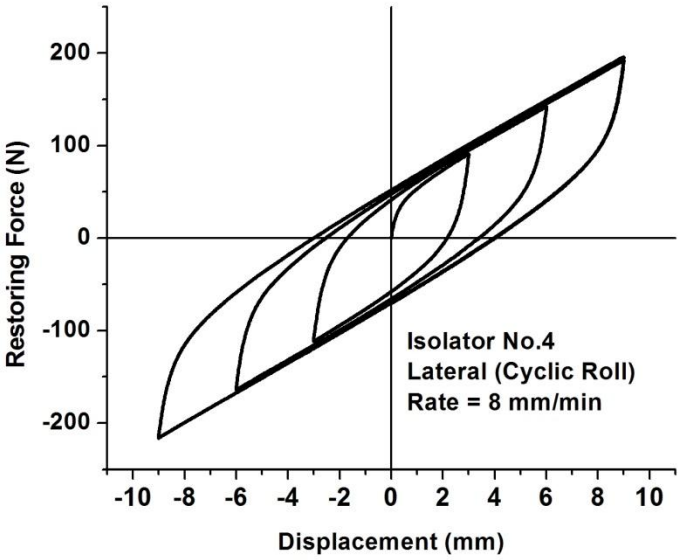

Figure 4.17 Hysteresis behavior under lateral cyclic loading (Cyclic Roll) at 8 mm/min of Isolator No.4

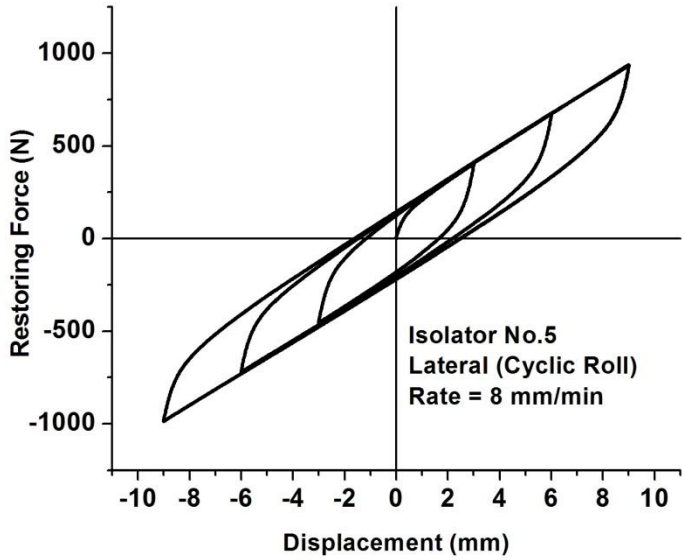

Figure 4.18 Hysteresis behavior under lateral cyclic loading (Cyclic Roll) at 8 mm/min of Isolator No.5

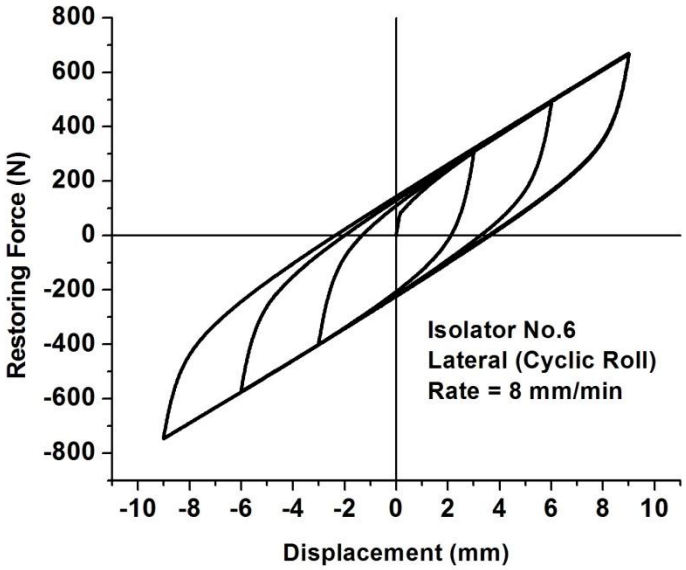

Figure 4.19 Hysteresis behavior under lateral cyclic loading (Cyclic Roll) at 8 mm/min of Isolator No.6

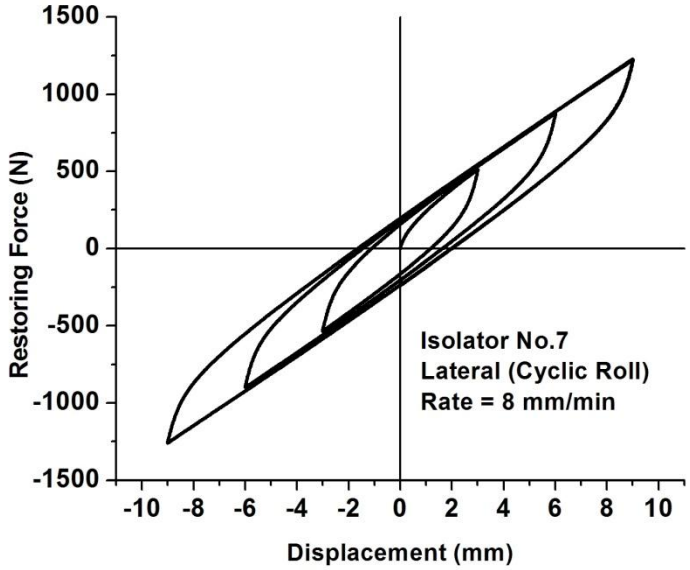

Figure 4.20 Hysteresis behavior under lateral cyclic loading (Cyclic Roll) at 8 mm/min of Isolator No.7

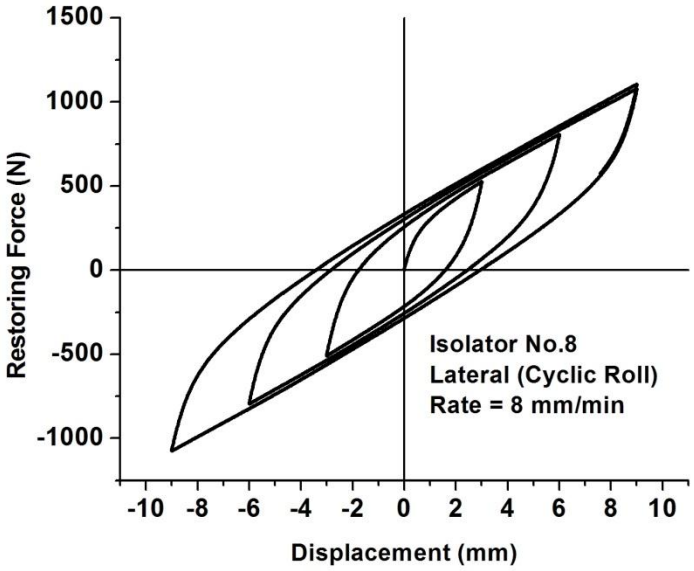

Figure 4.21 Hysteresis behavior under lateral cyclic loading (Cyclic Roll) at 8 mm/min of Isolator No.8

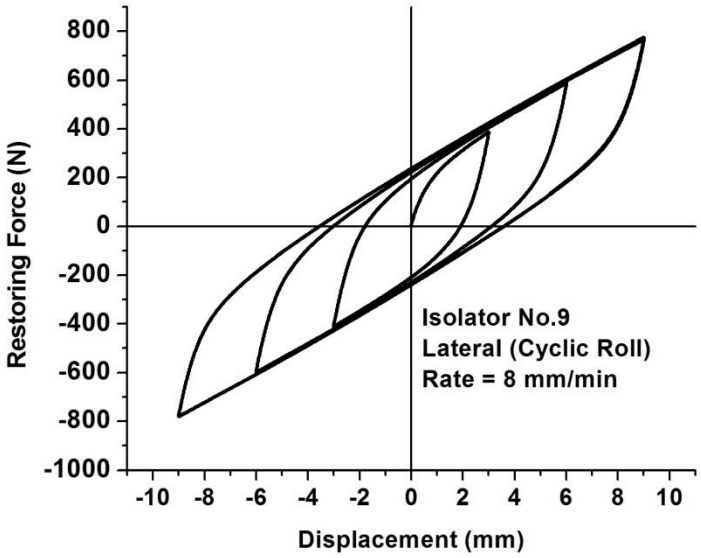

Figure 4.22 Hysteresis behavior under lateral cyclic loading (Cyclic Roll) at 8 mm/min of Isolator No.9

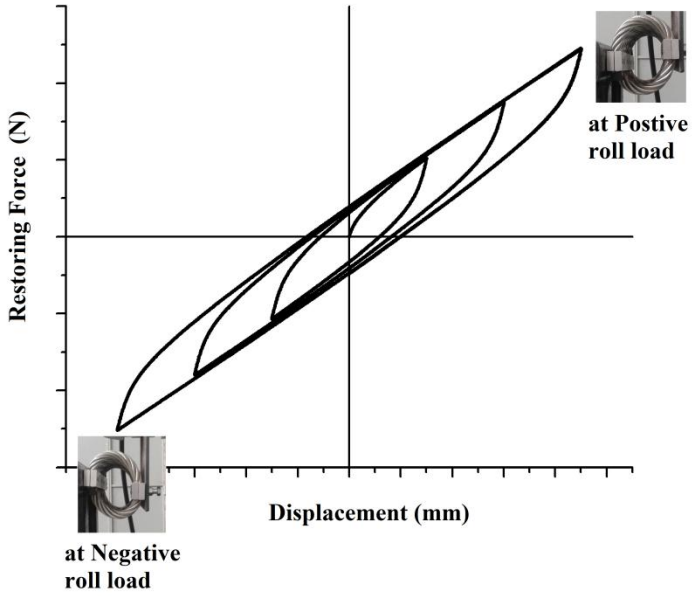

(a)

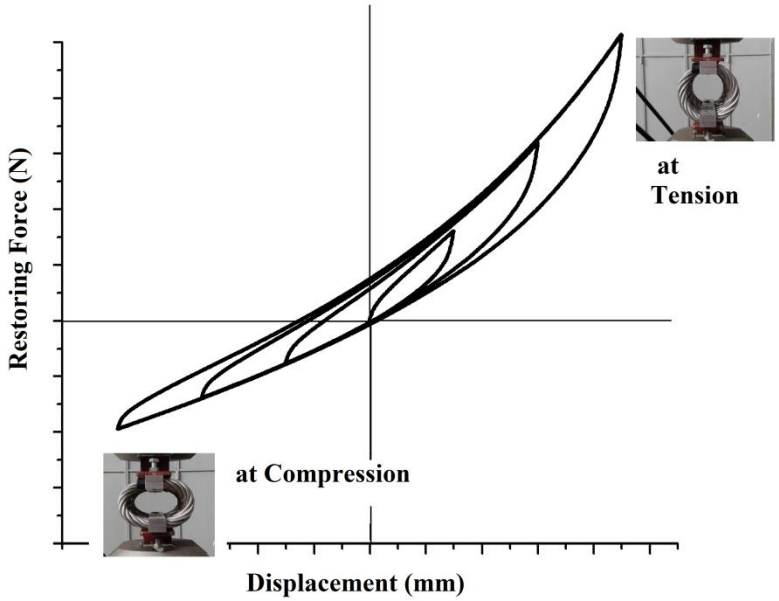

(b)

Figure 4.23 Displacement of the isolator (a) Cyclic Roll (b) Tension/Compression

The similarity in the hysteresis behavior under cyclic shear and cyclic roll was observed in all displacement amplitudes results (Figure 4.24). Due to this similarity, the lateral hysterics behaviour can be studied either along the x-axis or along the y-axis (Figure 4.1). In this study, cyclic behavior in the lateral direction was studied along the y-axis using a cyclic roll load. The effect of rate-of-loading on the WRI behavior was also investigated in the present study. The cyclic test was carried at 2 mm/min, 4 mm/min, 8 mm/min, 32 mm/min, 64 mm/min and 128 mm/mm in both directions at 6 mm displacement amplitude and the results are shown in the Figure 4.25.

It can be observed the cyclic loading behavior was rate independent in the test range. The rate independent behavior is due to its mechanism of energy dissipation, which is through the friction contact. The rate-independency enables the dynamic characteristics of WRI to be analysed using a quasi-static test when the inertial effects are neglected. The test was also conducted to study the effect of coil orientation such as right-hand and left-hand coil as shown in Figure 4.26. The hysteresis behaviors of both coil types of WRI are shown in Figure 4.27. It can be observed the hysteresis curve resulting from both types of WRI can be considered the same and hence it can be suggested that a WRI with the same geometric characteristics, except for coil

orientation, will exhibit a similar hysteresis curve in both the vertical and lateral direction.

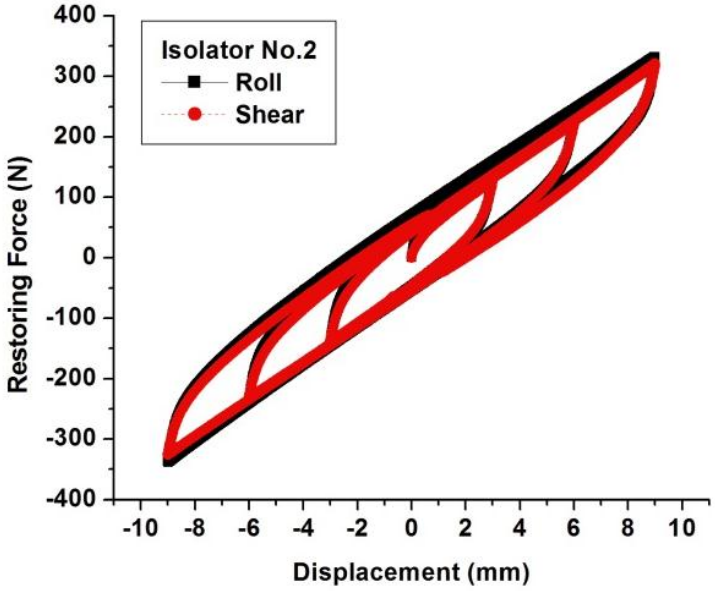

(a)

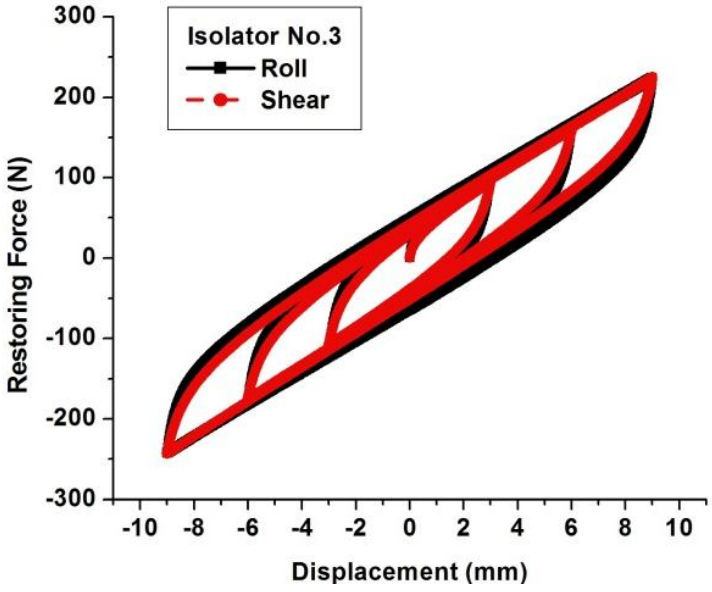

(b)

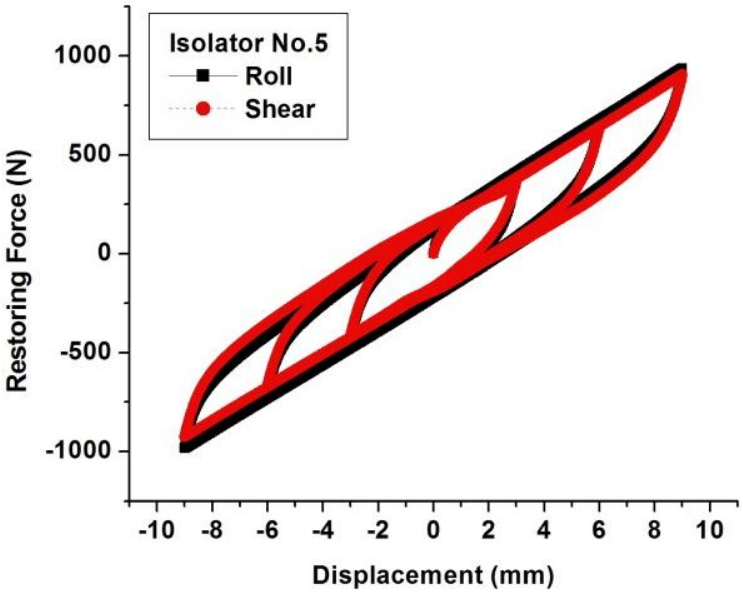

(c)

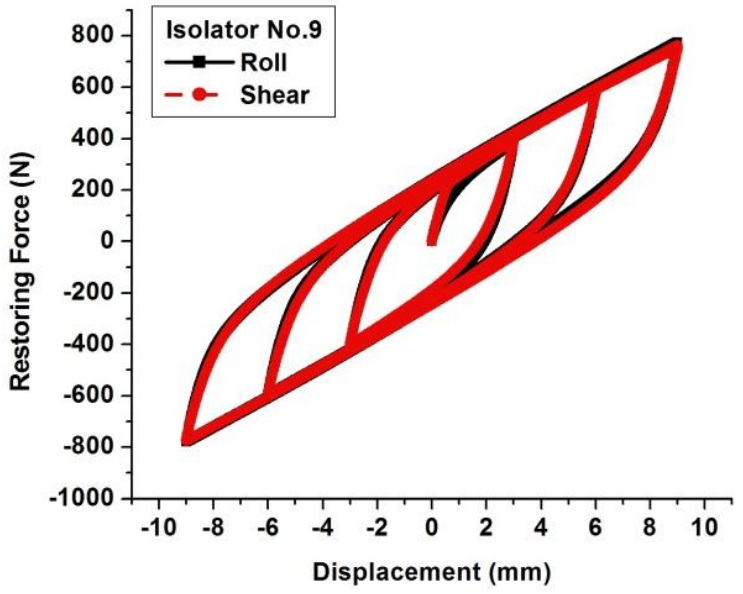

(d)

Figure 4.24 Hysteresis behavior under lateral cyclic loading (Roll and Shear) at 8 mm/min (a) Isolator No. 2 (b) Isolator No. 3 (c) Isolator No. 5 (d) Isolator No. 9

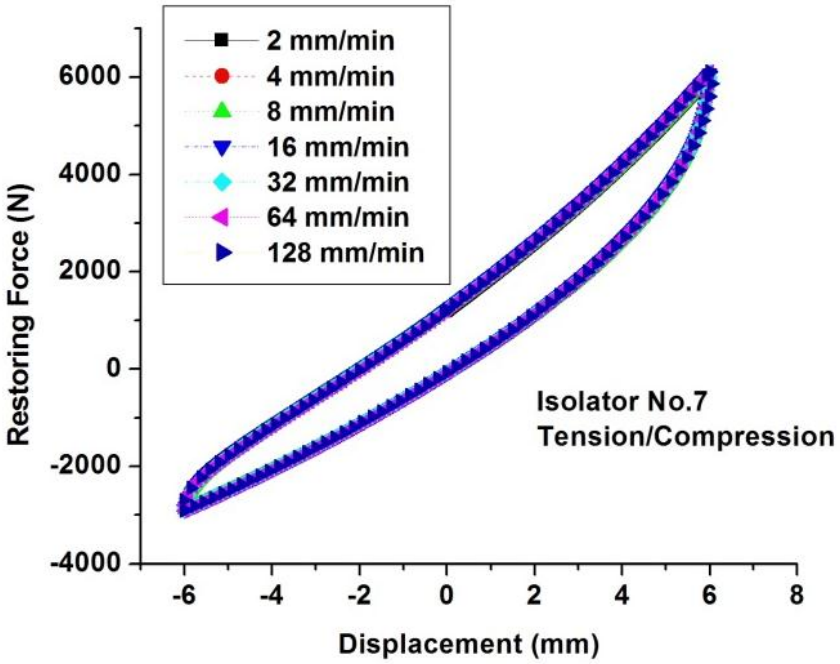

(a)

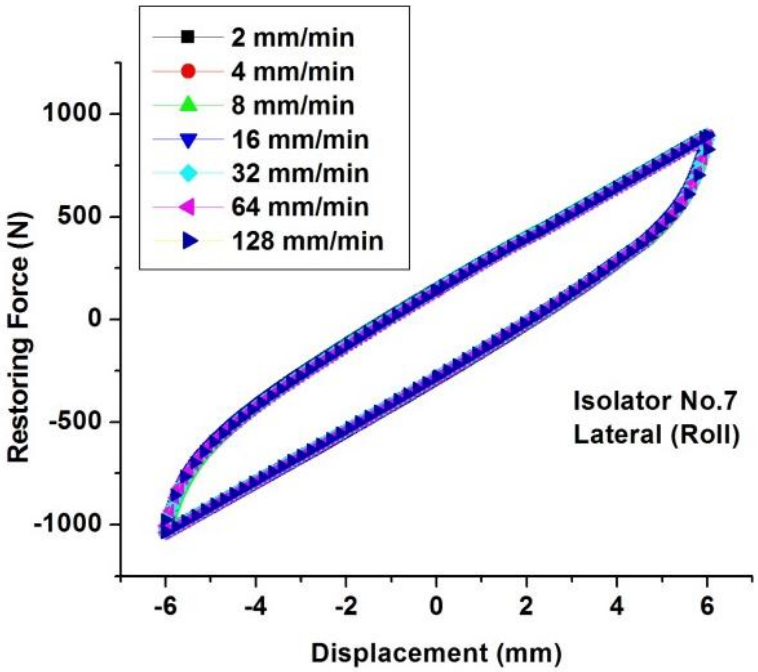

(b)

Figure 4.25 Effect of Rate of Loading on the hysteresis behavior of WRI under (a) Vertical (b) Lateral

Figure 4.26 Left hand and Right hand Coil of Isolator No. 7

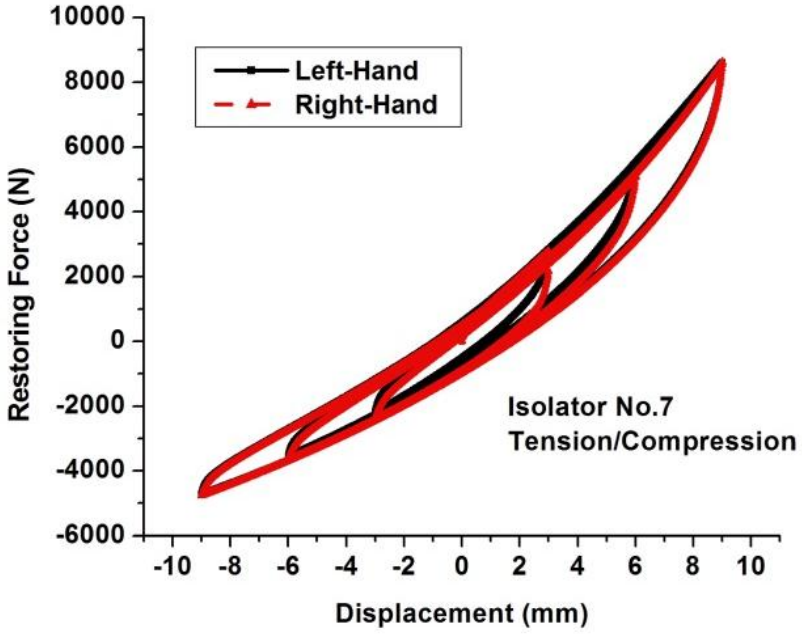

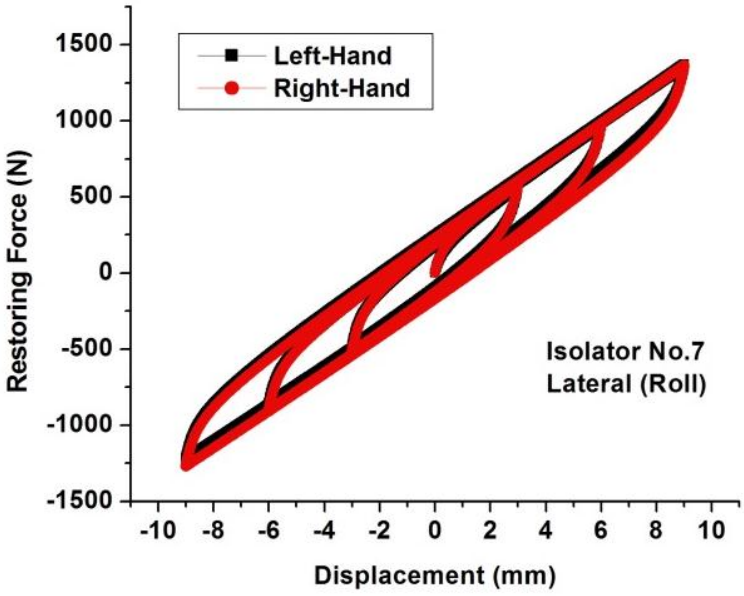

Figure 4.27 Comparison of hysteresis behavior between right and left coil of isolator No.7 (a) Vertical direction (b) Lateral direction

The test results also show that WRI under cyclic loading exhibits rate-independency and the memory effect. The memory effect of the WRI can be seen in Figure 4.28. The test was conducted in both vertical and lateral directions with increasing displacement amplitude from 1 mm to 10 mm in increments of 1 mm per cycle. The subsequent displacement input resulted in the overlapping of the behavior in both directions. This overlapping can be explained from the wire strand interaction from the input load. The frictional contact of the wire strands results in the wire strand displacing in a similar configuration and follows the displacement history. This memory effect of the WRI is a significant characteristic since it can be understood the WRI, under cyclic loading, undergoes similar displacement modes. The hysteresis behavior was studied using two parameters namely the equivalent damping ratio and the effective stiffness which were evaluated from the hysteresis curve. These parameters allow an estimation of the damping capability and stiffness characteristics.

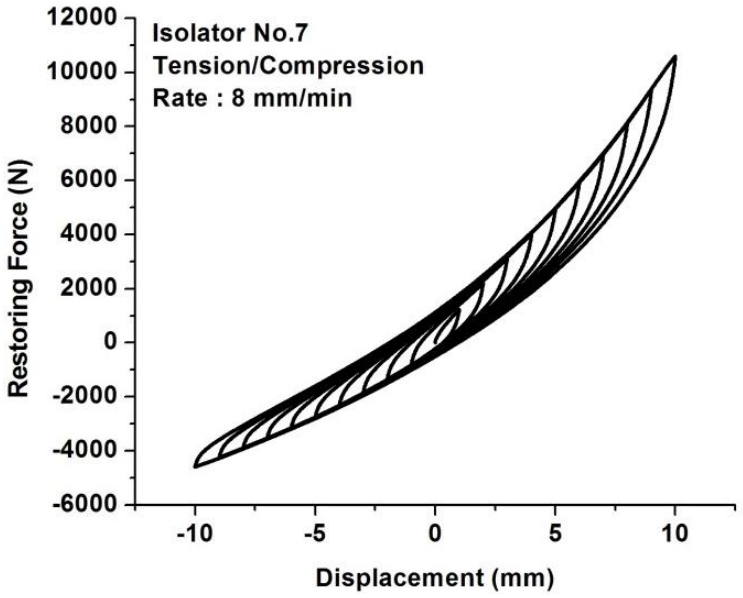

(a)

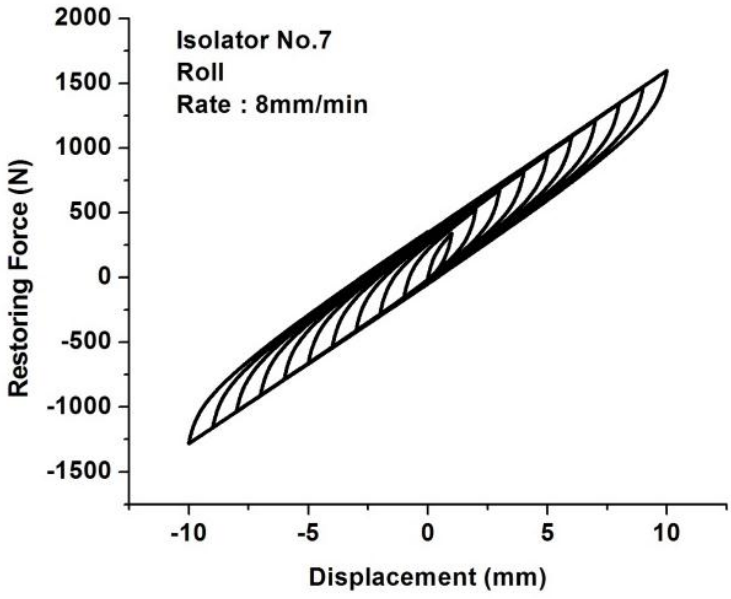

(b)

Figure 4.28 Hardening overlap (memory effect) under cyclic loading in (a) Vertical (b) Lateral

4.3.3. EQUIVALENT DAMPING RATIO

The Equivalent Damping Ratio (EDR) can be used to define the damping property of WRIs (Foss, 2006). The EDR is the amount of energy being dissipated due to frictional resistance between the wire strands and is evaluated as the equivalent viscous damping. It is represented by Eqs.4.1 and 4.2 (Foss, 2006).

$$Energy\ Loss\ Ratio = \frac{A_{loop}}{\pi \frac{(F_{\max} - F_{\min})}{2} \frac{(X_{\max} - X_{\min})}{2}} \tag{4.1}$$

$$EDR = \frac{Energy\ Loss\ Ratio}{2} \tag{4.2}$$

where A_{loop} is the area of the hysteresis loop and F_{max} and F_{min} are the maximum and minimum forces, respectively. X_{max} and X_{min} are the maximum and minimum displacements, respectively. Both forces and displacements are obtained from the hysteresis behavior of the corresponding isolator. The equivalent damping ratio provides information on the WRI's damping capabilities. The higher value of EDR represents the increased damping capabilities of WRI (Foss, 2006).

4.3.3.1. Equivalent damping ratio for Tension/Compression loading

Figure 4.29 shows the variation of EDR computed for each isolator with the variation of displacement amplitude in the tension/compression mode. For the 3 mm displacement amplitude, the equivalent damping ratio for all isolators were observed to be in the range of 0.13-0.23. For the 6 mm displacement amplitude, the equivalent damping ratio decreased on average by 30% for all isolators. For the 9 mm displacement amplitude, the equivalent damping ratio of isolators continually decreased by an average of 28%. The equivalent damping ratio of all isolators in this amplitude became closer at a range of about 0.13 to 0.07.

From the results in Figure 4.29, theequivalent damping ratio shows that all isolators have their highest damping effectiveness when they are loaded under small amplitude levels (i.e., 3 mm). However, as the amplitude increases, the hysteresis loops become narrower (i.e., their area decreases), indicating a decrease in the damping effectiveness.This can be due to, at higher displacments the wire rope strands move away from each other resulting in reduced contact surface and hence frictional resistance and damping effectivenss is reduced.The wire rope isolators with different geometries have different damping capacities (total energy dissipation). The WRI with higher wire rope diameters was observed to have a greater capability in dissipating energy.This could be due to the increase frictional contact in the higer wire rope diameter and hence

those isolators provide larger damping capacity than isolators with smaller wire rope diameter. The hystereiss curve of the WRI with a greater wire rope diameter (Isolator Nos. 7, 8 and 9) has shown an increased hysteresis area (Figure 4.30). This larger hysteresis area indicates these WRIs can dissipate larger amounts of energy per cycle.Thus, geometrically different isolators were found to have similar damping effectiveness, but different damping capacities.

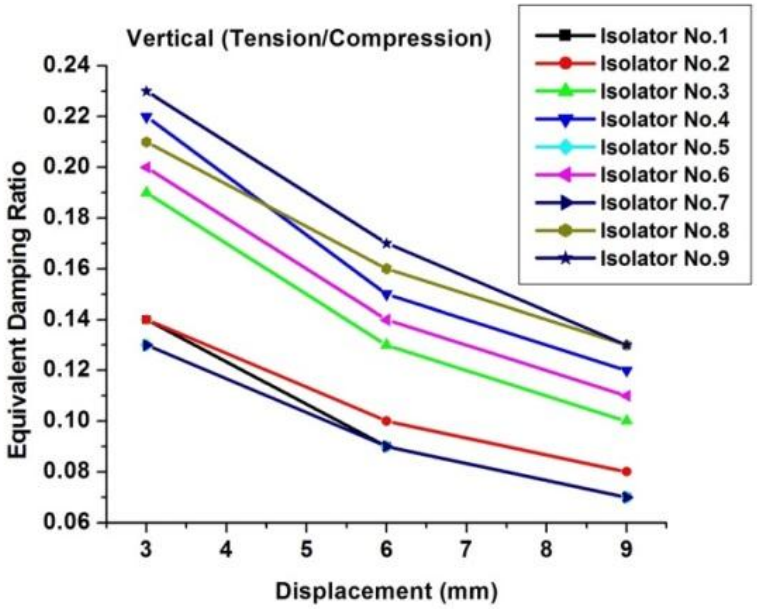

Figure 4.29 Equivalent damping ratio of the WRIs for various displacement amplitudes under vertical cyclic loading

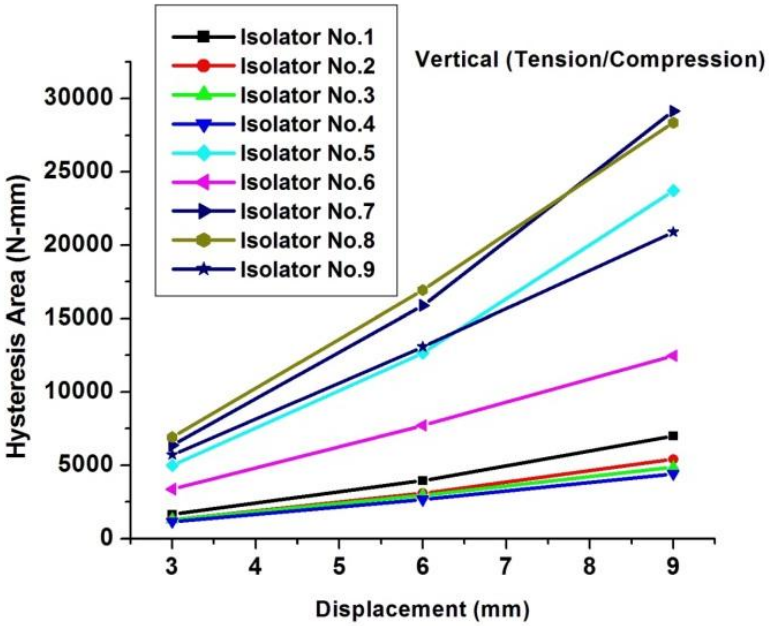

Figure 4.30 Hysteresis area of the WRIs under various displacement amplitudes under vertical cyclic loading

4.3.3.2. Equivalent damping ratio for Roll

Figure 4.31 shows the variation of the Equivalent Damping Ratio of various isolators during the roll test is a function of the displacement amplitude. For a 3 mm displacement amplitude, the EDR varied from 0.16 to 0.27. When the displacement amplitude was increased to higher values, the EDR decreased as observed in the vertical direction. For a 6 mm displacement, the equivalent damping ration decreased on average by 25 % which was lower than the vertical direction. The similar result in the decrease of the equivalent damping ratio with respect to wire rope diameter was observed. Based on this result, it can be understood that the WRI with a greater wire rope diameter has a higher damping capability. However, the amount of damping required for the application depends on the amount of isolation required. The hysteresis area (Figure 4.32) in the lateral direction also increased for higher displacment as seen in the case of the vertical direction. The larger wire rope diameter of a WRI showed a higher hysteresis area which shows that they can dissipiate more energy than the WRI with a smaller wire rope diameter.

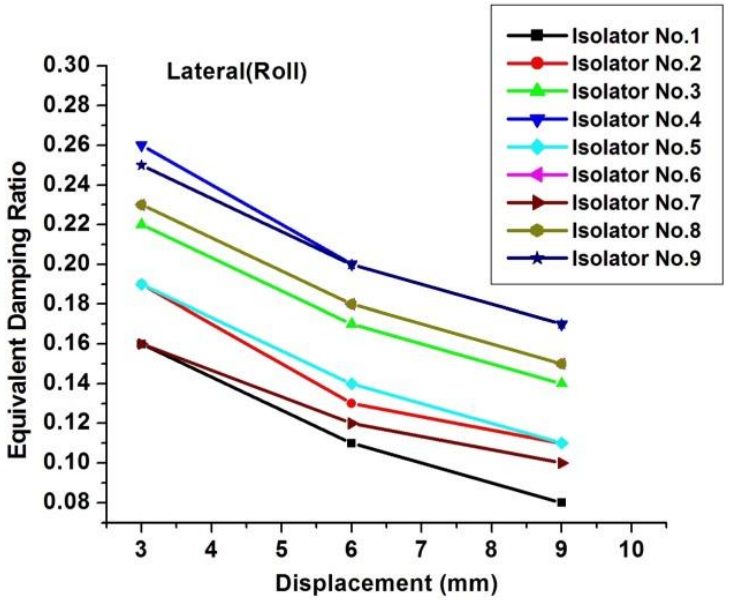

Figure 4.31 Equivalent damping ratio of the WRIs for various displacement amplitudes under lateral loading

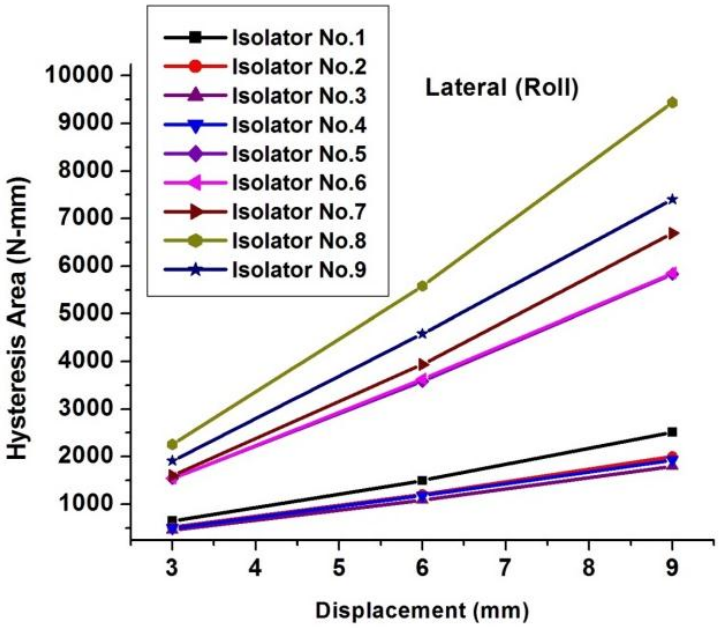

Figure 4.32 Hysteresis area of the WRIs under various displacement amplitudes under lateral cyclic loading

4.3.3.3. Effect of Height to Width ratio and Displacement amplitude

Figure 4.33 shows the equivalent damping ratio against the H\W ratio and it can be observed, as in the case of elastic force, increasing the value of H\W decreases the equivalent damping ratio in both directions. With respect to direction, lateral direction

provides better isolation than vertical for a equivalent displacement as in Figure 4.33**.** A similar observation also made on all the tested isolators. Figure 4.33 can be used in applications which demand better isolation and based on these curves, the WRI can be oriented to take the excitation in the lateral direction and further, can also be designed with a low H\W to achieve the desired level of damping. It can be observed that the equivalent damping ratio decreased by increasing displacement. Hence, in applications, which need high levels of damping, an isolator can be designed to achieve smaller displacements.

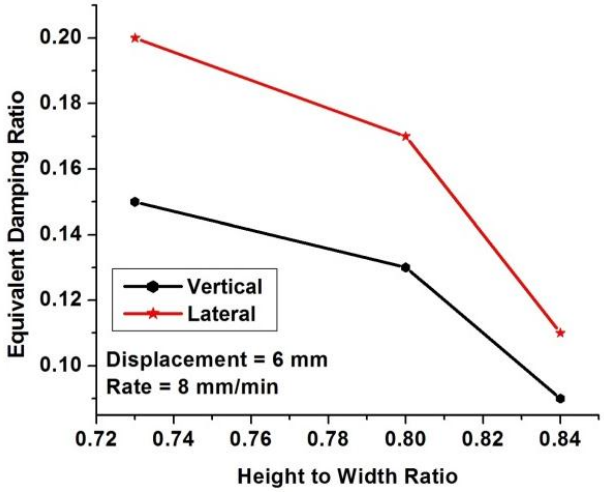

(a)

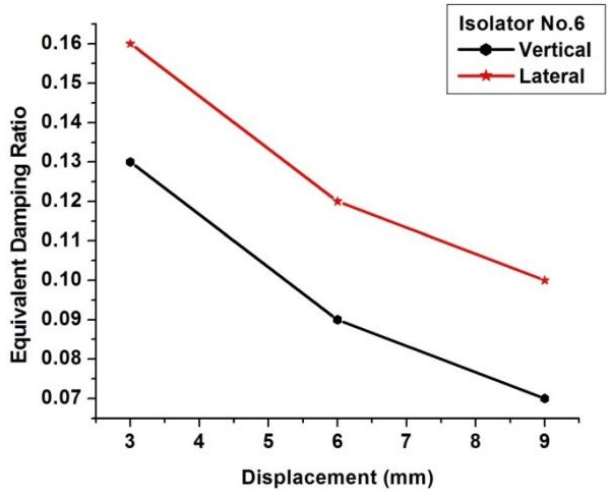

(b)

Figure 4.33 Equivalent damping ratio against (a) H\W Ratio (b) Loading direction

When the H\W ratio can be lowered to achieve an increased damping ratio, the low value of H/W may not always be suitable to the application in terms of the magnitude of the energy dissipation required. Figure 4.34 shows the hysteresis area against displacement and it can be observed that the hysteresis area increases because of higher displacement. The hysteresis area is the amount of energy dissipated from the cyclic loading. A closer examination of Figure 4.30 and Figure 4.32 reveals the isolators with higher values of H/W ratio have an increased hysteresis area than other isolators with the same wire rope diameter. Hence, in the application, which requires high energy dissipation, WRIs with a high H/W ratio can be preferred. Similarly, regarding the dependence of direction of loading on the energy dissipation, the vertical direction was found to dissipate relatively higher energy than the lateral direction (Figure 4.34). This fact can be used in the orientation of the WRI for this type of application.

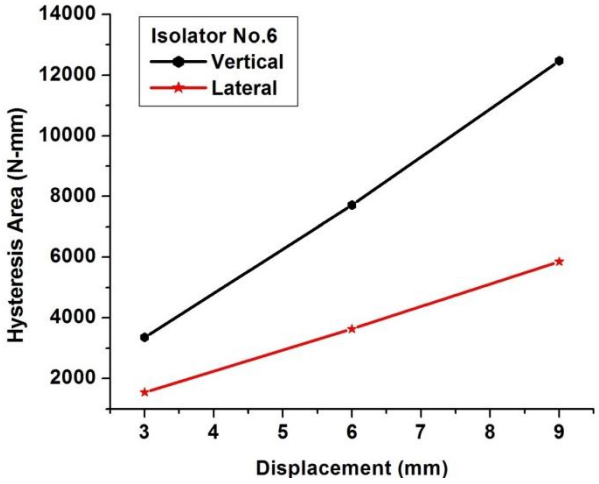

Figure 4.34 Hysteresis area against displacement in vertical and lateral direction

4.3.4. EFFECTIVE STIFFNESS

The effective stiffness of the WRI is defined as the ratio of the differences between the maximum and minimum forces to the maximum and minimum displacement amplitudes as given by Eq. (4.3).

$$K_{eff} = \frac{F_{\max} - F_{\min}}{X_{\min} - X_{\min}} \tag{4.3}$$

where *F* and *X* represents force and displacement respectively, and subscripts *max* and *min* represent the maximum and minimum ranges. The effective stiffness is dynamic and it is calculated after one complete cycle of loading and unloading. To determine the exact value of static stiffness, it is required to perform a static loading of the WRI. The dynamic effective stiffness is an indicative quantity, which helps us to understand the increment or decrement of the WRI's stiffness under cyclic loading. This effective stiffness can be viewed as the linear interpolation of the hysteresis curve. Furthermore, by evaluating the stiffness for tension and compression load individually, the hardening and softening of the isolator is also available.

Figure 4.35 shows the K_{eff} in vertical and lateral directions for various displacements. It was observed that the K_{eff} decreases with higher displacements. This decrease shows the softening behaviour of WRI under higher displacements. For both directions, a similar trend in K_{eff} was observed. The WRI with a greater wire rope diameter has a relatively higher value of K_{eff} and as can be seen No.7 has highest value of K_{eff} among all other WRI. However, it was also observed that another parameter, the Height to Width ratio (H/W) also significantly influences the K_{eff}. The Isolator No. 9 though has a greater value in diameter but a lower K_{eff} than Isolator No.5, which is due to the Higher Height to Width ratio.

This observation shows that the higher value of stiffness can be achieved from the smaller wire rope diameter by suitably adjusting the H\W ratio. As can be observed the effective stiffness declines for higher displacements. This is due to the fact that at a higher displacement, the wire rope strand moves further away, resulting in less contact surface and friction. The greater wire rope diameter has an increased value of effective stiffness due to increased wire rope diameter. However, the WRI with lesser H\W ratio for same diameter has higher value of EDR.

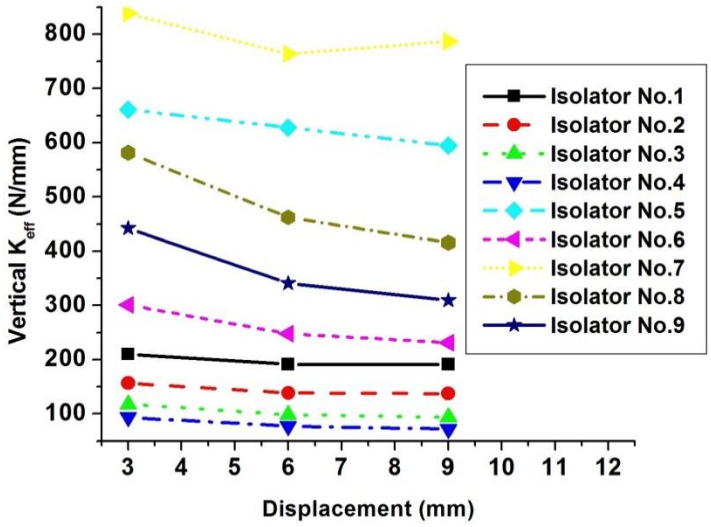

(a)

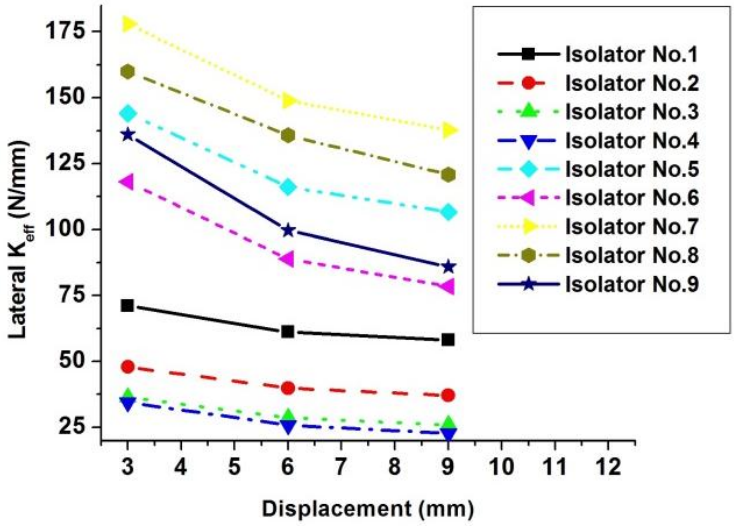

(b)

Figure 4.35 Effective stiffness under various displacements for all WRIs (a) Vertical (b) Lateral

The significance of the H\W ratio in the stiffness contribution can be understood from Figure 4.36. The isolators No.1, 3 and 4 which had the same wire rope diameter and length however, had different height to width ratios were compared. Figure 4.36 shows the effect of the H/W ratio against the effective stiffness. The effective stiffness was obtained in each loading for example, tension, compression and roll at 6 mm displacement amplitude. As can be observed for loading in both vertical and lateral directions, the higher H\W ratio shows a greater stiffness. The higher value of the H\W ratio induces greater hardening than the WRI with a similar wire rope diameter. From an

isolation of system point of view, softening is desirable since softening reduces the natural frequency of the system and hence better isolation at low frequency excitations can be achieved. Therefore, any hardening can be undesirable for the low frequency excitations. Hence, the lower H/W ratio can be used for isolation against low frequency excitation. On the other hand, orientation of the WRI can be adjusted, depending on the fitting provision to load the excitation in the lateral mode of WRI.

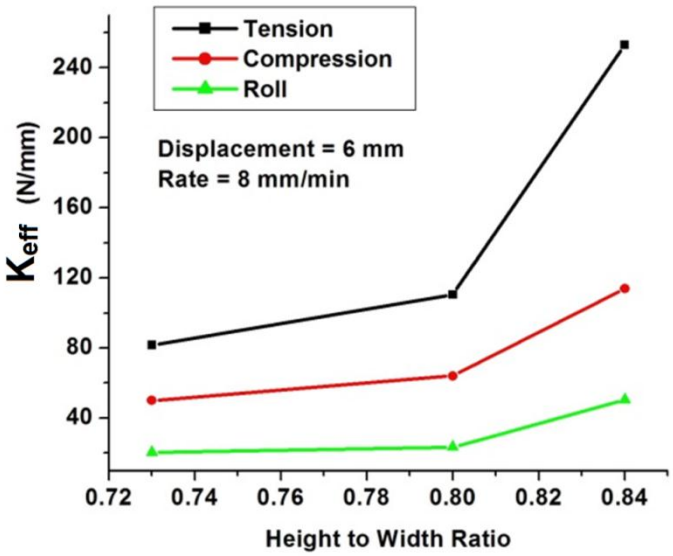

Figure 4.36 Effect of displacement on effective stiffness on various H\W ratio

Figure 4.37 shows the effective stiffness against displacments for tension, compression and roll load. The effective stiffness under compression declines with higher displacment, indicating softening behaviour. However, under tension elastic, sitffness increases due to the hardening. For the roll load, stiffness was constant for the tested displacement range and hence, the hysteresis curve was symmetric. This result suggests in the applications where the system is supported from the top, it may be supported in the compression mode rather than the tension mode as shown in the Figure 4.38. This is due to the softening behaviour of the WRI under compression which improves the isolation by reducing the natural frequency of the system. These findings are reported in this section and in the next section along with the mathematical model developed for the hysteresis behaviour of WRI. This mathematical model can be used to predict the hysteresis behaviour of WRI for various displacement amplitudes.

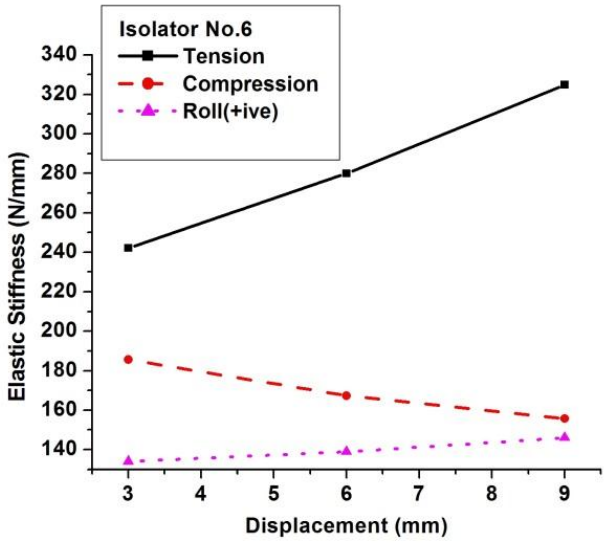

Figure 4.37 Effective stiffness in Tension, compression and roll loads for various displacement amplitudes

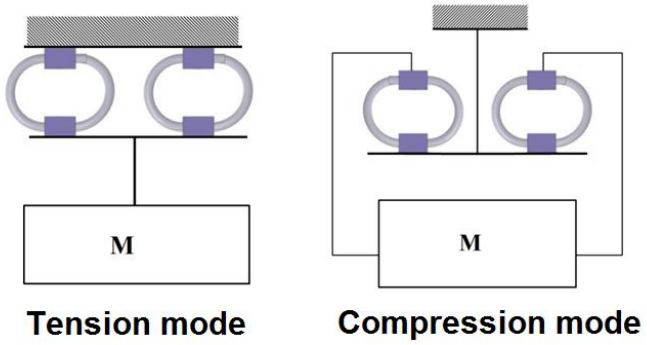

Figure 4.38 Loading modes of the WRI when supporting from top

4.4. MATHEMATICAL MODELING OF HYSTERESIS BEHAVIOUR

4.4.1. INTRODUCTION

In Section 4.3, the results of the hysteresis behaviour of the WRI were discussed and were observed the WRI exhibits hysteresis curve under cyclic loading, due to its frictional damping phenomenon. Further, the study also showed that the geometric characteristics of the WRI significantly influence the hysteresis behaviour. The cyclic loading test was performed under 3 different displacement amplitudes: 3 mm, 6 mm and 9 mm. The study was limited in terms of the inability to predict the hysteresis behaviour of the WRI in the other displacement amplitudes, which were not included in this test.

Hence, it is desirable to develop a mathematical model that can predict the hysteresis behaviour at any required displacement amplitude and further, such mathematical models can be used to study the performance of the WRI for various excitations. Hence, there is a requirement for the mathematical model for the hysteresis behaviour of the WRI. In this section, mathematical models for the WRI hysteresis behavior in both vertical and lateral directions are discussed.

The development of an analytical model for the hysteresis behaviour, with a closed form solution is a challenging task. The relation between the restoring force and displacement is highly dependent on the nonlinear contact between the wire strands and wires. The literature lacks any analytical understanding of the wire strands interaction (Ismail *et al.*, 2009a). Therefore, the study mathematically related the input and output through the physical understanding of the hysteresis system. Further, due to this type of approach, some researches also have referred their models as "Semi-Physical" (Ismail *et al.*, 2009a). Section 2.2 discussed the literatures on the mathematical models for the hysteresis behaviour.

In this study, Bouc-Wen Equations were used for the mathematical model of the WRI hysteresis behaviour. A hysteretic semi-physical model was proposed initially by Bouc in 1971 and later, generalized by Wen in 1976 (Ismail *et al.*, 2009a). Hence, the model is referred to as the Bouc-Wen model or Bouc-Wen equation in the literature. This equation has been used extensively in the modeling of hysteresis in mechanical and civil engineering. The Bouc-Wen model is a first-order non-linear differential equation that hysterically relates input displacement with the output restoring force (Demetriades *et al.*, 1993;Wen, 1976;Song and Kiureghian, 2006). The Bouc-Wen equation is used to model the hysteresis behavior under cyclic loading in both vertical and lateral directions. The available Bouc-Wen equation can be used to model a symmetric hysteresis loop as in the case of shear and roll load behaviour. However for tension/compression, the hysteresis loop is asymmetric, hence some modifications need to be incorporated. The model for the hysteresis curve can be used to predict the response of the WRI for any displacement amplitudes.

The Bouc-Wen equation has a set of parameters called the Bouc-Wen parameters and Bouc-Wen equation relates the restoring force and the displacement through these parameters. The Bouc-Wen equation is used to model the hysteresis behaviour of each WRI individually and the parameters of the Bouc-Wen are estimated using the corresponding hysteresis behaviour of the WRI. In this study, the mathematical model was performed using the Bouc-Wen model and the corresponding model parameters were identified using the least square method from the test results. The asymmetric hysteresis behaviour of the WRI in the vertical direction was modeled using a modification in the Bouc-Wen equation and is discussed in section 4.4.3.

4.4.2. LATERAL SYMMETRIC HYSTERESIS CURVE

The WRI exhibits non-linear hysteresis behaviour for the force-displacement relation when subjected to cyclic shear loading. This nonlinear input-output relation is due to the memory effect. The memory effect refers to the memory nature of these systems with inelastic behavior, in which the resorting force depends on both instantaneous deformation and the deformation history. The Bouc-Wen model(Bouc, 1971;Wen, 1976;Wen, 1980) is a first-order nonlinear differential algebraic equation, which hysterically relates input displacement and output restoring force. The generalized Bouc-Wen equation of the hysteresis curve (Figure 4.39) is represented by,

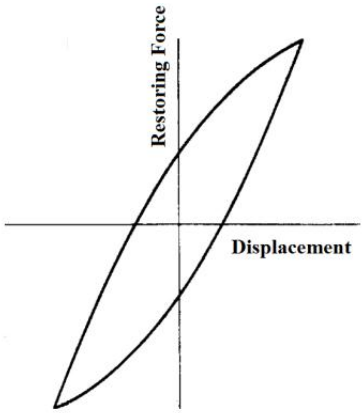

Figure 4.39 Symmetric hysteresis curve

$$F = \alpha \frac{F_Y}{Y} U + QZ \tag{4.4}$$

where F is the restoring force, U is the displacement and Q is the characteristic stregth given by $(1-\alpha)F_Y$. Z is a hysteresis dimensionless quantity defined by the following differential equations,

$$Y\dot{Z} + \gamma\left|\dot{U}\right|Z\left|Z\right|^{n-1} + \beta\dot{U}\left|Z\right|^{n} - A\dot{U} = 0 \tag{4.5}$$

In Eq.(4.5) the model parameters A, γ, β *and* n governs the amplitude, the shape of the hysteresis loop, and the smoothness of transition from the elastic to the inelastic region. Different choices of model parameters control the shape of the hysteresis curve. The parameter *A* controls the hysteresis loop's slope at Z =0 and an increase in parameter *A* and *n* makes the hystersis loop narrower (Ismail *et al.*, 2009a). When employing the Bouc-Wen model to a pratical application, it is required to identify the parameters with respect to the intial experimental data to enable the B-W model to predict the response. This identification of the model parameters use system identification techniques. In the present work the least square least square method (Loh and Chung, 1993) was used to identify the system paramters, so that the output of the model matches as accurately as possible with the research data. Generally, the Bouc-Wen equation can be used to model a symmetric hysteresis loop as in the case of lateral behaviour of WRI. However for tension/compression, the hysteresis loop of the WRI is asymmetric, hence some modifications need to be incorporated.

4.4.3. VERTICAL HYSTERESIS BEHAVIOR OF WRI

The hysteresis behaviour of the WRI is asymmetrical due to the hardening and softening effect. The WRI undergoes hardening and softening under tension and compression, respectively. A mathematical model for the asymmetric hysteresis can be developed using the Bouc-Wen equation by understanding the terms used in the equation. The Bouc-Wen equation (Eq.(4.4)) models the restoring force as a sum of the elastic force and the damping force. In the Eq.(4.4), the first term represents the elastic force and second term represents the history dependent damping force. The mathematical modelling of the hysteresis behaviour was developed by constructing the individual components of the Bouc-Wen model. For the symmetric hysteresis curve, the plot of the elastic and damping force is shown in Figure 4.40. The elastic force and

damping force for the asymmetric hysteresis curve is shown in the Figure 4.41. As can be observed the elastic force component of the restoring force induces the asymmetric nature and hence, it needs to be adjusted in the Bouc-Wen model. However, the available Bouc-Wen equation can satisfactorily model the damping force component. Therefore, a modification in the elastic force model is desired to agree with the test results. The nonlinearity in the elastic force of an isolator can be modeled using either multi-linear or bilinear depending on the amount of nonlinearity. In this work, this component is modeled as a bilinear model using a unit step function since, the bilinear was found to predict with good agreement. The modification as a bilinear model was demonstrated in the present work however, it can be extended to multi-linear using the same methodology.

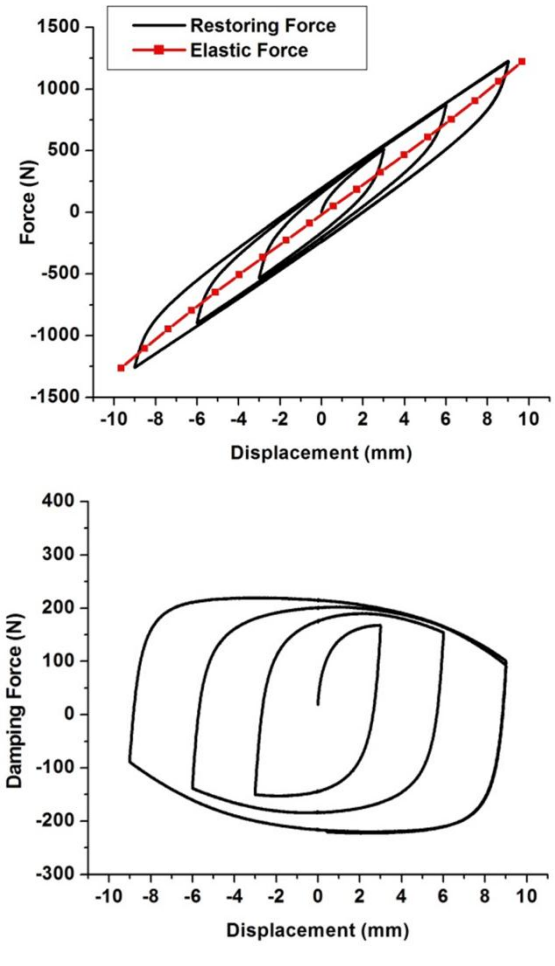

Figure 4.40 Bouc-Wen Equation in lateral direction (a) Elastic force (b) Damping force

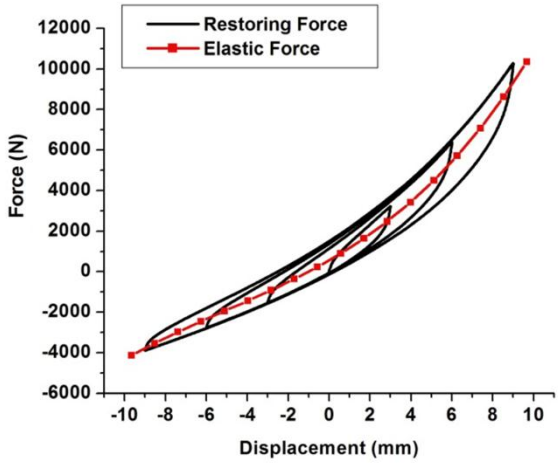

(a)

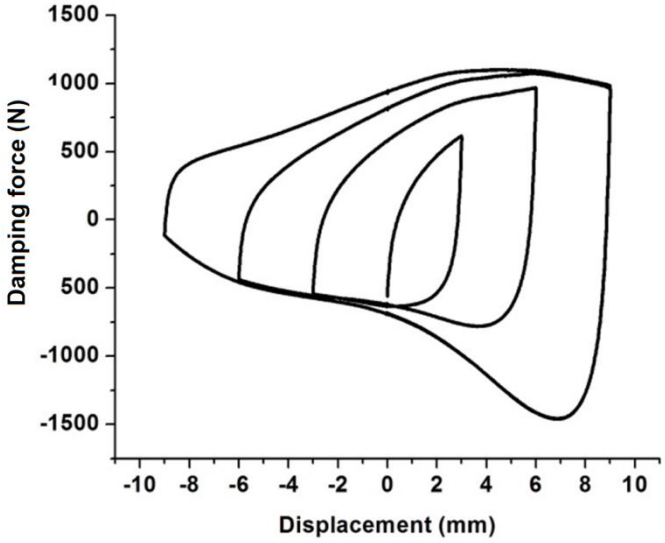

(b)

Figure 4.41 Restoring force components in vertical direction (a) Elastic force (b) Damping force

The nonlinear elastic force from the test results was modelled as a bilinear model. Figure 4.42 shows the bilinear model adopted and the parameters used in the mathematical model. Eqs (4.6)-(4.7) show the bilinear model. In this equation, the first term was modified with a bilinear formulation using the step function however; the second term was kept as per the original Bouc-Wen model. The parameter identification of this model was performed using the test results and the least square method.

$$F = f + (1-\alpha)F_Y z \tag{4.6}$$

$$f = kx + \begin{cases} 0 & x_1 \le x \ge x2 \\ k_1(x_1 - x) & x < x_1 \\ k_2(x - x_2) & x \ge x_2 \end{cases} \tag{4.7}$$

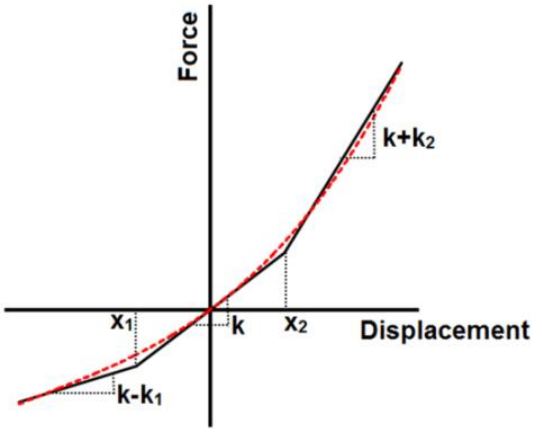

Figure 4.42 Bilinear model used in this work

4.4.4. SOLVING BOUC-WEN EQUATIONS

The Bouc-Wen equation for vertical (Eq. (4.6)) and lateral (Eq.(4.4)) are a class of mathematical equation called, "Differential Algebraic Equations" due to the combination of an algebraic term and a differential equation term. The differential equation term expresses the damping force and this term relates the restoring force with the history of displacement. Due to the complexity in the equation from differential and algebraic terms, the numerical method is preferred. This solving method was used in conjunction with the least square method to identify the Bouc-Wen parameters. The z term in the damping force is the differential equation and it was solved by using the numerical method as discussed in this section. This method is based on the work done by Haukaas and Kiureghian (2014)

z is a dimensionless hysteresis quantity given by Eq.(4.8),

$$\dot{z} = \frac{A\dot{x} - \{\beta|\dot{x}|z|z|^{n-1} + \gamma\dot{x}|z|^{n}\}\nu}{\eta} \tag{4.8}$$

The dimensionless parameters $\beta, n, \gamma,$ control the shape of the hysteresis loop. And A, ν and η are varibles which control the material degradation. A dot denotes the differentiation with respect to time and Eq.(4.8) can be rewritten as:

$$\dot{z} = \frac{A-|z|^n\{\beta sgn(\dot{x}z)+\gamma\}\nu}{\eta}\dot{x} = \frac{\partial z}{\partial x}\frac{\partial x}{\partial t} \tag{4.9}$$

The equations of Baber and Noori (Baber and Noori, 1985) were considered for the material degradation and are given by,

$$A = A_o - \delta_A e \tag{4.10}$$

$$\nu = 1 + \delta_\nu e \tag{4.11}$$

$$\eta = 1 + \delta_\eta e \tag{4.12}$$

where e is defined by the rate equations,

$$\dot{e} = (1-\alpha)\frac{F_y}{Y}\big(1 + (1-\alpha)\big)\dot{x}z \tag{4.13}$$

And $A_o, \delta_A, \delta_\nu,$ and δ_η are user defined parameters.

The numerical method used to solve the Bouc-Wen equation to obtain the hysteresis response of the WRI and its algorithm for the program is provided in Appendix D. The method discussed in Appendix D was used for both vertical and lateral hysteresis curve however the elastic term of the Bouc-Wen equation was replaced with the bilinear approximation for the vertical hysteresis curve. A coding was developed using this algorithm to plot the hysteresis curve from the model. The shape of the hysteresis curve can be controlled by the choice of the input parameters. The test results of the WRI were used to identify the parameters using the least square method.

4.4.5. DISCUSSIONS

The two mathematical models developed for hysteresis behaviour, one each for the vertical and lateral directions, was validated with the test results. The parameters of the models were identified from the least square method. For the parametric identification, a single loop of a hysteresis curve at particular displacement amplitude was used and upon identifying the parameters the plot of the hysteresis was generated using the Bouc-Wen equations. The comparison between the experimental and mathematical was verified at each point in the hysteresis curve. This process was performed for all the isolators at 6 mm displacement amplitude. Figure 4.43 shows the good agreement between the mathematical models and test results for Isolator No. 3 at 6 mm displacement amplitude

and a similar observation was also observed for all the isolators. However in the validation process, it was also required to verify the ability of the Bouc-Wen equations to predict the hysteresis at other displacement amplitudes. Hence, the Bouc-Wen equations were also validated against 3 mm, 6 mm and 9 mm displacement amplitudes as well. Figure 4.44 and 4.45 show the comparison between the mathematical and experimental test results at the tested displacement amplitudes for isolator No.3 and No.6 respectively and similar observations was made for all the isolators.

The Bouc-Wen parameters identified for each isolator are shown in the Table 4-2 and Table 4-3 for vertical and lateral directions, respectively. Those parameters can be used to generate a hysteresis curve at any required displacement amplitudes. The WRIs used in this study are commonly used WRI sizes and hence for many applications the WRI required for the vibration isolation applications can be selected from this list. Hence the identification of the Bouc-Wen parameters can ease the selection of the WRIs for different applications. The commonly accepted procedure to select the WRI is given in the catalogue of the WRI manufacture (ITT Enidine Inc, 2014) which is based on the static stiffness of the WRIs using the linear approach. Such a linearized selection process is suitable for a linear isolator however, for a nonlinear isolator; it is more conservation selection approach.

The linearized approach can be assumed suitable for the excitations, which has a specific frequency such as in the mechanical disturbance due to the operation of heavy machinery. However, for the isolation against the random excitations as in the case of an earthquake, it may be more suitable to use a nonlinear model for a more accurate prediction of the isolation capability. The major reason for using the linearized approach was due to the lack of Bouc-Wen parameters in the literature for the effective modelling of WRIs. Therefore, in this study, the Bouc-Wen parameters for a wide range of WRIs were identified and this model can effectively predict isolation capability of the WRIs. In chapter 5, the performance of the WRIs was investigated for a special case and the selection of the WRI was performed using the Bouc-Wen parameters.

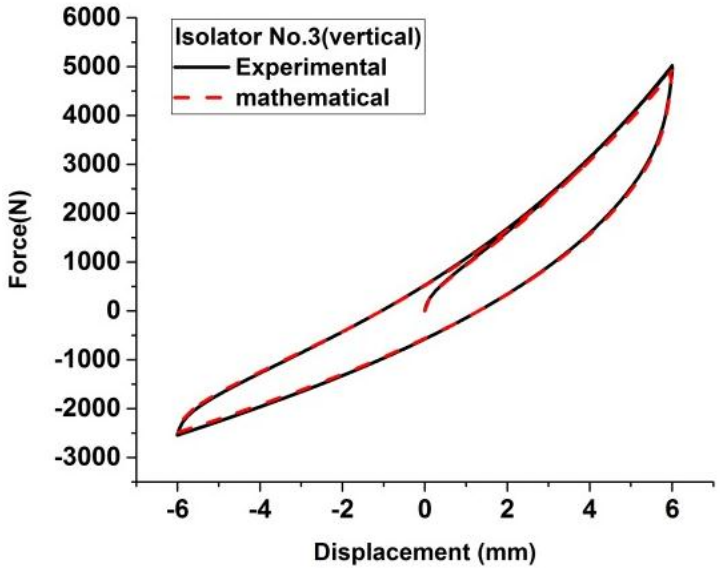

(a)

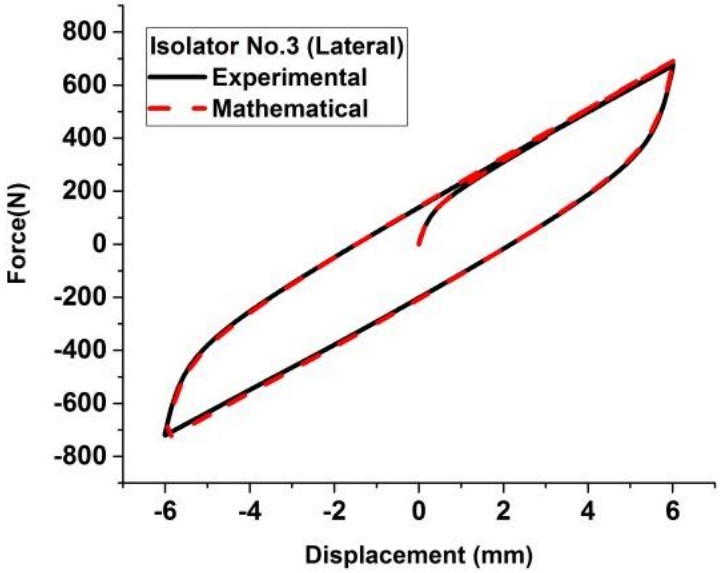

Figure 4.43 Comparison of mathematical and experimental test results (a) Vertical (b) Lateral

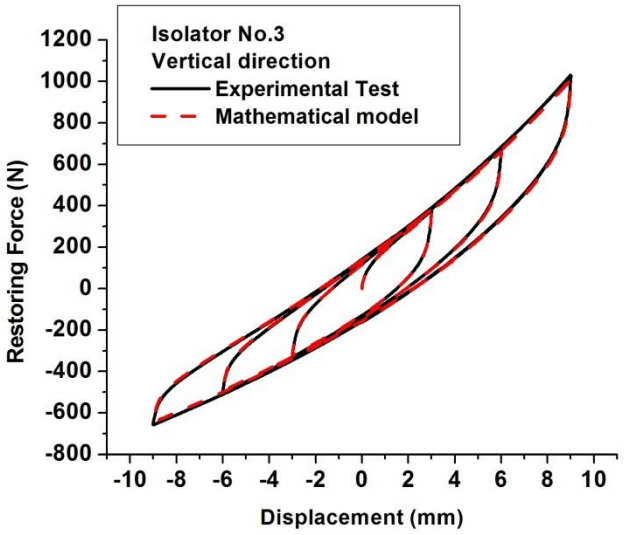

(a)

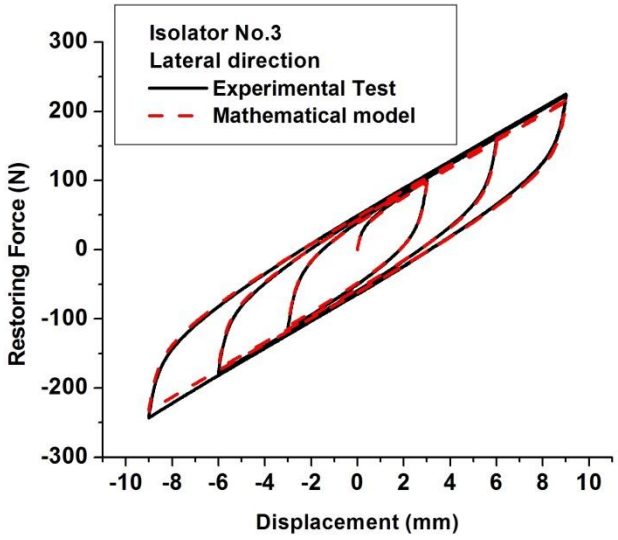

(b)

Figure 4.44 Comparison of Mathematical and Experimental results at all test displacement amplitudes doe isolator No.3 (a) Vertical (b) Lateral

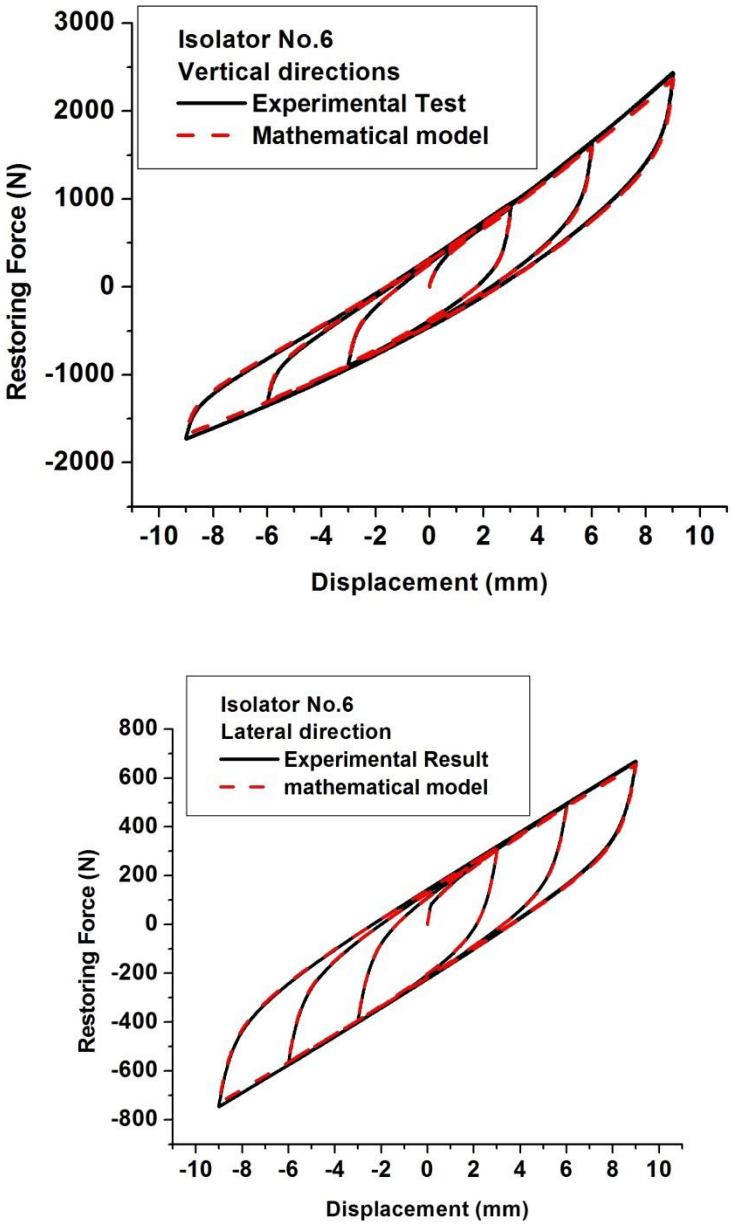

Figure 4.45 Comparison of Mathematical and Experimental results at all test displacement amplitudes doe isolator No.6 (a) Vertical (b) Lateral

Table 4-2. Model parameters for asymmetric hysteresis curve

Model Parameters	Isolator No.								
	1	2	3	4	5	6	7	8	9
k (N/mm)	146.65	119.83	68.47	58.84	552.49	180.12	366.00	317.46	218.76
k_1 (N/mm)	58.12	35.46	73.82	12.92	239.80	187.38	488.49	391.25	313.08
k_2 (N/mm)	122.91	59.37	36.15	16.13	746.39	71.04	550.06	87.60	76.54
x_1 (mm)	-4.61	-1.46	-7.55	-1.01	-1.03	-7.52	-8.14	-7.54	-7.88
x_2 (mm)	4.23	4.42	2.92	2.91	5.29	3.99	0.01	4.88	1.35
Q (N)	228.57	162.81	148.53	131.97	762.19	384.15	941.12	885.89	629.11
x_y(mm)	0.2549	0.2377	0.3565	0.345	0.2256	0.4058	0.5621	0.6378	0.4111
k_p (N/mm)	0.0138	0.0058	0.1	0.005	0.0146	0.095	0.0362	0.0368	0.0214

Table 4-3. Model parameters of symmetric hysteresis curve

Model Parameters	Isolator No.								
	1	2	3	4	5	6	7	8	9
k_e (N/mm)	205.15	151.69	105.30	103.37	300.35	270.65	350.64	310.45	290.33
Y (mm)	0.39	0.40	0.52	0.55	0.38	0.37	0.34	0.34	0.38
Q (N)	60.00	47.95	43.78	47.69	93.40	86.29	88.49	90.00	99.15
F_y (N)	79.45	60.42	54.49	57.18	113.45	99.41	118.51	104.18	111.12
α	0.2448	0.2065	0.1966	0.1660	0.1767	0.1320	0.2533	0.1361	0.1077
k_p(N/mm)	50.22	31.32	20.70	17.16	53.06	35.71	88.83	42.27	31.27

4.5. ENHANCEMENT OF STIFFNESS AND DAMPING CAPABILITY OF WRI

The selection and application of the WRI primarily depends on the amount of isolation required. However, especially in the retrofitting and in space applications, there is also another important factor to be considered which is the space requirement for placing the WRI. In the case of limited space applications to support a heavy weight and a higher energy dissipation capability, the WRI can be placed either underneath in tension/compression mode or in a roll or in shear model (Figure 4.2). Generally, the bigger the WRI size the higher the stiffness value for a heavy load. However, in the case of limited space, the larger size WRI may not be feasible to as shown in Figure 4.46. Hence, within the limited space available, the smaller-sized WRI need to be used to support a heavy mass. The smaller size has less weight carrying capacity and therefore,

there is a requirement to provide the required damping and stiffness within the limited space.

In the Section 4.3, it is shown that the stiffness and damping characteristics of the WRI is highly influenced by the geometric characteristics and hence by reducing the size of the WRI this will results in a reduction of stiffness and damping characteristics. In Chapter 3, the S-WRI design was discussed which mainly increases the vertical loading carrying ability However, the damping and lateral stiffness is not influenced. These designs may not serve the purpose of space limited applications. There is a need for a design which can support the loading and provide stiffness and damping along excitation directions.

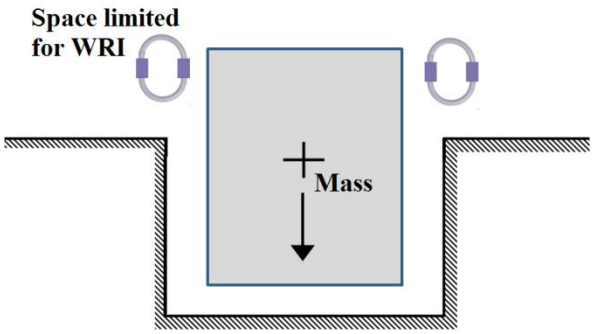

Figure 4.46 Limitation of space in the applications

4.5.1. DOUBLE-WRI (D-WRI)

In this study a new configuration called "Double-WRI (D-WRI)" was considered to enhance the stiffness and damping properties of the isolator. The D-WRI configuration is made by supporting the inside space of the 'big' WRI with a 'small' WRI as shown in Figure 4.47. The term "Big" refers to the outer WRI and the term "small" refers to the inner WRI. This design mainly depends on the geometric compatibility between the big and small WRI since the small needs to be placed inside the big WRI. Three samples of the D-WRI were fabricated in a mechanical lab (Figure 4.48). The big WRIs were Isolator No. 3, 5 and 8 for each sample respectively, each having different wire rope diameters. The combinations of the WRIs were selected based on the available WRIs and since three WRIs were already used for the S-WRI design, among the remaining WRIs in stock, the geometrically compactable were merged and for isolators No.3 and

No.5, two small WRIs Sm.1 and Sm.2 were purchased for this D-WRI design. The isolators used in the D-WRI configurations are shown in Table 4-4 and Table 4-5.

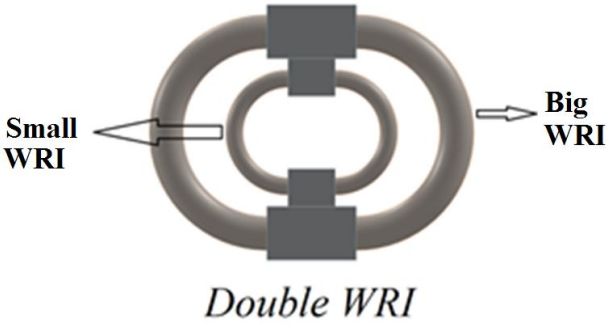

Figure 4.47 Schematic of D-WRI design

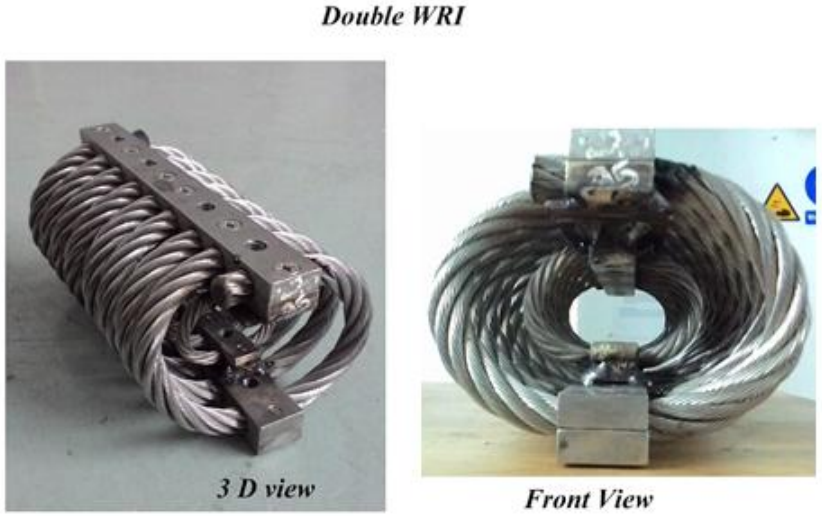

Figure 4.48 D-WRI fabricated in this work

The D-WRI design is different from the S-WRI design, which was discussed in Chapter 3. The S-WRI is designed to have an improved vertical loading carrying capacity however; the D-WRI is designed to have an improvement in both stiffness and damping in all directions. The small WRIs were welded together with the metal retainers of the big WRI as shown in Figure 4.49. This design was primarily developed to enhance the stiffness and damping characteristics of the WRI by compounding it with a small WRI inside. This configuration combines the benefits of both WRIs. From Figure 4.46 and Figure 4.50, it can be seen that within the limited space available, a single WRI

with required stiffness and damping was placed. By combining the two smaller size WRI for D-WRI design, the heavy mass can be supported and effective isolation can be provided. This proposed design can be tailored to suit any required stiffness and damping by a proper combination of WRIs and hence it is more robust and versatile in design.

(a)

(b)

Figure 4.49 Welding for joining two WRIs (a) Top metal retainer (b) Bottom Retainer

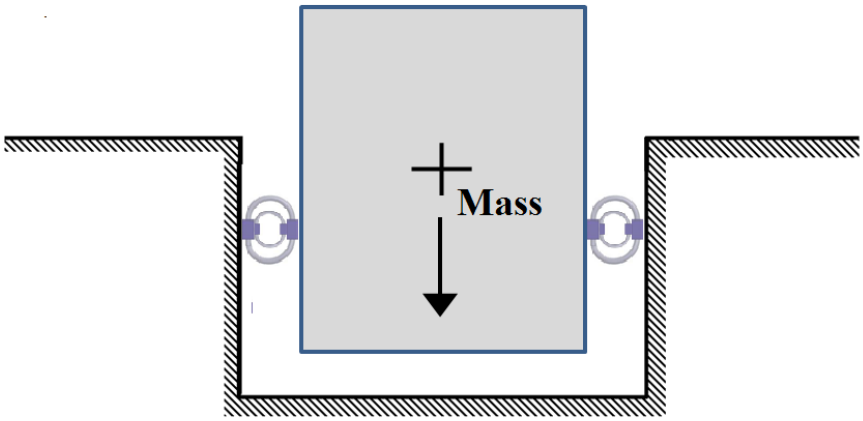

Figure 4.50 Application of D-WRI in the space limited applications

Table 4-4 Specifications of the small WRI used in this work

Isolator No	Wire rope diameter (D) (mm)	Number of coils	Width (W) (mm)	Length (L) (mm)	Height (H) (mm)
Sm.1	3.2	8	43	112	38
Sm.2	3.2	8	48	128	41

Table 4-5 Configuration of the D-WRI used in this work

D-WRI	Big WRI	Small WRI
D-WRI.1	Isolator No.8	Isolator No.1
D-WRI.2	Isolator No.6	Sm.2
D-WRI.3	Isolator No.3	Sm.1

4.5.2. STIFFNESS AND DAMPING ENHANCEMENT

The cyclic loading test was performed as mentioned in Section.4.3.1. The cyclic test was performed in both vertical and lateral directions to identify the effect of combining two WRIs and to evaluate the enhancement of the stiffness and damping of the D-WRI. The study's setup is shown in Figure 4.51. The metal retainers of the two WRIs were welded together and act as one WRI in all directions. This design is very versatile and robust since a number of WRIs can be placed one inside the other to achieve the stiffness and damping enhancement. However in the case of having more than 2 WRI, the care should be taken in providing adequate space between the WRIs so

displacements can be made without hindering each other. The tests were carried out to study how the WRIs act together. Figure 4.52 show the hysteresis behaviour of the D-WRI under cyclic loading.

The effective stiffness and equivalent damping ratio were evaluated for each D-WRI at various displacement amplitudes and is shown in Table 4-6 to 4-10. A comparison of the effective stiffness and equivalent ratio were made with a single WRI (Big) to understand enhancement for the equivalent height of the isolator. It can be seen that both stiffness and damping were enhanced with this D-WRI design. The proper combination of the WRI can be made based on individual requirements. This study shows the hysteresis characteristics of the D-WRI can be expressed as the sum of the hysteresis curve of big and small WRIs as shown in Figure 4.53. Furthermore, the improvement in the D-WRI can be estimated using the individual hysteresis curve of the WRIs, provided both WRIs are geometrically compatible.

(a)

(b)

Figure 4.51 Experimental setup for cyclic loading test of D-WRI (a) Vertical (b) Lateral

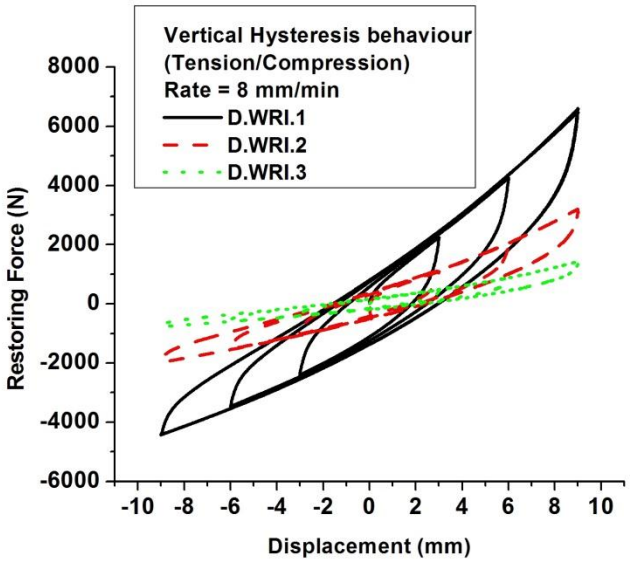

(a)

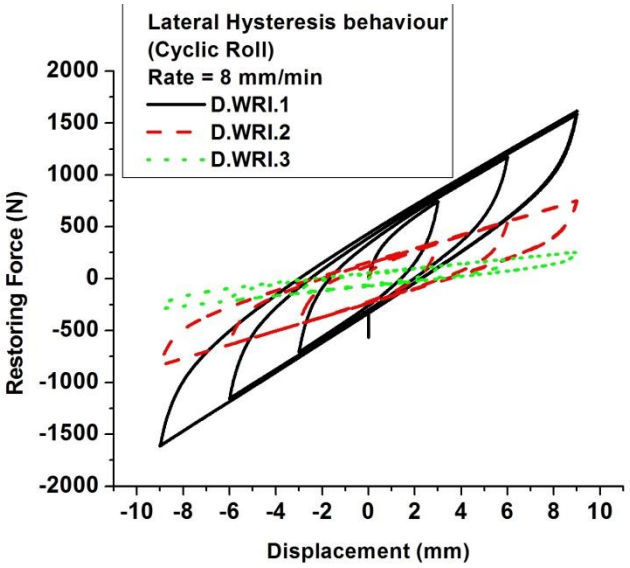

(b)

Figure 4.52 Cyclic loading test results of D-WRIs (a) Vertical (b) Lateral

Table 4-6 Effective stiffness comparison for D-WRI and WRI in vertical direction

D.WRI	Displacement amplitude (mm)	Effective stiffness (N/mm)	
		D-WRI	WRI
D.WRI.1	3	774.50	581.25
	6	643.74	462.16
	9	602.99	415.68
D.WRI2	3	351.51	300.77
	6	296.73	248.00
	9	286.59	231.06
D.WRI.3	3	142.02	117.57
	6	121.55	98.27
	9	119.15	93.60

Table 4-7 Effective stiffness comparison for D-WRI and WRI in the lateral direction

D.WRI	Displacement amplitude (mm)	Effective stiffness (N/mm)	
		D-WRI	WRI
D.WRI.1	3	241.99	176.81
	6	194.28	135.76
	9	177.47	120.87
D.WRI2	3	129.20	118.14
	6	98.43	88.87
	9	87.92	78.49
D.WRI.3	3	41.20	36.42
	6	32.72	28.67
	9	30.19	25.87

Table 4-8 Equivalent damping ratio comparison for D-WRI and WRI in the vertical direction

D.WRI	Displacement amplitude (mm)	Equivalent Damping Ration	
		D-WRI	WRI
D.WRI.1	3	0.23	0.21
	6	0.17	0.16
	9	0.14	0.13
D.WRI2	3	0.22	0.20
	6	0.17	0.14
	9	0.13	0.11
D.WRI.3	3	0.21	0.19
	6	0.15	0.13
	9	0.12	0.10

Table 4-9 Equivalent damping ratio comparison for D-WRI and WRI in the lateral direction

D.WRI	Displacement amplitude (mm)	Equivalent damping Ratio	
		D-WRI	WRI
D.WRI.1	3	0.25	0.23
	6	0.19	0.18
	9	0.17	0.15
D.WRI2	3	0.25	0.23
	6	0.19	0.18
	9	0.16	0.15
D.WRI.3	3	0.23	0.22
	6	0.18	0.17
	9	0.15	0.14

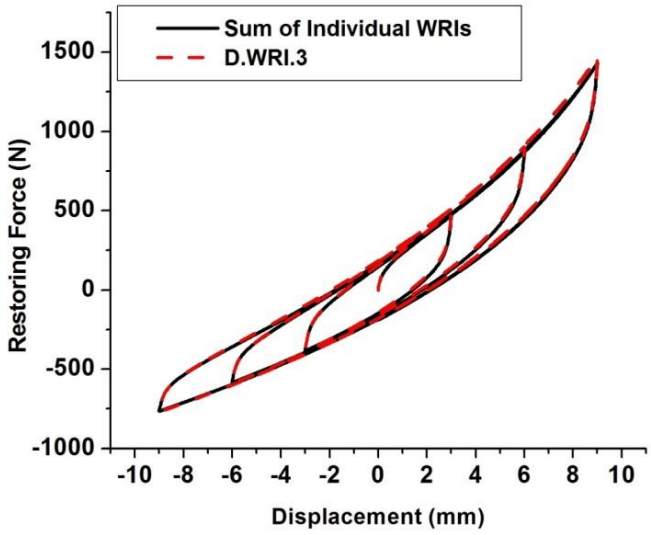

Figure 4.53 Comparison between sums of individual WRIs with D-WRI

4.6. SUMMARY

This study presented an analysis of the restoring force-displacement relation of the WRI under cyclic loading in vertical and lateral directions. The hysteresis behavior in the vertical direction was obtained from tension\compression loading and roll loading was used to determine the hysteresis behaviour in the lateral direction. The following conclusion can be drawn from this research:

1. The vertical hysteresis behavior of the WRI is asymmetric however, in the lateral direction, the WRI exhibits symmetrical hysteresis behavior.
2. The hysteresis behavior of the WRI is rate independent in both vertical and lateral direction
3. The WRI with a left and right coil orientation produces similar hysteresis and hence coil orientation effect can be ignored.
4. The WRI exhibits hardening under tension and softening under compression
5. An increased value of H\W, increases the hardening of the WRI.
6. An equivalent damping ratio reduces the higher displacement and hence the WRI can be designed for small displacements.

7. An increased value of the H\W ratio decreases the equivalent-damping ratio however, possesses a higher energy dissipation effect. Therefore, in case of a high-energy dissipation application, a higher H\W ratio can be used.
8. The mathematical model for the hysteresis behaviour was developed in this study using the Bouc-Wen equation.
9. For the vertical asymmetric hysteresis behaviour, the original Bouc-Wen equation was modified to model the asymmetric hysteresis curve. The model was validated with the test results and good agreement was observed.
10. The model identification for both models was performed using the least Square method. Furthermore, the modification of the Bouc-Wen model was proposed using the bilinear model.
11. The study shows that the effective stiffness and damping ratio was significantly influenced by the size of the wire rope diameter and furthermore, the height to width ratio can be used to achieve a wide variety of effective stiffness and the equivalent damping for similar wire rope diameters.
12. D-WRI configuration was developed and tested in this study. The test results show that the proper combination of the WRIs can provide enhanced stiffness and damping characteristics in both vertical and lateral direction.

Chapter 5. WIRE ROPE ISOLATORS FOR VIBRATION ISOLATION – A PERFORMANCE STUDY

5.1. INTRODUCTION

Vibration isolation techniques are used to protect a system from external excitations by isolating the system from its surroundings. In some cases, such as the operation of heavy machinery, a system is isolated to prevent the excitation from affecting the surrounding structures. It can be observed from Section 1.2 that low transmissibility can be achieved by reducing the natural frequency of the system using flexible isolators. The required amount of isolation can be achieved by designing an isolator with suitable stiffness and damping characteristics. In Chapter 3, analytical models of the vertical and lateral stiffness of the WRI were discussed to enable the effective design of the WRI. Furthermore in Chapter 4, the damping characteristics of the WRI was studied using a cyclic loading test and the mathematical models for the hysteresis behavior using the Bouc-Wen equation were also developed. To summarize the previous chapters, the understanding of the stiffness and damping characteristics of the WRI were discussed and in this chapter, the performance of the WRI in vibration applications is presented.

In this study, a special case of the performance of the WRI in vibration isolation using the raised floor approach in a three-storey structure was analyzed. This study involved the development of a set of simulation models subjected to a set of real time earthquake ground motions to study the performance of the WRI. The study evaluated the performance using the acceleration reduction and displacement of the isolated equipment. This study can enhance the understanding of the WRI in vibration isolation applications for various external excitations and extend the application of the raised floor approach using the WRI.

5.2. APPROACHES IN VIBRATION ISOLATION

In general, the mitigation of the vibrational response of equipment and structures can be performed through three approaches (Hamidi and El Naggar, 2007;Ismail *et al.*,

2009b): (1) Isolation of the entire housing structure, (2) Isolation of a single piece of equipment, or (3) Isolation of a raised floor system. The first approach (Figure 5-1 (a)) is suitable for new construction where isolators are installed between the structure and foundation to reduce the damage to both the primary structure and the equipment (Naeim and Kelly, 1999). The second approach (Figure 5-1(b)) concentrates only on the equipment; the isolation system is inserted at the base of the equipment to reduce the transmission of vibration. However, both of these approaches are confronted with a difficulty in achieving the desired long period effect within an affordable displacement (Demetriades *et al.*, 1993).

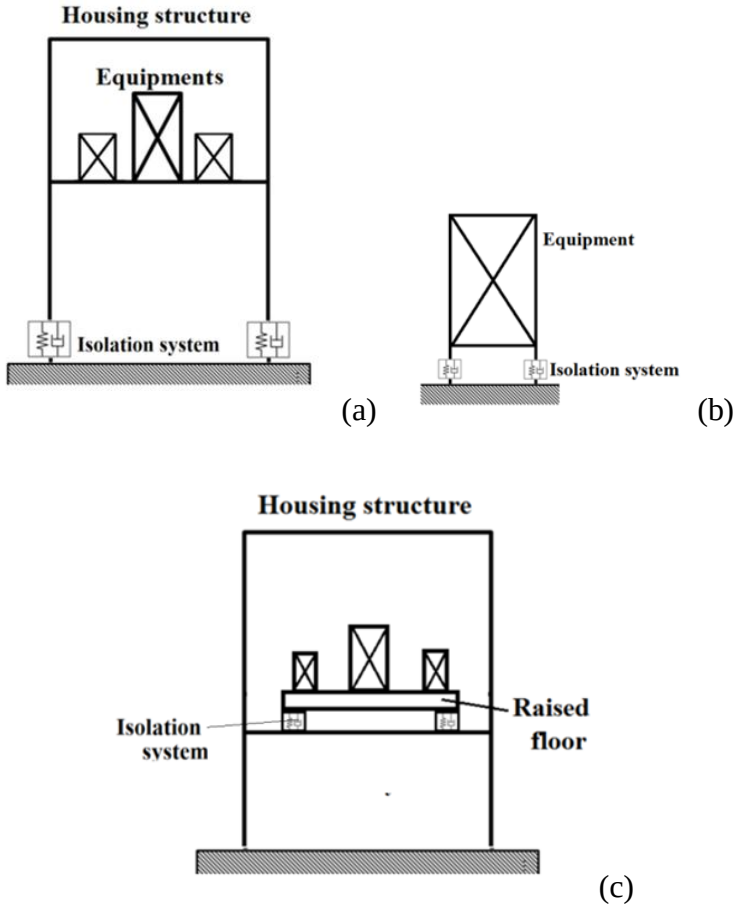

Figure 5-1 Types of isolation methods (a) Entire structure (b) individual equipment (c) raised floor method (de Silva, 2005)

In the third approach (Figure 5-1 (c)); several pieces of equipment are fixed to a secondary floor, which is then decoupled from the structural floor by an isolation

system. This approach provides the potential benefit to both new and existing constructions. The raised floor approach also possesses other advantages such as low cost when compared with the first and second approach and it can also provide a long period while maintaining affordable displacements (Ismail *et al.*, 2012a;Ismail *et al.*, 2012b). The raised floor isolation system also provides free space beneath the raised floor, which can be used for other purposes such as cooling air circulations, ventilation, passages for telephone and computer cables (Chang *et al.*, 1986).

Furthermore, the raised floor system enables easy access to the service area beneath the raised floor hence; the room facility can be relocated and reconnected conveniently (Chang *et al.*, 1986). Therefore, the raised floor approach is well established as an effective technique for the vibration mitigation of equipment (Ismail *et al.*, 2009b). The studies (Demetriades *et al.*, 1993;Ni *et al.*, 1999a;Alessandri *et al.*, 2015b;Alessandri *et al.*, 2015a;Massa *et al.*, 2013) on the performance of the WRI and have focused on the first two approaches but the literature lacks the study on the raised floor approach using WRI. Therefore, research on the perfromance of the WRI in a raised floor concept has been undertaken in this work.

5.2.1. WRI IN THE RAISED FLOOR APPROACH

The raised floor concept using WRI involves challenges in providing vertical support for the heavy mass of a raised floor-equipment configuration (Figure 5-2). The heavy mass of the system, often seen as advantageous in the application of vibration isolation, entails unique challenges to the WRI in terms of vertical loading carrying capacity (along Z in Figure 5-3). The WRI is available a in variety of sizes and the larger sizes of WRIs can handle a heavy mass. However, larger sizes have an increased lateral stiffness, which can reduce the lateral flexibility compared with the smaller WRIs. Furthermore, smaller WRIs have lateral flexibility yet lack the ability to support a heavy mass (along Z) due to its limited vertical loading carrying capacity. Hence, there is a requirement for a method to enable soft (small) WRIs to be used in heavy mass applications for better vibration isolation. The application of a raised floor together with a soft WRI can provide a solution to enhanced vibration isolation. In the previous chapters, the S-WRI and D-WRI designs were discussed and showed enhanced stiffness

and damping characteristics. However, those types of designs need more research and in this study, only preliminary tests to verify their effectiveness were performed. Therefore in this study, the challenge of supporting the heavy raised floor was overcome through a wire cable support technique as used in the work of Ni *et al.*(1999b).

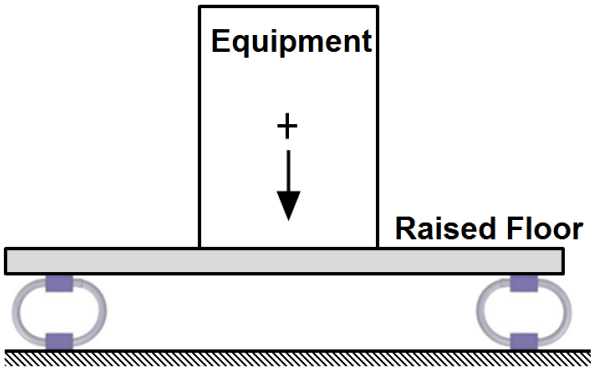

Figure 5-2 Equipment on Raised floor isolated using WRI

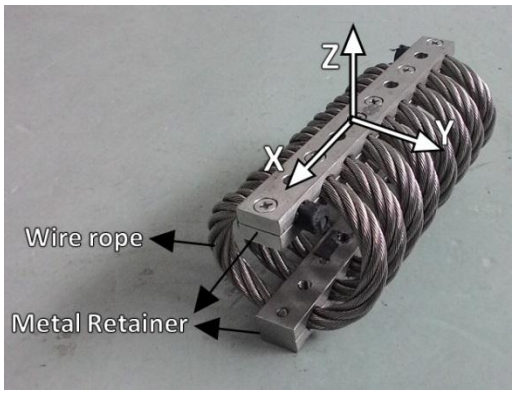

Figure 5-3 Wire Rope Isolators and its loading axis

Metal wire cables possess high loading carrying capacity along its axis (Velinsky, 1988). The cables are used in application to support weight and to lift the heavy machinery. The cables support the heavy mass vertically, but still allow the lateral movement of the mass as in the case of a pendulum (Ni *et al.*, 1999b). Ni *et al.*(1999b) performed the cyclic loading test on the WRI using setup shown in Figure 5-4. This setup consisted of two plates, a top and bottom plates, which were connected with the metal retainer of the WRI. The cyclic loading was applied from the bottom plate and in this; the weight of the top plate is supported with the wire cables. These cables vertically

support the top plate to avoid the preloading of the WRI due to the weight of the top loading and these cables provide lateral flexibility for cyclic loading. The length of the wire cables used in Figure 5-4 were large enough to provide the displacement of the WRI and therefore the influence of the wire cables can be ignored in the displacement of WRI.

Earlier, the wire cable support technique was also used by Ko *et al.*(1992) for their cyclic loading test and the results showed the wire cable system can be used to support the heavy mass to enable the application of WRIs for vibration isolation. In this research, the performance of the WRI was examined in the raised floor concept by using cables as a vertical load-carrying member. The equipment and the raised floor were vertically supported by the cables and laterally supported by the WRI. The performance of the WRI was analysed through the seismic response of the equipment mounted on an isolated raised floor.

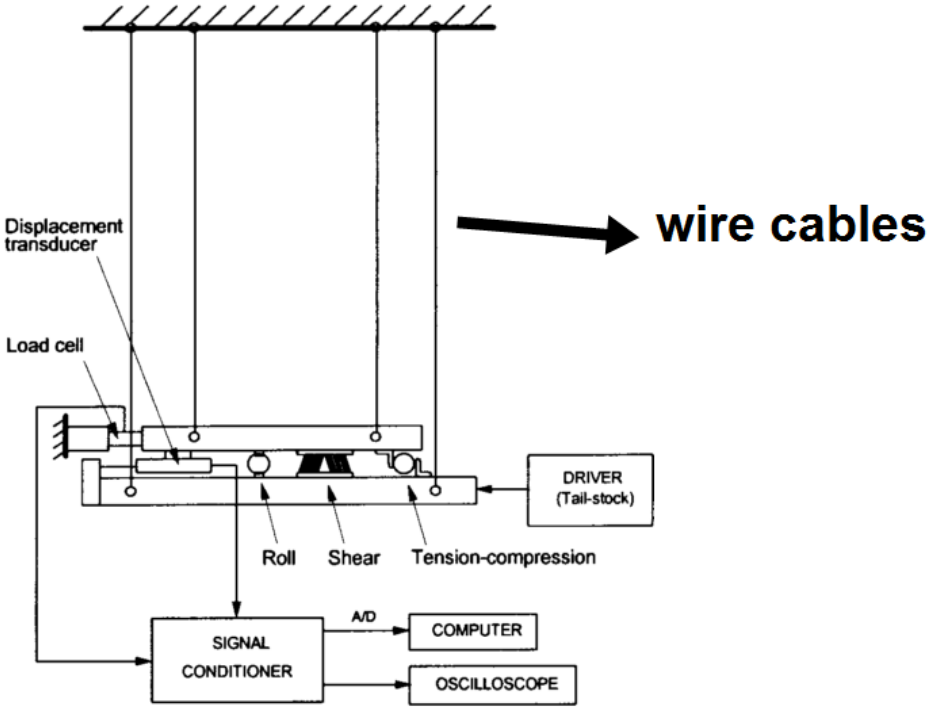

Figure 5-4 Cyclic Loading Setup used by (Ni *et al.*, 1999b)

5.3. METHODOLOGY

This section discusses the methodology used in this work. The numerical study is performed by considering equipment isolated by WRIs using the raised floor approach from the top floor of a 3-storey building. The raised floor was supported by the cables from the ceiling to support the weight of the raised floor and the equipment. Figure 5-5 shows the raised floor arrangement considered in the present study. The equipment used was referenced from Demetriades *et al.*(1992). Accordingly, the equipment is the computer cabinet having the weight of 1886 N and the fundamental time period of 0.097 seconds (Demetriades *et al.*, 1992). The numerical model was developed using the SAP2000 (2010) simulation program and the methodology used in this work was referenced from the work of Ismail *et al.*(2009b). They studied the performance of the type of isolator called "Roll-N-Cage Isolators" in the raised floor approach and this isolator provided the necessary isolation by reducing the natural frequency of the system and providing viscous damping. The wire rope isolator also provided isolation in a similar fashion but the damping is frictional damping. Therefore, the methodology used by Ismail *et al.*(2009b) was also adopted for this study.

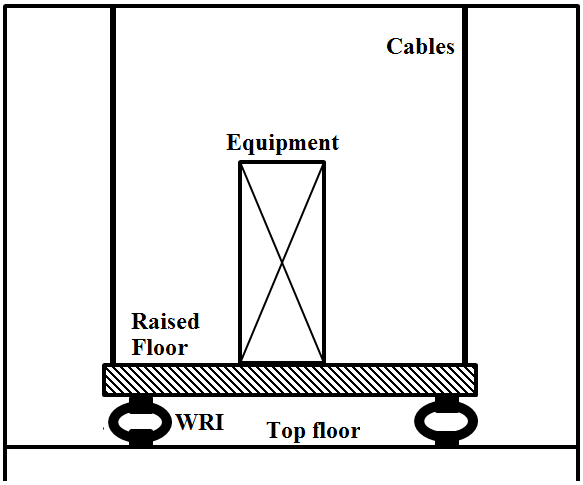

Figure 5-5 Isolated raised floor supported by the cable approach used in the present work

The raised floor was vertically supported using the wire rope cables and laterally by the WRI. The lateral behavior of the WRI was modelled using the Bouc-Wen model, which was explained in Chapter.4. The numerical model was subjected to 34 earth

quake excitations in the lateral direction to study the isolation ability of the WRI for a wide variety of earthquake excitations. The WRI to be used for this application was selected from the available isolators as given in Table 4-1. The selection of the WRI was based on the response spectrum of the equipment to earthquake excitations (de Silva, 2005). The earthquake records were obtained from the SAP2000 time history database. The performance of the WRI was evaluated using the acceleration response between fixed equipment on the top floor against the equipment isolated under the raised floor approach. The displacement of the isolator was also evaluated to analyse the compatibility of the WRI for the displacement demanded by the application. The numerical model details and the selection of isolation system will be discussed in the Sections 5.5-5.7. Finally, at the end of this study, the performance of all the WRIs for the raised floor approach under earthquake and harmonic excitations are reviewed.

5.4. MODELING OF LATERAL HYSTERESIS BEHAVIOR OF WRI

The raised floor was vertically supported by the wire cables and hence the vertical loading on the WRI can be ignored. The three-storey structure was subjected to the lateral earthquake excitation, and the isolation of equipment from the lateral excitation was provided through the lateral displacement of the WRI. Therefore, modelling the lateral behavior of the WRI was vital for the numerical model. This section presents model for the WRI in the lateral direction. Previous studies (Demetriades *et al.*, 1993;Paolacci and Giannini, 2008) on the cyclic behavior of WRI, found that it exhibits nonlinear hysteresis in the lateral direction. The mathematical model of the hysteresis curve was developed using the Bouc-Wen model of hysteresis, which provides smooth transition between elastic and plastic regions by avoiding gradient discontinuities (Wen, 1989). The Bouc-Wen model of hysteresis was used in this study to simulate the lateral cyclic behavior of the WRI. The Bouc-Wen model (Wen, 1980) is a first-order nonlinear differential algebraic equation, which hysterically relates the input displacement and the output restoring force. Its general form is given by:

$$F = \alpha \frac{F_y}{Y} x + (1-\alpha) F_y z \qquad (5.1)$$

where F is the restoring force, x is the displacement, F_y is the yield force, Y is the yield displacement and z is a dimensionless hysteresis quantity in the range of [-1, +1] and is given by:

$$Y\dot{z} = A\dot{x} - \{\beta|\dot{x}|z|z|^{n-1} + \gamma\dot{x}|z|^{n}\} \quad (5.2)$$

The dimensionless parameters $A, \beta, \gamma,$ and n control the shape of the hysteresis loop. The above hysteresis model was implemented using the SAP2000 (2010) as the Plastic Wen NL-Link element, which is recommended for 2D static and dynamic analysis. The parameters involved in the Bouc-Wen model (such as F_y, Y, α, $A, \beta, \gamma,$ and n) were used to mathematically define the behavior of the WRI in the simulation model to determine the response. The Bouc-Wen parameters can be determined using various techniques as discussed in Ismail *et al.*,(2009a) and this present study used the least square method due to its simplicity. Identification of the Bouc-Wen parameters requires initial experimental data and this data will then be used in the least square method, which performs the sequential regression analysis to obtain the values of the Bouc-Wen parameters. The Bouc-Wen parameters of the all the test WRIs was identified in Chapter 4 and used for this study.

5.5. NUMERICAL MODELING AND SIMULATION

To assess the performance of wire rope isolators in protecting equipment against earthquake-induced vibrations, the three-storey structure was considered. The equipment was mounted on a raised floor, which was connected to the 2nd floor through a wire rope isolator system. In this study, 4 WRIs were used to isolate the raised floor and equipment. The raised floor was vertically supported by the cables from the roof of the second floor. The analysis was conducted for the two cases (Figure 5-6): case (1) Equipment fixed to the hosting floor and case (2) Equipment is mounted on an isolated raised floor. The hosting structure consisting of reinforced concrete Moment Resisting Frame (MRF) and it was modelled as a linear shear building. This study mainly focuses on the performance of the isolation system and hence the nonlinearity is concentrated only at the isolation system level to reduce the computational time. For all structural

vibration modes, a 2% of critical damping was considered to incorporate the inherent structural damping (Ismail *et al.*, 2009b)

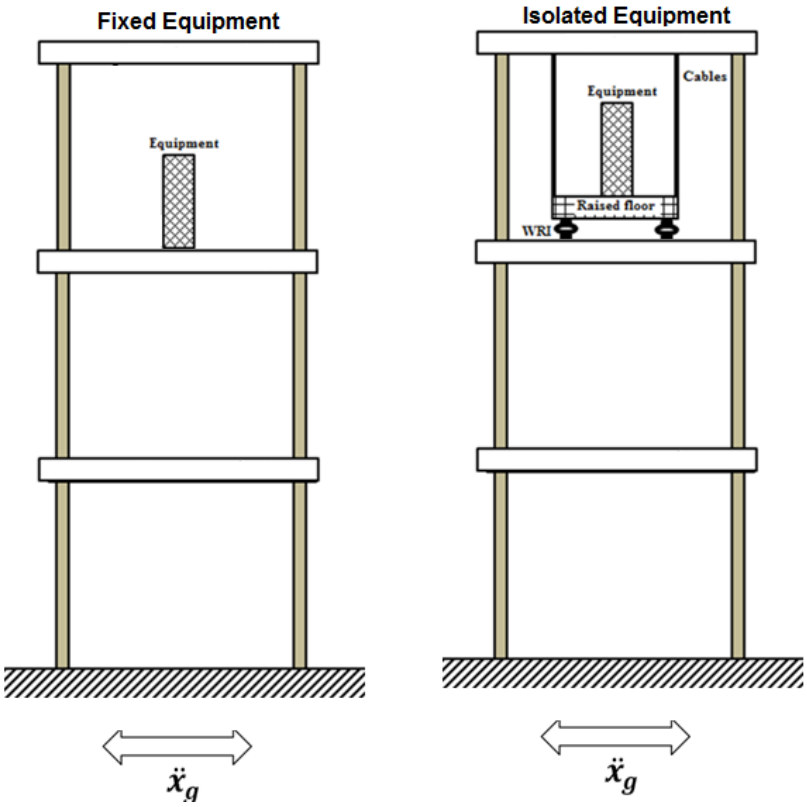

Figure 5-6 Fixed based equipment and isolated equipment using raised floor approach studied in this work

The numerical model of the three-storey structure is shown in Figure 5-7. The raised floor was modelled as rigid in the horizontal direction while the equipment is modelled as a linear single-degree of freedom system (SDOF) system with mass m_e , stiffness k_e and damping coefficient c_e. The equipment's damping was considered equal to the structural damping. Nonlinear earthquake response history analyses (RHA) were performed for the structure and equipment using the structural analysis program SAP2000 (2010). The Fast Nonlinear Analysis method (FNA) (Wilson *et al.*, 1998) was selected since the nonlinearity is concentrated at the isolation level only. As the name suggests, the FNA runs as fast as a linear analysis while maintaining a level of accuracy comparable to direct iteration methods. Preliminary simulation was performed to

determine the influence of the cable in the lateral displacement of the isolated raised floor. The preliminary results showed that the influence of the cables in the lateral displacement could be ignored due to the higher value of the length of the cable compared to the isolator displacement. Further, the equipment was found to have a significant lateral displacement with negligible vertical displacement. This shows that the weight of the raised floor–equipment was primarily carried by the cables and laterally supported by the WRI.

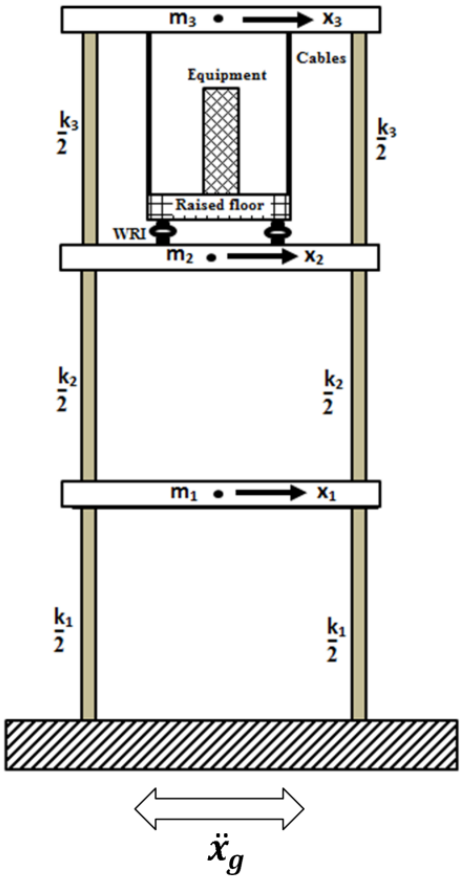

(a)

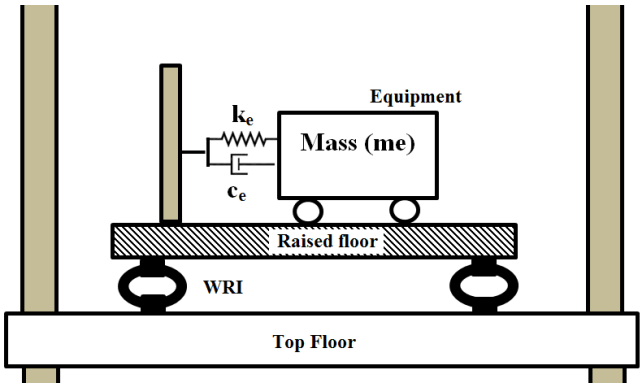

(b)

Figure 5-7 (a) Numerical model of the superstructure (b) Isolated equipment using raised floor system model for lateral excitation

5.5.1. EQUATIONS OF MOTION

The governing equation of motion for the superstructure subjected to an earthquake ground motion is given by (Ismail *et al.*, 2009b):

$$M_s\ddot{X}_s + C_s\dot{X}_s + K_sX_s = -M_sr\ddot{x}_g \tag{5.3}$$

where M_s, K_s and C_s are the mass, stiffness, and damping matrices of the superstructure, respectively. $\ddot{X}_s$, $\dot{X}_s$andX_s are the floor acceleration, velocity, and displacement vectors respectively. $r$is the vector of influence coefficients and $\ddot{x}_g$is the vector of earthquake ground accelerations. For the system raised floor-equipment, the governing equation of motion can be expressed as (Ismail *et al.*, 2009b):

$$m_e\ddot{x}_e + c_e\dot{x}_e + k_ex_e = -m_e(\ddot{x}_f + \ddot{x}_r) \tag{5.4}$$

$$m_r\ddot{x}_r - c_e\dot{x}_e - k_ex_e + \varphi F_b = -m_r\ddot{x}_f \tag{5.5}$$

where the subscripts r, e, and f denote raised floor, equipment, and mounting floor respectively. φ denotes the number of isolator and $\ddot{x}_f = \ddot{x}_2 + \ddot{x}_g$, where the 2nd floor is the hosting floor of the equipment. The force F_b mobilized in the isolation system is modelled using the Bouc-wen model of hysteresis. In developing the governing equation of motion, shear elastic superstructure with a rigid diaphragm was assigned to every floor. The modal frequencies and corresponding periods of vibration of the superstructure are summarized in Table 5-1.

Table 5-1 Modal properties of the three-story reinforced concrete MRF structure

	Mode number					
	1	**2**	**3**	**4**	**5**	**6**
Frequency (Hz)	4.902	14.165	14.642	24.179	30.904	63.347
Periods (s)	0.204	0.071	0.068	0.041	0.032	0.015
Mass participation ratio	0.340	0.044	0.016	0.016	0.000	0.000

5.6. VALIDATION OF THE NUMERICAL MODEL

The validation of the numerical model was performed by comparing the peak in the response spectrum of the isolated equipment from the numerical model with the analytical calculation. An acceleration response spectrum was plotted between the maximum response of single degree of freedom system when subjected to specific earthquake excitations and its time period (or frequency). The peak response of a system for various frequencies (time periods) can be obtained from the response spectra (de Silva, 2005). The earthquake excitations consist of a wide range of frequencies and if any of the frequencies of the excitation is in-line with the natural frequency of the system, then the system exhibits peak response at that frequencies. For the case of earthquake excitation, it is convenient to use the time period instead of frequency, since the time period can provide more details in the low frequency range. The response spectra with system time period on x-axis and response quantity on y-axis at specified damping ratio and input ground motion is then plotted.

The time period of the isolated raised floor equipment for each of the 9 WRIs were calculated analytically using the Eq. (5.6) (Ismail *et al.*, 2012b).

$$T = 2\pi\sqrt{\frac{M_{RE}}{K_{Total}}} \tag{5.6}$$

where T is the time period (s), M_{RE} is the mass of the raised floor and equipment, K_{Total} is the sum of the stiffness of the isolators used to support the raised floor. This is the fundamental time period of the isolated system. The WRI was modelled using the Bouc-Wen equation in the numerical model by providing Bouc-Wen parameters from Table 4-3 and the three-storey structure was excited by the El-centro 1947 in the lateral

directions. The response spectrum of the acceleration of the isolated equipment was obtained from the SAP2000 for the comparison as shown in Figure5-8. The comparison of the time period from the numerical model and analytical calculation is given in Table 5-2. As can be seen, there is a good agreement between them.

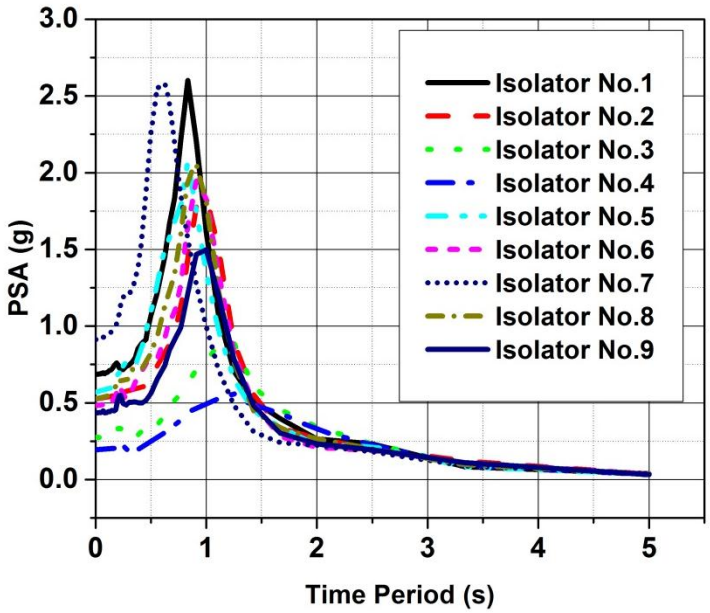

Figure5-8 Acceleration response of the isolated equipment for El-Centro

Table 5-2 Validation of Numerical model with analytical calculation

Isolated System	Time period (s)	
	Numerical	Analytical
WRI.1	0.80	0.79
WRI.2	1.01	1.00
WRI.3	1.25	1.23
WRI.4	1.36	1.35
WRI.5	0.65	0.60
WRI.6	0.75	0.72
WRI.7	0.56	0.51
WRI.8	0.69	0.58
WRI.9	0.75	0.70

5.7. SELECTION OF THE ISOLATION SYSTEM

The selection of the isolation, in general, depends on the amount of isolation required for the applications. The isolation is provided by increasing the fundamental

time period of the system greater than the dominant time period of the external excitations. The fixed equipment considered in the present study has the fundamental period of 0.095s and the equipment was situated on the top floor of the 3-storey building. In this case, the isolation system required isolating the equipment from the external excitation as well from the building when the building vibrates at its resonance frequency due to external excitation. The prime focus was on the equipment to be isolated from the building floor through the raised floor configurations.

The WRIs, from Table 4-1, were tested in the present study and the selection of the WRI was made to provide suitable lateral flexibility, which increased the time period of the isolated raised floor. The Pseudo Spectral Acceleration (PSA) was evaluated for the fixed equipment case using the numerical modelling for various earthquake excitations. The PSA of the fixed equipment was analyzed to understand the time periods at which the floor accelerates due to external excitations. The WRI is required to effectively decouple the raised floor –equipment from the floor of the three-storey structure and hence, it is required to first determine the time period at which the response of the fixed equipment attains peak.

Upon identifying the peak response time period, the WRI can be selected so that the time period of the isolated raised floor-equipment is further away from the peak response time period. A greater amount of isolation can be achieved by increasing the time period of the isolated raised floor-equipment greater than the peak response time period (Ismail *et al.*, 2012b). In this study, the selection of the WRI was performed based on the El-Centro 1947 and this methodology can be used for the selection against any required earthquake excitation. Further, the effectiveness of the WRI for other earthquakes was also examined by subjecting the numerical model to 34 different earthquake conditions.

For obtaining the PSA, the average of the damping of isolators in the lateral direction from the cyclic loading test was considered which was 10%.Figure 5-9 shows the PSA of the fixed equipment and the isolated equipment using each WRI for El Centro Earthquake exactions at 10% damping. As can be observed, the fixed equipment accelerated in high magnitude in the time period at the first fundamental time of the

building which was 0.204 s. Hence, the time period of the isolated raised floor needs to be shifted further away from this region to provide the isolation. The raised floor was isolated using each of the nine isolators and their PSA were compared with the fixed condition. The evaluation for the time period of the isolated system under each WRI is given in Table 5-2. Accordingly, the peak in the PSA for the isolated equipment, using each isolator, occurred in their respective fundamental time period. However, the magnitude was lower than the fixed condition and furthermore, at the fundamental period of the building, the equipment was efficiently decoupled.

From Table 5-2, it can be seen isolator's No 2, 3, and 4 have a higher time period and their time period was much further away from the peak response time period of the fixed equipment which was 0.204 s. Evidently, the selection of an isolator for this study can be determined as isolator No.4 due to the increased time period, which was 1.35 s, than the other WRIs and additionally, due to the reduced magnitude of equipment acceleration. Hence, the raised floor system was isolated using isolator No. 4. The Bouc-wen model (Table 4-3) of isolator No.4 was used in the numerical model to study the reduction of acceleration as well as on the displacement for every excitation and will be discussed in the subsequent section.

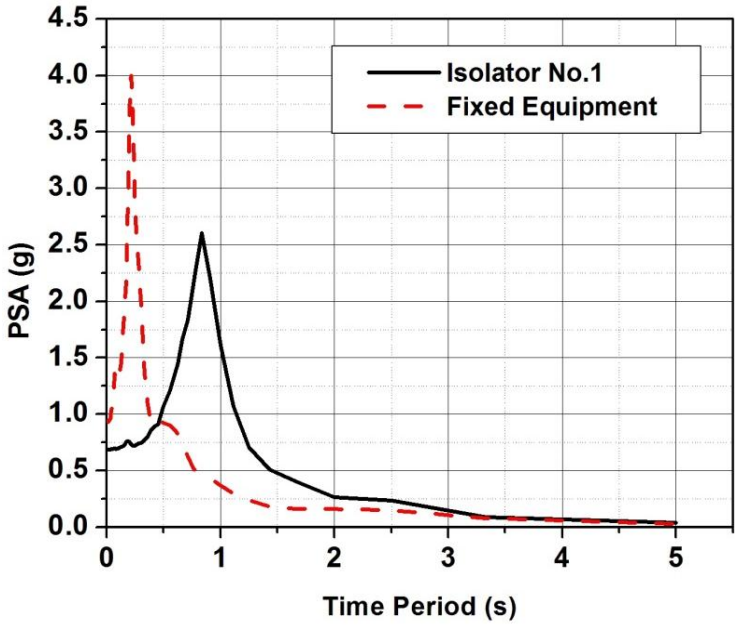

(a)

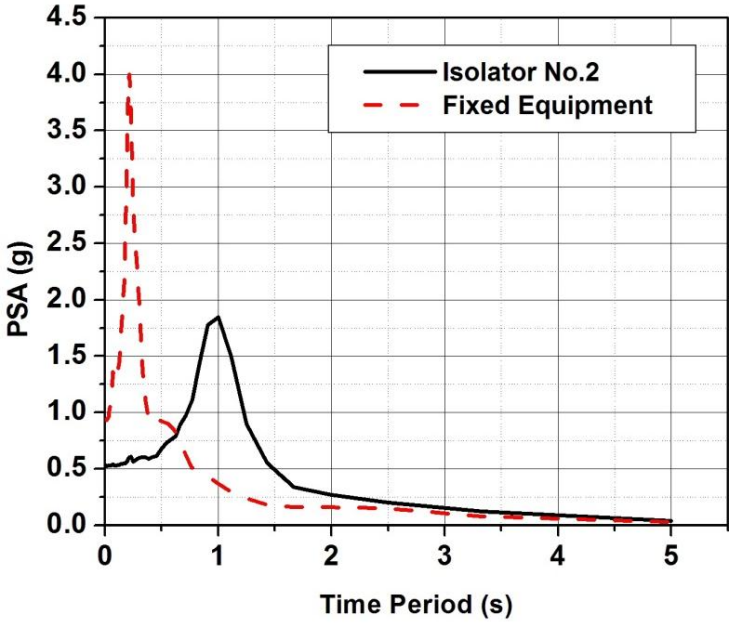
Isolator No.2
Fixed Equipment
PSA (g)
Time Period (s)
0.0
0.5
1.0
1.5
2.0
2.5
3.0
3.5
4.0
4.5
0
1
2
3
4
5

(b)

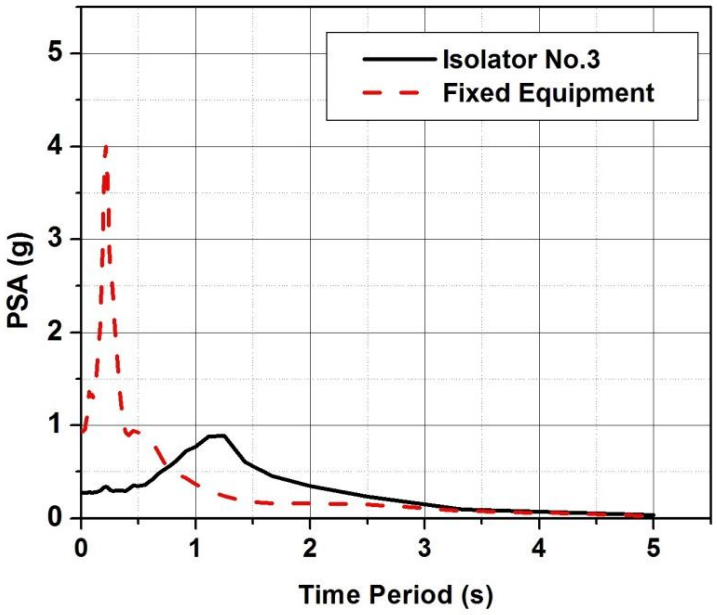
Isolator No.3
Fixed Equipment
PSA (g)
Time Period (s)
0
1
2
3
4
5
0
1
2
3
4
5

(c)

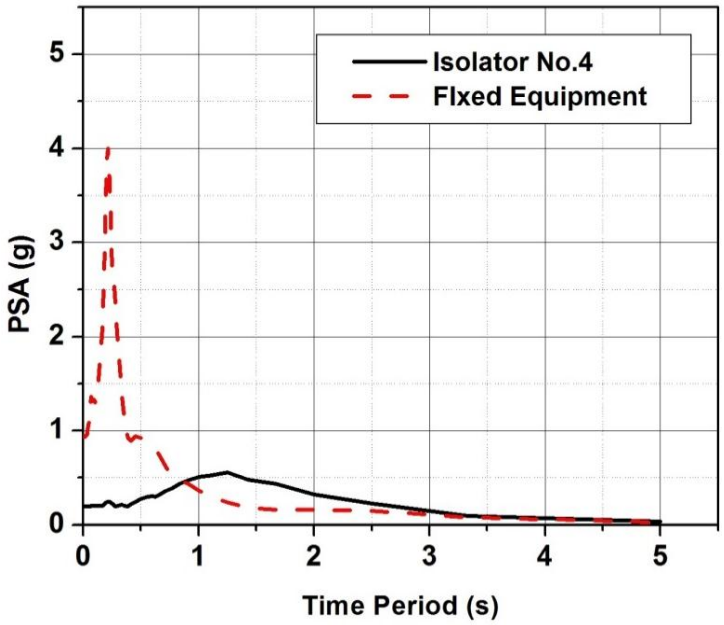
Isolator No.4
FIxed Equipment
PSA (g)
Time Period (s)
0
1
2
3
4
5

(d)

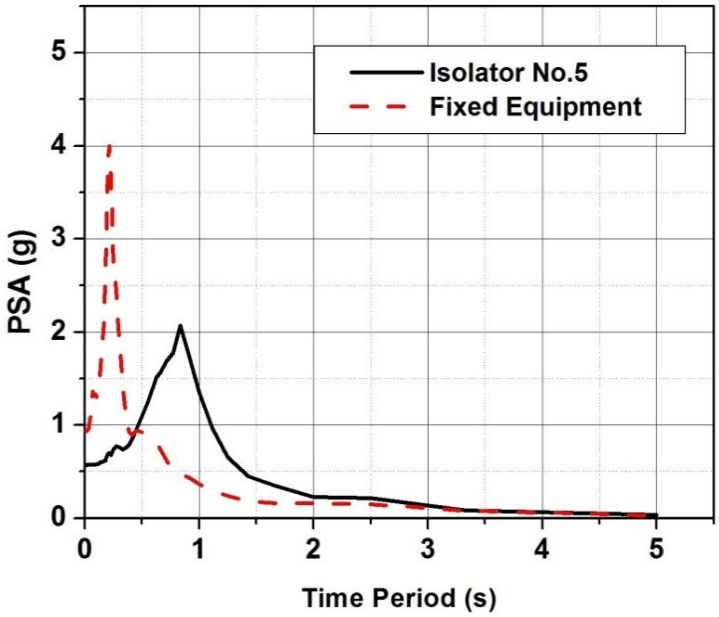
Isolator No.5
Fixed Equipment
PSA (g)
Time Period (s)
0
1
2
3
4
5

(e)

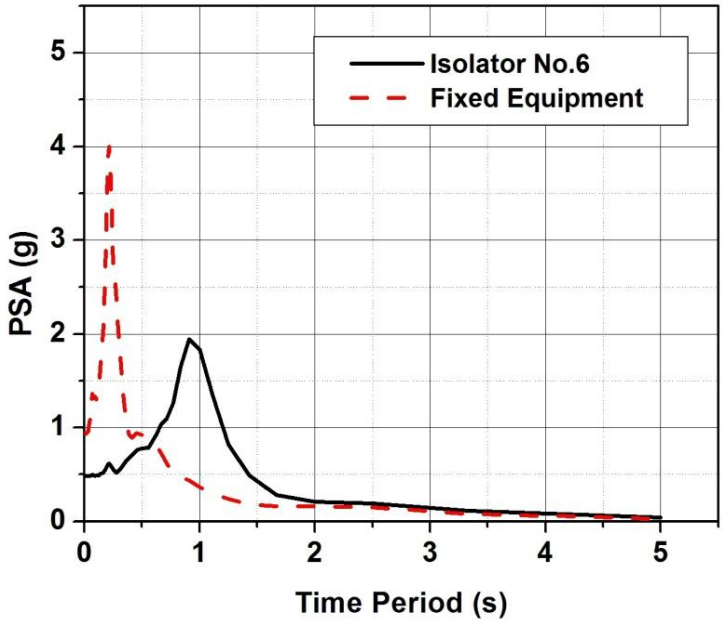
Isolator No.6
Fixed Equipment
PSA (g)
Time Period (s)
0
1
2
3
4
5

(f)

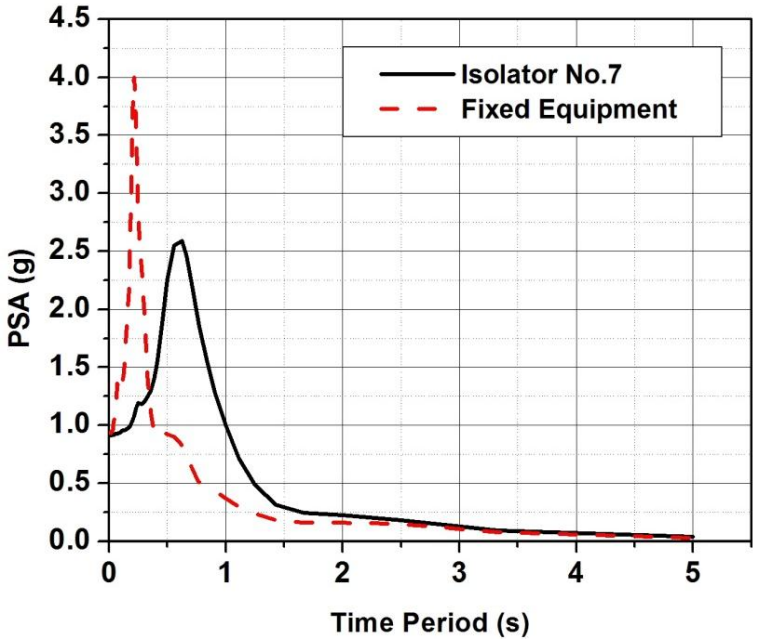
Isolator No.7
Fixed Equipment
PSA (g)
Time Period (s)
0.0
0.5
1.0
1.5
2.0
2.5
3.0
3.5
4.0
4.5
0
1
2
3
4
5

(g)

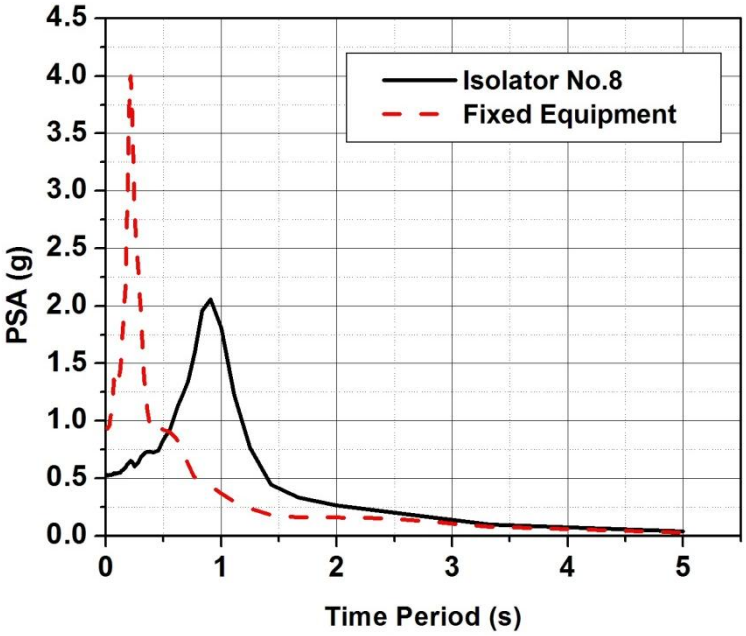

(h)

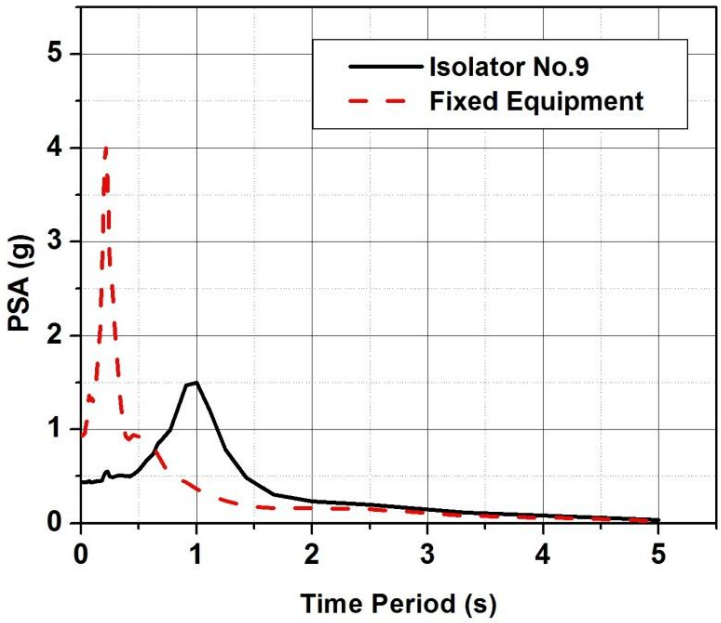

(i)

Figure 5-9 PSA spectrum for fixed and isolated cases under El-Centro 1940 excitation using (a) Isolator No.1 (b) Isolator No.2 (c) Isolator No.3 (d) Isolator No.4 (e) Isolator No.5 (f) Isolator No.6 (g) Isolator No.7 (h) Isolator No.8 (i) Isolator No.9

5.8. RESULTS AND DISCUSSIONS

In this section, the performance of the WRI in the vibration isolation of the raised floor is discussed. The numerical model was subjected to 34 earthquake excitations and the acceleration and displacement response of the equipment was evaluated. The performance of the WRI in the vibration isolation is studied by comparing the isolated case with the fixed case. The acceleration and displacement response of the fixed and isolated cases under El-Centro, Altadena_0 and Parkfield is shown in Figure 5-10, 5-11 and 5-12 respectively. Figure 5-10(a), 5-11(a) and 5-12(a) demonstrate the effectiveness of the WRI in reducing the equipment acceleration; Table 5-3shows the summary of the equipment acceleration response and the relative displacement with respect to the fixed case and the corresponding plots are provided in the Appendix E and F.

As can be observed, the WRI isolation system was capable of reducing up to 68% of the equipment acceleration on average for the earthquake excitations considered in this study. This reduction was mainly due to the decoupling offered by the nonlinear behavior of the WRI through its nonlinear frictional contact surfaces between the individual wire strands. A maximum reduction of 83.8 % was observed for the Northridge earthquake data. The decrease in acceleration was achieved at the expense of increased lateral displacement. Figure 5-10(b), 5-11(b) and 5-12 (b) show the equipment's peak lateral displacement corresponding to El-Centro, Altadena_0 and Parkfield earthquake excitations, respectively. This is the typical property of most passive isolation systems; the isolation system decouples the equipment from the structure resulting in a relatively high lateral displacement compared to the fixed case. This feature prevents permanent distortion of the equipment after an earthquake ground motion.

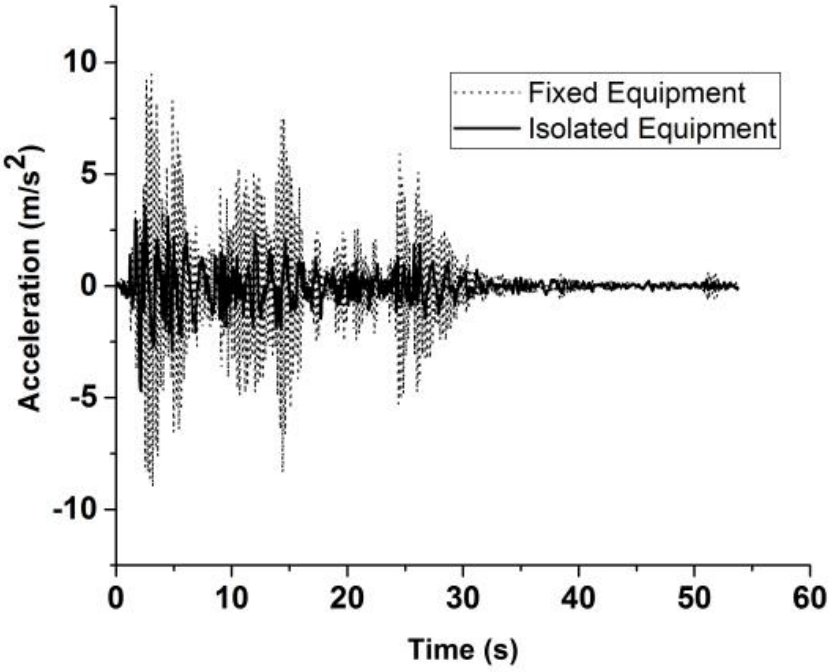

(a)

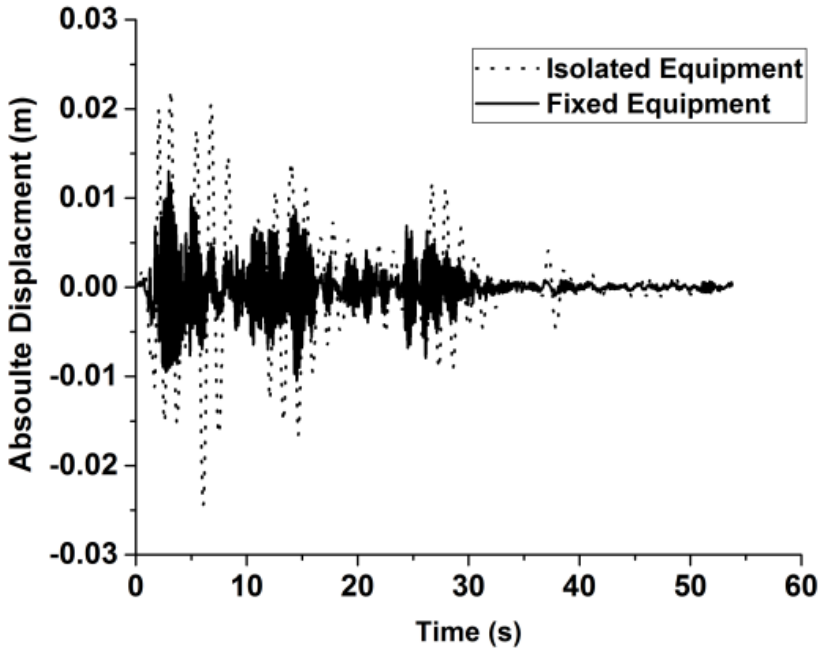

(b)

Figure 5-10 Comparison of response between fixed and isolated case under El-Centro Excitation (a) acceleration response (b) Displacement response

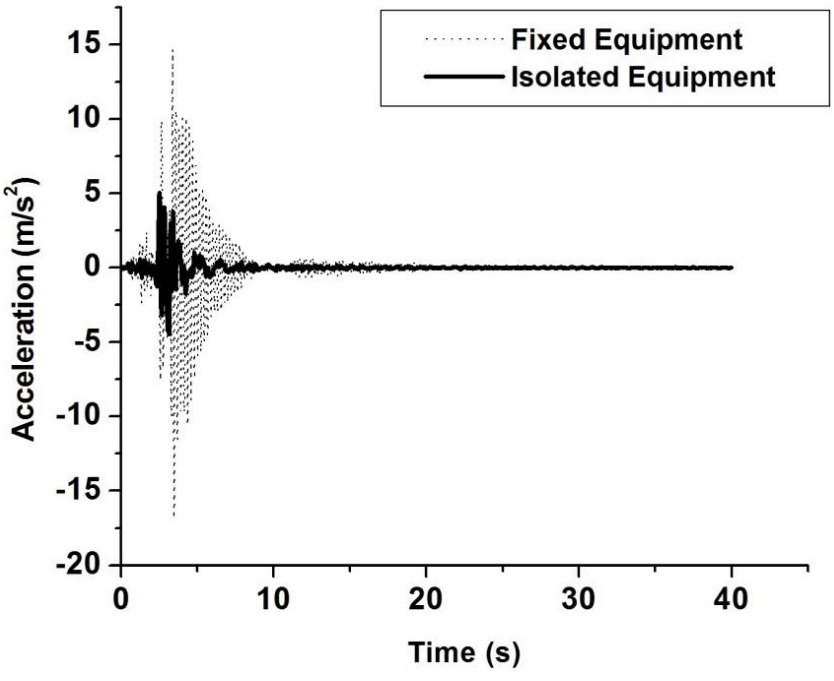

(a)

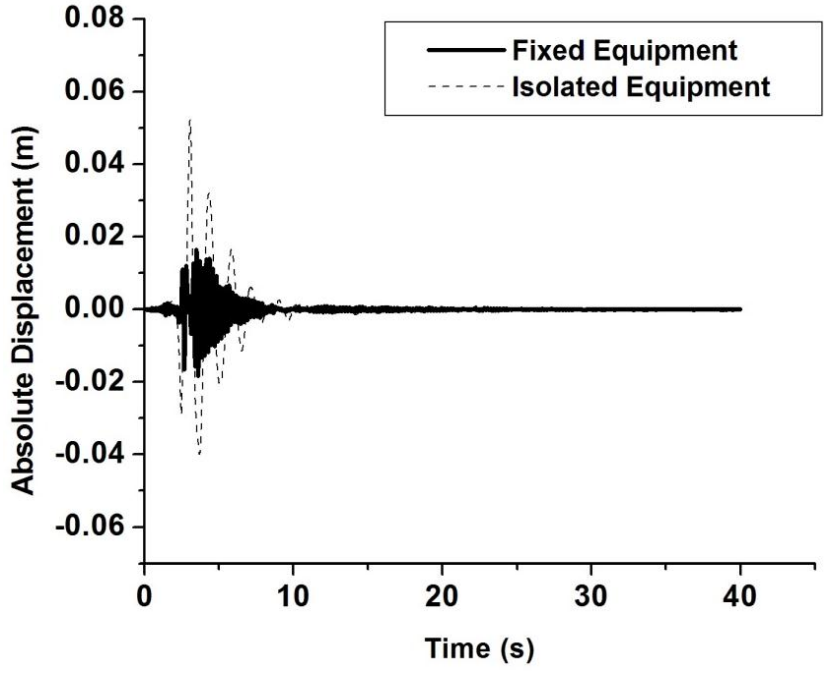

(b)

Figure 5-11 Comparison of response between fixed and isolated case under Altadena_0 excitations (a) acceleration response (b) Displacement response

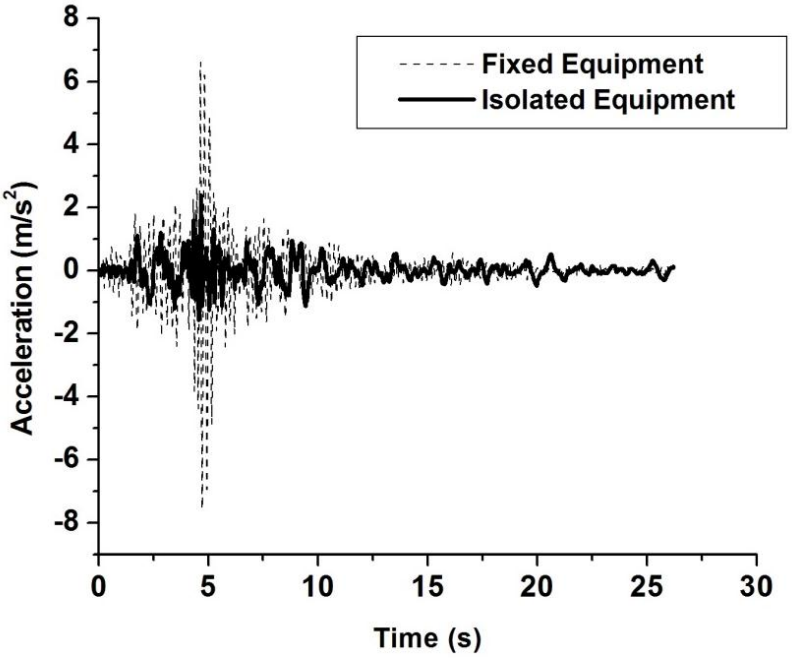

(a)

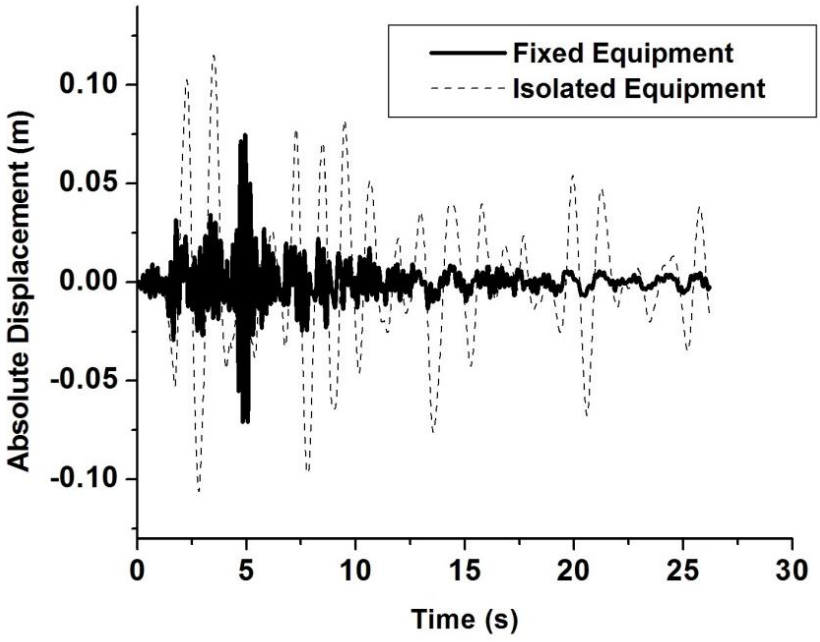

Figure 5-12 Comparison of response between fixed and isolated case under PARKFIELD excitations (a) acceleration response (b) Displacement response

The displacement demand of the earthquake motion has to be taken into consideration to evaluate whether for the WRI isolation system is compatible with the design requirements; the WRI used in the present simulation study possesses maximum lateral displacement of about 40 mm(ITT Enidine Inc, 2014). The average displacement for the considered cases was 39.1 mm. This is within the affordable limits of the WRI selected for the present study. However the percentage of relative displacement that is within the given WRI limits is 80%. The displacement demand for cases, which fall outside this limit, can be compensated by using a larger sized WRI. On the other hand, the increased lateral stiffness of the larger WRI can reduce the flexibility and results in reduced acceleration reduction. The displacement limit primarily depends on the height of the WRI and a general observation was made from the manufacture's catalogue (2014b) that the WRI are preferred to use in the applications having the displacement demand within the 60% of the WRI height. The analytical model for the stiffness was developed in Chapter 3 and these models can be used to design the geometric characteristics of the WRI for a given height and stiffness. Depending on the significance and sensitivity of the application, for external excitations the displacement demand can be achieved either by the use of a larger WRI or by designing the WRI using the analytical models.

The simulation results show the efficiency of the WRI in mitigating the acceleration response and satisfying the displacement demand for the considered earthquake cases. The raised floor approach for the vibration isolation using the WRI is a feasible solution also for isolating lightweight equipment and can be used as a common platform for isolating groups of equipment. The present study has considered the case of equipment on the 2^{nd} floor of a 3-storey building and selected the WRI based on a 2^{nd} floor spectrum. The time period of the isolated system was selected to be higher than the floor predominant time period. A similar procedure can also extend to any floor and the simulation model was extended to examine the effect of floor acceleration. Furthermore, the present numerical model was also extended to analyse the influence of isolator characteristics and earthquake intensity on vibration isolation to develop an overall understanding of the performance of WRI.

Table 5-3 Response Summary under 34 earthquake excitations

S.No	Earthquake Records	Peak Accel.(g)	Peak acceleration (m/s^2)		Reduction ratio (%)	Isolated Equipment Relative Disp. (mm)
			Fixed Equipment	Isolated Equipment		
1	Altadena_0	0.448	16.84	4.52	73.2	34.1
2	Altadena_90	0.179	4.48	1.75	60.9	11.99
3	Array06_0	0.376	21.69	5.08	76.6	51.11
4	Array06_90	0.437	8.67	2.87	66.9	28.60
5	Corralit_0	0.63	17.64	6.34	64.0	12.55
6	Corralit_90	0.479	14.51	5.32	63.3	26.16
7	Holliste_0	0.369	4.41	2.05	53.5	37.88
8	Holliste_90	0.178	4.71	2.38	49.5	13.17
9	Lacc-Nor-0	0.222	6.35	3.04	52.1	15.99
10	Lacc-Nor-90	0.256	11.17	2.59	76.8	12.68
11	Lexingt_0	0.442	6.76	2.42	64.2	45.55
12	Lexingt_90	0.41	9.83	2.49	74.6	50.17
13	Lucerne_0	0.681	22.94	5.86	74.5	22.33
14	Lucerne_90	0.703	25.26	6.37	74.8	8.24
15	New Hall_0	0.59	26.19	11.42	56.4	65.42
16	New Hall_90	0.583	24.61	8.07	67.2	47.04
17	Oak Whaf_0	0.287	4.87	1.97	59.6	28.52
18	Oak Whaf_90	0.271	4.88	1.83	62.5	32.91
19	Petrolia_0	0.59	16.15	6.61	59.1	15.55
20	Petrolia_90	0.662	13.13	5.60	57.4	34.63
21	Pomona_0	0.186	9.58	2.01	79.0	41.95
22	Pomona_90	0.207	7.39	1.76	76.2	41.58
23	Santa Monica_0	0.37	17.49	3.41	80.5	20.13
24	Santa Monica_90	0.883	47.99	7.77	83.8	13.66
25	Sylmar_0	0.843	15.18	5.95	60.8	69.16
26	Sylmar_90	0.604	9.33	5.62	39.8	39.60
27	Yermo_0	0.151	7.44	3.10	58.4	21.00
28	Yerma_90	0.245	5.64	1.23	78.2	38.71
29	EL-CENTRO	0.348	9.48	3.62	61.8	13.28
30	KERN	0.179	0.73	0.21	70.9	6.13
31	KOBE	0.679	24.20	10.54	56.4	82.63
32	NORTHRIDGE	0.883	47.90	7.77	83.8	20.8
33	PARKFIELD	0.237	7.60	1.56	79.5	3.8
34	SAN-FRENANDO	1.717	50.71	13.96	72.5	67.04

5.8.1. INFLUENCE OF ISOLATOR CHARACTERISTIC AND EARTHQUAKE INTENSITY

The design of the isolation system was performed to select the most apprpriate WRI for the present application. The isolation system, which has a higher fundamental period, was selected. However, in the study, the performance of the isolator having a different time period and its influence in the vibration isolation of equipment was assessed. This study was designed to understand the effect of time period and earthquake intensity on the performance of the WRI. The El-Centro 1940, was used in various intensities; 50%, 100% and 200% in this study. The floor spectrum showed the floor was accelerating in the first fundamental time period which was 0.204s. The isolator stiffness was suitably varied to the time periods; 1s, 1.5s and 2s.Table 5-4 summarizes the influence of time period and earthquake intensity. As can be observed from Table 5-4 the increased time period of the isolated system improves the acceleration reduction at increased displacement of the isolator. The influence of the earthquake intensity is largely influenced by the displacement of the isolator however; the acceleration reduction is similar for other considered levels of intensity. These results show that moving the time period of the isolators further away and also having a higher intensity earthquake will needs to be verified within the displacement limit.

Table 5-4 Summarize of isolator characteristics and earthquake intensity

	50 % El-Centro			100 % El-Centro			200 % El-Centro		
Time period	Iso. Equip (m/s^2)	Rel. Disp (mm)	Red. %	Iso. Equip (m/s^2)	Rel. Disp (mm)	Red. %	Iso. Equip (m/s^2)	Rel. Disp (mm)	Red. %
1	3.02	7.97	35.8	6.22	16.58	34.4	12.64	35.57	32.5
1.5	2.16	7.52	54.04	4.46	13.38	52.9	9.1	31.09	51.4
2	1.65	10.28	64.89	3.01	24.41	68.2	6.04	54.42	67.8

5.8.2. INFLUENCE OF FLOOR ACCELERATION

The design of the isolation system was approached based on the floor spectrum. Hence, the isolation system design and selection can vary for each floor. The isolation

system designed for the second floor was placed in the first floor to study the influence of floor acceleration in the vibration isolation. The floor spectrum of first and second floor was observed to be similar and hence the isolation system was also effectively functioning in the first floor. Table 5-5 shows the results of the influence of floor acceleration. As can be observed, the isolated equipment accelerates to a similar level however; the reduction percentage was less on the lower floor. This difference was due to the reduced floor acceleration in the lower floor compared to the higher floor.

Table 5-5 Comparison of WRI performance for floor acceleration

	KERN				NORTHRIDGE				PARKFIELD			
Floor	**Iso. Eqiup (m/s2)**	**Fixed Equip**	**Rel.Disp (mm)**	**Red. %**	**Iso. Eqiup (m/s2)**	**Fixed Equip**	**Rel.Disp (mm)**	**Red. %**	**Iso. Eqiup (m/s2)**	**Fixed equip**	**Rel.Disp (mm)**	**Red. %**
2nd	2.13	7.32	6.13	70.90	7.77	47.9	20.8	83.78	1.56	7.6	3.8	79.47
1st	2.08	4.87	6.94	57.29	7.79	34.78	21.5	77.60	1.5	5.1	4.25	70.59

5.9. DISCUSSION OF THE OVERALL PERFORMANCE OF WRIS

In this section, the discussion of the overall performance of all the WRIs used in the study is presented. The analysis of the performance of these WRIs was examined under earthquake excitations and mechanical vibrations using the numerical model, which was the raised floor method supported by wire cables, as discussed in Section 5.5. The performance against the mechanical vibration was acheived by evaluating the natural frequencies under WRI for a given mass ranging from 50 kg to 500kg. In this study, a plot was made to facilitate the selection process of the WRI for harmonic vibrations.

5.9.1. UNDER EARTHQUAKE EXICTATIONS

The analysis under earthquake excitations was accomplished by subjecting the numerical model to real time earthquake records from the SAP2000 database. The earthquake excitations can be categorized as three types: high, medium and low based on their peak ground acceleration (PGA) to Peak ground velocity (PGV) ratio (Naumoski *et al.*, 1988;Zhu *et al.*, 1988). The effectiveness of the WRI was examined for each type of earthquake record (Table 5-6). The excitation of the fixed equipment is shown in Figure 5-13 and it can be observed the acceleration response of the fixed equipment peaked at the first fundamental period of the three-storey structure.

The equipment was isolated using each of the WRIs (Table 4-1) and these WRIs were modeled using the Bouc-Wen parameters (Table 4-3) in the lateral directions. The time period for each WRI is given in Table 5-2. As can be seen, the time period corresponding to each WRI was greater more than the peak response of the fixed equipment and hence, those WRIs can provide isolation against these earthquake excitations. Table 5-7 Performance of WRIs under earthquake excitations shows the peak acceleration of the fixed and isolated equipment and also the relative displacement. As can be seen, the peak acceleration of the isolated equipment was less than the fixed equipment indicating isolation ability of these WRIs. As can also be observed the lower category earthquake has increased displacement of the isolators and hence, this numerical model can be used to verify the displacement demand of the isolator with the maximum possible displacement of the isolators.

Table 5-6 Earthquake Records (Naumoski, 2014)

Record#	Earthquakes	PGA (g)	A/V ratio	Class
1	ParkField California , 1966	0.085	1.67	High
2	Kern County California,1952	0.179	1.01	Intermediate
3	San Fernando California,1971	0.132	0.61	Low

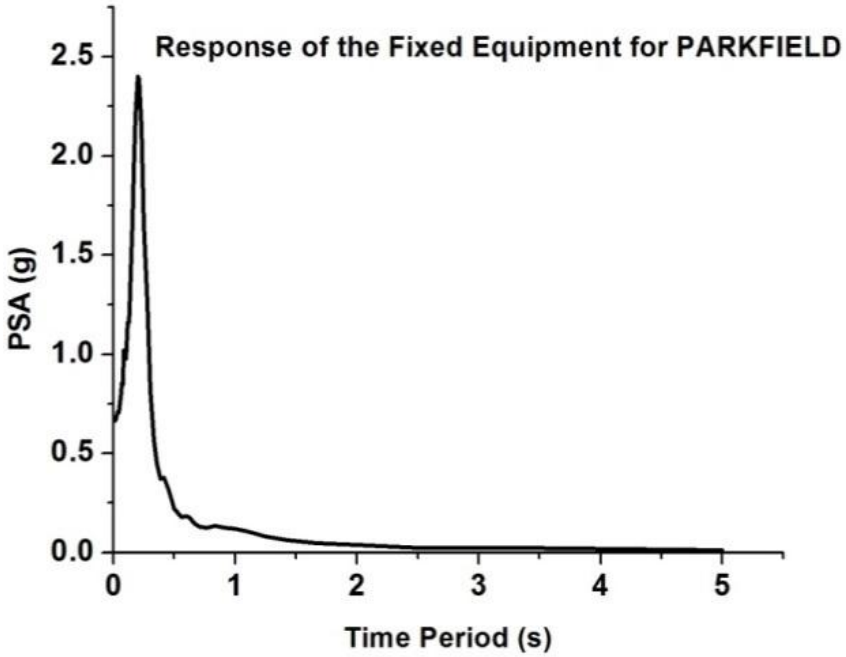
Response of the Fixed Equipment for PARKFIELD
PSA (g)
Time Period (s)
0.0
0.5
1.0
1.5
2.0
2.5
0
1
2
3
4
5

(a)

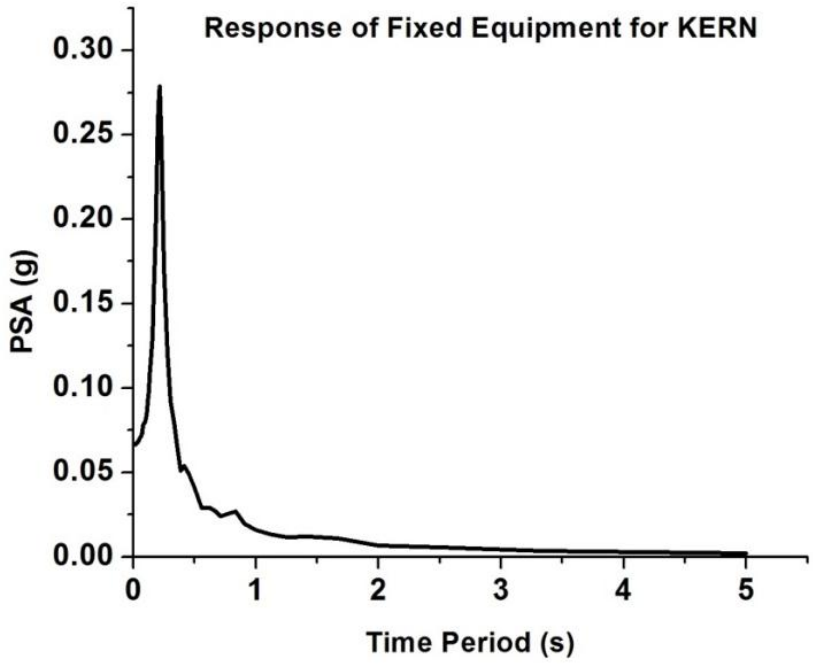
Response of Fixed Equipment for KERN
PSA (g)
Time Period (s)
0.00
0.05
0.10
0.15
0.20
0.25
0.30
0
1
2
3
4
5

(b)

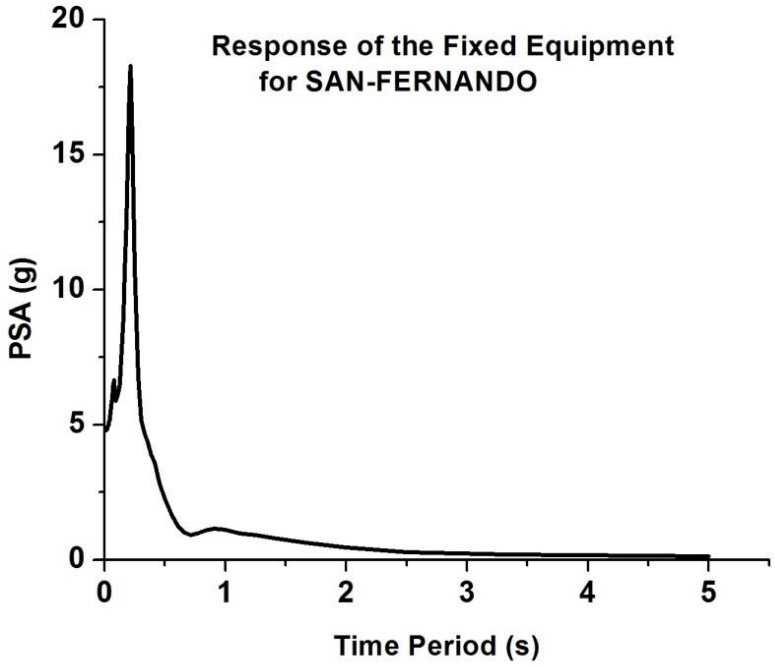

(c)

Figure 5-13 Acceleration response of the fixed equipment under (a) PARKFIELD (b) KERN (c) SAN-FRENDO

Table 5-7 Performance of WRIs under earthquake excitations

			Isolated Equipment								
Earthquakes	**Parameters**	**Fixed Equipment**	**WRI.1**	**WRI.2**	**WRI.3**	**WRI.4**	**WRI.5**	**WRI.6**	**WRI.7**	**WRI.8**	**WRI.9**
PARKFIELD	**A (m/s^2)**	7.57	2.53	3.06	2.21	1.56	2.58	2.82	2.44	2.69	2.76
	Relative Displacement (mm)	-	2.78	4.73	4.21	3.81	1.88	2.77	1.60	2.41	2.72
KERN	**A (m/s^2)**	0.73	0.27	0.25	0.22	0.21	0.34	0.31	0.38	0.32	0.30
	Relative Displacement (mm)	-	6.68	7.07	7.03	6.31	8.13	7.12	9.12	8.51	7.51
SAN-FRENDO	**A (m/s^2)**	50.71	19.15	17.5	13.8	13.96	18.80	13.40	15.37	16.47	15.96
	Relative Displacement (mm)	-	24.30	52.67	70.41	67.40	20.24	40.07	30.69	31.59	47.04

5.10. UNDER MECHANCIAL VIBRATIONS

The selection of the WRI for mechanical vibration isolation is relatively easy when compared to seismic vibration isolation. This is due to the nature of the mechanical vibrations. Most mechanical disturbances, such as the operation of heavy machinery, are harmonic in nature with a definitive frequency. Hence, by identifying this frequency, which in most cases is the rpm of a rotatory machine, isolation can be effectively provided. The fundamental concept for vibration isolation is to reduce the natural frequency of the system smaller than the external excitation frequency, by providing flexible isolators. The isolator contributes to the natural frequency of the system through its stiffness component. The amount of isolation required can be designed for a system by the proper control of stiffness, which influences the natural frequency of the system. The selection procedure of isolators for the harmonic frequencies can be made through the principles of the SDOF system response (Figure 1.2). In most industries, the selection procedure is based on this SDOF approach (ITT Enidine Inc, 2014).

ITT ENDINE Inc (2014b) has established the procedure for the selection of the WRI for applications and is shown in Table 5-8. The selection procedure has two parts, part 1 for system data and part 2 for vibration data. In part 1, the general information of the system is identified and the number of isolators is defined based on the number of support point for the system. Part 2 is the vibration data where the stiffness of the isolator required for 80% isolation is estimated. The isolator can be selected for any amount of isolation, which can be determined based on the transmissibility curve (Figure 1.2) of the SDOF. The frequency ratio of the system with respect to excitation frequency for 80% isolation is obtained from the transmissibility ratio (Figure 1.2) and from this frequency ratio, the required natural frequency of the system for 80% isolation is determined. Upon estimating the required natural frequency of the system, the stiffness of the isolator is selected to obtain the suitable frequency ratio.

Figure 5-14 Natural Frequency of the isolated equipment for various mass of the equipment (a) Vertical (b) Lateral shows the plot between mass and the natural frequency of the isolated system with each WRI in vertical and lateral directions. This plot was developed to

assist in the selection process of the nine WRIs assessed in this study. Figure 5-14 was plotted using the Eq.(5.6) and the natural frequency was 1/T. As can be noted, the increased mass reduces the natural frequency and it implies that the heavier mass are ease to be protected against the vibrations. However for lighter mass, a WRI with the proper stiffness needs to be selected. The selection process can be made by calculating the mass and the forcing frequency. As can be seen from Figure 5-14, in lateral directions the isolators have less natural frequency for a given mass than in the vertical directions. This shows the WRI can be effectively isolated in the lateral directions and the favourable position for the WRI can be load supported vertically and for the lateral isolation.

Table 5-8 Selection procedure of WRI from ITT ENDINE Inc

Selection procedure of WRI from ITT ENDINE Inc(2014b)		
S.No	**Part 1. System Data**	
1	Total weight of the system	W_T kg
2	Number of isolators	N
3.	Static weight on an individual isolator (W_i)	(W_T/N) kg
4	Excitation direction	Vertical/Lateral
	Part 2. Vibration data	
1	Excitation frequency	F_e Hz
2	System response frequency for 80% isolation, F_s	F_e/3.0
3	Maximum stiffness of the isolator K	(W_i $2\pi F_s$)/g

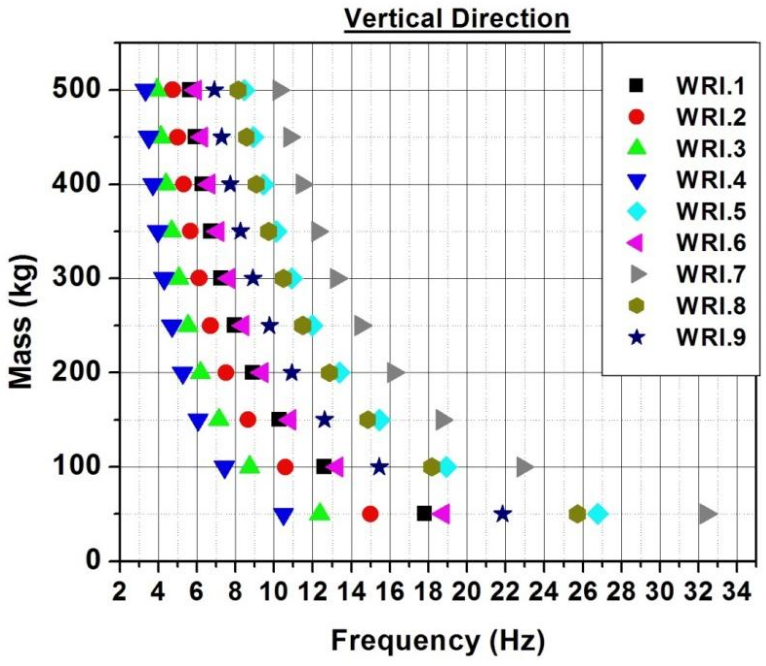

(a)

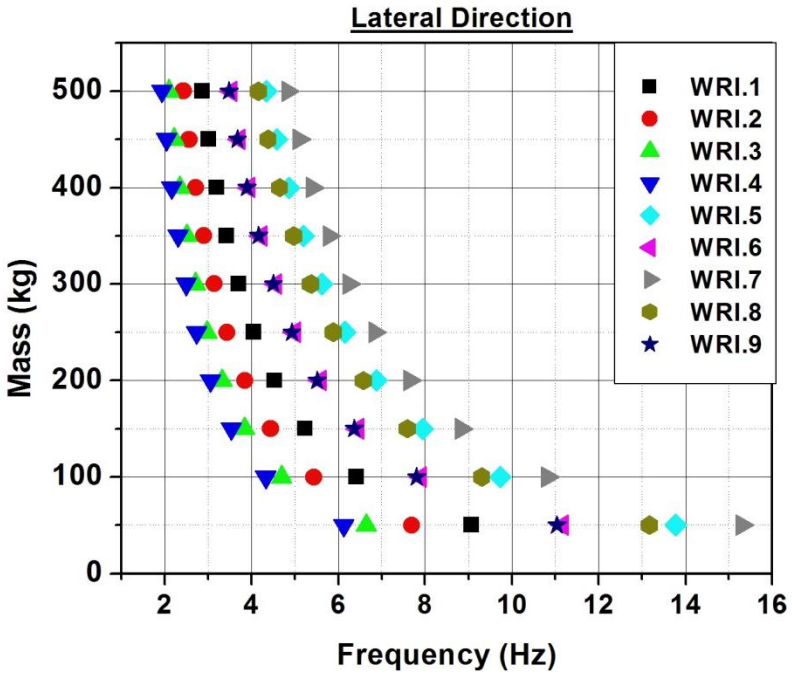

(b)

Figure 5-14 Natural Frequency of the isolated equipment for various mass of the equipment (a) Vertical (b) Lateral

5.11. CONCLUSIONS

The performance of the wire rope isolators in the vibration isolation of equipment using the raised floor approach was studied in this work. This study shows that the WRI is effective in reducing the acceleration response and hence, protects the equipment from external excitations. This acceleration reduction was achieved at the expense of the lateral displacement.

The following conclusions are drawn from the present study:

1. The WRI is effective in reducing the acceleration of equipment;
2. The WRI reduced the acceleration of the equipment by 68% on average with a maximum 83.8 % reduction observed for NORTHRIDGE.
3. The average displacement demand for the applied earthquake excitations was 39.1 mm. Furthermore, the present simulation model also provides a way to determine the displacement demand required for the application and a suitable WRI can be selected to provide the required displacement demand.
4. For the chosen excitation intensities, the WRI isolation system was found to be effective in providing vibration isolation however; this increased lateral displacements at higher intensities.
5. The WRI isolation system can provide effective isolation for equipment situated on various floors by selecting the proper WRI determined by the floor spectrum.

Chapter 6. CONCLUSIONS AND RECOMMENDATION FOR FUTURE WORK

6.1. CONCLUSIONS

Nonlinear isolators can provide better isolation than linear isolators however; the lack of relevant literature on nonlinear isolators restricts their potential application area. In this research a type of nonlinear isolator, the Wire Rope Isolator (WRI) was studied for its stiffness and damping characteristics. Furthermore, the performance in the isolation of a system using raised floor approach was also assessed using the numerical study. This study can further the understanding of the WRI and widen the potential application area.

The aims of this research work were:

I. To evaluate the static stiffness and damping characteristics in both vertical and lateral directions of the wire rope isolators through an analytical and experimental study.

II. To investigate a case study on the performance of wire rope isolators in the vibration isolation of equipment by the raised floor method.

The objectives of the proposed work are listed below:

1. To develop an analytical model of the static stiffness of wire rope isolators in both vertical and lateral directions and to validate the model with monotonic loading tests.

2. To study the damping characteristics of the wire rope isolators in both vertical and lateral directions using mathematical modelling and cyclic loading tests.

3. To numerically study the performance of wire rope isolators, in the vibration isolation of equipment by raised floor method, using the static stiffness and damping characteristics obtained from objective 1 and 2.

In this chapter, the results from each objective are summarized. Furthermore, a discussion on possible future research is also provided.

6.1.1. CONCLUSIONS FROM OBJECTIVE 1:

To develop an analytical model of the static stiffness of wire rope isolators in both vertical and lateral directions and to validate the model with monotonic loading tests.

1. Two analytical models were developed for stiffness of the wire rope isolators in the vertical and lateral directions respectively using Castigliano's second theorem.
2. The validation of these analytical models was performed with the experimental data obtained from a series of monotonic loading tests and found to have a good agreement with experimental results.
3. The developed models can be effectively used in the analysis and design of wire rope isolators for vibration protection of equipment and lightweight structures.
4. The transverse bending test was used to estimate the flexural rigidity, *EI*, of the 6x19 IWSC wire rope cables. A simple equation was developed to estimate EI for similar wire ropes with different diameters (Figure 3.10).
5. The WRI is almost four times stiffer in the vertical direction than the lateral direction (Figure 3.14)
6. The wire rope diameter significantly influences the vertical and lateral stiffness more than the other geometric characteristics such as width, height, and number of turns.
7. An increase in the wire rope diameter increases the WRI stiffness (vertical and lateral), however, decreasing either the width or height results in the decrease of the stiffness.

8. A new configuration of the WRI called the S-WRI was developed in this study and tested (Figure 3.24). The test results show the springs can be used to enhance the vertical stiffness of the WRI.

6.1.2. CONCLUSIONS FROM OBJECTIVE 2:

To study the damping characteristics of the wire rope isolators in both vertical and lateral directions using mathematical modelling and cyclic loading tests.

1. The damping characteristic of the WRI was analysed from its hysteresis behavior under cyclic loading. The hysteresis behavior in the vertical direction was obtained from tension\compression loading; a roll loading was used for the lateral direction.
2. The vertical hysteresis behavior of WRI is asymmetric however in lateral WRI exhibits symmetrical hysteresis behavior.
3. The hysteresis behavior of WRI was rate independent in both the vertical and lateral direction (Figure 4.25).
4. The WRI with a left and right coil orientation produces similar hysteresis and therefore the coil orientation effect can be ignored (Figure 4.27).
5. An increased value of Height to Width ratio increases the hardening of the WRI (Figure 4.33).
6. The WRI exhibits hardening under tension and softening under compression (Figure 4.37)
7. An equivalent damping ratio reduces for higher displacement and therefore the WRI can be designed having small displacements, for high energy dissipation requirement applications.
8. An increased value of the H\W Ratio decreases the equivalent-damping ratio however this possesses greater energy dissipation. Therefore, in cases of high-energy dissipation applications a higher H\W ratio can be used.
9. The mathematical model for the lateral hysteresis behavior was developed using the Bouc-Wen equations and the Bouc-Wen parameters were identified from the least square method

10. For the vertical asymmetric hysteresis behavior, the Modified Bouc-Wen model was developed. The modification in the Bouc-Wen model was developed using the bilinear model. The model validated the test results and good agreement was observed.
11. The study showed that the effective stiffness and damping ratio is significantly influenced by the wire rope diameter and further, the Height to Width ratio can be used to achieve a wide variety of effective stiffness and equivalent damping results for similar wire rope diameters.

6.1.3. CONCLUSIONS FROM OBJECTIVE. 3:

To numerically study the performance of wire rope isolators, in the vibration isolation of equipment by raised floor method, using the static stiffness and damping characteristics obtained from objectives 1 and 2.

1. The performance of the wire rope isolators in the vibration isolation of equipment using the raised floor approach was analysed studied in this study (Chapter. 5).
2. This study shows the WRI is effective in reducing the acceleration response and protects the equipment from external excitations. This acceleration reduction was achieved at the expense of the lateral displacement.
3. The WRI is effective in reducing the acceleration of equipment.
4. The WRI reduced the acceleration of the equipment by 68% on average and a maximum of 83.8 % reduction was observed for NORTHRIDGE.
5. The average displacement demand for the applied earthquake excitations was 39.1 mm (Table 5-3). Furthermore, the present simulation model also provides a method to determine the displacement demand required for the application and therefore a suitable WRI can be selected to provide the required displacement demand.
6. For the considered excitation intensities, the WRI isolation system was found to be effective in providing the vibration isolation however; this increased lateral displacements at higher intensities (Table 5-4).
7. The WRI isolation system can provide effective isolation for the equipment situated on various floors by selecting the proper WRI by using the floor spectrum.

6.2. RECOMMENDATION FOR FUTURE WORK

1. The WRI used in the study was fabricated from the metal wire rope having the configuration of 6 x 19 WSC. The flexural rigidity of the 6 x 19 WSC wire rope was used it, in the stiffness analytical model. However the flexural rigidity test can be extended to other metal wire rope configurations such as; 6 x 6, 6 x 21, 6 x 36 as well as different cores such as IWSC and IWRC cores. So the analytical model can also be used for the WRI made with wire rope having different configurations.
2. The analytical model of the stiffness in both vertical and lateral directions was developed in the linear region of the force-displacement relation. However, the force-displacement was nonlinear for higher displacements and therefore, this study can be extended into the area of nonlinear by performing a detailed study on the wire strand interaction.
3. The Bouc-Wen parameters were identified for nine WRIs used in this study. Though these nine WRIs can be used for most applications, there are additional samples of WRIs available with the supplier. Therefore, the methodology used in this study can be used to identify the Bouc-Wen parameters of these other WRI samples.
4. In this study two new configurations, the S-WRI and the D-WRI were developed to enhance the stiffness and damping characteristics, respectively. However, only preliminary tests to study the benefits of these designs were carried out in this study. These designs can be subjected to further detailed analysis to understand fully their characteristics.
5. A Performance study on the WRI was carried out using a numerical technique and however; the performance of the WRI can also be examined studied using the scaled model of the raised floor approach.
6. Primarily, this research work and other work on WRI have focused on the stiffness, damping and performance characteristics of the WRI. However the durability study can also be performed to find the long term performance.

References

2010. SAP 2000 Release 14, Documentation. *Computers & Structures Inc, New York*

2014a. Shock & Vibration Control Wire rope Isolators. *In:* WUXI HONGYUAN DEVFLEX CO., L. (ed.). China.

2014b. Wire rope Isolators, ITT Enidine Inc, New York. *www.enidine.com*.

ABOLFATHI, A. 2012. *Nonlinear Vibration Isolators with Asymmetric Stiffness.* Doctor of Philosophy, UNIVERSITY OF SOUTHAMPTON.

ALESSANDRI, S., GIANNINI, R., PAOLACCI, F., AMORETTI, M. & FREDDO, A. 2015a. Seismic retrofitting of an HV circuit breaker using base isolation with wire ropes. Part 2: Shaking-table test validation. *Engineering Structures,* 98**,** 263-274.

ALESSANDRI, S., GIANNINI, R., PAOLACCI, F. & MALENA, M. 2015b. Seismic retrofitting of an HV circuit breaker using base isolation with wire ropes. Part 1: Preliminary tests and analyses. *Engineering Structures,* 98**,** 251-262.

BABER, T. & NOORI, M. 1985. Random Vibration of Degrading, Pinching Systems. *Journal of Engineering Mechanics,* 111**,** 1010-1026.

BARRY, O., OGUAMANAM, D. C. & LIN, D. C. 2013. Aeolian vibration of a single conductor with a Stockbridge damper. *Proceedings of the Institution of Mechanical Engineers, Part C: Journal of Mechanical Engineering Science,* 227**,** 935-945.

BARRY, O., ZU, J. W. & OGUAMANAM, D. C. D. 2015. Nonlinear Dynamics of Stockbridge Dampers. *Journal of Dynamic Systems, Measurement, and Control,* 137**,** 061017-061017.

BOUC, R. 1971. A Mathematical Model for Hysteresis. *Acta Acustica united with Acustica,* 24**,** 16-25.

BUDYNAS, R. G., NISBETT, J. K. & SHIGLEY, J. E. 2008. *Shigley's mechanical engineering design*, McGraw-Hill.

CHANG, I.-K., LIU, S.-C. & SHAH, H. C. 1986. Seismic support of electronic and computer equipment on raised floors. *Soil Dynamics and Earthquake Engineering,* 5**,** 159-169.

CHAUDHURI, S. & KUSHWAHA, B. 2008. Wire Rope Based Vibration Isolation Fixture For Road Transportation Of Heavy Defence Cargo. *In:* İNAN, E., SENGUPTA, D., BANERJEE, M., MUKHOPADHYAY, B. & DEMIRAY, H. (eds.) *Vibration Problems ICOVP-2007.* Springer Netherlands.

CHUNGUI, Z., XINONG, Z., SHILIN, X., TONG, Z. & CHANGCHUN, Z. 2009. Hybrid modeling of wire cable vibration isolation system through neural network. *Mathematics and Computers in Simulation,* 79**,** 3160-3173.

CONSTANTINOU, M. C., REINHORN, A. M. & ENGINEERING, S. U. O. N. Y. D. O. C. 1991. *Seismic Testing of Equipment Isolated by Wire-rope Isolators*, Department of Civil Engineering, State University of New York.

COSTELLO, G. A. 1997. *Theory of Wire Rope*, Springer New York.

COSTELLO, G. A. & BUTSON, G. J. 1982. Simplified Bending Theory for Wire Rope. *Journal of the Engineering Mechanics Division,* 108**,** 219-227.

CUTCHINS, M. A., COCHRAN, J. E., JR, GUEST, S., FITZ-COY, N. G. & TINKER, M. L. 1987. An investigation of the damping phenomena in wire rope isolators. *The role of damping in vibration and noise control (11th Sept. 27-30, 1987).* Boston, MA; United States: United States.

DE SILVA, C. W. 2005. *Vibration and Shock Handbook*, CRC Press.

DE SILVA, C. W. 2006. *Vibration: Fundamentals and Practice, Second Edition*, Taylor & Francis.

DEMETRIADES, G. F., CONSTANTINOU, M. C. & REINHORN, A. M. 1992. *Study of wire rope systems for seismic protection of equipment in buildings (NCEER-92-0012).* State Univeristy of New York.

DEMETRIADES, G. F., CONSTANTINOU, M. C. & REINHORN, A. M. 1993. Study of wire rope systems for seismic protection of equipment in buildings. *Engineering Structures,* 15**,** 321-334.

DEN HARTOG, J. P. 1985. *Mechanical Vibrations*, Dover Publications.

DUTTA, S. & CHAKRABORTY, G. 2014. Performance analysis of nonlinear vibration isolator with magneto-rheological damper. *Journal of Sound and Vibration,* 333**,** 5097-5114.

FOSS, G. C. 2006. Modal Damping Estimates from Static Load-Deflection Curves. *24th Conference and Exposition on Structural Dynamics 2006 (IMAC - XXIV).* Missouri.

GERGES, R. 2008. Model for the Force–Displacement Relationship of Wire Rope Springs. *Journal of Aerospace Engineering,* 21**,** 1-9.

GUYOMAR, D., RICHARD, C. & MOHAMMADI, S. 2008. Damping Behavior of Semi-passive Vibration Control using Shunted Piezoelectric Materials. *Journal of Intelligent Material Systems and Structures,* 19**,** 977-985.

HABERMAN, M. R. 2007. *DESIGN OF HIGH LOSS VISCOELASTIC COMPOSITES THROUGH MICROMECHANICAL MODELING AND DECISION BASED MATERIALS DESIGN.* Doctor of Philosophy, Georgia Institute of Technology.

HAIYAN, H. & YUEFENG, L. 1989. Parametric Identification of Nonlinear Vibration Isolators with Memory. *Journal of Vibration Engineering,* 2**,** 17-27.

HAMIDI, M. & EL NAGGAR, M. H. 2007. On the performance of SCF in seismic isolation of the interior equipment of buildings. *Earthquake Engineering & Structural Dynamics,* 36**,** 1581-1604.

HAUKAAS, T. & KIUREGHIAN, A. D. 2014. Finite element reliability and sensitivity methods for performance-based engineering. Berkeley: Pacific Earthquake Engineering Research Center, University of California.

HAYASHI, C. 1964. *Nonlinear Oscillations in Physical Systems*, McGraw-Hill.

IBRAHIM, R. A. 2008. Recent advances in nonlinear passive vibration isolators. *Journal of Sound and Vibration,* 314**,** 371-452.

ISMAIL, M., IKHOUANE, F. & RODELLAR, J. 2009a. The Hysteresis Bouc-Wen Model, a Survey. *Archives of Computational Methods in Engineering,* 16**,** 161-188.

ISMAIL, M., RODELLAR, J., CARUSONE, G., DOMANESCHI, M. & MARTINELLI, L. 2012a. Characterization, modeling and assessment of Roll-N-

Cage isolator using the cable-stayed bridge benchmark. *Acta Mechanica,* 224**,** 525-547.

ISMAIL, M., RODELLAR, J. & IKHOUANE, F. 2009b. An innovative isolation bearing for motion-sensitive equipment. *Journal of Sound and Vibration,* 326**,** 503-521.

ISMAIL, M., RODELLAR, J. & IKHOUANE, F. 2012b. Seismic protection of low- to moderate-mass buildings using RNC isolator. *Structural Control and Health Monitoring,* 19**,** 22-42.

ITT ENIDINE INC 2014. Wire rope Isolators, ITT Enidine Inc, New York. *www.enidine.com*.

J.M.KO, Y.CHEN, G.ZHENG & Y.Q.NI 1992. Hysteresis behaviour and empirical modelling of wire-cable vibration isolator. *International Journal of Analytical and Experimental Modal Analysis,* 7**,** 111-127.

JEEN-SHANG, L. & YIGONG, Z. 1994. Nonlinear structural identification using extended kalman filter. *Computers & Structures,* 52**,** 757-764.

KLEMBCZYK, A. R. 2014. Introduction to Shock and Vibration Isolation and Damping Systems. Available: http://taylordevices.com/Tech-Paper-archives/literature-pdf/74-Introduction_ShockandVibration.pdf [Accessed 25/04/2014].

LEBLOUBA, M., ALTOUBAT, S., EKHLASUR RAHMAN, M. & PALANI SELVARAJ, B. 2015. Elliptical Leaf Spring Shock and Vibration Mounts with Enhanced Damping and Energy Dissipation Capabilities Using Lead Spring. *Shock and Vibration,* 2015**,** 12.

LO, H. R., HAMMOND, J. K. & SAINSBURY, M. G. 1988. Non-linear system identification and modelling with applicaiton to an isolator with hysteresis. *Proceedings of the Sixth Interational Modal Analysis Conference.* Kissimmee, Florida, USA.

LOH, C.-H. & CHUNG, S.-T. 1993. A three-stage identification approach for hysteretic systems. *Earthquake Engineering & Structural Dynamics,* 22**,** 129-150.

LOZIUK, L. A. 1988. A wire rope seismic support. *Nuclear Engineering and Design,* 107**,** 201-204.

MALLICK, P. K. 1987. Static Mechanical Performance of Composite Elliptic Springs. *Journal of Engineering Materials and Technology,* 109**,** 22-26.

MALLIK, A. K. 1990. *Principles Of Vibration Control*, Affiliated East-West Press,India.

MASSA, G., PAGANO, S., ROCCA, E. & STRANO, S. 2013. Sensitive equipments on WRS-BTU isolators. *Meccanica,* 48**,** 1777-1790.

MCCALLION, H. & DAVIES, D. M. 1955. Behaviour of Rubber in Compression under Dynamic Conditions. *Proceedings of the Institution of Mechanical Engineers,* 169**,** 1125-1140.

MICHAEL LOYD, T. 1989. *Damping Phenomena in a Wire Rope Vibration Isolation System.* Doctor of Philosophy, Auburn University.

MILLER, B. A. 2004. Wire Ropes. *In:* VEYSSIÈRE, K. H. J. B. W. C. C. F. I. J. K. M. (ed.) *Encyclopedia of Materials: Science and Technology (Second Edition).* Oxford: Elsevier.

NAEIM, F. & KELLY, J. M. 1999. *Design of Seismic Isolated Structures: From Theory to Practice*, Wiley.

NAUMOSKI, N. 2014. Representative ensembles of strong earthquake records, CAEE ACGP. [Accessed 20-Nov-2014].

NAUMOSKI, N., HEIDEBRECHT, A. C., TSO, W. K. & GROUP, M. U. E. E. R. 1988. *A Selection of Representative Strong Motion Earthquake Records Having Different A/V Ratios*, McMaster University, Earthquake Engineering Research Group.

NAYFEH, A. H. & MOOK, D. T. 2008. *Nonlinear Oscillations*, Wiley.

NI, Y. Q., KO, J. M., WONG, C. W. & ZHAN, S. 1999a. Modelling and identification of a wire-cable vibration isolator via a cyclic loading test. *Proceedings of the Institution of Mechanical Engineers, Part I: Journal of Systems and Control Engineering,* 213**,** 173-182.

NI, Y. Q., KO, J. M., WONG, C. W. & ZHAN, S. 1999b. Modelling and identification of a wire-cable vibration isolator via a cyclic loading test. *Proceedings of the Institution of Mechanical Engineers, Part I: Journal of Systems and Control Engineering,* 213**,** 163-172.

ORTIZ, G. A., ALVAREZ, D. A. & BEDOYA-RUÍZ, D. 2013. Identification of Bouc–Wen type models using multi-objective optimization algorithms. *Computers & Structures,* 114-115**,** 121-132.

PAGANO, S. & STRANO, S. 2013. Wire rope springs for passive vibration control of a light steel structure. *WSEAS Transactions on Applied and Theoretical Mechanics,* 8**,** 212-221.

PAOLACCI, P. & GIANNINI, R. 2008. Study of The Effectiveness of Steel Cable Dampers For The Seismic Protection of Electrical Equipment. *The 14th World Conference on Earthquake Engineering.* Beijing, China.

PLATUS, D. L. 1992. Negative-stiffness-mechanism vibration isolation systems. *Vibration Control in Microelectronics, Optics, and Metrology, Proceedings OF SPIE,* 1619**,** 44-54.

RAVINDRA, B. & MALLIK, A. K. 1994. Performance of Non-linear Vibration Isolators Under Harmonic Excitation. *Journal of Sound and Vibration,* 170**,** 325-337.

RIVIN, E. I. 2003. *Passive Vibration Isolation,* ASME Press.

SHASKA, K., IBRAHIM, R. A. & GIBSON, R. F. 2006. Influence of excitation amplitude on the characteristics of nonlinear butyl rubber isolators. *Nonlinear Dynamics,* 47**,** 83-104.

SIMMONS, R. 2007. Vibration isolation. *ASHRAE,* 49**,** 30-40.

SNOWDON, J. C. 1968. *Vibration and shock in damped mechanical systems,* J. Wiley.

SONG, J. & KIUREGHIAN, A. D. 2006. Generalized Bouc-Wen Model for Highly Asymmetric Hysteresis. *JOURNAL OF ENGINEERING MECHANICS,* 132**,** 610-618.

TANDON, I., MALLIK, A. K. & BHAYA, P. G. 1999. PERFORMANCE CHARACTERISTICS OF A VIBRATION ISOLATOR WITH ELECTRO-RHEOLOGICAL FLUIDS. *Journal of Sound and Vibration,* 219**,** 395-404.

TIMOSHENKO, S. 1983. *Strength of Materials, Pt. 2: Advanced Theory and Problems,* R. E. Krieger Publishing Company.

TINKER, M. L. & CUTCHINS, M. A. 1992. Damping phenomena in a wire rope vibration isolation system. *Journal of Sound and Vibration,* 157**,** 7-18.

TINKER, M. L. & CUTCHINS, M. A. 1994. Instabilities In A Non-linear Model Of A Passive Damper. *Journal of Sound and Vibration,* 176**,** 415-428.

TSE, P. C., LAU, K. J., WONG, W. H. & REID, S. R. 2002. Spring stiffnesses of composite circular springs with extended flat contact surfaces under unidirectional line-loading and surface-loading configurations. *Composite Structures,* 55**,** 367-386.

TUSTIN, W. & JARIWALA, D. 2005. *Random Vibration and Shock Testing,* Equipment Reliability Institute.

VELINSKY, S. A. 1988. Design and Mechanics of Multi-Lay Wire Strands. *Journal of Mechanisms, Transmissions, and Automation in Design,* 110**,** 152-160.

VELINSKY, S. A. 1989. On the Design of Wire Rope. *Journal of Mechanisms, Transmissions, and Automation in Design,* 111**,** 382-388.

VELINSKY, S. A. 2004. Compressive Loading of Stiffened, Wire-Strand Based Structures. *Mechanics Based Design of Structures and Machines,* 32**,** 101-113.

VEPRIK, A. M. & BABITSKY, V. I. 2000. VIBRATION PROTECTION OF SENSITIVE ELECTRONIC EQUIPMENT FROM HARSH HARMONIC VIBRATION. *Journal of Sound and Vibration,* 238**,** 19-30.

VIRGIN, L. N. & DAVIS, R. B. 2003. Vibration isolation using buckled struts. *Journal of Sound and Vibration,* 260**,** 965-973.

VISINTIN, A. 2013. *Differential Models of Hysteresis,* Springer Berlin Heidelberg.

WANG, H.-X., GONG, X.-S., PAN, F. & DANG, X.-J. 2015. Experimental Investigations on the Dynamic Behaviour of O-Type Wire-Cable Vibration Isolators. *Shock and Vibration,* 2015**,** 12.

WANG, S., ZHAO, Y., ZHOU, J., LI, C. & LI, X. 2013. Static response of stranded wire helical springs to axial loads: A two-state model. *Proceedings of the Institution of Mechanical Engineers, Part C: Journal of Mechanical Engineering Science,* 227**,** 1608-1618.

WEIMIN, C., GANG, L. & WEI, C. 1997. Research on ring structure wire-rope isolators. *Journal of Materials Processing Technology,* 72**,** 24-27.

WEN, Y.-K. 1976. Method for random vibration of hysteretic systems. *Journal of the engineering mechanics division,* 102**,** 249-263.

WEN, Y. K. 1980. Equivalent Linearization for Hysteretic Systems Under Random Excitation. *Journal of Applied Mechanics,* 47**,** 150-154.

WEN, Y. K. 1989. Methods of Random Vibration for Inelastic Structures. *Applied Mechanics Reviews,* 42**,** 39-52.

WILSON, E. L., COMPUTERS & STRUCTURES, I. 1998. *Three dimensional static and dynamic analysis of structures: a physical approach with emphasis on earthquake engineering*, Computers and Structures Inc.

WINTERFLOOD, J., BARBER, T. A. & BLAIR, D. G. 2002a. Mathematical analysis of an Euler spring vibration isolator. *Physics Letters A,* 300**,** 131-139.

WINTERFLOOD, J., BLAIR, D. G. & SLAGMOLEN, B. 2002b. High performance vibration isolation using springs in Euler column buckling mode. *Physics Letters A*, 300**,** 122-130.

XIE, S. L., ZHANG, Y. H., CHEN, C. H. & ZHANG, X. N. 2013. Identification of nonlinear hysteretic systems by artificial neural network. *Mechanical Systems and Signal Processing,* 34**,** 76-87.

ZHOU, J., WANG, S., KANG, L. & CHEN, T. 2011. Design and modelling on stranded wires helical spring. *Chinese Journal of Mechanical Engineering,* 24**,** 626-637.

ZHU, T. J., HEIDEBRECHT, A. C. & TSO, W. K. 1988. Effect of peak ground acceleration to velocity ratio on ductility demand of inelastic systems. *Earthquake Engineering & Structural Dynamics,* 16**,** 63-79.

ZHU, Z. H. & MEGUID, S. A. 2007. Nonlinear FE-based investigation of flexural damping of slacking wire cables. *International Journal of Solids and Structures,* 44**,** 5122-5132.

Appendices

Appendix A: Fixture Design

The cyclic loading test was carried out in the INSTRON machine 5982 (Figure A.1). The cyclic test was performed in three loading modes (Figure A.2) namely, tension and compression, cyclic roll and cyclic shear. In INSTRON machine, the bottom grip is fixed and the top grip is moveable in both upward and downward direction. The INSTRON machine can be controlled using the control system through the software called BLUEHILL® software. The cyclic test was performed in the displacement control mode in the three displacement amplitudes namely 3 mm, 6 mm, and 9 mm. The default upward and downward movement of the top grip can be used to apply tension/compression displacement however for the lateral cyclic shear and cyclic roll a suitable fixture was designed for this work. Figure A.3 shows the cyclic loading test performed on the WRI and the Figure A.4-7 shows the specifications of the fixture. Table A-1 shows the specification of the individual parts of the fixture assembly and each part was welded together. The material of the fixture is Mild Steel.

Figure A.1 INSTRON machine 5982 used in this work

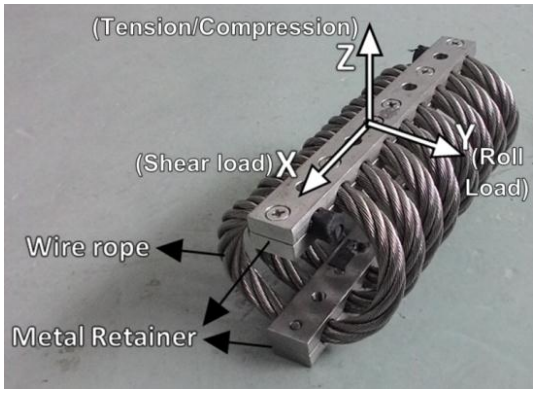

Figure A.2 Wire Rope Isolator and Loading directions

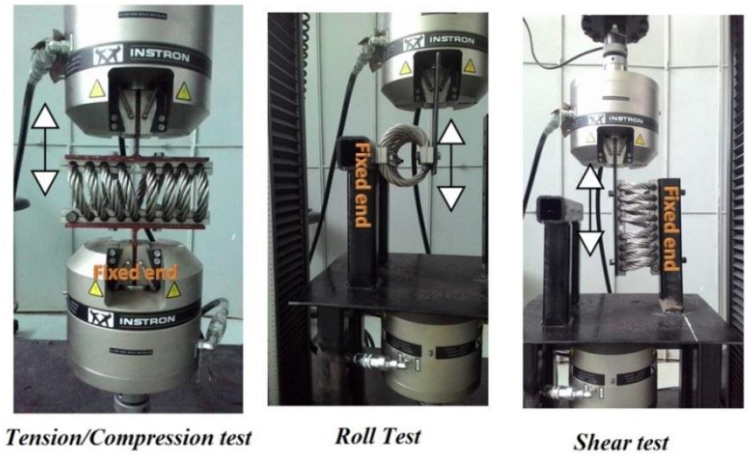

Figure A.3 Cyclic Loading setup

Figure A.4 Fixture used for cyclic shear and cyclic roll

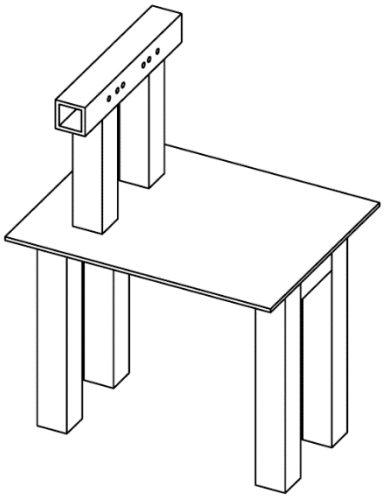

Figure A.5 Isometric view of the fixture

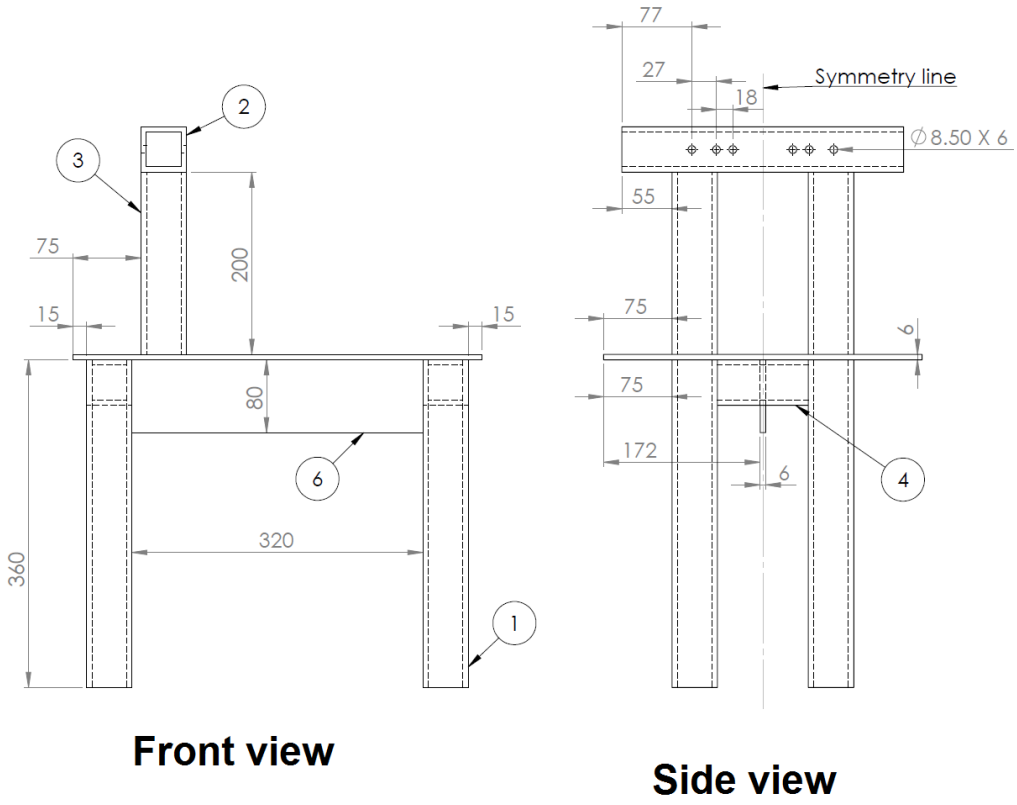

Figure A.6 Front and side view of the fixture

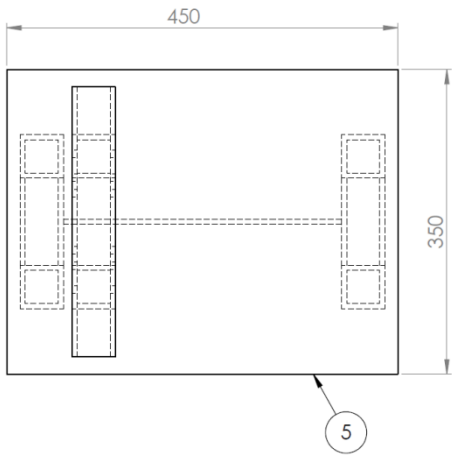

Figure A.7 Top view of the fixture

Table A-9 Specification of the fixture

Balloon No	Size	Quantity
1	50 mm x 50 mm x 6 mm steel square tube Length = 360 mm	4
2	50 mm x 50 mm x 6 mm steel square tube Length = 310 mm Through holes (6 x Dia 8.5) are required. Details of the position are given in the assembly drawing.	1
3	50 mm x 50 mm x 6 mm steel square tube Length = 200 mm	2
4	50 mm x 50 mm x 6 mm steel square tube Length = 100 mm	2
5	Steel plate 450 mm x 350 mm x 6 mm	1
6	Steel plate 320 mm x 80 mm x 6 mm	1

Appendix B: Data points of Vertical cyclic loading test

The vertical cyclic loading test was performed in INSTRON 5982 using tension/compression mode. The test was conducted in a displacement-controlled manner and at a rate of 8 mm/min. The displacements were applied in three amplitudes namely 3 mm, 6 mm and 9 mm. The displacements and corresponding restoring forces were evaluated in the BLUEHILL® software. This software also able to provide all the data points of the cyclic loading test in MICROSOFT EXCEL ® format. In this appendix, the data points of the cyclic test are provided. However, since the test is carried out at slow rate, there are over 6800 points for one complete test of each WRI. In this appendix only selected 150 points are provided in a way that the hysteresis behaviour of each WRI can be effectively represented using these points with reasonable smoothness.

ISOLATOR NO.1
Loading Direction = Tension/Compression. Rate: 8 mm/min

D (mm)	F(N)
0.577	202.8
1.1763	323.84
1.7769	443.26
2.3771	563.62
2.9762	688.8
2.4726	301.53
1.8719	152.26
1.2727	36.27
0.6727	-66.865
0.0723	-160.96
-0.4941	-243.93
-1.0941	-326.96
-1.6934	-405.52
-2.2943	-481.15
-2.8934	-552.47
-2.5536	-327.53
-1.9535	-204.51
-1.353	-98.694
-0.7538	4.2509
-0.1529	107.66
0.4133	207.09
1.0142	315.86
1.6132	428.15
2.2139	545.92
2.8137	668.02
3.4132	794.94
4.0143	927.21
4.6135	1065.1
5.214	1211
5.8139	1361.5
5.6329	976.97
5.0334	749.78
4.4324	589.86
3.8332	454.03
3.2327	331.55
2.6328	219.21
2.0335	114.21
1.4328	15.207
0.8333	-77.753
0.2328	-166.04
-0.3334	-245.49
-0.9343	-326.18
-1.5338	-403.32
-2.1336	-477.34
-2.7344	-548.03
-3.3336	-615.99
-3.9342	-681.17
-4.5339	-743.52
-5.1337	-804.26
-5.7343	-862.98
-5.7271	-729.49
-5.1269	-613.49
-4.5276	-522.48
-3.9267	-436
-3.3272	-351.72
-2.727	-265.94
-2.1268	-178.44
-1.5276	-89.131
-0.9266	3.4112
-0.3272	99.213
0.2409	193.1
0.8402	296.24
1.4406	404.89
2.0405	517.11
2.6401	635.61
3.2408	759.57
3.8399	888.98
4.4406	1027.1
5.0404	1170.5
5.6398	1323.2
6.241	1480.9
6.8402	1637.1
7.4405	1799.5
8.0403	1966.6
8.6399	2142.7
8.8062	1833.7
8.2055	1451
7.6063	1223.5
7.0056	1039
6.4059	878.25
5.8064	732.36
5.2056	598.44
4.6063	474.7
4.0056	358.31
3.4057	249.3
2.8062	147.09
2.2054	49.872
1.6062	-42.308
1.0057	-130
0.4058	-213.39
-0.1612	-289.17
-0.7605	-365.86
-1.3604	-439.51
-1.9607	-510.6
-2.56	-577.99
-3.1609	-643.79
-3.7604	-706.42
-4.3603	-767.85
-4.9609	-827.1
-5.56	-884.58
-6.1609	-940.6
-6.7606	-993.55
-7.3602	-1046.1
-7.9608	-1097.4
-8.5601	-1147.3
-8.8869	-1095.1
-8.2863	-963.51
-7.6866	-880.94
-7.0869	-805.55
-6.4863	-733.03
-5.8874	-661.99
-5.2864	-590.08
-4.6864	-517.52
-4.0868	-443.15
-3.486	-367.02
-2.887	-288.99
-2.2862	-207.51
-1.6866	-124.28
-1.0869	-37.364
-0.4863	52.865
0.0805	141.5
0.6809	238.95
1.2799	340.89
1.8808	448.57
2.4804	560.61
3.0804	678.57
3.6806	802.15
4.2798	932.17
4.881	1070.5
5.4805	1214.8
6.0804	1368.1
6.681	1528.7
7.2802	1699.7
7.8808	1882.6
8.4804	2075.6
8.9664	2102
8.3661	1513.6
7.7659	1263.7
7.166	1071.2
6.5654	906.25
5.9659	758.03
5.3658	621.62
4.7656	496.7
4.1664	379.45
3.566	268.91
2.9662	165.32
2.3661	66.281
1.7657	-26.44
1.1665	-114.79
0.5656	-199.1

ISOLATOR NO.2
Loading Direction = Tension/Compression. Rate: 8 mm/min

D (mm)	F(N)
0.57609	169.83
1.1753	258.96
1.7762	344.31
2.3758	429.24
2.9755	516.18
2.473	230.93
1.8725	124.84
1.2723	39.29
0.67322	-37.518
0.07258	-108.43
-0.49328	-171.65
-1.094	-235.31
-1.6932	-295.18
-2.294	-353.7
-2.8937	-408.85
-2.5664	-227.26
-1.9673	-133.99
-1.3664	-54.354
-0.76699	22.398
-0.16648	99.611
0.39905	172
1.0001	250.78
1.5999	330.88
2.1997	413.5
2.8004	498.51
3.3996	585.17
4.0001	675.06
4.5998	766.86
5.1994	862.47
5.8	961.39
5.646	699.08
5.0461	548.46
4.4466	438.12
3.8459	342.09
3.2464	255.68
2.6461	174.22
2.0459	97.957
1.4466	25.822
0.84573	-43.167
0.24635	-109.27
-0.3205	-169.41
-0.91968	-230.38
-1.5206	-289.36
-2.1204	-346.15
-2.7199	-401.9
-3.3205	-454.21
-3.9198	-504.64
-4.5205	-553.73
-5.1201	-600.85
-5.7197	-646.72
-5.7404	-535.09
-5.1394	-439.53
-4.5404	-367.91
-3.94	-300.27
-3.3398	-234.43
-2.7404	-169.39
-2.1395	-103.21
-1.5404	-36.6
-0.93966	32.356
-0.33951	103.08
0.22673	171.51
0.82637	246.22
1.4262	323.65
2.0267	402.98
2.626	484.78
3.2267	570.34
3.8264	658.01
4.4261	749.31
5.0267	843.83
5.6257	942.01
6.2266	1043.9
6.8265	1148
7.4262	1256.9
8.0267	1369.7
8.6259	1485.7
8.8318	1307.8
8.2327	1056.4
7.6326	906.81
7.0324	783.67
6.433	673.91
5.8324	573.04
5.233	479.81
4.6327	391.65
4.0324	309.78
3.4328	231.19
2.832	155.89
2.2325	84.744
1.6325	15.667
1.0324	-49.679
0.43308	-113.44
-0.13391	-171.55
-0.73337	-231.28
-1.3341	-288.51
-1.9333	-343.54
-2.5336	-397.48
-3.1338	-449.32
-3.7332	-500.14
-4.334	-548.75
-4.9332	-596.81
-5.5337	-643.34
-6.1338	-688.09
-6.7333	-730.53
-7.3344	-772.33
-7.9336	-813.41
-8.5337	-853.09
-8.9266	-826.09
-8.3267	-701.65
-7.7271	-632.34
-7.1262	-570.74
-6.5269	-512
-5.9266	-453.74
-5.3265	-396.26
-4.7272	-337.83
-4.1264	-279.07
-3.5269	-219.55
-2.9269	-159.29
-2.3264	-97.255
-1.7272	-33.685
-1.1262	31.914
-0.52674	99.497
0.04091	165.55
0.63929	236.41
1.24	311.09
1.8398	387.38
2.4395	467.02
3.0403	549.2
3.6393	633.95
4.2398	722.77
4.8398	814.21
5.4391	909.25
6.0402	1008.4
6.6394	1111.1
7.2399	1219.9
7.8399	1333.1
8.4394	1452.2
9.0003	1567.9
8.4197	1118.5
7.8192	952.94
7.2195	823.36
6.6195	708.99
6.0189	605.61
5.4198	510.18
4.8189	420.13
4.2191	336.14
3.6194	256.11
3.0187	180.39
2.4195	107.99
1.8188	37.458
1.2194	-28.429
0.61948	-93.262
0.01883	-155.4

ISOLATOR NO.3
Loading Direction = Tension/Compression. Rate: 8 mm/min

D(mm)	F (N)
0.57675	140.83
1.177	205.44
1.7773	262.72
2.3763	318.01
2.9773	373.97
2.4725	124.59
1.8733	41.146
1.2726	-21.623
0.67326	-75.482
0.07307	-124.36
-0.49338	-165.36
-1.0941	-207.96
-1.6936	-247.56
-2.2931	-285.41
-2.8937	-322.71
-2.553	-149.03
-1.9521	-68.427
-1.3531	-5.7725
-0.75253	51.146
-0.1528	105.53
0.41404	156.52
1.0132	206.44
1.6136	259.12
2.2142	312.64
2.8133	367.11
3.4144	422.31
4.0136	478.24
4.6137	536.4
5.2141	595.93
5.8132	657.34
5.6329	435.12
5.0331	321.16
4.4332	242.87
3.8326	176.61
3.2338	117.23
2.6328	62.42
2.0333	11.462
1.4333	-37.391
0.83289	-83.646
0.23363	-127.77
-0.33377	-165.71
-0.93301	-206.58
-1.5338	-245.66
-2.1331	-283.13
-2.7335	-320.04
-3.3339	-355.36
-3.9332	-389.63
-4.5339	-423.29
-5.1335	-456.19
-5.7337	-488.52
-5.7131	-375.1
-5.1128	-291.55
-4.5127	-234.07
-3.9133	-182.56
-3.3124	-133.27
-2.7132	-85.484
-2.113	-36.813
-1.5125	11.621
-0.91329	60.535
-0.3125	109.38
0.25347	156.29
0.85412	205.98
1.4534	253.03
2.054	305.26
2.6538	358.36
3.2533	413.54
3.8542	469.46
4.4534	526.86
5.0538	586.76
5.6537	647.91
6.2533	710.88
6.8543	775.54
7.4533	842.46
8.054	913.23
8.654	984.69
8.7932	811.62
8.1922	641.87
7.5928	542.01
6.9926	459.71
6.3924	388.03
5.793	321.57
5.1923	260.06
4.593	202.21
3.9928	147.78
3.3924	96.175
2.793	46.961
2.1922	0.08084
1.5931	-45.553
0.99289	-90.186
0.39241	-132.27
-0.17363	-168.95
-0.77358	-208.43
-1.3733	-247.02
-1.9741	-284.23
-2.5732	-319.62
-3.1738	-354.84
-3.7738	-389.21
-4.3733	-422.86
-4.9741	-455.53
-5.5732	-487.41
-6.1736	-518.78
-6.7738	-549.1
-7.3733	-578.74
-7.9739	-608.24
-8.5732	-637.19
-8.8725	-584.52
-8.2734	-484.12
-7.6722	-428.65
-7.0724	-381.73
-6.4729	-337.32
-5.8723	-294.48
-5.2734	-251.97
-4.6727	-209.16
-4.073	-166.68
-3.473	-123.04
-2.8724	-79.157
-2.2734	-34.93
-1.6725	10.909
-1.0726	56.92
-0.47302	103.83
0.09355	148.52
0.69378	197.56
1.2941	244.11
1.8933	292.83
2.4943	345.35
3.0937	398.37
3.6936	454.34
4.2939	510.97
4.8931	569.49
5.4939	629.96
6.0936	692.43
6.6935	757.46
7.2941	824.62
7.8932	894.5
8.4941	968.32
8.9528	944.36
8.3531	674.12
7.7527	563.93
7.1536	478.21
6.5527	402.86
5.953	335.11
5.3532	272.39
4.7526	213.75
4.1531	158.83
3.5523	106.28
2.9525	56.306
2.353	9.0663
1.7524	-36.706
1.1531	-81.199
0.55271	-123.98

ISOLATOR NO.4
Loading Direction = Tension/Compression. Rate: 8 mm/min

D(mm)	F (N)
0.57336	121.88
1.1744	176.25
1.7735	222.26
2.3739	265.15
2.9739	306.64
2.4726	96.532
1.8727	28.205
1.2733	-21.084
0.67255	-62.225
0.07331	-98.56
-0.49407	-129.97
-1.0932	-161.41
-1.6939	-191.53
-2.2935	-220.05
-2.8937	-247.42
-2.5522	-99.713
-1.953	-32.189
-1.3523	18.679
-0.7523	63.838
-0.15298	107.47
0.41394	146.71
1.0137	188.3
1.6142	229.03
2.2133	269.42
2.8141	309.61
3.4139	348.74
4.0137	389.38
4.6143	430.67
5.2134	472.96
5.8143	516.77
5.6327	332.49
5.032	239.92
4.4327	179.1
3.8328	128.22
3.2325	82.733
2.6332	40.753
2.0321	1.4225
1.4327	-35.315
0.83264	-70.932
0.23201	-104.01
-0.33346	-134.15
-0.93377	-164.53
-1.5333	-193.73
-2.1342	-221.77
-2.7336	-248.58
-3.334	-274.62
-3.934	-300.13
-4.5333	-324.8
-5.1341	-349.21
-5.7333	-373.22
-5.7125	-277.33
-5.1121	-203.94
-4.513	-156.21
-3.912	-114.11
-3.3125	-75.188
-2.7125	-36.58
-2.1122	1.1904
-1.513	38.79
-0.91233	76.843
-0.31296	115.28
0.25421	151.21
0.85317	190.25
1.4538	229.84
2.0539	269.06
2.653	310.02
3.2539	350.13
3.8534	390.89
4.4539	432.54
5.0541	474.73
5.6532	517.58
6.2544	561.09
6.8535	605
7.4536	650.71
8.0539	697.65
8.6531	746.72
8.7929	608.29
8.1931	472.69
7.5925	396.87
6.9935	335.72
6.3926	281.76
5.793	232.68
5.1936	187.4
4.5928	144.31
3.9934	103.87
3.3928	64.799
2.7929	27.89
2.1934	-7.8552
1.5925	-41.895
0.99322	-74.931
0.39285	-106.79
-0.1732	-135.77
-0.77421	-166.06
-1.3738	-194.82
-1.9736	-222.95
-2.574	-249.97
-3.1731	-276.24
-3.774	-301.72
-4.3735	-326.53
-4.9732	-351.39
-5.5739	-375.35
-6.1732	-398.38
-6.7741	-421.64
-7.3737	-443.83
-7.9734	-465.87
-8.5741	-488.15
-8.8734	-444.41
-8.2728	-353.56
-7.6728	-306.2
-7.0731	-266.56
-6.4724	-230.14
-5.8732	-195.16
-5.2728	-160.72
-4.6727	-126.9
-4.0734	-92.85
-3.4724	-58.525
-2.873	-24.764
-2.2726	10.205
-1.6726	45.807
-1.0732	81.84
-0.47229	118.16
0.09365	153
0.69423	190.7
1.2932	229
1.8942	268.04
2.4937	307.33
3.0935	347.9
3.6941	388.7
4.2932	430.18
4.8942	472.85
5.4935	516.19
6.0935	561
6.6943	605.75
7.2934	651.85
7.8941	699.68
8.4939	748.2
8.9526	723.74
8.3532	497.65
7.7531	411.38
7.1527	346.28
6.5536	290.32
5.9529	240.32
5.3533	194
4.7531	150.18
4.1528	109.32
3.5534	70.149
2.9526	32.881
2.3532	-2.6291
1.7532	-37.458
1.1527	-70.562
0.55356	-102.74

ISOLATOR NO.5
Loading Direction = Tension/Compression. Rate: 8 mm/min

D(mm)	F (N)
0.57457	660.24
1.1755	1067.9
1.7744	1463.2
2.375	1875.5
2.9748	2307.5
2.4731	1018.3
1.8727	515.11
1.2732	135.42
0.67252	-189.4
0.07332	-478.54
-0.49364	-725.25
-1.0929	-965.83
-1.6937	-1191.1
-2.2931	-1402.7
-2.8932	-1605.6
-2.5523	-1004.2
-1.9535	-630.38
-1.353	-302.69
-0.75297	17.614
-0.15348	348.7
0.41395	671.57
1.0138	1029.9
1.6142	1405.5
2.2132	1802.9
2.8143	2225.3
3.414	2668.2
4.0137	3147.4
4.6145	3659.2
5.2136	4207.8
5.8144	4803.1
5.6337	3441.7
5.0328	2557
4.4334	1957
3.8333	1471.7
3.2329	1058.4
2.6336	692.33
2.0328	362.89
1.4333	62.361
0.83358	-216.82
0.2331	-477.16
-0.33376	-708.48
-0.93361	-939.64
-1.533	-1158.9
-2.1339	-1368.2
-2.7332	-1566.8
-3.3335	-1757.7
-3.9337	-1941.5
-4.5332	-2121.7
-5.1339	-2297.4
-5.7332	-2465.8
-5.7127	-2119.4
-5.1123	-1766.4
-4.5131	-1490.8
-3.9121	-1235.4
-3.3129	-986.1
-2.7126	-733.49
-2.1121	-476.44
-1.513	-209.51
-0.91227	69.051
-0.3127	364.54
0.25427	661.68
0.85355	992.51
1.4541	1347.4
2.0542	1722.3
2.6536	2124.9
3.2545	2555.9
3.8535	3020.1
4.4539	3525
5.0542	4067.2
5.6536	4658.5
6.2544	5293.4
6.8536	5972.7
7.4541	6735.5
8.0543	7569.5
8.6535	8480
8.7938	7427.1
8.1943	5645.8
7.5932	4603
6.9938	3807.4
6.3933	3150.9
5.7933	2592.8
5.1939	2105.3
4.5932	1673.9
3.994	1286.6
3.3935	934.05
2.7936	611.54
2.1944	312.65
1.5936	33.753
0.99404	-227.23
0.39349	-474.92
-0.17296	-695.3
-0.77372	-919.27
-1.3733	-1132.1
-1.9732	-1336.3
-2.574	-1532.5
-3.173	-1720.8
-3.7741	-1904.2
-4.3737	-2082.3
-4.9732	-2256.7
-5.5737	-2426.3
-6.1728	-2589.9
-6.7738	-2748.9
-7.3733	-2902.3
-7.973	-3052.9
-8.5738	-3201.1
-8.8734	-3070.2
-8.2728	-2682.1
-7.6731	-2425.3
-7.0735	-2194.8
-6.4726	-1975.7
-5.8733	-1762.8
-5.2729	-1549.3
-4.6729	-1337.2
-4.0734	-1120.3
-3.4725	-898.41
-2.8735	-669.45
-2.2729	-428.55
-1.673	-178.59
-1.0736	85.492
-0.47254	366.16
0.09371	646.69
0.69417	960.84
1.2934	1296.9
1.8941	1656.6
2.4937	2040.2
3.0936	2453.6
3.6944	2899.5
4.2934	3379.4
4.8941	3901.5
5.4937	4465.6
6.0936	5085.2
6.6943	5754.1
7.2933	6493.6
7.8941	7318.2
8.4938	8221.8
8.9532	8494.4
8.3536	5993
7.7535	4838.9
7.1532	3993.1
6.554	3308.8
5.9535	2726.9
5.3538	2225.3
4.7538	1780.1
4.1534	1382
3.5542	1024.1
2.9535	695.21
2.3536	392.18
1.7538	109.36
1.1531	-154.37
0.55394	-404.34

ISOLATOR NO.6
Loading Direction = Tension/Compression. Rate: 8 mm/min

D(mm)	F (N)
0.575	332.11
1.1756	499.76
1.7748	637.97
2.3757	765.35
2.9753	900.24
2.4727	256.56
1.8727	39.558
1.2735	-112.68
0.67278	-244.73
0.07326	-365.49
-0.49415	-475.01
-1.0933	-583.21
-1.6942	-686.83
-2.2939	-785.2
-2.8936	-881.39
-2.5523	-437.81
-1.953	-219.14
-1.352	-56.508
-0.75239	89.946
-0.15254	232.72
0.41357	363.26
1.0138	500.64
1.6143	632.53
2.2135	758.57
2.8144	883.14
3.4136	1018.2
4.0139	1157.4
4.6143	1298.8
5.2133	1443.3
5.8142	1591.2
5.6337	1034.7
5.0329	722.63
4.4331	524.92
3.8334	360
3.2328	212.73
2.6336	77.831
2.033	-47.222
1.4331	-163.64
0.83332	-275.07
0.23254	-382.67
-0.33379	-481.85
-0.93411	-584.19
-1.5334	-683.98
-2.1343	-780.65
-2.7339	-874.2
-3.3339	-964.53
-3.9342	-1051.2
-4.5333	-1136.2
-5.1341	-1220.4
-5.7336	-1301.8
-5.713	-1026.7
-5.1127	-795.31
-4.5135	-644.7
-3.9125	-511.36
-3.3132	-385.21
-2.7127	-260.52
-2.1128	-137.44
-1.5135	-13.958
-0.91243	111.23
-0.31319	236.7
0.25423	357.36
0.85333	486.36
1.4539	616.6
2.0537	745.54
2.6534	870.03
3.2542	993.75
3.8533	1132.7
4.4541	1276.6
5.0538	1421.8
5.6533	1569.7
6.2542	1717
6.8535	1866
7.4539	2020.4
8.0538	2175.7
8.6532	2335.8
8.7923	1954.9
8.193	1503.8
7.5925	1258.2
6.9934	1061.4
6.3931	886.78
5.7929	727.74
5.1933	578.42
4.5925	437.22
3.993	303.33
3.3927	175.04
2.7925	52.535
2.1931	-64.83
1.5923	-176.14
0.99318	-282.83
0.39316	-385.96
-0.17367	-480.1
-0.77445	-578.63
-1.3742	-674.68
-1.9737	-770.03
-2.5741	-862.72
-3.1736	-952.85
-3.7739	-1041.3
-4.374	-1127.1
-4.9736	-1211.2
-5.5746	-1293.3
-6.1737	-1372.6
-6.7742	-1450.8
-7.3744	-1526.9
-7.9737	-1602.6
-8.5743	-1676.8
-8.8733	-1567.3
-8.2726	-1288.8
-7.6727	-1143.1
-7.0728	-1019.8
-6.4724	-905.02
-5.8734	-794.43
-5.2726	-683.98
-4.6729	-574.66
-4.0732	-464.45
-3.4726	-353.78
-2.8734	-241.73
-2.2725	-127.31
-1.6728	-12.477
-1.0731	105.52
-0.47246	225.19
0.0939	341.56
0.69421	466.18
1.2934	592.33
1.8944	721.52
2.4939	849.09
3.0941	967.74
3.694	1096.1
4.2932	1235.9
4.8942	1380.4
5.4937	1525.6
6.0936	1674.8
6.6942	1825.8
7.2934	1981
7.8942	2140.5
8.4938	2302.2
8.9523	2274.8
8.353	1587.7
7.7532	1313.3
7.1525	1105.5
6.5531	926.82
5.9523	763.97
5.3526	613.45
4.7531	471.33
4.1523	335.78
3.5531	207.22
2.9525	83.161
2.3529	-35.403
1.7533	-149.86
1.1525	-258.82
0.55344	-363.05

ISOLATOR NO.7
Loading Direction = Tension/Compression. Rate: 8 mm/min

D(mm)	F (N)	1.4593	791.93	8.8325	8939.8	-4.1261	-854.27
0.5766	991.22	0.85929	427.09	8.2329	7062.9	-3.5267	-542.36
1.1758	1577.9	0.25933	83.087	7.6322	5999.1	-2.9266	-222.54
1.7764	2119.4	-0.30746	-227.92	7.0324	5172	-2.326	105.95
2.3759	2653.6	-0.9071	-541.54	6.4332	4467.9	-1.7269	445.87
2.9758	3196.7	-1.5067	-842.6	5.8325	3844	-1.1262	798.37
2.4732	1804.6	-2.1072	-1133.9	5.2332	3291.4	-0.52682	1164.1
1.8727	1201.9	-2.7065	-1412.2	4.6329	2787.6	0.04019	1527
1.2725	738.13	-3.3072	-1679.7	4.0328	2330.9	0.63941	1924.6
0.67298	334.71	-3.9069	-1933.9	3.4333	1904.3	1.2399	2344.8
0.07242	-30.137	-4.5063	-2182.7	2.8326	1503.9	1.8401	2783.3
-0.49332	-341.36	-5.1071	-2425.9	2.2329	1127.4	2.4395	3243.1
-1.0938	-646.52	-5.7066	-2662	1.6325	768.34	3.0402	3722.3
-1.693	-937.91	-5.7533	-2267	1.0325	426.71	3.6395	4222.1
-2.2937	-1218.1	-5.1534	-1767.4	0.43314	97.823	4.24	4757.5
-2.8935	-1487.4	-4.5527	-1381.2	-0.13358	-198.92	4.8401	5322.6
-2.5665	-766.84	-3.9533	-1023.5	-0.73322	-503.09	5.4393	5919.9
-1.9672	-261.92	-3.3527	-671.77	-1.3342	-796.44	6.0403	6560.5
-1.366	177.89	-2.7534	-324.1	-1.9333	-1080.2	6.6397	7228.5
-0.76659	599.86	-2.1533	28.466	-2.5341	-1356.6	7.2399	7940.9
-0.16664	1022.9	-1.5525	389.19	-3.1337	-1620.8	7.8403	8696.2
0.39897	1428.6	-0.95357	758.99	-3.7332	-1878.2	8.4394	9500.2
0.99963	1873.4	-0.35293	1144.6	-4.3337	-2130.3	9.0044	10264
1.5994	2329.9	0.21264	1521.8	-4.9329	-2373.7	8.406	7455.8
2.1992	2808.1	0.81356	1939	-5.5338	-2614.8	7.8061	6276.6
2.8001	3303.4	1.4128	2372.8	-6.1336	-2846.5	7.2066	5393.5
3.3991	3812.1	2.0132	2830.5	-6.7331	-3072.1	6.6057	4657.1
3.9996	4348.3	2.6134	3304.8	-7.334	-3293.8	6.0063	4014.9
4.5995	4912.3	3.2126	3798.9	-7.9334	-3510.6	5.4057	3439.5
5.1989	5522	3.8135	4318.7	-8.5339	-3726.4	4.806	2926.9
5.7997	6168.6	4.4128	4868.5	-8.9265	-3657.3	4.2065	2458.3
5.6601	4838	5.013	5454.8	-8.326	-3060.9	3.6059	2024.6
5.0592	3819.8	5.6136	6078.1	-7.7269	-2698	3.0065	1619.8
4.4598	3118.4	6.2127	6730.6	-7.1261	-2373	2.4062	1236.6
3.8592	2538.4	6.8135	7417.2	-6.5268	-2063.8	1.8061	874.45
3.2589	2036.6	7.4128	8139.4	-5.9267	-1760.7	1.2067	528.38
2.6598	1587.2	8.0131	8914.8	-5.3261	-1461	0.60591	195.36
2.0589	1174.7	8.6135	9733	-4.7271	-1161.4	0.00638	-121.36

ISOLATOR NO.8
Loading Direction = Tension/Compression. Rate: 8 mm/min

D(mm)	F (N)	1.4466	-572.1	8.8322	3536.4	-4.1132	-746.51
0.57478	518.4	0.84599	-775.54	8.2329	2497.1	-3.5135	-542.55
1.1741	799.7	0.24651	-969.96	7.6328	1972.3	-2.9126	-338.46
1.7749	1057.7	-0.32075	-1145.8	7.0326	1581.5	-2.3135	-132.68
2.3743	1303.7	-0.92001	-1323.5	6.4333	1254.4	-1.713	74.58
2.9744	1547.8	-1.5206	-1495.6	5.8326	961.4	-1.1132	281.86
2.4727	359.96	-2.1206	-1659.4	5.233	694.56	-0.51359	494.36
1.8724	-105.59	-2.7202	-1815.3	4.6326	445.6	0.05242	694.88
1.2724	-421.43	-3.3209	-1959.8	4.0322	213.6	0.65286	913.23
0.67318	-685.49	-3.92	-2101.6	3.4331	-8.0803	1.2535	1133.7
0.07235	-914.18	-4.5206	-2243.5	2.8322	-218.47	1.8523	1355.5
-0.49375	-1110.5	-5.1205	-2381.1	2.2325	-417.01	2.453	1584.2
-1.0945	-1300.9	-5.72	-2519.6	1.6326	-611.32	3.0526	1814.5
-1.6934	-1478.5	-5.7403	-2030.1	1.0325	-798.24	3.6527	2052.7
-2.2939	-1645.6	-5.1392	-1513.2	0.43315	-980.73	4.2531	2291.8
-2.8938	-1804.4	-4.5404	-1193.1	-0.13406	-1146.2	4.8524	2535.3
-2.5537	-968.83	-3.9398	-922.73	-0.73352	-1317.3	5.453	2785.6
-1.9528	-510.66	-3.3401	-677.09	-1.3341	-1483	6.0528	3039.1
-1.3531	-181.89	-2.7405	-440.56	-1.9334	-1644.3	6.6526	3300
-0.75336	105.92	-2.1395	-211.35	-2.534	-1802	7.2533	3563.2
-0.1528	374.11	-1.5404	15.32	-3.1338	-1952.5	7.8524	3831.3
0.41284	615.22	-0.93981	241.8	-3.7332	-2099.6	8.4531	4103.2
1.0132	861.35	-0.33973	465.44	-4.3339	-2244.6	9.0043	4330
1.6124	1102.5	0.2264	677.22	-4.9335	-2383.7	8.4055	2763.4
2.2131	1340.6	0.82601	901.32	-5.5341	-2519.3	7.8056	2137
2.8128	1573.6	1.4259	1130.4	-6.1342	-2650.3	7.2063	1701.9
3.4129	1803	2.0267	1359.6	-6.7335	-2780.4	6.6057	1348.1
4.0132	2035.2	2.6259	1591	-7.3344	-2907.6	6.0064	1046.4
4.6125	2275	3.2265	1827.5	-7.9337	-3030.7	5.4062	768.4
5.2135	2519.3	3.8262	2064.7	-8.5338	-3151.9	4.806	514.99
5.813	2766.6	4.4261	2307.4	-8.9125	-3026.4	4.2065	276.3
5.6462	1780.6	5.0267	2551.4	-8.3135	-2398.9	3.6058	51.311
5.0462	1112.9	5.6257	2798.2	-7.7128	-2078.2	3.0061	-160.51
4.4467	715.08	6.2262	3045.2	-7.1131	-1818.8	2.4058	-367.14
3.846	398.1	6.8261	3292.3	-6.5137	-1586	1.8056	-561.73
3.2466	123.83	7.4259	3547.4	-5.9128	-1370.1	1.2064	-751.18
2.6463	-127.13	8.0266	3808.7	-5.3137	-1158.7	0.60557	-935
2.046	-357.53	8.6257	4070.2	-4.713	-949.95	0.00603	-1110.6

ISOLATOR NO.9
Loading Direction = Tension/Compression. Rate: 8 mm/min

D(mm)	F (N)
0.5744	482.76
1.175	761.16
1.775	975.66
2.3744	1173.2
2.9753	1362.2
2.4728	341.7
1.8736	10.261
1.2728	-204.19
0.67303	-379.96
0.07375	-535.83
-0.4937	-670.84
-1.0939	-807.99
-1.6941	-938.35
-2.2934	-1064.1
-2.8941	-1185.3
-2.5521	-468.51
-1.952	-120.67
-1.3528	112.93
-0.75188	315.11
-0.15286	503.42
0.41434	677.56
1.0134	858.12
1.6142	1036.7
2.2138	1212.1
2.8137	1387.3
3.4145	1556.2
4.0134	1728.5
4.6141	1905.5
5.2139	2083
5.8136	2263.4
5.6336	1388.6
5.0331	908.46
4.4339	642.07
3.8333	430.77
3.2339	242.74
2.6334	67.87
2.0334	-94.205
1.4341	-248.07
0.83343	-395.67
0.2338	-536.85
-0.33406	-666.15
-0.93333	-798.29
-1.5339	-927.37
-2.1337	-1052.6
-2.7333	-1172.7
-3.334	-1286.3
-3.9334	-1397.5
-4.5342	-1510.1
-5.1341	-1618.8
-5.7333	-1725.4
-5.7135	-1265.7
-5.1124	-874.65
-4.5129	-647.32
-3.9132	-454.1
-3.3127	-277.29
-2.7135	-106.85
-2.1126	61.694
-1.5129	226.27
-0.91304	390.96
-0.31246	554.87
0.25386	712.11
0.85416	878.42
1.4534	1046.4
2.0543	1215.8
2.6538	1384
3.2537	1555.9
3.8541	1727
4.4533	1900.9
5.0543	2077.1
5.6537	2253.6
6.2537	2430
6.8541	2606.9
7.4533	2789.5
8.0543	2975.7
8.6538	3163.3
8.8063	2615.4
8.2072	1881.6
7.6064	1550.8
7.0071	1301.7
6.4066	1085.3
5.8065	888.44
5.207	704.56
4.6064	530.21
4.0069	364.39
3.4063	203.69
2.8062	50.156
2.207	-100.12
1.6063	-245.8
1.0068	-384.72
0.4066	-520.85
-0.16	-645.19
-0.76097	-775.39
-1.3604	-901.21
-1.9601	-1026.3
-2.5606	-1147.4
-3.1599	-1265
-3.7606	-1379.4
-4.3606	-1491.2
-4.9601	-1603.1
-5.5608	-1711.4
-6.1602	-1813.3
-6.7609	-1913.7
-7.3607	-2012.5
-7.9598	-2110.1
-8.5609	-2207.2
-8.8856	-2037.6
-8.2862	-1553.1
-7.6865	-1323.5
-7.0861	-1141.6
-6.4868	-976.25
-5.8859	-818.27
-5.2862	-664.51
-4.6861	-511.31
-4.0858	-361.4
-3.4867	-211.04
-2.8857	-59.997
-2.2862	91.172
-1.6865	244.92
-1.0858	398.69
-0.48672	553.71
0.08076	703.43
0.68014	864.71
1.2811	1027.7
1.88	1189.9
2.4803	1357.1
3.0807	1523.8
3.6801	1693.7
4.281	1865.4
4.8805	2038.3
5.4807	2215.4
6.0806	2393
6.6799	2573.6
7.281	2759.1
7.8804	2945.9
8.4804	3137.2
8.9803	3181.7
8.3794	2029.5
7.7801	1646.5
7.1797	1378.3
6.58	1155.3
5.9806	952.16
5.3799	762.33
4.7803	586.2
4.18	416.66
3.5796	255.64
2.9803	99.181
2.3793	-52.41
1.78	-198.34
1.1797	-341.29
0.57954	-478.1

Appendix C: Data points of Lateral cyclic loading test

The lateral cyclic loading test was performed in INSTRON 5982 using cyclic roll mode. The test was conducted in a displacement-controlled manner and at a rate of 8 mm/min. The displacements were applied in three amplitudes namely 3 mm, 6 mm and 9 mm. The displacements and corresponding restoring forces are evaluated in the BLUEHILL® software. This software also able to provide all the data points of the cyclic loading test in MICROSOFT EXCEL ® format. In this appendix, the data points of the cyclic test are provided. However, since the test is carried out at slow rate, there are over 6800 points for one complete test of each WRI. In this appendix only selected 150 points are provided in a way that the hysteresis behaviour of each WRI can be effectively represented using these points with reasonable smoothness.

ISOLATOR NO.1
Loading Direction = Cyclic Roll. Rate: 8 mm/min

D(mm)	F (N)
0.57612	80.363
1.1763	121.33
1.7757	155.9
2.3767	188.1
2.9759	218.51
2.4726	105.12
1.8722	60.402
1.2731	24.74
0.67247	-8.4753
0.07282	-39.599
-0.4943	-68.977
-1.0936	-99.51
-1.6943	-130.36
-2.294	-161.2
-2.8935	-192.46
-2.5524	-86.831
-1.953	-34.92
-1.3523	4.6118
-0.75293	39.288
-0.15295	72.2
0.41333	101.41
1.014	132.1
1.6141	161.39
2.2134	191.1
2.8141	219.8
3.4133	247.62
4.0138	276.17
4.614	303.75
5.2133	331.16
5.8143	358.78
5.6326	271.14
5.032	218.95
4.4321	181.45
3.8327	148.2
3.2321	116.1
2.6328	85.244
2.0323	54.852
1.4322	24.716
0.83267	-5.2461
0.23157	-35.512
-0.33354	-63.775
-0.93411	-93.802
-1.5334	-124.42
-2.1342	-155.46
-2.7339	-186.56
-3.334	-217.91
-3.9345	-249.29
-4.5336	-281.18
-5.1342	-313.86
-5.7337	-346.63
-5.7127	-270.58
-5.1128	-202.49
-4.5132	-156.66
-3.9122	-117.33
-3.3131	-81.724
-2.7128	-47.48
-2.113	-14.617
-1.5134	16.622
-0.91248	47.49
-0.31344	76.898
0.25424	104.91
0.85303	134.2
1.4539	162.58
2.0536	191.19
2.6537	218.89
3.2542	246.95
3.8533	274.2
4.4542	301.62
5.0538	328.81
5.6534	356.24
6.2541	383.45
6.8532	410.28
7.454	437.28
8.0533	464.15
8.6534	491.56
8.7924	436.49
8.193	371
7.5919	330.88
6.9928	296.51
6.3926	264.14
5.7924	233.4
5.1932	203.54
4.5923	173.85
3.993	144.53
3.3929	115.55
2.7924	86.852
2.193	57.864
1.592	28.857
0.99256	-0.03947
0.39279	-29.132
-0.17345	-56.459
-0.77384	-86.386
-1.3742	-115.92
-1.9735	-145.88
-2.5743	-176.98
-3.1737	-208.08
-3.7737	-239.86
-4.374	-272.11
-4.9732	-305.31
-5.5742	-338.89
-6.1735	-372.94
-6.7737	-407.16
-7.3742	-442.04
-7.9736	-477.48
-8.5745	-513.46
-8.8736	-482.51
-8.2727	-382.53
-7.6732	-327.26
-7.0732	-281.43
-6.4728	-241.31
-5.8736	-203.22
-5.2726	-167.03
-4.6732	-132.71
-4.0732	-99.323
-3.4729	-67.113
-2.8736	-35.721
-2.2727	-5.1321
-1.6732	24.228
-1.0732	54.037
-0.47282	82.794
0.09403	109.78
0.69393	137.74
1.2934	166
1.8943	193.48
2.4935	220.61
3.0938	247.99
3.6938	274.94
4.2932	301.64
4.8941	328.52
5.4935	355.16
6.0937	381.98
6.694	408.91
7.2932	435.6
7.8942	462.71
8.4936	489.7
8.9523	487.56
8.3525	388.96
7.7532	346.02
7.1525	310.46
6.5532	277.85
5.9524	246.82
5.3526	216.85
4.7533	187.23
4.1524	157.98
3.553	129.31
2.9525	100.65
2.3525	71.796
1.7531	43.063
1.1524	14.204
0.55309	-14.257

ISOLATOR NO.2
Loading Direction = Cyclic Roll. Rate: 8 mm/min

D(mm)	F (N)
0.5761	53.823
1.1771	77.848
1.7761	99.494
2.3768	119.58
2.9767	138.75
2.473	52.611
1.8732	20.653
1.2736	-3.0833
0.67282	-23.939
0.07362	-44.286
-0.49399	-62.482
-1.0932	-81.762
-1.6942	-101.05
-2.2937	-119.77
-2.8939	-138.19
-2.5522	-59.119
-1.9529	-22.753
-1.3523	3.2332
-0.75196	25.548
-0.15277	46.501
0.41403	65.708
1.0137	84.965
1.6144	104.52
2.2135	122.83
2.8145	141.17
3.4142	158.71
4.0137	176.83
4.6143	194.45
5.2134	212.08
5.8142	230.17
5.6336	161.88
5.0328	121.82
4.4337	95.743
3.8334	73.121
3.2331	51.843
2.6338	31.871
2.0329	12.189
1.4334	-6.8687
0.83322	-25.776
0.23304	-44.495
-0.3341	-62.157
-0.93392	-80.385
-1.5336	-99.249
-2.1344	-117.89
-2.7335	-135.98
-3.334	-155.05
-3.934	-173.2
-4.5335	-191.9
-5.1341	-210.5
-5.7333	-229.46
-5.7133	-172.5
-5.1126	-124.56
-4.5135	-95.656
-3.9126	-71.053
-3.313	-48.507
-2.713	-27.15
-2.1125	-6.556
-1.5135	13.433
-0.91284	33.012
-0.31302	52.116
0.25426	69.494
0.8537	87.896
1.4541	106.64
2.0543	124.33
2.6535	142.45
3.2544	160.25
3.8537	178.13
4.454	195.8
5.0545	213.1
5.6536	230.56
6.2545	247.99
6.8537	265.15
7.454	282.76
8.0545	300.38
8.6533	318.06
8.793	274.61
8.1935	222.27
7.5929	194.16
6.9939	170.34
6.3931	148.51
5.7933	127.85
5.1936	107.6
4.593	87.822
3.9935	68.465
3.3927	49.501
2.7929	30.766
2.1936	12.322
1.5929	-5.9686
0.99371	-24.212
0.39314	-42.321
-0.17366	-59.413
-0.77449	-77.716
-1.3737	-95.912
-1.9738	-114.55
-2.574	-132.79
-3.1733	-151.03
-3.774	-169.84
-4.3737	-188.43
-4.9737	-207.45
-5.5742	-226.73
-6.1736	-245.78
-6.7745	-265.06
-7.3739	-284.18
-7.9735	-303.95
-8.574	-324.06
-8.8731	-299.11
-8.2725	-230.26
-7.6726	-196.89
-7.0731	-169.29
-6.472	-144.5
-5.873	-121.73
-5.2727	-99.492
-4.6727	-78.772
-4.0733	-58.062
-3.4722	-38.047
-2.8731	-18.306
-2.2725	0.75596
-1.6725	19.566
-1.0733	38.229
-0.47228	56.254
0.09373	73.589
0.69448	91.412
1.2936	109.41
1.8944	126.98
2.4939	144.5
3.0939	162.02
3.6946	179.65
4.2935	196.67
4.8942	214.34
5.4938	231.51
6.0936	248.72
6.6944	265.95
7.2936	283.07
7.8942	301.11
8.4942	318.75
8.953	314.52
8.3538	235.58
7.7534	204.16
7.1529	179.39
6.5538	156.85
5.9531	135.67
5.3535	115.37
4.7531	95.159
4.1529	76.041
3.5539	56.983
2.9531	38.101
2.3536	19.433
1.7534	0.82504
1.1531	-17.075
0.55393	-35.148

ISOLATOR NO.3
Loading Direction = Cyclic Roll. Rate: 8 mm/min

D(mm)	F (N)
0.57513	42.644
1.1755	59.989
1.7746	73.806
2.3755	86.953
2.9747	99.87
2.4729	28.924
1.8725	1.3501
1.2731	-17.485
0.67221	-33.429
0.07315	-48.245
-0.49394	-61.298
-1.093	-74.44
-1.6937	-87.64
-2.2937	-100.49
-2.893	-112.9
-2.5526	-47.312
-1.9534	-15.453
-1.3526	4.3146
-0.75287	20.671
-0.15308	35.644
0.41352	48.423
1.014	62.026
1.6138	74.896
2.2132	87.53
2.8143	99.864
3.4136	111.61
4.0138	123.64
4.6141	135.29
5.2134	146.82
5.8143	158.64
5.6333	102.4
5.0324	66.625
4.4328	45.701
3.8332	28.774
3.2322	13.485
2.6331	-1.1863
2.0324	-15.309
1.4326	-28.851
0.8332	-41.703
0.23252	-54.529
-0.33337	-65.914
-0.93381	-78.001
-1.5328	-90.224
-2.1337	-102.51
-2.7331	-114.21
-3.3331	-125.98
-3.9337	-137.69
-4.533	-149.96
-5.1339	-161.86
-5.7333	-173.75
-5.7126	-127.77
-5.1123	-86.375
-4.513	-64.192
-3.9122	-45.947
-3.313	-30.249
-2.7125	-15.203
-2.1122	-1.1411
-1.5131	12.308
-0.91215	25.434
-0.3129	38.645
0.2541	50.107
0.85348	62.632
1.4542	75.039
2.0539	87.372
2.6536	99.031
3.254	110.98
3.8531	122.74
4.454	134.52
5.0538	146.39
5.6535	157.81
6.2542	169.47
6.8533	180.66
7.4542	192.51
8.0539	204.07
8.6534	215.87
8.7927	180.68
8.1936	134.02
7.5927	110.34
6.9932	92.366
6.3927	75.7
5.7926	60.452
5.1934	46.081
4.5926	32.125
3.9932	18.683
3.3931	5.7912
2.7928	-6.8775
2.1935	-19.355
1.5929	-31.435
0.99306	-43.92
0.39314	-55.908
-0.17306	-67.286
-0.77369	-79.306
-1.3735	-90.856
-1.9729	-102.56
-2.5737	-114.36
-3.173	-126.05
-3.7736	-138.01
-4.3737	-149.77
-4.973	-161.05
-5.5737	-173.19
-6.173	-185.27
-6.7735	-197.27
-7.3735	-209.22
-7.9727	-221.22
-8.5736	-234.05
-8.8735	-213.63
-8.2727	-157.12
-7.6734	-130.84
-7.0733	-111.65
-6.4728	-94.766
-5.8738	-78.811
-5.2731	-64.262
-4.6735	-50.234
-4.0735	-36.12
-3.4728	-22.774
-2.8737	-10.281
-2.2728	2.607
-1.6732	15.046
-1.0735	27.353
-0.47268	39.884
0.09396	51.121
0.69424	62.996
1.2935	75.139
1.8943	87.2
2.4936	98.55
3.094	110.47
3.6942	122.52
4.2934	133.79
4.8941	145.42
5.4935	157.06
6.0939	168.82
6.6943	180.51
7.2935	192.18
7.8945	203.73
8.4938	215.17
8.9523	211.46
8.3527	143.74
7.753	116.43
7.1523	96.708
6.5534	79.747
5.953	63.957
5.353	49.841
4.7535	35.317
4.1526	22.146
3.5535	8.7798
2.9528	-3.8871
2.3527	-16.75
1.7531	-29.377
1.1525	-40.93
0.5531	-53.055

ISOLATOR NO.4
Loading Direction = Cyclic Roll. Rate: 8 mm/min

D(mm)	F (N)
0.57783	42.219
1.1772	57.146
1.7774	69.479
2.3777	80.484
2.9769	90.997
2.473	16.856
1.872	-11.351
1.2729	-29.216
0.67233	-43.418
0.07214	-56.312
-0.49413	-67.447
-1.0938	-78.346
-1.6938	-89.331
-2.2944	-99.305
-2.8936	-109.55
-2.5532	-41.722
-1.9534	-8.8795
-1.3532	10.352
-0.75395	24.962
-0.15321	38.193
0.4129	49.639
1.0137	60.789
1.6131	71.901
2.2134	82.137
2.8137	92.033
3.413	101.4
4.014	111.34
4.6134	120.42
5.2133	130.16
5.8138	139.33
5.6323	82.063
5.0324	46.217
4.4317	25.993
3.8325	10.204
3.2315	-3.5798
2.6321	-16.313
2.0323	-28.529
1.4317	-39.652
0.83263	-50.787
0.23169	-61.464
-0.3336	-71.256
-0.93459	-81.758
-1.5339	-92.104
-2.1336	-101.82
-2.7341	-111.27
-3.3335	-120.94
-3.9343	-130.39
-4.5336	-140.43
-5.134	-149.9
-5.7343	-159.82
-5.7126	-112
-5.1132	-68.673
-4.513	-46.845
-3.9125	-30.539
-3.3135	-16.612
-2.7126	-3.6266
-2.1134	8.4227
-1.5129	20.252
-0.91257	31.155
-0.31354	42.039
0.2536	52.065
0.853	62.263
1.4537	72.852
2.0528	83.074
2.6536	92.663
3.2534	102.48
3.853	112.04
4.4538	121.66
5.0529	130.74
5.6536	140.5
6.2536	149.36
6.8529	158.67
7.4537	167.84
8.0531	177.38
8.6534	187.38
8.7921	151.01
8.1927	103.92
7.5921	80.785
6.992	63.96
6.3925	49.534
5.7916	36.077
5.1925	23.855
4.5919	11.903
3.9919	0.51071
3.3927	-10.737
2.7922	-21.646
2.1926	-32.216
1.5922	-42.877
0.99206	-53.242
0.39273	-63.28
-0.17361	-72.637
-0.77332	-82.641
-1.3741	-92.56
-1.9734	-102.37
-2.5742	-112.41
-3.174	-121.81
-3.7736	-131.41
-4.3743	-140.91
-4.9736	-150.71
-5.5742	-160.59
-6.1741	-170.1
-6.7735	-179.52
-7.3742	-189.21
-7.9734	-198.96
-8.574	-208.9
-8.8872	-190.13
-8.2866	-129.74
-7.6865	-103.52
-7.0872	-85.119
-6.4863	-69.937
-5.887	-56.404
-5.2866	-43.09
-4.6865	-31.466
-4.0873	-19.803
-3.4863	-8.6562
-2.887	2.0056
-2.2866	12.788
-1.6863	23.143
-1.0872	33.587
-0.48623	43.652
0.07981	53.436
0.68045	63.422
1.2796	73.042
1.8803	82.935
2.4802	92.938
3.0796	102.52
3.6803	112.17
4.2796	121.76
4.8802	131.46
5.4801	140.69
6.0796	150.53
6.6805	159.79
7.2796	169.24
7.8802	178.64
8.4803	188.2
8.9661	186.02
8.3653	113.93
7.7656	86.65
7.1662	68.064
6.5655	52.962
5.9661	39.47
5.3654	26.461
4.7653	14.475
4.1659	2.7436
3.5651	-8.2872
2.9658	-19.3
2.3653	-29.826
1.7655	-40.553
1.1662	-50.458
0.56536	-61.046

ISOLATOR NO.5
Loading Direction = Cyclic Roll. Rate: 8 mm/min

D(mm)	F (N)
0.57507	156.36
1.1743	226.77
1.7747	287.73
2.3748	345.33
2.9742	401.05
2.4727	140.85
1.872	29.477
1.2723	-45.758
0.67257	-111.6
0.072	-172.83
-0.49399	-227.24
-1.094	-283.03
-1.6934	-337.8
-2.2941	-391.14
-2.8934	-444.16
-2.5666	-225.21
-1.9674	-102.85
-1.3664	-23.817
-0.76688	44.391
-0.16713	107.63
0.39899	164.76
0.9992	224.33
1.5993	281.33
2.1988	337.68
2.7999	392.68
3.3992	445.21
3.9994	498.34
4.5999	550.9
5.199	603.48
5.7999	656.01
5.6596	470.23
5.0585	325.88
4.4593	241.42
3.8586	171.22
3.2589	107.11
2.6597	46.951
2.0589	-11.913
1.4595	-67.936
0.859	-124.37
0.25899	-178.85
-0.30744	-230.06
-0.90658	-283.03
-1.5065	-336.42
-2.1071	-388.7
-2.7063	-439.81
-3.3074	-490.25
-3.907	-541.19
-4.5068	-592.25
-5.1073	-643.64
-5.7067	-695
-5.7533	-568.29
-5.1537	-406.77
-4.5531	-319
-3.9537	-248.39
-3.3531	-184.29
-2.7534	-123.69
-2.1538	-64.72
-1.5528	-6.8038
-0.95367	49.61
-0.35315	106.21
0.21231	158.36
0.81303	213.52
1.4125	267.87
2.0126	323
2.6131	376.96
3.212	430.5
3.8131	484.55
4.4124	537.42
5.0123	590.79
5.6131	643.08
6.2121	694.07
6.8129	745.8
7.4125	797.18
8.0124	848.8
8.6131	900.26
8.8459	818.91
8.2456	620.65
7.6461	523.03
7.0452	446.97
6.4458	379.07
5.8457	316.01
5.2455	255.82
4.6464	197.53
4.0456	141.15
3.4465	86.186
2.8462	31.345
2.2458	-22.019
1.6464	-75.275
1.0454	-127.94
0.44583	-179.87
-0.12067	-229.01
-0.71978	-280.59
-1.3205	-332.45
-1.9207	-383.64
-2.5202	-434.66
-3.121	-485.57
-3.7202	-536.12
-4.3206	-587.23
-4.9205	-637.94
-5.5199	-688.58
-6.1205	-738.93
-6.7199	-789.63
-7.32	-840.94
-7.9206	-892.49
-8.52	-943.75
-8.9404	-936.51
-8.3399	-710.75
-7.7397	-608.52
-7.1405	-532.29
-6.5396	-464.74
-5.9402	-402.17
-5.34	-342.62
-4.7398	-284.27
-4.1404	-227.83
-3.5396	-172.85
-2.9404	-118.38
-2.3398	-63.739
-1.7396	-10.842
-1.1405	42.634
-0.53963	96.099
0.01822	143.79
0.62634	199.02
1.2253	252.02
1.8263	305.05
2.426	357.54
3.0256	410.51
3.6264	463.56
4.2254	516.12
4.8263	569.51
5.4261	622.3
6.0256	675.69
6.6264	728.59
7.2255	781.16
7.8263	834.75
8.4262	888.56
9.0002	939.19
8.4327	665.49
7.8325	551.42
7.2321	471.14
6.6329	401.26
6.0322	336.75
5.4326	276.18
4.8325	217.31
4.2323	160.43
3.6332	105.02
3.0323	50.249
2.4327	-3.2605
1.8325	-56.592
1.2321	-109.42
0.63286	-161.75
0.03218	-213.97

ISOLATOR NO.6
Loading Direction = Cyclic Roll. Rate: 8 mm/min

D(mm)	F (N)
0.57434	124.37
1.1753	177.16
1.775	222.94
2.3748	265
2.9753	304.93
2.473	75.674
1.8737	-36.216
1.2733	-102.53
0.67313	-154.53
0.07388	-199.99
-0.49322	-240.48
-1.0928	-280.93
-1.6934	-318.91
-2.2926	-356.65
-2.8933	-393.73
-2.5667	-200.82
-1.9658	-74.247
-1.3665	-4.4707
-0.7659	49.953
-0.16563	97.103
0.40073	138.1
1.0006	179.07
1.6005	219.43
2.2009	258.13
2.8001	296.16
3.4011	332.54
4.0007	369.12
4.6004	405.63
5.2009	442.18
5.7999	477.82
5.6467	314.6
5.0465	174.28
4.4464	100.64
3.847	45.99
3.2463	-1.4528
2.6466	-45.019
2.0461	-86.574
1.446	-126.13
0.84671	-164.74
0.24592	-203.05
-0.31937	-238.94
-0.92026	-275.63
-1.5196	-312.21
-2.1203	-348.82
-2.72	-384.18
-3.3195	-418.96
-3.9201	-453.73
-4.5191	-488.18
-5.12	-523.38
-5.7197	-557.58
-5.7261	-434.8
-5.1262	-280.12
-4.5256	-201.15
-3.9265	-143.8
-3.3255	-94.594
-2.7259	-50.123
-2.1257	-7.799
-1.525	32.39
-0.92624	71.401
-0.32536	109.61
0.24023	145.09
0.84116	182.16
1.4403	219.03
2.0406	255.86
2.6407	291.94
3.2399	328.32
3.8409	364.21
4.4401	400.11
5.0404	436.22
5.6408	471.21
6.24	506.29
6.8408	541.35
7.4404	575.94
8.0406	610.4
8.6409	645.14
8.8199	563.06
8.22	384.94
7.6206	299.7
7.0196	240.68
6.4202	191.79
5.8197	146.48
5.2199	104.4
4.6205	64.509
4.0196	24.912
3.4205	-13.178
2.82	-51.206
2.22	-88.436
1.6205	-124.75
1.0199	-161.38
0.42036	-197.53
-0.14646	-231.55
-0.74567	-267.38
-1.3467	-303.38
-1.9461	-338.57
-2.5459	-374.13
-3.1469	-409.61
-3.7461	-444.57
-4.3468	-479.89
-4.9464	-514.58
-5.5459	-550.04
-6.1465	-583.67
-6.7458	-617.56
-7.3465	-652
-7.9464	-686.02
-8.5458	-720.18
-8.8989	-685.44
-8.2987	-490.56
-7.6995	-397.86
-7.0988	-334.7
-6.4994	-282.59
-5.8991	-234.9
-5.2989	-191.13
-4.6996	-149.59
-4.0985	-109.32
-3.4991	-71.338
-2.8991	-32.954
-2.2986	4.0728
-1.6996	40.736
-1.0988	77.443
-0.49925	113.03
0.06758	147
0.66682	182.62
1.2674	218.37
1.8674	253.62
2.4667	289.05
3.0675	324.62
3.6668	359.52
4.2672	395.39
4.8675	429.67
5.4668	465.06
6.0678	500.53
6.6669	535.24
7.2673	569.91
7.8675	604.67
8.4667	639.74
8.9986	663.3
8.3938	426.25
7.7931	324.88
7.1939	261.43
6.593	209.65
5.9933	164.21
5.3939	121.14
4.793	80.238
4.1937	40.748
3.5931	1.8773
2.9932	-35.707
2.3938	-73.452
1.7931	-110.26
1.1937	-146.72
0.59318	-182.95

ISOLATOR NO.7
Loading Direction = Cyclic Roll. Rate: 8 mm/min

D(mm)	F (N)
0.57393	166.49
1.173	267.05
1.7738	353.63
2.3733	433.53
2.9736	509.27
2.4725	246.39
1.8726	112.93
1.2721	13.893
0.67282	-72.969
0.07178	-154.69
-0.49309	-227.22
-1.0938	-302.84
-1.6933	-376.38
-2.2934	-449.44
-2.8936	-520.92
-2.5533	-290.1
-1.9523	-142.37
-1.3527	-38.211
-0.75252	52.146
-0.15224	135.85
0.41333	211.51
1.0133	289.15
1.6131	364.67
2.2139	438.21
2.8129	510.19
3.4136	580.95
4.0133	649.78
4.6127	718.73
5.2136	787.66
5.813	854.98
5.6461	664.54
5.0456	499.96
4.4461	391.87
3.8452	298.55
3.2457	213.45
2.6459	131.31
2.0456	52.449
1.4463	-23.988
0.84554	-99.519
0.24607	-173.14
-0.3208	-242.04
-0.91996	-314.27
-1.5202	-385.42
-2.1202	-455.96
-2.7196	-525.65
-3.3206	-595.31
-3.9199	-663.46
-4.5201	-732.42
-5.1205	-800.92
-5.7199	-868.58
-5.7402	-735.06
-5.1393	-547.62
-4.5404	-433.2
-3.9395	-337.33
-3.3399	-250.37
-2.7398	-167.62
-2.1391	-88.219
-1.5402	-11.074
-0.93934	64.99
-0.33979	139.63
0.22701	209.35
0.82629	282.1
1.4268	354.52
2.0269	425.37
2.6261	496.2
3.2269	566.42
3.8261	636.02
4.4265	706.19
5.0269	774.88
5.6261	844.03
6.227	912.74
6.8265	979.11
7.4266	1046.4
8.027	1112.8
8.6261	1179.1
8.8188	1090.4
8.2194	879.43
7.6187	757.71
7.0196	659.6
6.4195	570.54
5.8192	486.99
5.2199	406.58
4.6189	328.08
4.0192	251.55
3.4192	176.21
2.8189	101.95
2.2193	28.944
1.6185	-43.512
1.0193	-114.97
0.41942	-186.31
-0.14662	-252.97
-0.74707	-323.51
-1.3473	-392.78
-1.9466	-462.22
-2.5473	-531.25
-3.1464	-599.87
-3.7467	-668.73
-4.3469	-736.66
-4.9463	-804.21
-5.5474	-871.88
-6.1467	-938.7
-6.7471	-1006.4
-7.3473	-1072.9
-7.9466	-1140.2
-8.5476	-1207.5
-8.8998	-1182.2
-8.299	-940.67
-7.6995	-812.61
-7.0996	-711.54
-6.4986	-621.33
-5.8997	-537.39
-5.2994	-456.92
-4.6993	-378.43
-4.0999	-301.56
-3.4989	-226.07
-2.8997	-152.34
-2.2992	-78.58
-1.6991	-6.2817
-1.0998	65.615
-0.49875	136.83
0.06625	203.58
0.66699	273.97
1.2662	343.51
1.8668	413.77
2.4665	482.3
3.0666	551.69
3.6671	620.74
4.266	689.09
4.8668	758.35
5.4665	827.16
6.0662	895.33
6.6671	963.68
7.2662	1031.6
7.8668	1100.4
8.4667	1168.3
8.9985	1220.1
8.3921	927.93
7.7927	791.51
7.1926	687.16
6.5924	595.8
5.993	510.26
5.3921	428.48
4.7929	349.69
4.1928	271.84
3.5924	196.1
2.9932	121.65
2.3923	47.565
1.7929	-24.972
1.1927	-97.275
0.59228	-168.81

ISOLATOR NO.8
Loading Direction = Cyclic Roll. Rate: 8 mm/min

D(mm)	F (N)
0.57699	224.22
1.1764	326.5
1.7774	400.61
2.3767	464.52
2.9773	524.14
2.4727	226.34
1.8731	56.113
1.2723	-51.943
0.67296	-135.12
0.0721	-206.74
-0.49303	-267.06
-1.0937	-327.23
-1.6932	-385.32
-2.2935	-442.5
-2.8937	-498.26
-2.5662	-238.22
-1.9665	-42.432
-1.3656	73.994
-0.7666	162.2
-0.16586	237.84
0.39958	302.06
1.0004	365.57
1.5998	424.97
2.2	481.69
2.8006	535.37
3.3996	587.43
4.0005	639.13
4.5998	689.74
5.2001	740.57
5.8003	791.05
5.6462	593.89
5.0458	392.16
4.4466	268.1
3.8455	175.02
3.2461	96.008
2.6461	23.764
2.0456	-43.674
1.4465	-108.01
0.84554	-170.75
0.24637	-231.19
-0.32099	-287.2
-0.92007	-344.51
-1.5206	-401.58
-2.1206	-456.09
-2.7199	-510.04
-3.3206	-563
-3.92	-615.11
-4.5203	-667.54
-5.1205	-719.44
-5.72	-771.3
-5.74	-618.41
-5.1394	-377.3
-4.5401	-242.4
-3.9395	-143.25
-3.3398	-61.05
-2.7398	13.236
-2.1394	81.949
-1.5403	146.9
-0.93941	209.19
-0.33981	269.52
0.2273	324.89
0.82637	382.3
1.4266	438.71
2.0271	493.41
2.6262	546.79
3.2269	599.21
3.8265	650.87
4.4268	702.41
5.0272	753.17
5.6262	803.22
6.2271	852.58
6.8264	901.24
7.4266	950.8
8.0271	999.75
8.6262	1048.7
8.8192	949.91
8.2196	700.87
7.6187	566.64
7.0195	468.5
6.4193	385.03
5.8192	311.07
5.2198	241.14
4.619	174.91
4.0197	111.29
3.4195	49.282
2.819	-11.402
2.2197	-70.641
1.6188	-129.96
1.0194	-187.43
0.4194	-245.48
-0.14667	-298.71
-0.74709	-355.06
-1.3471	-410.13
-1.9467	-464.97
-2.5475	-519.7
-3.1466	-574.04
-3.7471	-628.07
-4.3471	-681.78
-4.9464	-734.3
-5.5472	-785.95
-6.1466	-835.92
-6.7469	-886.3
-7.3472	-936.37
-7.9466	-986.63
-8.5475	-1037.2
-8.8996	-998.52
-8.2993	-715.26
-7.6994	-557.11
-7.0998	-447.01
-6.4988	-357.16
-5.8996	-277.7
-5.2989	-204.32
-4.699	-135.61
-4.0997	-69.986
-3.4987	-6.4358
-2.8995	54.579
-2.2991	114.85
-1.6995	173.01
-1.0999	230.43
-0.49886	287.23
0.06651	339.6
0.66712	394.66
1.2661	448.69
1.8669	502.37
2.4667	554.24
3.0665	605.94
3.6673	657.71
4.2665	708.5
4.8672	760.19
5.4669	810.71
6.0664	862.05
6.6673	912.93
7.2664	962.66
7.8667	1012.9
8.4667	1062.2
8.9788	1081.4
8.3795	771.1
7.7798	611.92
7.1791	501.64
6.5798	412.35
5.9789	333.13
5.3791	261.1
4.7794	192.03
4.1788	127.04
3.5795	63.507
2.9788	1.7212
2.3792	-58.506
1.7798	-118.1
1.179	-176.98
0.57981	-234.69

ISOLATOR NO.9
Loading Direction = Cyclic Roll. Rate: 8 mm/min

D(mm)	F (N)
0.57682	156.78
1.1773	238.44
1.7765	294.92
2.3774	342.54
2.977	385.52
2.4724	141.18
1.8727	-6.7129
1.2734	-90.8
0.67258	-151.61
0.07336	-202.07
-0.49378	-244.92
-1.0931	-286.67
-1.694	-327.11
-2.2933	-364.87
-2.8933	-403.41
-2.552	-193.14
-1.9528	-29.104
-1.3523	63.948
-0.75239	128.63
-0.15311	181.89
0.41383	227.79
1.0137	272.76
1.6144	314.74
2.2133	354.92
2.814	393.67
3.4138	431.15
4.0138	468.66
4.6144	504.99
5.2134	541.04
5.8144	577.12
5.6331	405.11
5.0323	228.79
4.433	132.32
3.8328	65.535
3.2329	10.551
2.6334	-38.752
2.0326	-84.967
1.4329	-128.87
0.83273	-171.91
0.23239	-212.96
-0.33378	-251.17
-0.93377	-290.37
-1.5333	-329.2
-2.134	-367.25
-2.7337	-403.68
-3.3342	-440.22
-3.9341	-475.9
-4.5333	-511.57
-5.1341	-547.32
-5.7335	-582.55
-5.7128	-450.23
-5.1124	-258.47
-4.5132	-152.87
-3.9121	-82.018
-3.3126	-25.346
-2.7125	25.54
-2.1127	72.601
-1.5133	117.41
-0.91258	160.32
-0.31287	202.02
0.2545	240.59
0.85363	279.99
1.454	319.63
2.0541	357.65
2.6535	395.79
3.2544	433.49
3.8538	469.71
4.4541	506.5
5.0543	541.96
5.6536	577.52
6.2546	612.18
6.854	645.74
7.4539	679.99
8.0541	713.59
8.6532	746.97
8.7931	655.87
8.1933	453.14
7.5925	342.72
6.9936	271.76
6.393	214.67
5.793	164.72
5.1937	117.63
4.5927	72.517
3.9936	29.183
3.3931	-13.389
2.7932	-54.073
2.1935	-94.715
1.5926	-134.38
0.99347	-173.43
0.39293	-212.81
-0.1731	-249.48
-0.77399	-288.07
-1.3737	-325.78
-1.9737	-363.27
-2.5741	-400.35
-3.1733	-437.17
-3.774	-473.76
-4.3735	-509.92
-4.9735	-545.77
-5.574	-581.79
-6.1731	-616.22
-6.774	-651.54
-7.3738	-685.54
-7.9736	-720.68
-8.5742	-755.17
-8.8732	-706.29
-8.2728	-485.85
-7.6726	-367.01
-7.0732	-290.11
-6.4724	-229.54
-5.8732	-176.68
-5.2725	-127.41
-4.6727	-81.257
-4.0734	-36.744
-3.4727	5.88
-2.8734	47.54
-2.2728	88.497
-1.6726	128.82
-1.0731	168.03
-0.47239	207.02
0.09364	243.51
0.69434	281.42
1.2933	319
1.8943	356.58
2.4941	393.56
3.0937	429.78
3.6942	466.67
4.2933	502.8
4.8942	538.96
5.4938	574.16
6.0934	609.06
6.6943	644.4
7.2932	678.85
7.8941	713.28
8.4942	746.51
8.9527	742.74
8.3533	503.95
7.7534	374.08
7.1532	294.22
6.5538	234.22
5.9528	181.66
5.3534	133.68
4.7535	88.227
4.1529	44.471
3.5536	1.6803
2.9527	-39.682
2.3532	-80.233
1.7534	-120.46
1.1528	-160.5
0.55365	-199.63

Appendix D: Algorithm for solving Bouc-Wen Equation

This appendix provides the methodology used for solving the Bouc-Wen equations. This method is based on the work by Haukaas and Kiureghian (2014)

D.1. NUMERICAL SOLUTION FOR THE BOUC-WEN EQUATION USING BABER-NOORI EQUATIONS

Eq.(4.4)-(4.13) mathematically models the hysteresis behaviour of WRI under roll loading. These Differential Algebraic Equations (DAE) which are the combination of differential and algebraic equation needs to be solved to obtain displacement response of the WRI for a given value of load. The solution of DAE was obtained using the numerical methods and obtained solution is then used for response of the WRI for the earthquake ground motions to conduct the performance study. The algorithm for solving the DAE is provided in this section. The time is incremented to Δt and the value of the parameters for the incremented time $t_{(n+1)}$ is represented by the subscript (n+1).

D.1.1. INCREMENT RESPONSE EQUATION

The response for the time t_{n+1} , can be obtained as,

$$F_{(n+1)} = \alpha \frac{F_y}{Y} x_{(n+1)} + (1-\alpha) F_y z_{(n+1)} \tag{D.1}$$

The rate equation for the Z when time is t_{n+1}, is discretized using Backward Euler solution scheme. According to the Backward Euler scheme, for the first order differential equations of the form $y = f(y(t))$, the scheme can be used for time increment Δt,

$$y_{(n+1)} = y_n + \Delta t f(y_{(n+1\_)}) \tag{D.2}$$

On applying Eq.(4.15) to Eq.(4.8), the following is obtained

$$z_{(n+1)} = z_n + \Delta t \frac{A_{(n+1)} - |z_{(n+1)}|^n \left\{\gamma + \beta sgn\left(\frac{(x_{(n+1)} - x_n)}{\Delta t} z_{(n+1)}\right)\right\} \nu_{(n+1)}}{\eta} \frac{(x_{(n+1)} - x_n)}{\Delta t} \tag{D.3}$$

It can be seen, that the Δt cancels out from the Eq.(D.3) and non-linear equation in $z_{(n+1)}$is yielded. The obtained nonlinear equation can be solved by the newton scheme for $z_{(n+1)}$. Similarly, the equation for the degrading behaviour can also be written for time incrementΔt,

$$\mathrm{A}_{(\mathrm{n}+1)} = \mathrm{A}_{\mathrm{o}} - \delta_{\mathrm{A}}\mathrm{e}_{(\mathrm{n}+1)} \tag{D.4}$$

$$\nu_{(n+1)} = 1 + \delta_{\nu} e_{(n+1)} \tag{D.5}$$

$$\eta_{(n+1)} = 1 + \delta_{\eta} e_{(n+1)} \tag{D.6}$$

The rate equation $e_{(n+1)}$ for the time increment Δt was also written utilizing backward Eulers scheme,

$$e_{(n+1)} = e_{(n)} + \Delta t(1-\alpha)\frac{F_y}{Y}\left(1 + (1-\alpha)\right)\frac{\left(x_{(n+1)} - x_n\right)}{\Delta t} z_{(n+1)} \tag{D.7}$$

From the Eq.(4.14), it can be observed that $z_{(n)}$, $\mathrm{x}_{(n+1)}$,and $e_{(n)}$ are vairables based on history and is saved at each converged step.

D.1.2. ALGORITHM TO COMPUTE THE RESPONSE

This section summarizes the algorithm developed by Haukaas and Kiureghian(2014) and used to solve Bouc-Wen-Baber-Noori model for developing the hysteresis curve. The main components of the algorithm are two major sections. First for the identification of the $z_{(n+1)}$ and secondly, to obtain the response based on obtained $z_{(n+1)}$ and to determine the tangent of the curve.

1. While $\left(\left|z_{(n+1)}^{old} - z_{(n+1)}^{new}\right| > tol\right)$

a) Evaluate the function $f\left(z_{(n+1)}\right)$:

(i). $e_{(n+1)} = e_{(n)} + (1-\alpha)\frac{F_y}{Y}\left(1 + (1-\alpha)\right)\left(x_{(n+1)} - x_n\right)z_{(n+1)}$

(ii). $A_{(n+1)} = A_o - \delta_A e_{(n+1)}$

(iii). $\nu_{(n+1)} = 1 + \delta_{\nu} e_{(n+1)}$

(iv). $\eta_{(n+1)} = 1 + \delta_{\eta} e_{(n+1)}$

(v). $\Psi = \gamma + \beta sgn\left(\left(x_{(n+1)} - x_n\right)z_{(n+1)}\right)$

(vi). $\Phi = A_{(n+1)} - \left|z_{(n+1)}\right|^{n}\Psi\upsilon_{(n+1)}$

(vii). $f\left(z_{(n+1)}\right) = z_{(n+1)} - z_{(n)} - \frac{\Phi}{\eta_{(n+1)}}\left(x_{(n+1)} - x_n\right)$

b) Evaluating the derivatives of the function (prime denotes the derivate with respect to $z_{(n+1)}$

(i). $e'_{(n+1)} = (1-\alpha)\frac{F_y}{Y}\left(1 + (1-\alpha)\right)\left(x_{(n+1)} - x_n\right)$

(ii). $A'_{(n+1)} = -\delta_A e'_{(n+1)}$

(iii). $\nu'_{(n+1)} = \delta_v e'_{(n+1)}$

(iv). $\Phi' =$

$A'_{(n+1)} - n\left|z_{(n+1)}\right|^{(n-1)}\mathrm{sgn}\left(z_{(n+1)}\right)\Psi\upsilon_{(n+1)} - \left|z_{(n+1)}\right|^{n}\Psi\upsilon'_{(n+1)}$

(v). $f'\left(z_{(n+1)}\right) = 1 - \frac{\Phi'\eta_{(n+1)} - \Phi\eta'_{(n+1)}}{\eta^2_{(n+1)}}\left(x_{(n+1)} - x_n\right)$

c) Obtaining the trail value in the Newton scheme :

$$z^{new}_{(n+1)} = z_{(n+1)} - \frac{f\left(z_{(n+1)}\right)}{f'\left(z_{(n+1)}\right)}$$

d) Updating $z_{(n+1)}$ and saving the old value for convergence test.

$z^{old}_{(n+1)} = z_{(n+1)}$ and $z_{(n+1)} = z^{new}_{(n+1)}$

2. Compute the force-displacement response : $F_{(n+1)} = \alpha\frac{F_y}{Y}x_{(n+1)} + (1-\alpha)F_y Z_{(n+1)}$

a) Compute material degradation parameters

(i). $e_{(n+1)} = e_{(n)} + (1-\alpha)\frac{F_y}{Y}\left(1 + (1-\alpha)\right)\left(x_{(n+1)} - x_n\right)z_{(n+1)}$

(ii). $A_{(n+1)} = A_o - \delta_A e_{(n+1)}$

(iii). $\nu_{(n+1)} = 1 + \delta_v e_{(n+1)}$

(iv). $\eta_{(n+1)} = 1 + \delta_\eta e_{(n+1)}$

b) Computing Auxiliary parameters

(i). $\mathrm{b}_1 = (1-\alpha)\frac{F_y}{Y}\left(1 + (1-\alpha)\right)z_{(n+1)}$

(ii). $b_2 = (1-\alpha)\frac{F_y}{Y}\big(1+(1-\alpha)\big)\big(x_{(n+1)} - x_n\big)$

(iii). $b_3 = \frac{\left(x_{(n+1)} - x_n\right)}{\eta_{(n+1)}}$

(iv). $b_4 = -b_3\delta_A b_1 - b_3\left|z_{(n+1)}\right|^n \Psi\delta_v b_1 - \frac{\Phi}{\eta^2_{(n+1)}}\big(x_{(n+1)} - x_n\big)\delta_\eta b_1 + \frac{\Phi}{\eta_{(n+1)}}$

(v). $b_5 = 1 + b_3\delta_A b_2 + b_3\left|z_{(n+1)}\right|^{(n-1)} sgn\big(z_{(n+1)}\big)\Psi\upsilon_{(n+1)} + b_3\left|z_{(n+1)}\right|^n \Psi\delta_v b_2$

(vi). $+\frac{\Phi}{\eta^2_{(n+1)}}\big(x_{(n+1)} - x_n\big)\delta_\eta b_2$

c) Computing $\frac{\partial z_{(n+1)}}{\partial x_{(n+1)}}$ and tangent :

$$\frac{\partial z_{(n+1)}}{\partial x_{(n+1)}} = \frac{b_4}{b_5}$$

$$k = \frac{\partial f_{(n+1)}}{\partial x_{(n+1)}} = \alpha\frac{F_y}{Y} + (1-\alpha)F_y\frac{\partial z_{(n+1)}}{\partial x_{(n+1)}}$$

This Appendix.D presented the algorithm for the numerical method to solve the Bouc-Wen equation to obtain the hysteresis response of the WRI. This method was used for both vertical and lateral hysteresis curve however elastic term of the Bouc-Wen equation was replaced with Bilinear approximation for the vertical hysteresis curve. A coding was developed using this algorithm to plot the hysteresis curve from the model. The shape of the hysteresis curve can be controlled by the choice of the input parameters. The experimental test results of the WRI were used to identify the parameters using Least Square method.

Appendix E: Acceleration plots from the numerical model

In this appendix the acceleration response of the fixed and isolated equipment is given. These plots are corresponding to data summarized in the Table 5-3

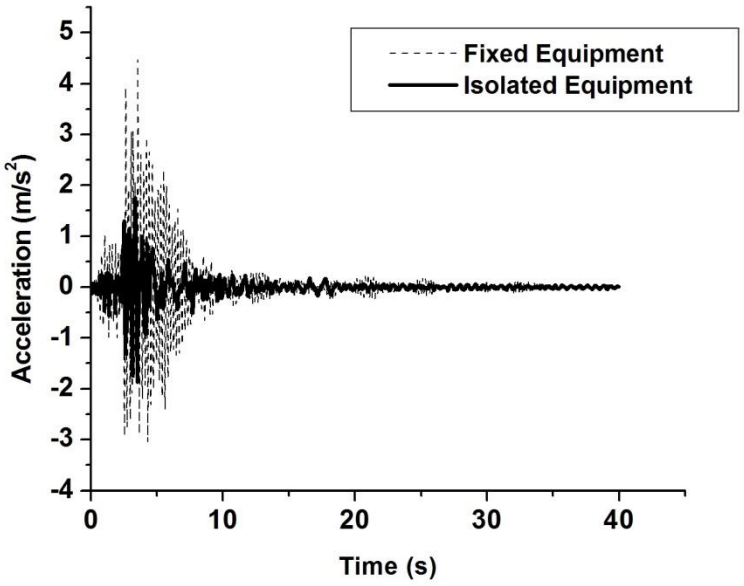

Figure E.1. Acceleration response of fixed and isolated case under Altadena_90 Excitation

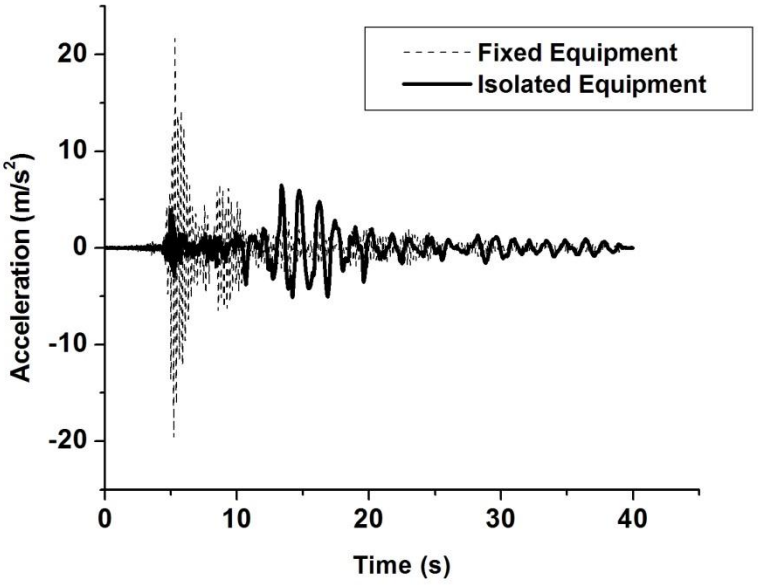

Figure E.2. Acceleration response of fixed and isolated case under Array_0 Excitation

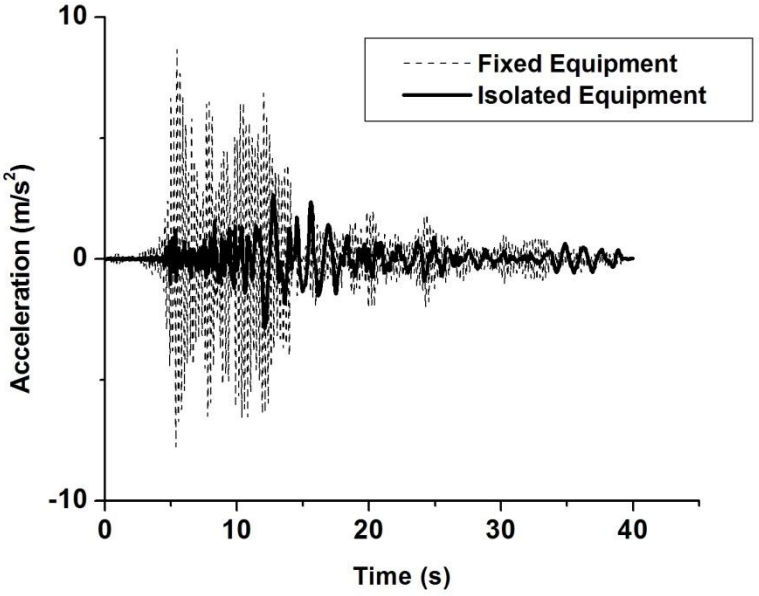

Figure E.3. Acceleration response of fixed and isolated case under Array_90 Excitation

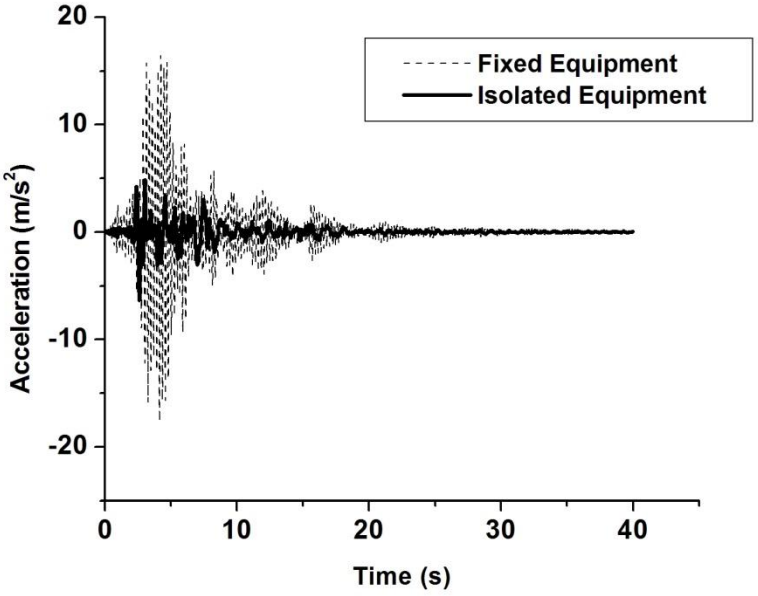

Figure E.4. Acceleration response of fixed and isolated case under Corralit_0 Excitation

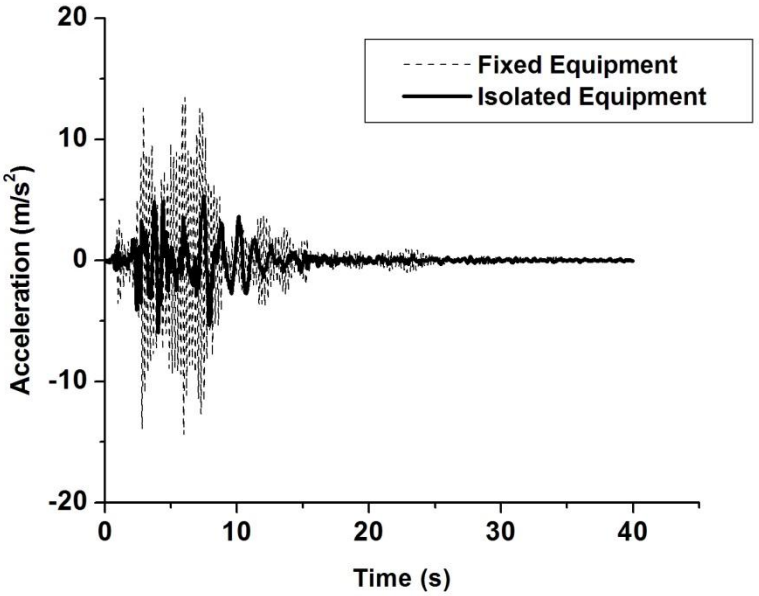

Figure E.5. Acceleration response of fixed and isolated case under Corralit_90 Excitation

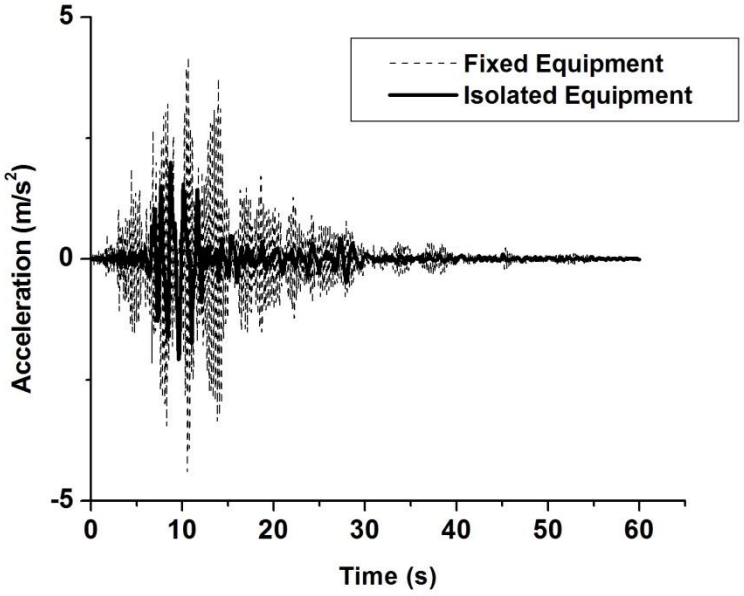

Figure E.6. Acceleration response of fixed and isolated case under Holliste_0 Excitation

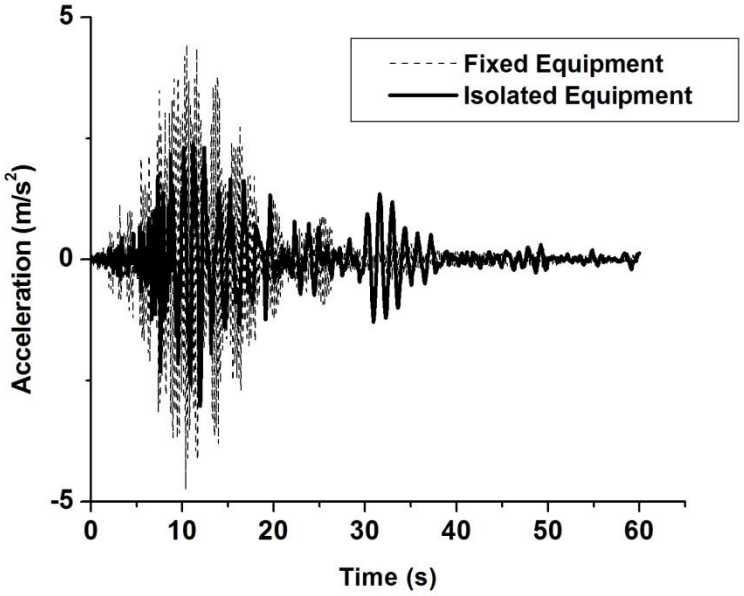

Figure E.7. Acceleration response of fixed and isolated case under Holliste_90 Excitation

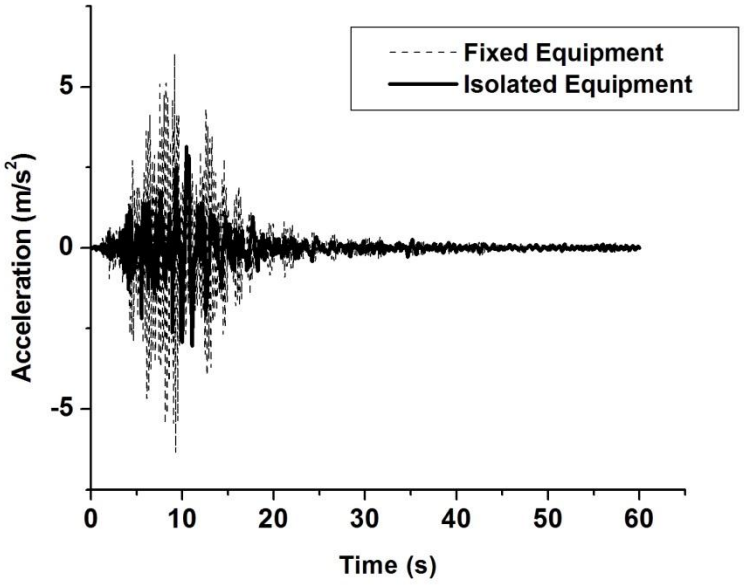

Figure E.8. Acceleration response of fixed and isolated case under Lacc-Nor_0 Excitation

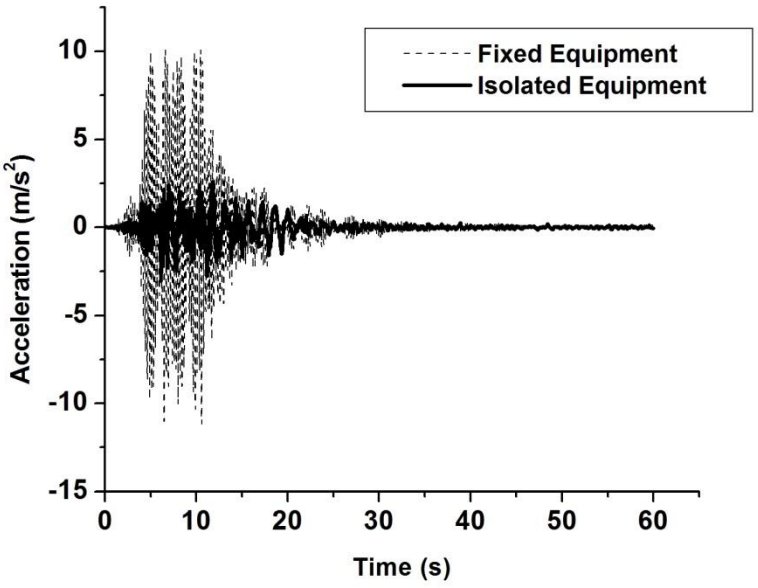

Figure E.9. Acceleration response of fixed and isolated case under Lacc-Nor_90 Excitation

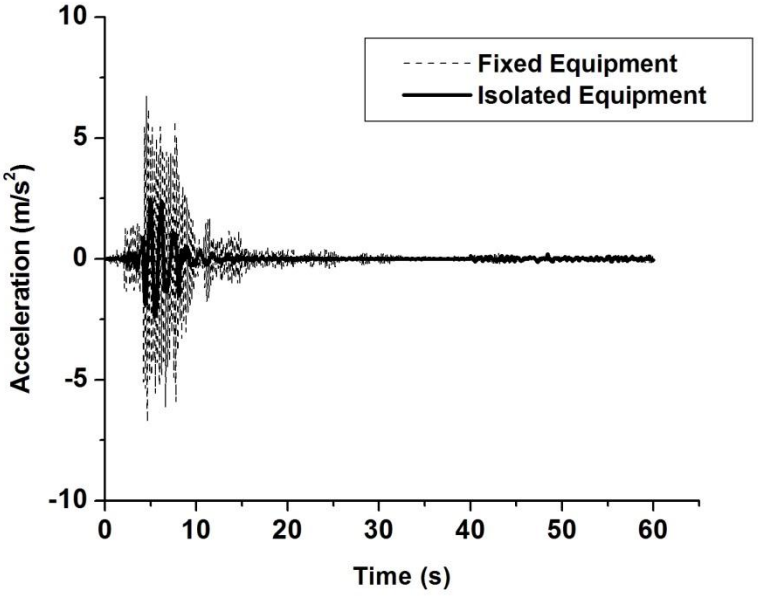

Figure E.10. Acceleration response of fixed and isolated case under Lexingt_0 Excitation

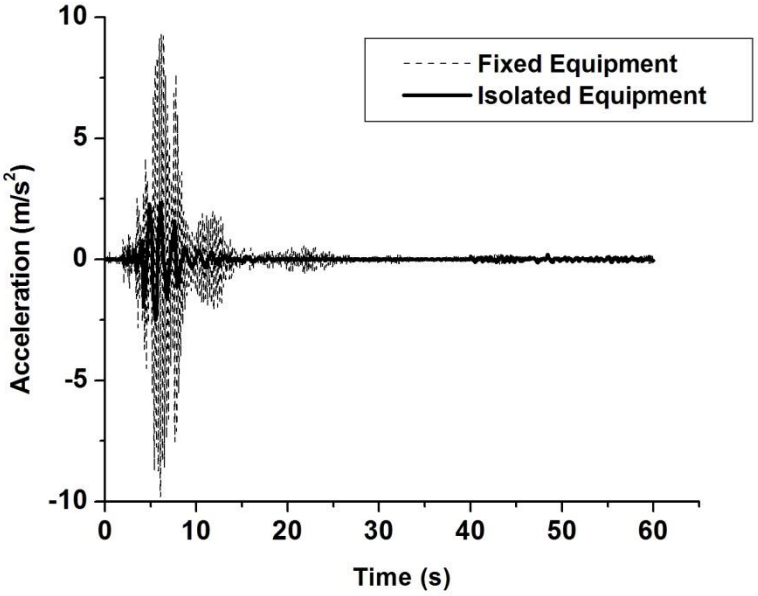

Figure E.11. Acceleration response of fixed and isolated case under Lexingt_90 Excitation

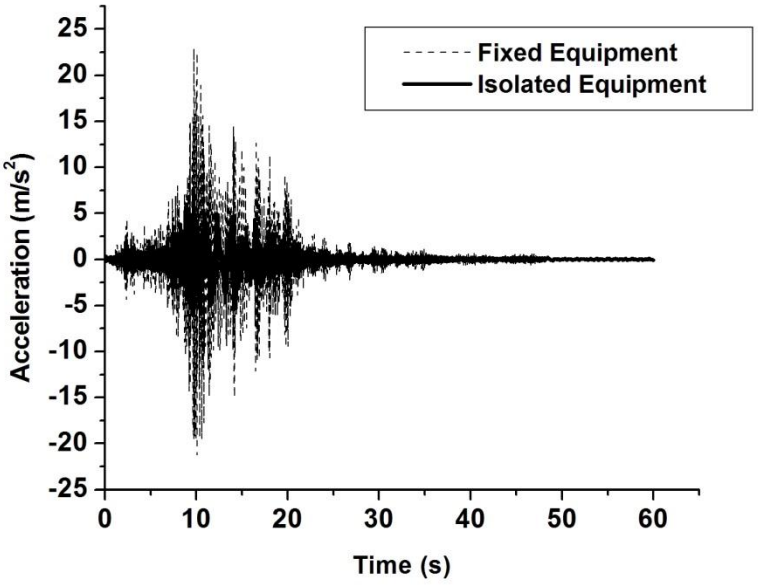

Figure E.12. Acceleration response of fixed and isolated case under Lucerne_0 Excitation

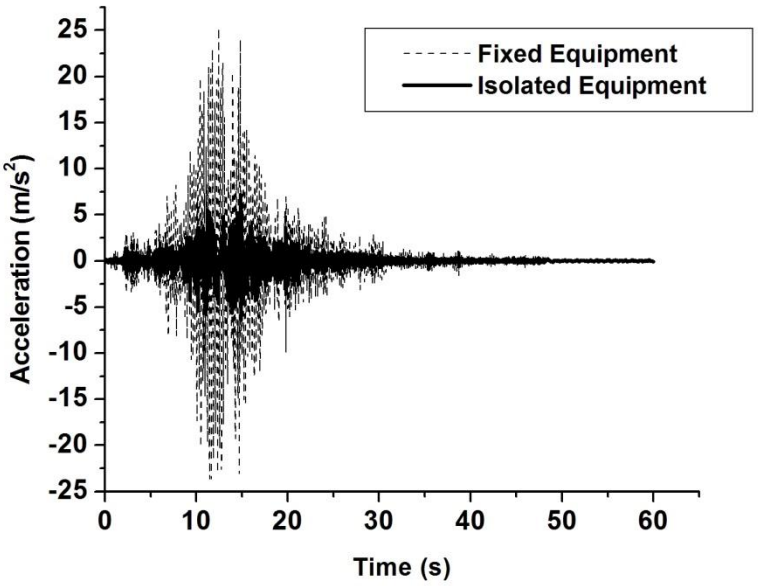

Figure E.13. Acceleration response of fixed and isolated case under Lucerne_90 Excitation

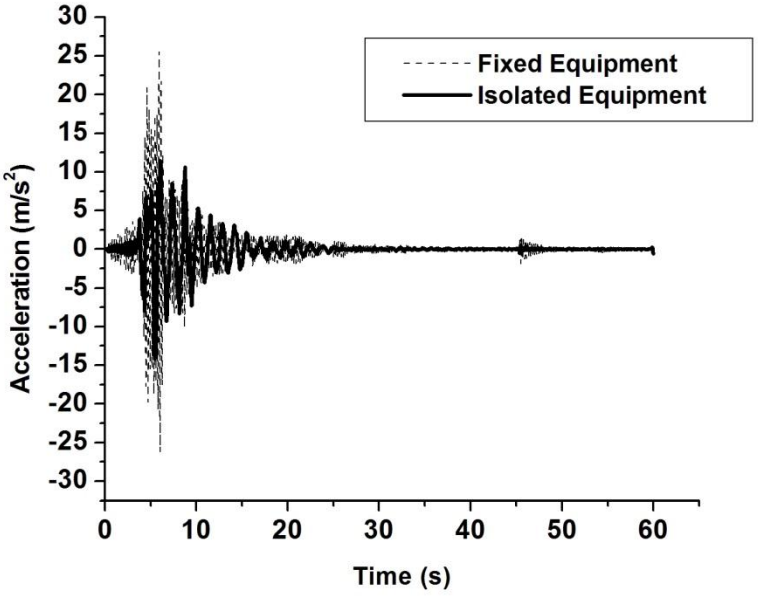

Figure E.14. Acceleration response of fixed and isolated case under Newhall_0 Excitation

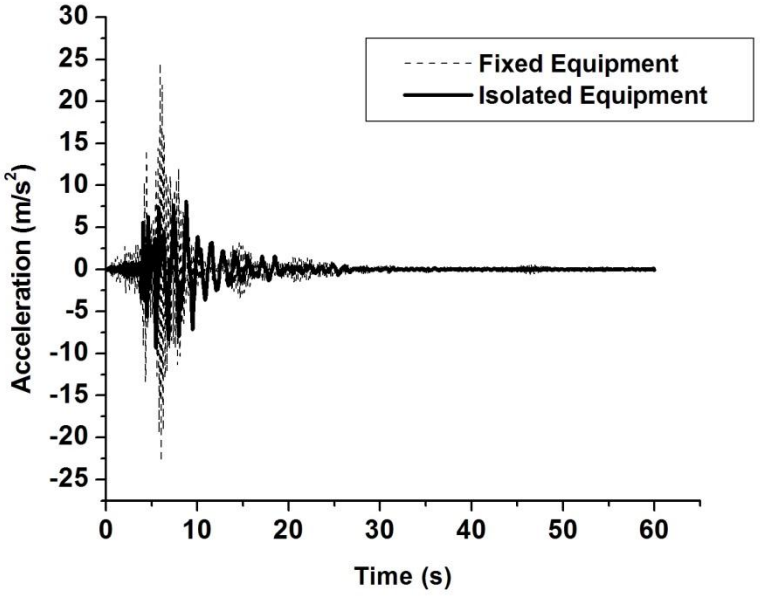

Figure E.15. Acceleration response of fixed and isolated case under Newhall_90 Excitation

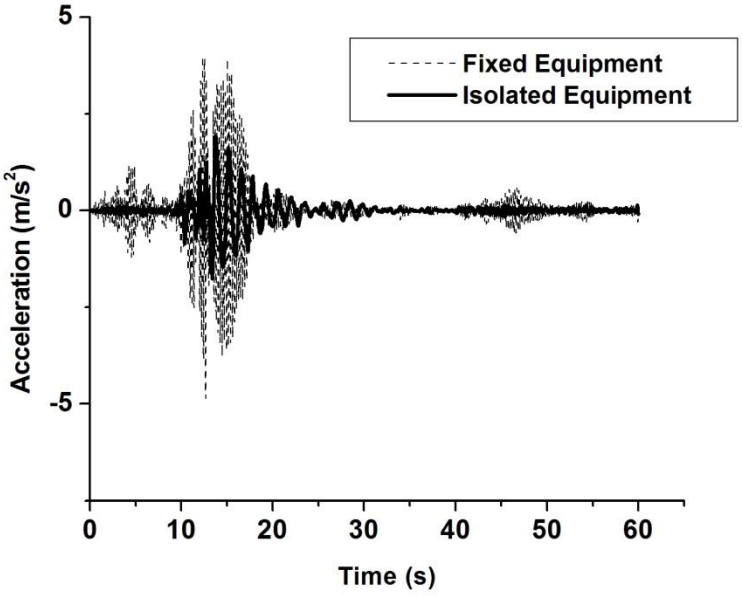

Figure E.16. Acceleration response of fixed and isolated case under Oak Whaf_0 Excitation

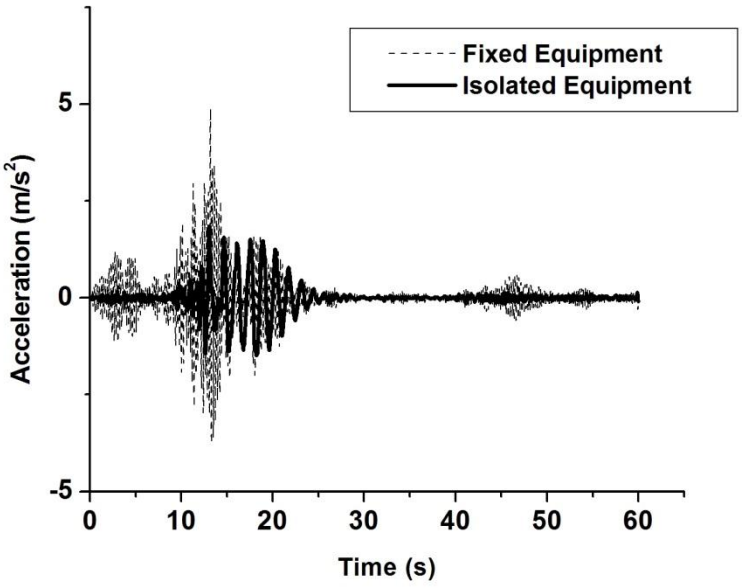

Figure E.17. Acceleration response of fixed and isolated case under Oak Whaf_90Excitation

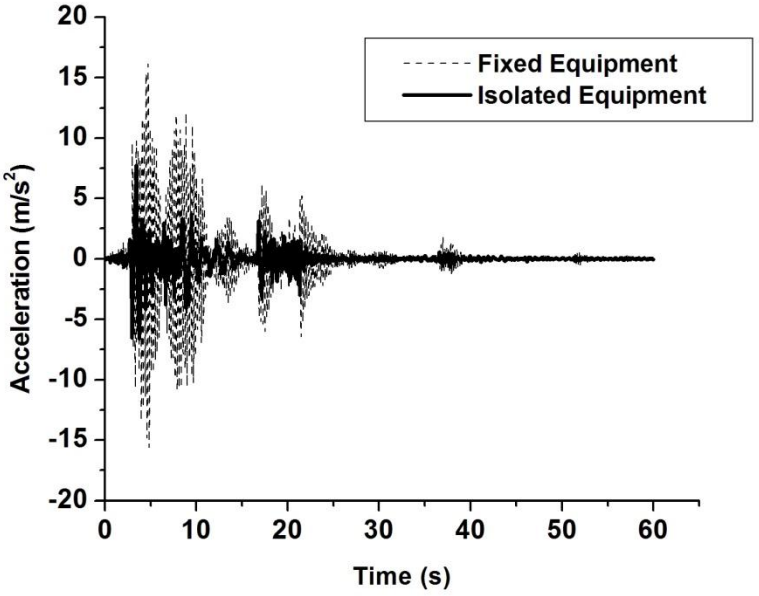

Figure E.18. Acceleration response of fixed and isolated case under Petrolia_0 Excitation

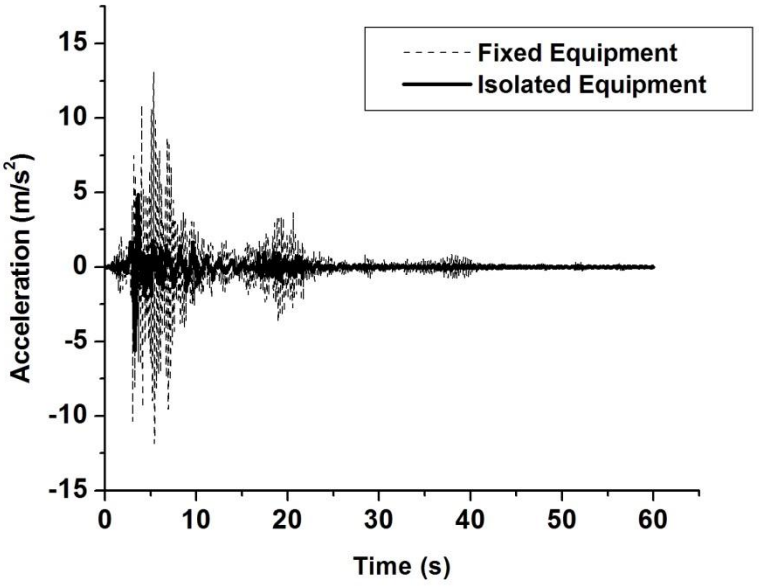

Figure E.19. Acceleration response of fixed and isolated case under Petrolia_90 Excitation

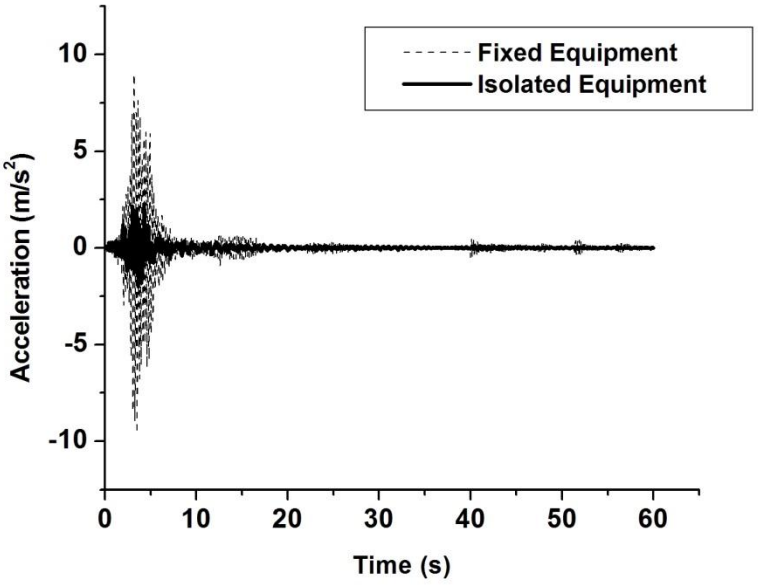

Figure E.20. Acceleration response of fixed and isolated case under Pomona_0 Excitation

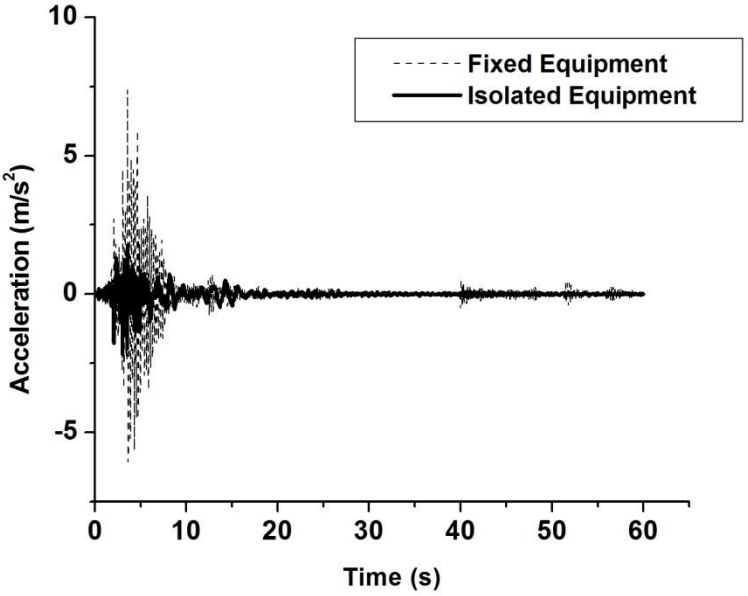

Figure E.21. Acceleration response of fixed and isolated case under Pomona_90 Excitation

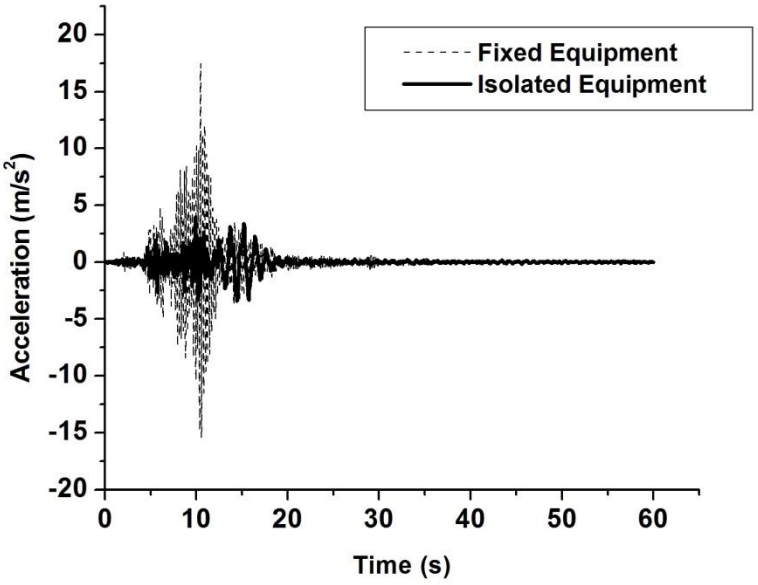

Figure E.22. Acceleration response of fixed and isolated case under Santa Monica_0 Excitation

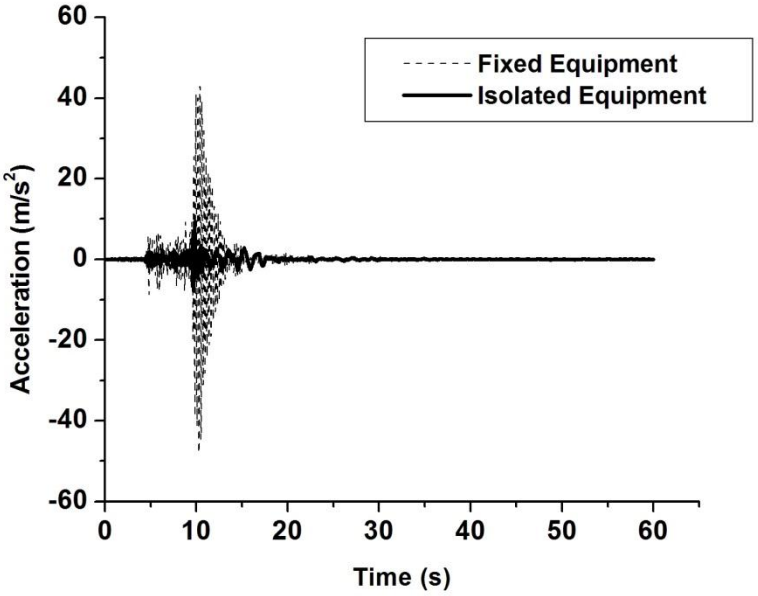

Figure E.23. Acceleration response of fixed and isolated case under Santa Monica_90 Excitation

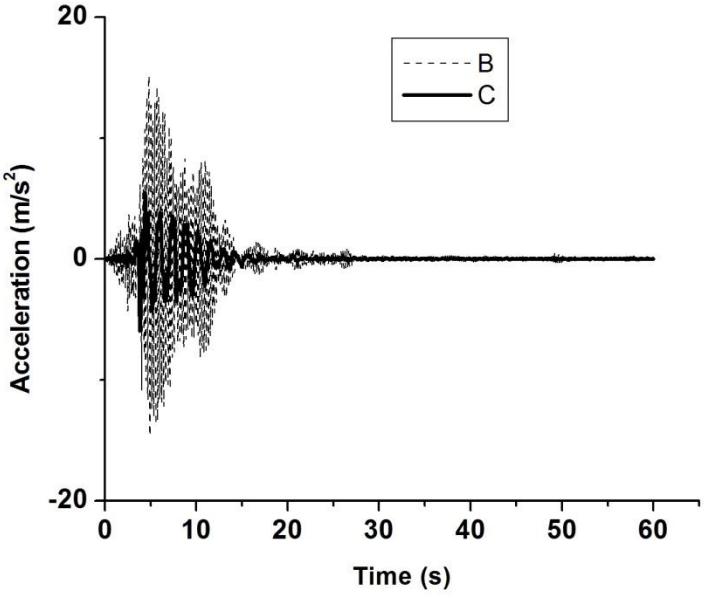

Figure E.24. Acceleration response of fixed and isolated case under Oak Sylmar_0 Excitation

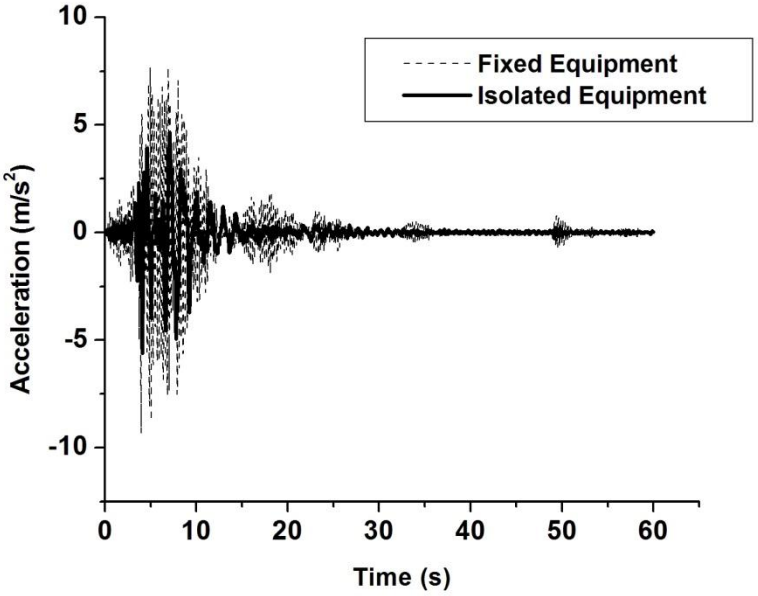

Figure E.25. Acceleration response of fixed and isolated case under Sylmar_90 Excitation

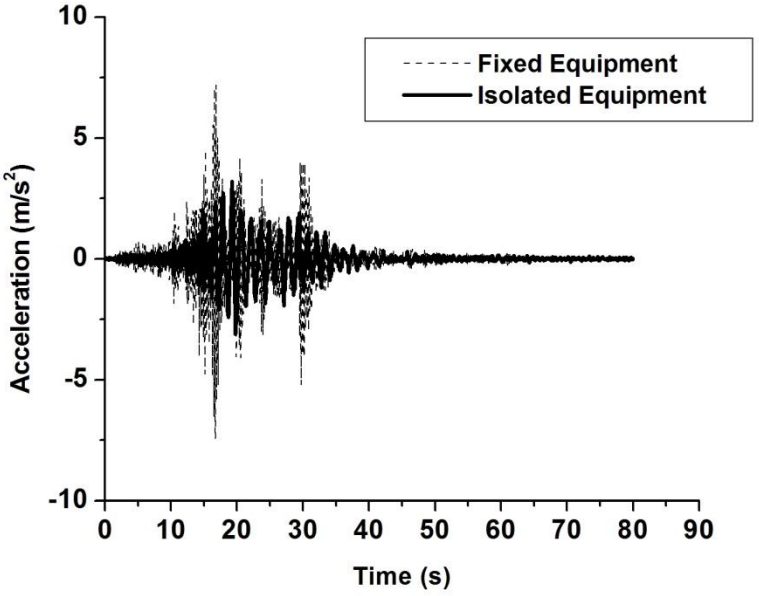

Figure E.26. Acceleration response of fixed and isolated case under Yermo_0 Excitation

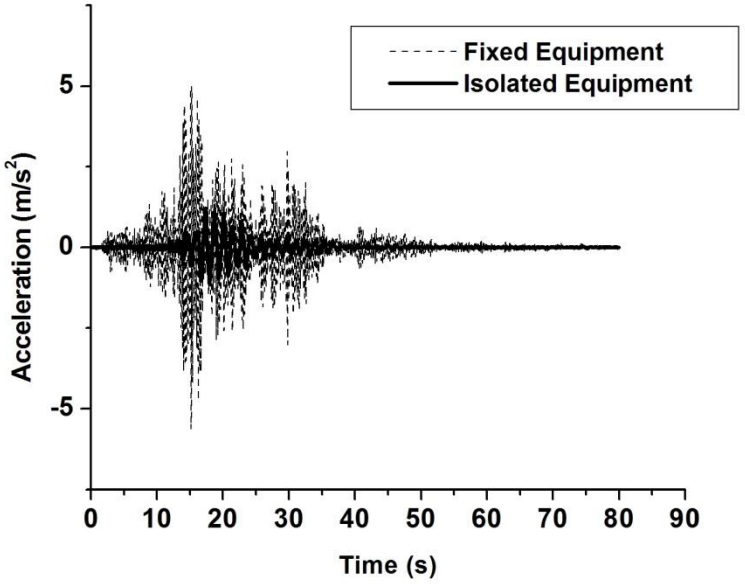

Figure E.27. Acceleration response of fixed and isolated case under Yermo_90 Excitation

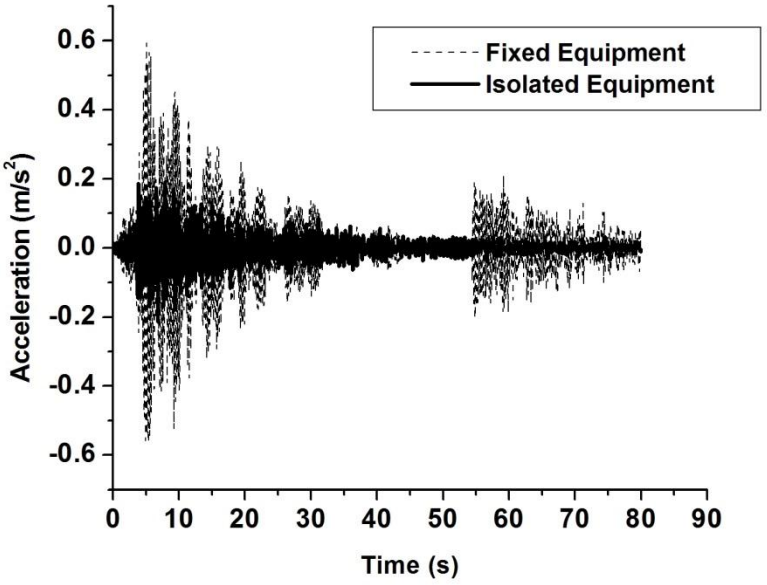

Figure E.28. Acceleration response of fixed and isolated case under Kern Excitation

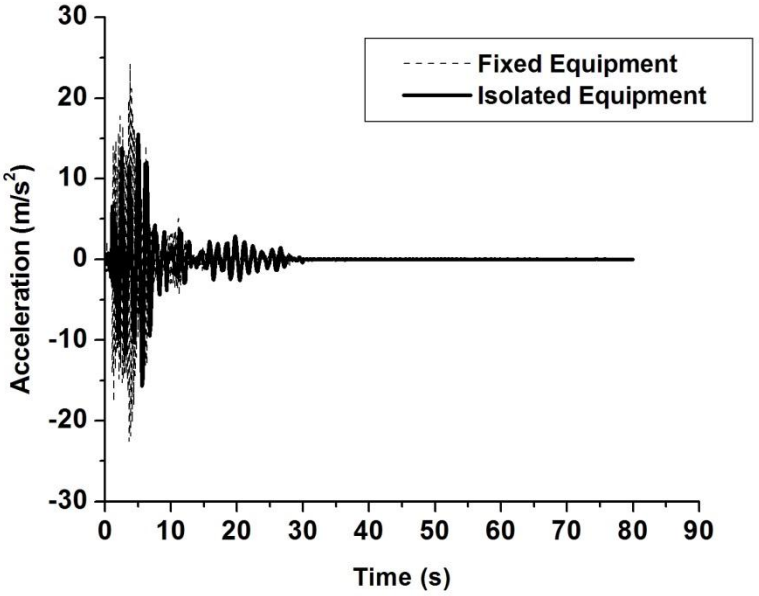

Figure E.29. Acceleration response of fixed and isolated case under Kobe Excitation

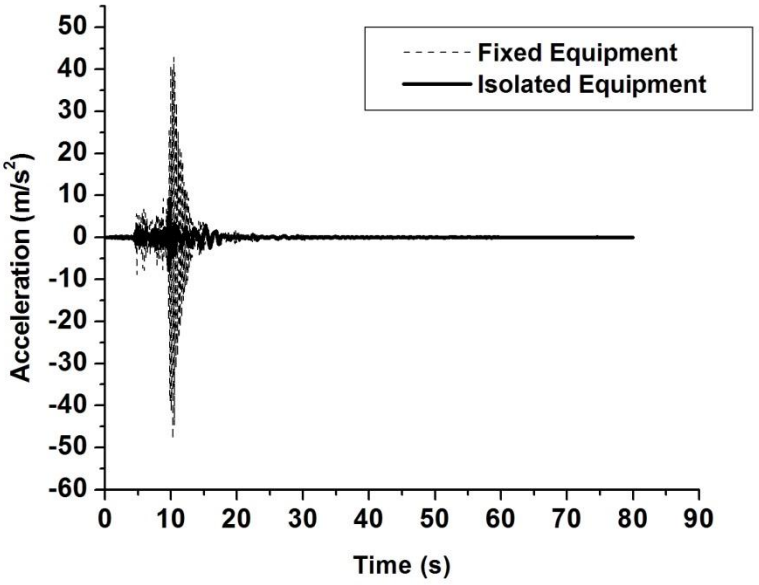

Figure E.30. Acceleration response of fixed and isolated case under NorthRidge Excitation

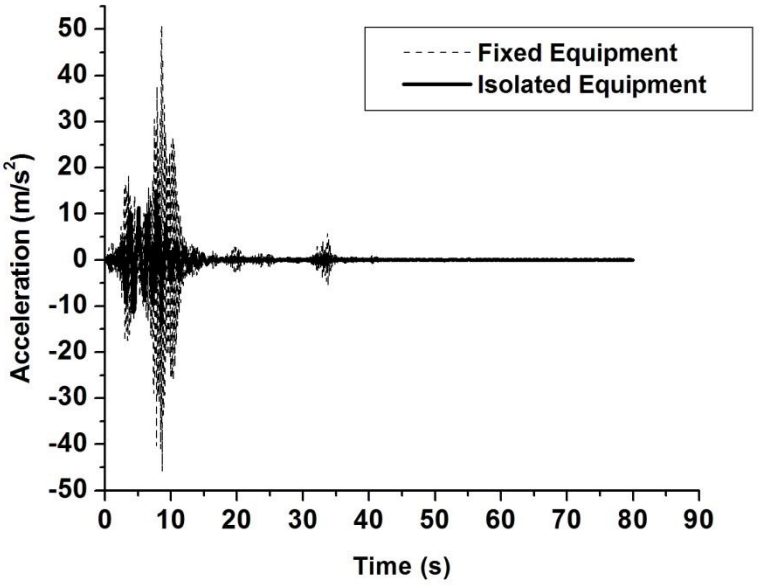

Figure E.31. Acceleration response of fixed and isolated case under San Frendo Excitation

Appendix F: Displacement plots from the numerical model

In this appendix the displacement response of the fixed and isolated equipment is given. These plots are corresponding to data summarized in the Table 5-3.

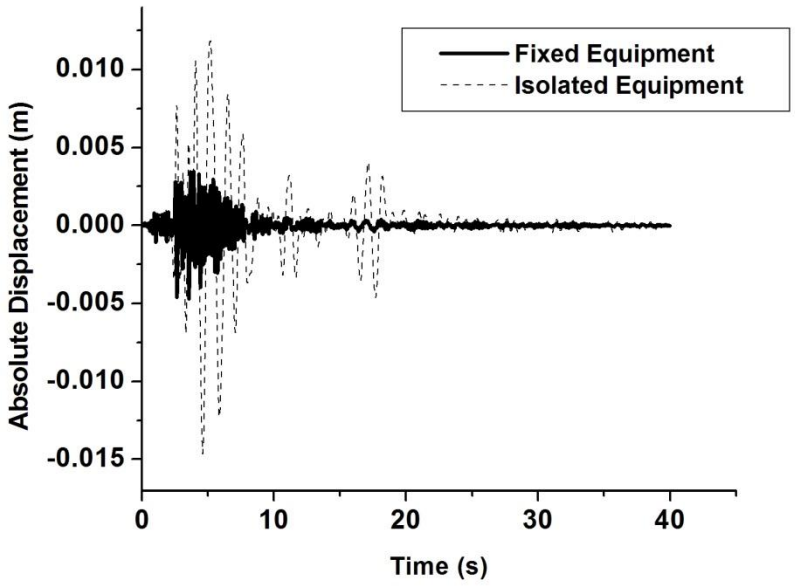

Figure F.1. Displacement response of fixed and isolated case under Altadena_90 Excitation

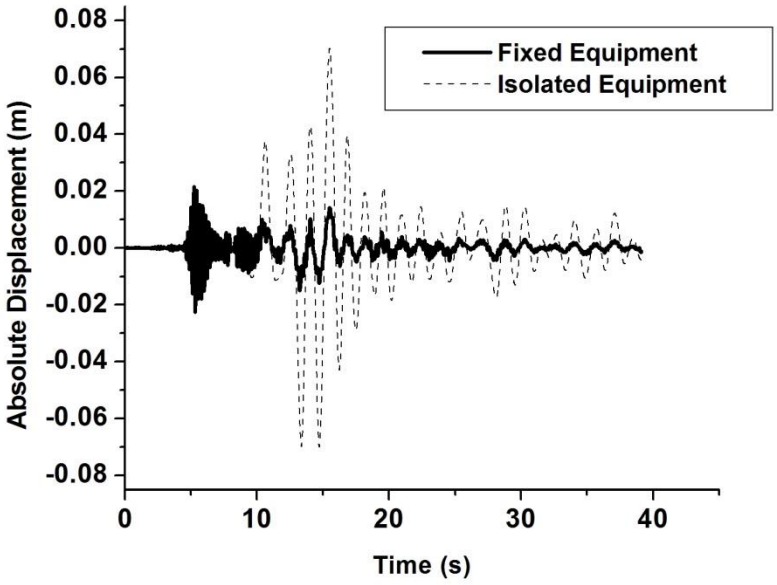

Figure F.2. Displacement response of fixed and isolated case under Array_0 Excitation

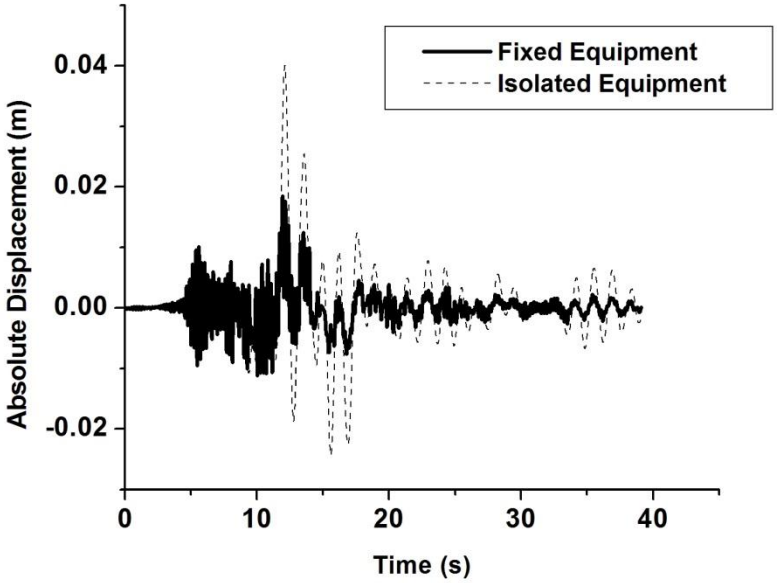

Figure F.3. Displacement response of fixed and isolated case under Array_90 Excitation

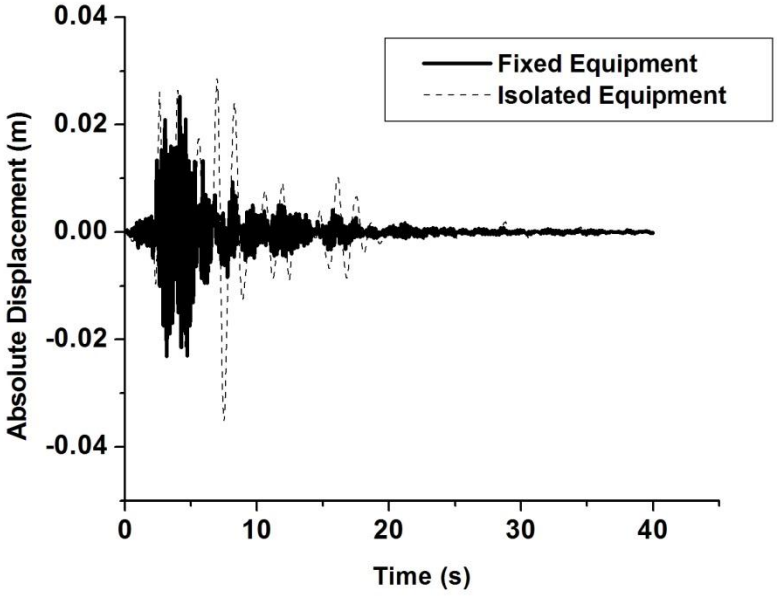

Figure F.4. Displacement response of fixed and isolated case under Corralit_0 Excitation

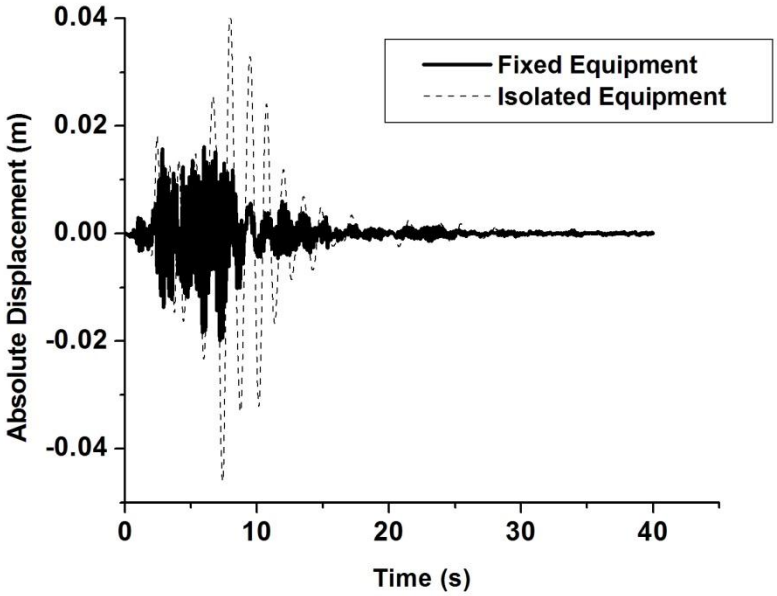

Figure F.5. Displacement response of fixed and isolated case under Corralit_90 Excitation

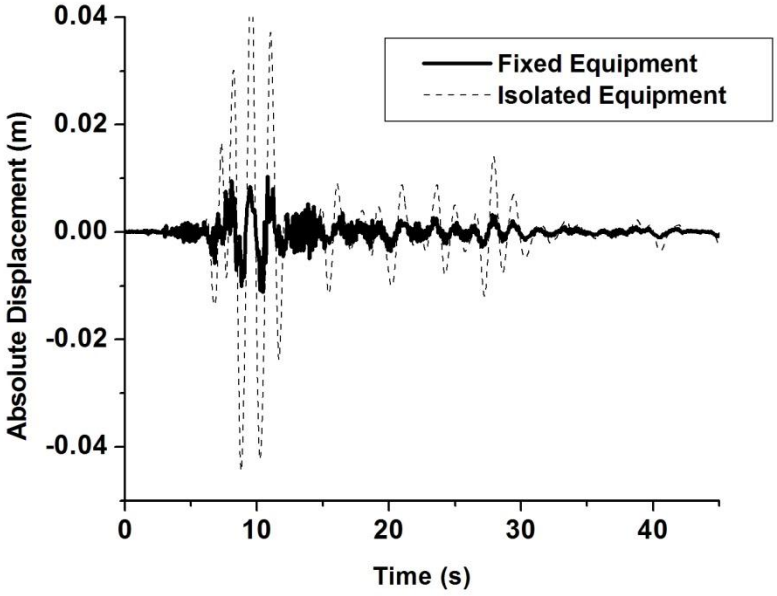

Figure F.6. Displacement response of fixed and isolated case under Holliste_0 Excitation

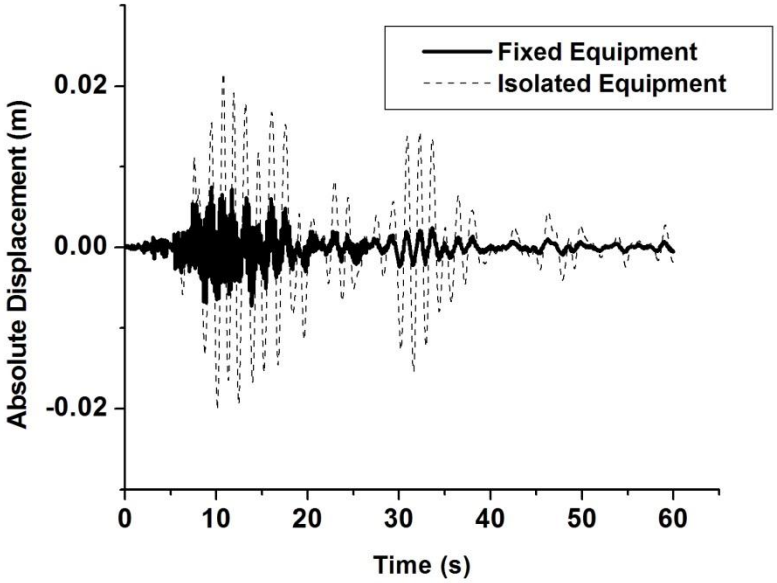

Figure F.7. Displacement response of fixed and isolated case under Holliste_90 Excitation

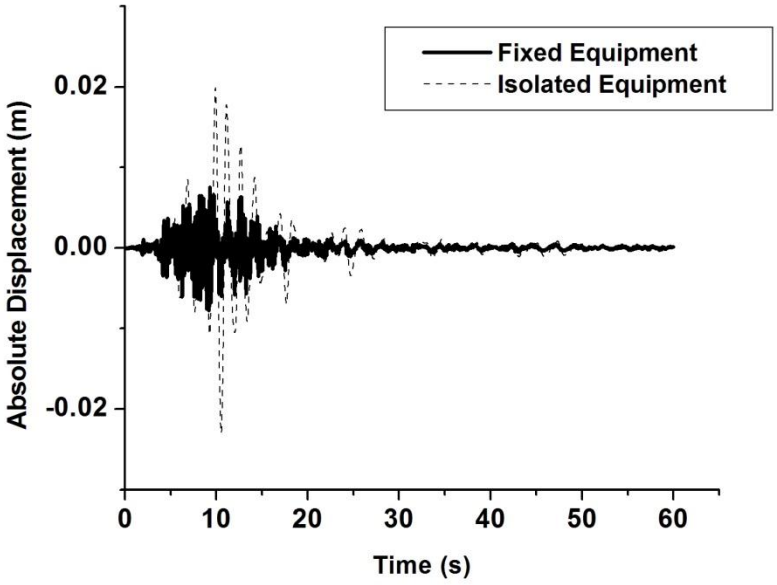

Figure F.8. Displacement response of fixed and isolated case under Lacc- Nor_0 Excitation

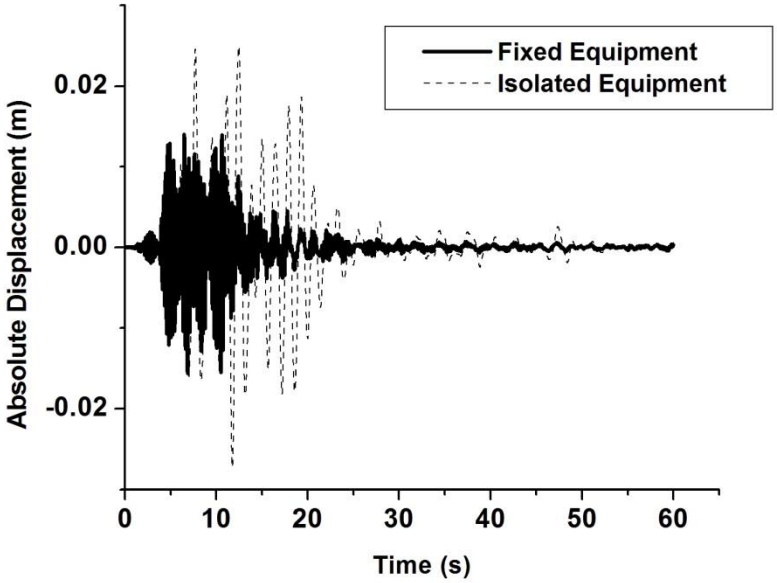

Figure F.9. Displacement response of fixed and isolated case under Lacc-Nor_90 Excitation

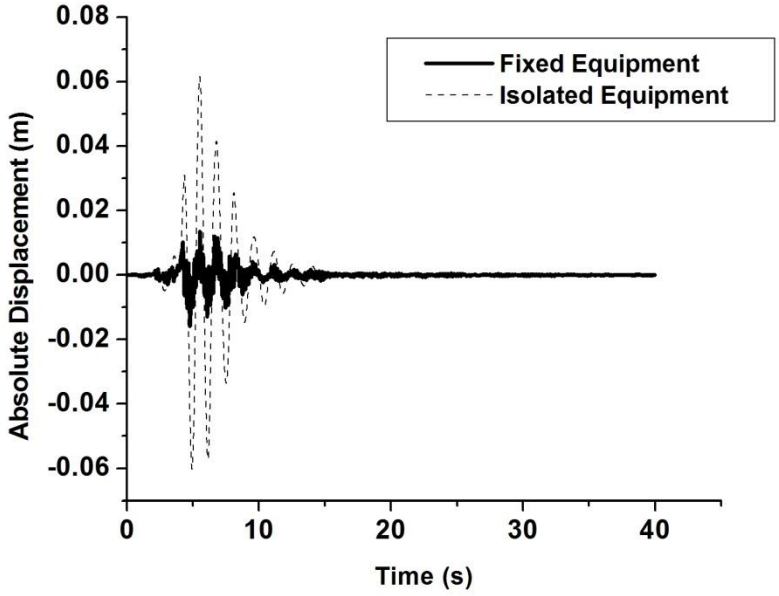

Figure F.10. Displacement response of fixed and isolated case under Lexingt_0 Excitation

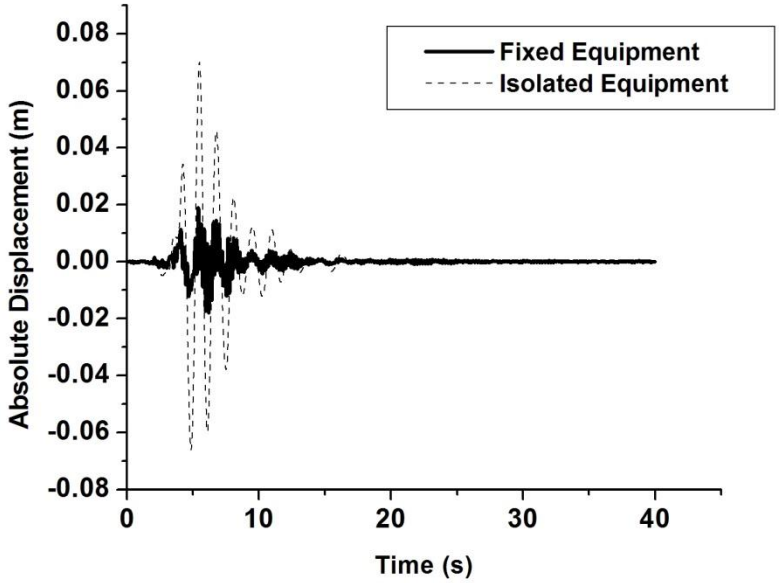

Figure F.11. Displacement response of fixed and isolated case under Lexingt_90 Excitation

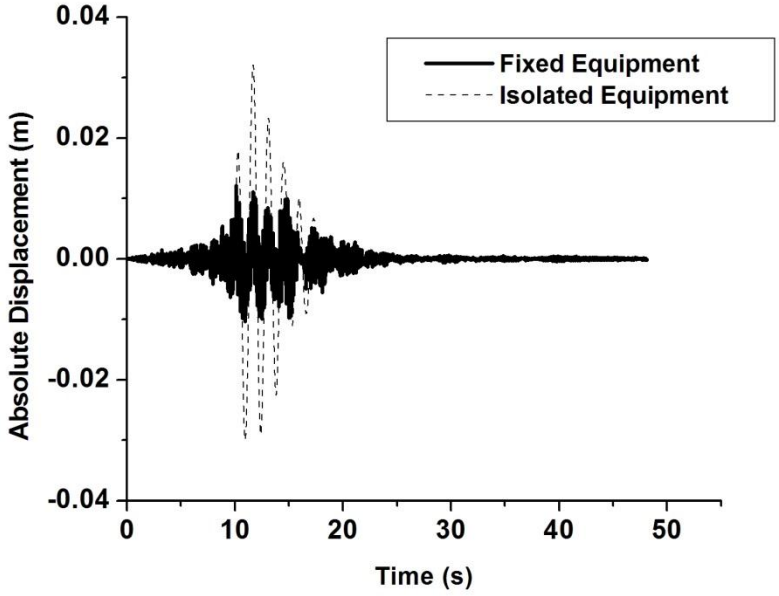

Figure F.12. Displacement response of fixed and isolated case under Lucerne_0 Excitation

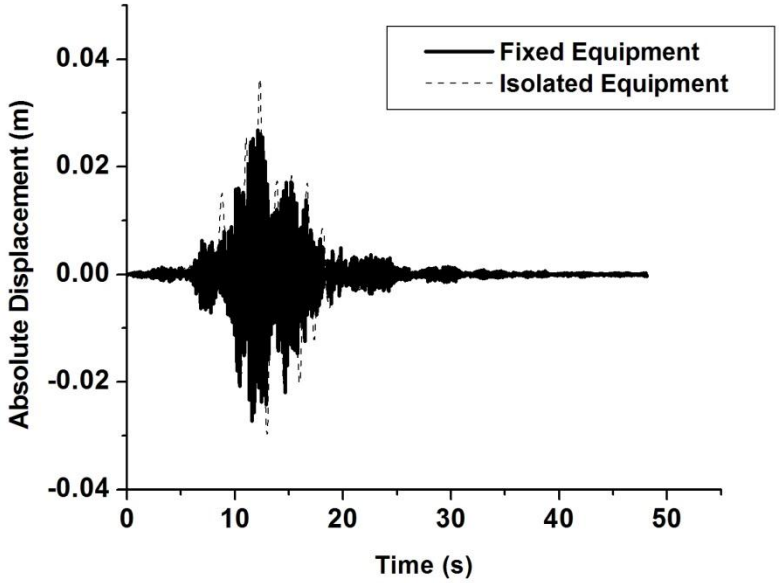

Figure F.13. Displacement response of fixed and isolated case under Lucerne_90 Excitation

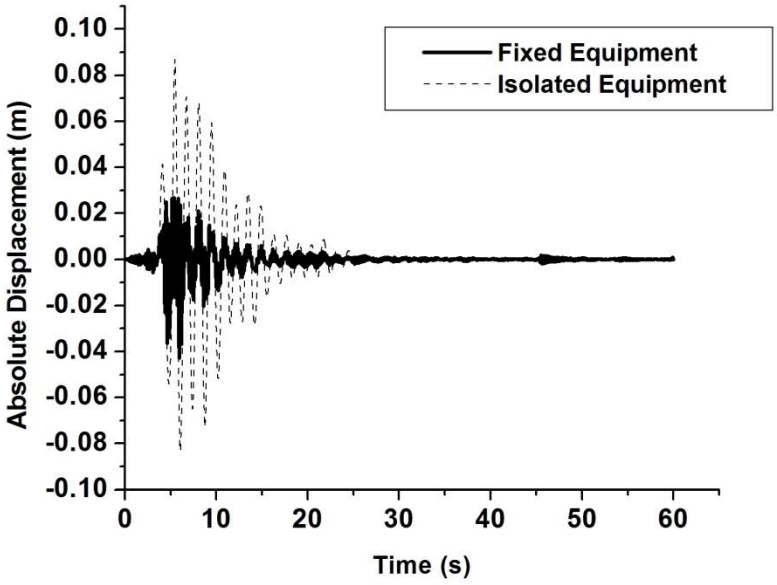

Figure F.14. Displacement response of fixed and isolated case under Newhall_0 Excitation

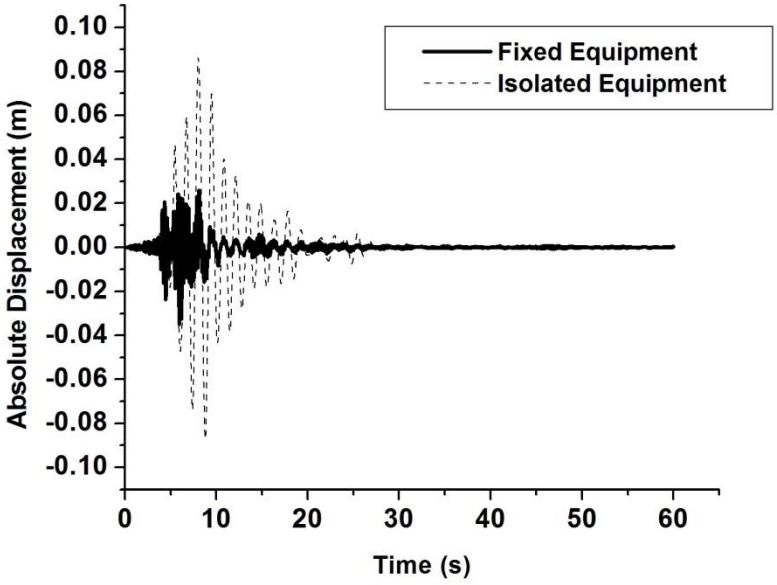

Figure F.15. Displacement response of fixed and isolated case under Newhall_90 Excitation

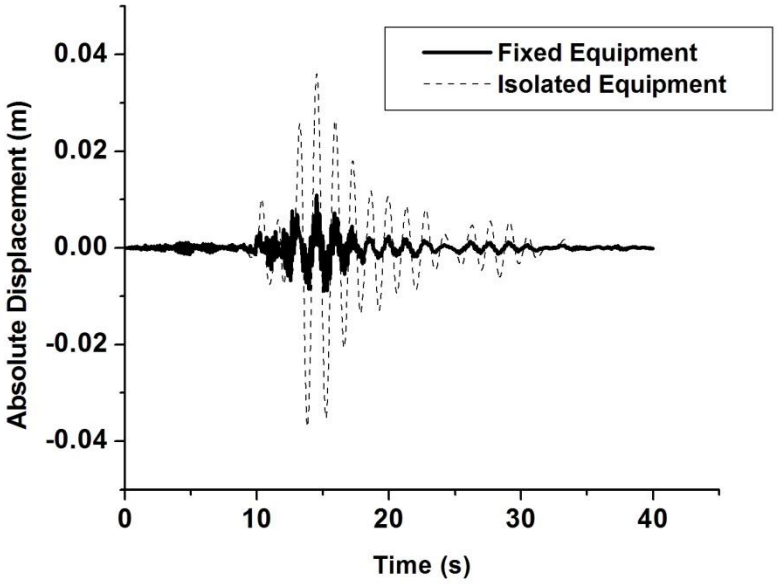

Figure F.16. Displacement response of fixed and isolated case under OakWhaf_0 Excitation

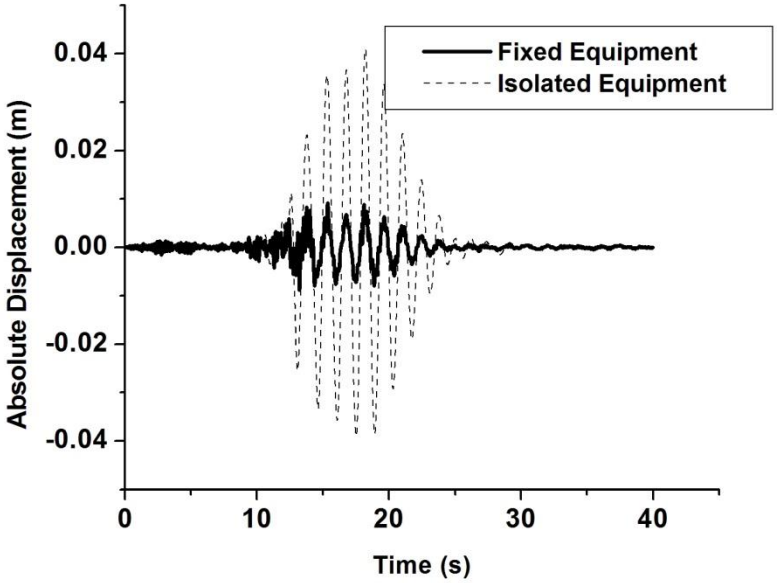

Figure F.17. Displacement response of fixed and isolated case under OakWhaf_90 Excitation

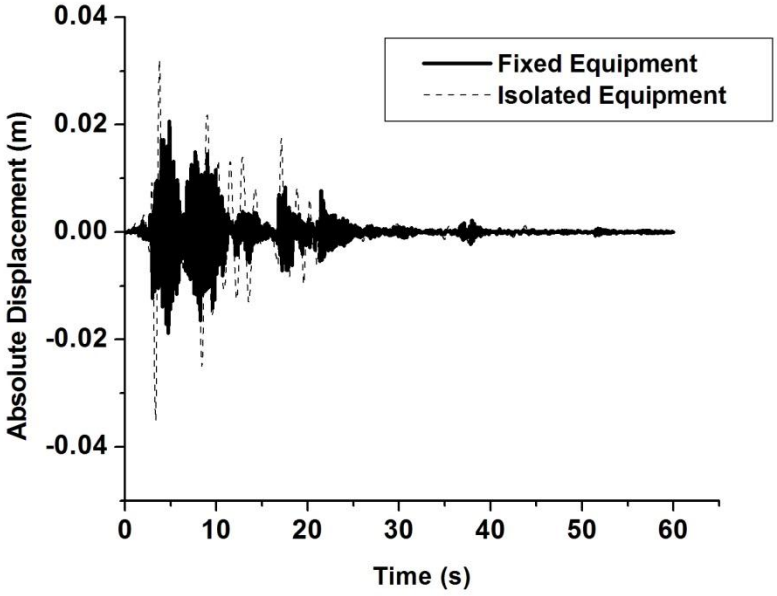

Figure F.18. Displacement response of fixed and isolated case under Petrolia_0 Excitation

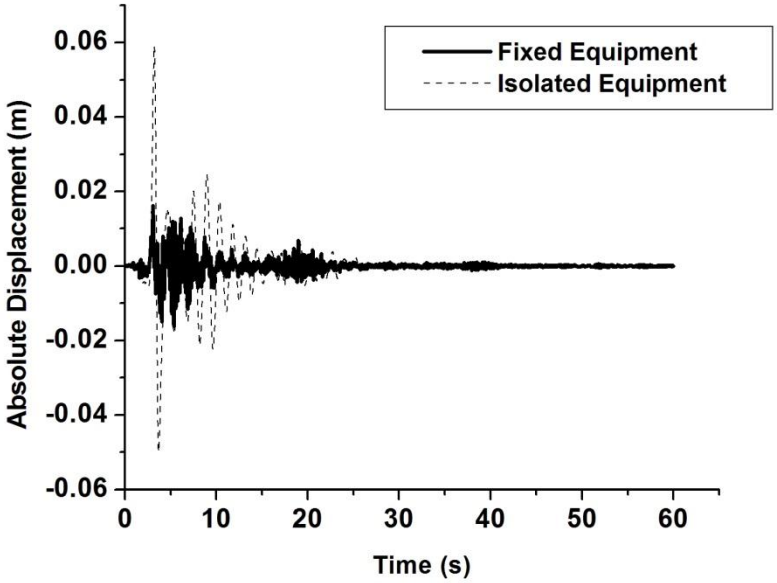

Figure F.19. Displacement response of fixed and isolated case under Petrolia_90 Excitation

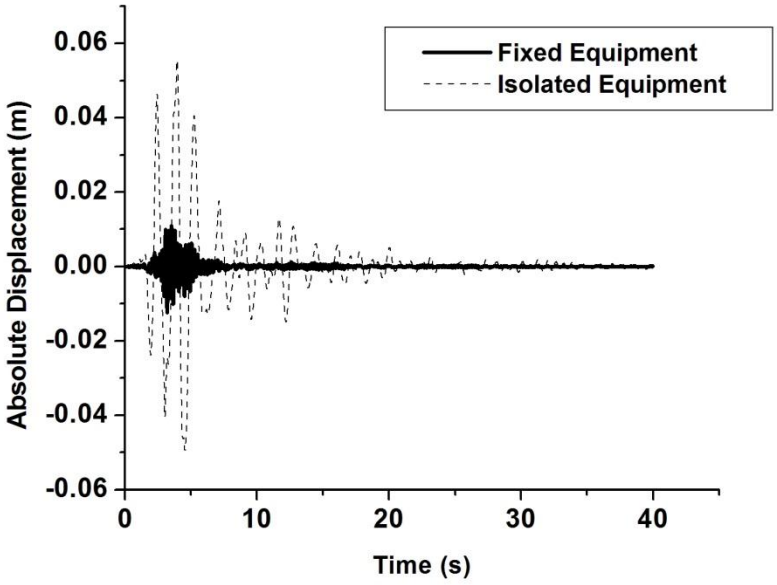

Figure F.20. Displacement response of fixed and isolated case under Pomona_0 Excitation

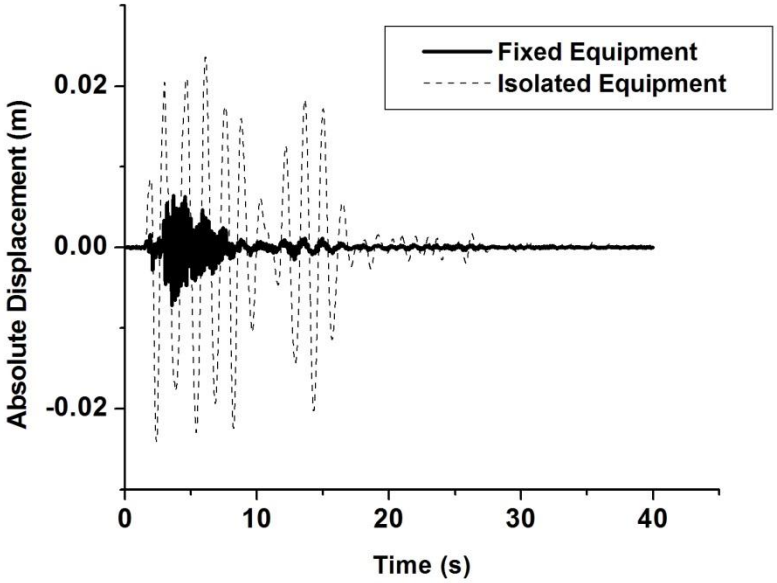

Figure F.21. Displacement response of fixed and isolated case under Pomona_90 Excitation

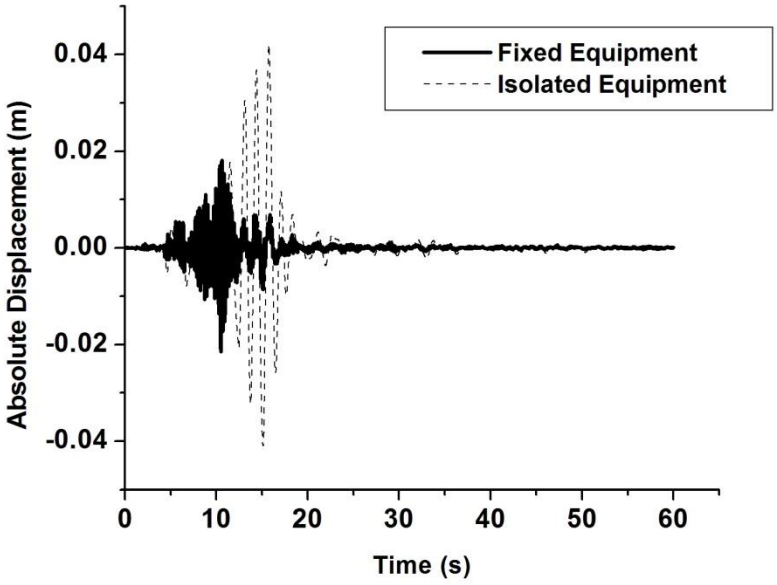

Figure F.22. Displacement response of fixed and isolated case under Santa Monica_0 Excitation

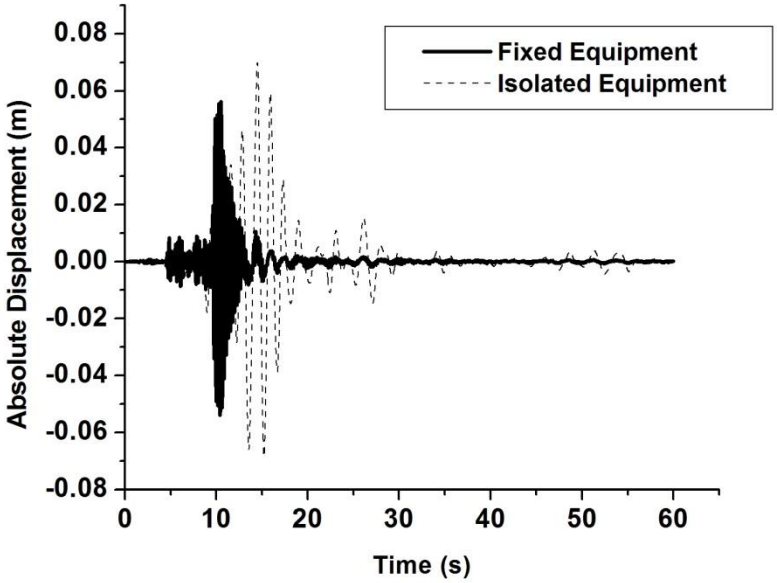

Figure F.23. Displacement response of fixed and isolated case under Santa Monica_90 Excitation

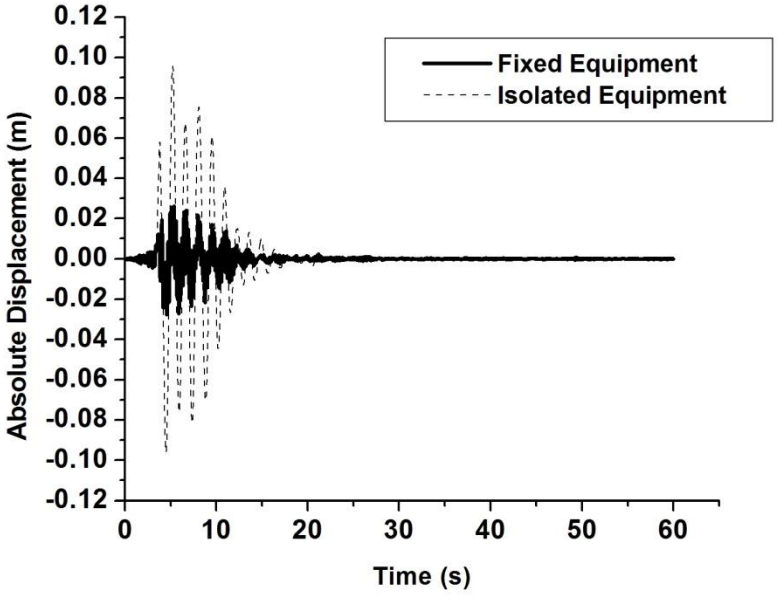

Figure F.24. Displacement response of fixed and isolated case under Sylmar_0 Excitation

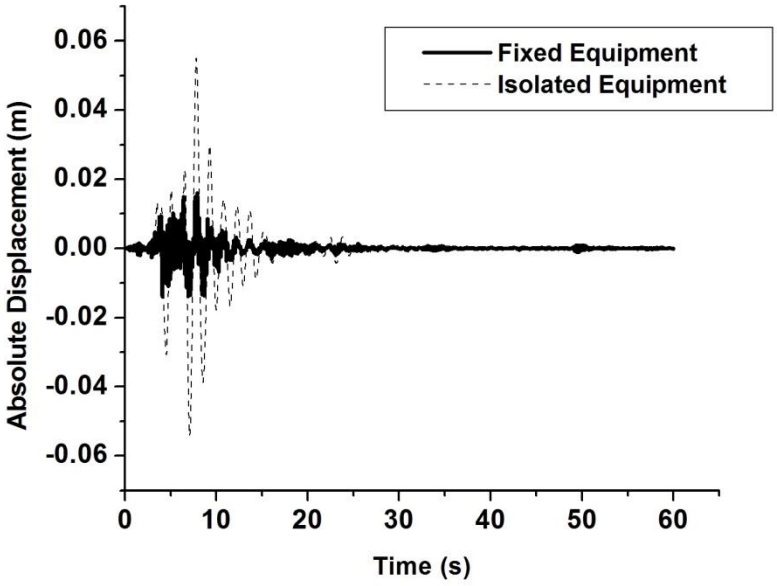

Figure F.25. Displacement response of fixed and isolated case under Sylmar_90 Excitation

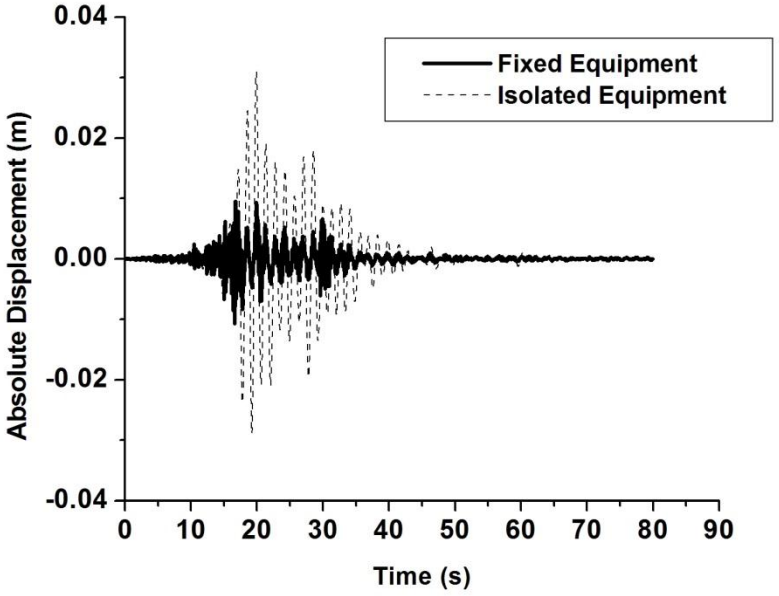

Figure F.26. Displacement response of fixed and isolated case under Yermo_0 Excitation

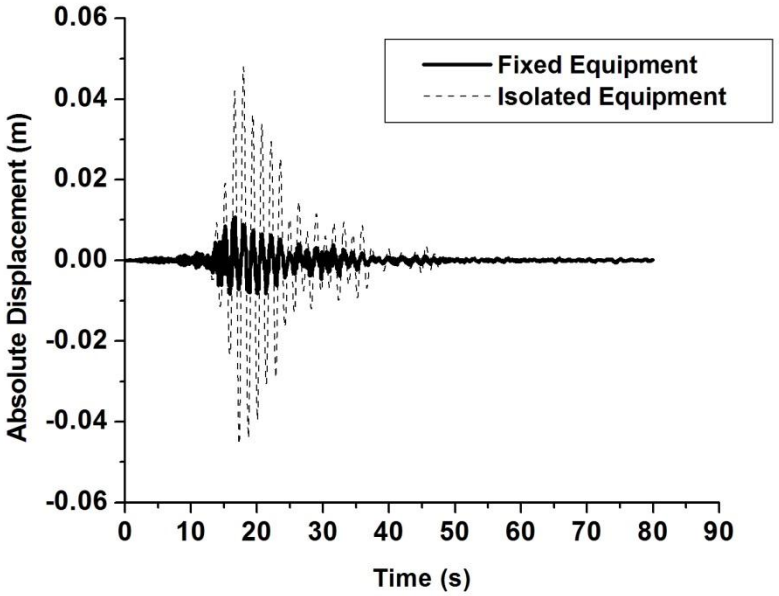

Figure F.27. Displacement response of fixed and isolated case under Yermo_90 Excitation

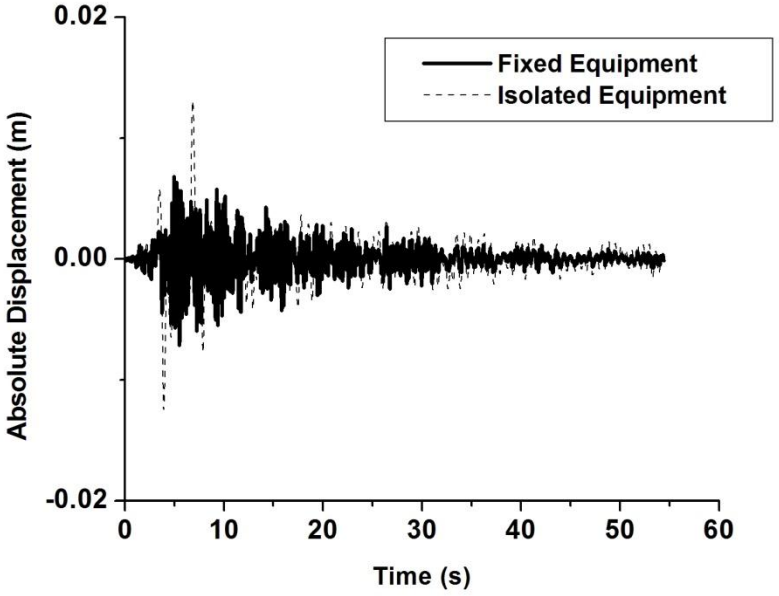

Figure F.28. Displacement response of fixed and isolated case under Kern Excitation

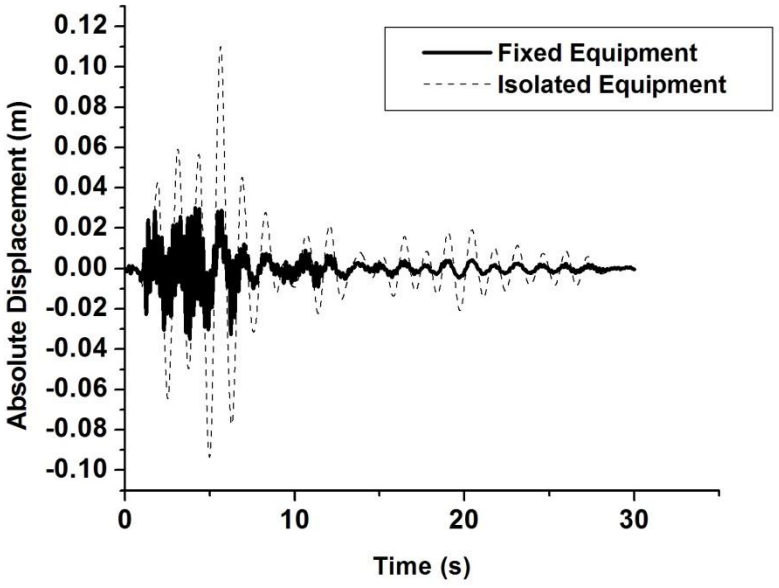

Figure F.29. Displacement response of fixed and isolated case under Kobe_90 Excitation

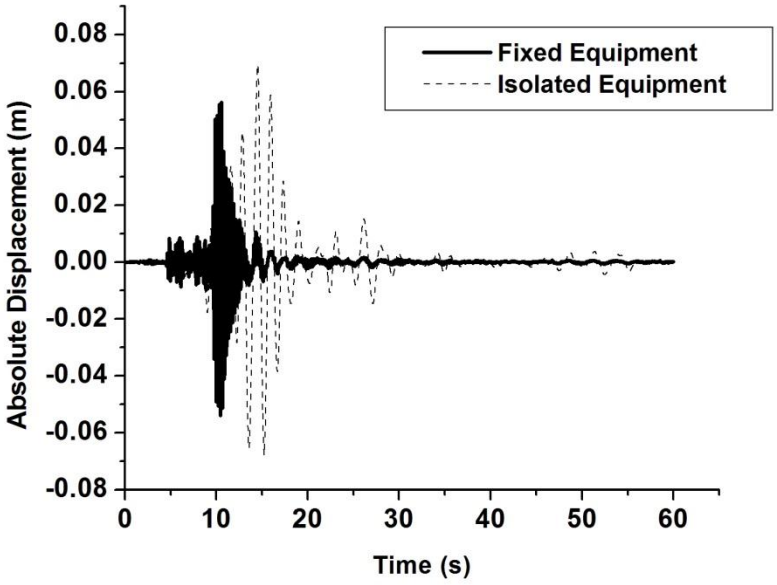

Figure F.30. Displacement response of fixed and isolated case under NorthRidge Excitation

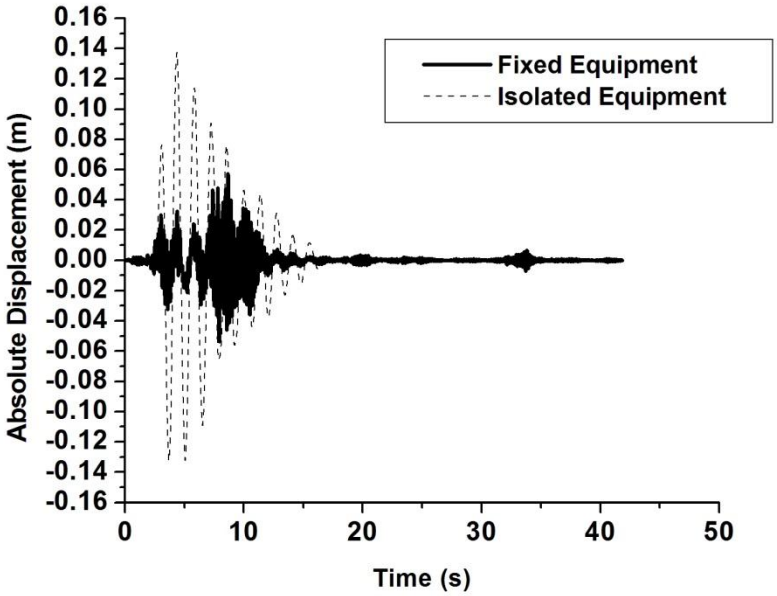

Figure F.31. Displacement response of fixed and isolated case under SanFrendo Excitation